NASA CR-72461

ANALYTICAL DESIGNS OF A SPACE-BORNE MAGNETICALLY-FOCUSED KLYSTRON AMPLIFIER

by

Dr. G. M. Branch and Dr. T. G. Mihran

prepared for

NATIONAL AERONAUTICS AND SPACE ADMINISTRATION

CONTRACT NAS3-11514

Requests for copies of this report should be referred to

National Aeronautics and Space Administration
Office of Scientific and Technical Information
Attention: AFSS-A
Washington, D.C. 20546

CR-72461

FINAL REPORT

ANALYTICAL DESIGNS OF A SPACE-BORNE MAGNETICALLY-FOCUSED KLYSTRON AMPLIFIER

by

Dr. G. M. Branch and Dr. T. G. Mihran

prepared for

NATIONAL AERONAUTICS AND SPACE ADMINISTRATION

October 25, 1968

CONTRACT NAS3-11514

Technical Management
NASA Lewis Research Center
Cleveland, Ohio
Dr. H. G. Kosmahl

GENERAL ELECTRIC COMPANY
Tube Department
Microwave Tube Business Section
Schenectady, New York

FOREWORD

This final report covering a six-month study of design approaches for very high-efficiency magnetically focused klystron amplifiers was conducted under Contract NAS3-11514 from the National Aeronautics and Space Administration, Lewis Research Center. Dr. Henry Kosmahl was the technical program manager for NASA. The study was performed by Drs. G. M. Branch and T. G. Mihran with assistance from personnel in three General Electric Company groups: Research and Development Center, Valley Forge Space Technology Center, and Microwave Tube Business Section. Principal technical contributors, in addition to Drs. Branch and Mihran, include E. C. Conway, R. A. Dehn, E. M. Gilbert, G. J. Griffin, and W. Neugebauer.

TABLE OF CONTENTS

LIST OF ILLUSTRATIONS

LIST OF TABLES

Section I
SUMMARY

An analytic study leading to the development of high-efficiency magnetically-focused klystron designs for use in satellite-borne television broadcasting service is reported herein. An accurate and detailed large-signal computer simulation of a klystron was employed for developing space-adapted, heat-pipe cooled klystron designs having internal conversion efficiencies in excess of 60 percent and meeting all specifications for phase linearity, gain, power output and bandwidth. During the course of the study, a new principle of reflex collection of the spent beam at reduced collector potentials was discovered. Preliminary analyses of the collector indicates that a power klystron with a reflex depressed collector could have an overall stable output-power efficiency in excess of 80 percent in FM television service.

The computer klystron gain and overall efficiency characteristics while transmitting a television signal at average picture levels in the five services considered are as follows:

Service	Beam Voltage (KV)	Beam Current (Amperes)	Power Output (KW)	Gain (dB)	Efficiency (Percent)
850-MHz AM	15.9	1.00	3.0	42	50
2000-MHz AM	13.5	0.78	2.0	52	51
2000-MHz FM	11.9	0.65	5.0	47	82
8000-MHz FM	12.3	0.68	5.0	40	77
11,000-MHz FM	12.9	0.73	5.0	38	70

The above characteristics were computed for klystrons with state-of-art beam transmission efficiencies between 95 and 98 percent, with a reflex collector energy conversion efficiency of 85 percent, and with a solenoid providing a collimating magnetic field of twice the Brillouin value.

Section II
INTRODUCTION

STUDY OBJECTIVES

National Aeronautics and Space Administration Contract No. NAS3-11514 was initiated February 6, 1968, for conducting an analytic study leading to the development of theoretical designs for space-borne magnetically-focused klystron amplifiers for television broadcasting. Klystron power amplifiers for amplitude modulation service at 850 MHz and 2000 MHz, and for frequency modulation service at 2000 MHz, 8000 MHz and 11,000 MHz, were to be studied, critical design areas identified, and verification experiments designed.

Trade-off analyses and engineering evaluations of designs for each of these five klystron amplifiers were made in order to develop an optimum design compatible with the space environment and meeting the required specifications for power output, bandwidth, signal-to-noise ratio, phase linearity, life, gain, minimum weight, and maximum efficiency.

The specifications, as amended, include the following:

1. Power output

   (a) 850-MHz AM (vestigial sideband)

Peak synchronizing pulse power	7.5 kW
Peak picture power	3.5 kW
Average picture power	2.6-3.0 kW
Minimum picture power	1.3 kW
Sound power	0.75 kW

   (b) 2000-MHz AM (vestigial sideband)

Peak synchronizing pulse power	5.0 kW
Peak picture power	2.3 kW
Average picture power	1.75-2.0 kW
Minimum picture power	0.9 kW
Sound power	0.5 kW

(c) 2000-MHz FM . . . . . 5.0 kW

(d) 8000-MHz FM . . . . . 5.0 kW

(e) 11,000-MHz FM . . . . . 5.0 kW

2. Linear dynamic range for AM . . . . . 20 dB, min.

3. Deviation of small-signal gain from linearity 3 dB below saturation (for AM only) . . . . . 0.5 dB, max.

4. Signal-to-noise ratio over bandwidth (AM) . . 42 dB, min.
. . 55 dB, desired

5. Signal-to-noise ratio over bandwidth (FM) . . 32 dB, min.
. . 45 dB, desired

6. Deviation from phase linearity (AM) . . . . . 1.2^{o} max.

7. Magnitude of second derivative of phase response across band (FM) . . . . . $0.05\ deg/MHz^2$, max.
. . . . . $0.015\ deg./MHz^2$, desired

8. 3-dB bandwidth . . . . . 6 MHz (AM)

9. Gain of amplifier or amplifier chain . . . . . 40 dB, min.

10. Input and output VSWR . . . 1.05 max., into 50-ohm impedance

11. Life . . . . . 20,000 hours, min.

12. Vibration capability

(a) Sinusoidal . . . . . 5.0 g (20-400 Hz)
. . . . . 15.0 g (400-3000 Hz)

(b) Random density . . . . . 5.4 g RMS ($0.082\ g^2/Hz$)
. . . . . 17.9 g RMS ($0.15\ g^2/Hz$)

(c) Shock . . . . . 8-msec duration, 30 g, min.

STATE-OF-THE-ART BACKGROUND

At the start of this study, the overall efficiency of klystron amplifiers of "kilowatt" size was less than 50 percent under saturation drive conditions. Efficiency is defined here as the ratio of RF output at a transmission line terminal to total power supply input including heater power and magnet power as well as beam power. Klystrons used in television broadcasting have slightly lower efficiency -- generally in the range of 30 to 40 percent. Of course, in AM service the actual operating efficiency is much lower due to the characteristics of the amplitude modulation and the need to operate below the maximum output capability of the device in order to maintain amplitude linearity.

Although most commercial klystrons operate with efficiencies ranging from 30 to 50 percent, a few commercial klystrons achieve efficiencies in the 50-60 percent range. Reported klystron efficiencies above 60 percent are rare, even in experimental tubes. High efficiency in a klystron may be achieved with or without the use of additional features such as extended interaction and voltage jumping. The use of a properly designed depressed collector may result in increased efficiency.

Perhaps the earliest and still one of the best achievements in obtaining high efficiency was the four-cavity, 400-MHz klystron[1] built at SERL in England in 1961. This tube achieved an efficiency of 61 percent under optimum conditions without resorting to collector depression or other efficiency-enhancing schemes. Another noteworthy achievement is that of Walder[2] in 1965, with a four-cavity tube at 750 MHz. Walder measured an efficiency of 59 percent at a beam voltage of 9 KV, again without the use of additional efficiency-enhancing schemes. This efficiency could be raised to 62.5 percent by jumping the voltage by 3 KV at the penultimate cavity. By collector depression alone, Walder reported he could increase the efficiency to 63.5 percent. Finally, by a judicious combination of penultimate voltage jumping, collector depression, and magnetic field shaping, Walder reports efficiencies of 68.2 and 70.7 percent, the latter figure corresponding to an extremely unstable mode of operation due to reflected electrons. It should be noted that the collector on the tube was not especially designed for potential depression; thus the numbers reported above should not be regarded as the ultimate upper limit for depressed-collector operation.

The use of extended interaction cavities in klystrons has been suggested as another means for enhancing efficiency. In 1961 Chodorow and Wessel-Berg[3] reported an efficiency of 47 percent in a three-cavity tube

with 20 dB gain. In 1963 Priest and Leidigh[4] reported an efficiency of 56 percent when two separate cavities were used to extract output power. When the two power outputs were combined, the efficiency dropped to 53 percent. In 1964 Priest and Leidigh[5] reported an efficiency of 65 percent and a "stable gain in excess of 15 dB" from a two-cavity extended-interaction klystron with collector depression. With no depression, the efficiency of this tube was 36 percent. With voltage jumping this figure was raised to 42 percent.

Summarizing the above results, it is evident that a conventional klystron of optimum design -- namely, the SERL tube -- outperforms both extended interaction klystrons and klystrons with voltage jumps. This suggests that the first task at hand is to develop a systematic design procedure which will lead to conventional klystrons of optimum design. Once this optimum design has been achieved, the next largest improvement in efficiency should come from the addition of a properly designed depressed collector. Upon completion of these two tasks, it is possible that the use of voltage jumps or extended interaction cavities could yield a modest additional increase in the efficiency of energy conversion.

Although intensive efforts had been made over several years to devise a segmented collector electrode to be operated at reduced potentials and thus recover some of the unused beam energy,[6] these were only partially successful. In some special cases, a low interaction efficiency amplifier could be improved from the 20 to 30 percent range to the 50 percent range. These methods were not successfully applied to klystrons for television broadcasting, mainly because the designs employed resulted in signal distortion and amplifier instability due to the return of electrons from the collector region to the RF interaction region of the tube.

Modern large-signal computer programs for the design of multicavity klystrons have not been discussed in detail in the literature. The most complete published study was made by Webber[7] in 1958. Because he employed a distance-stepping formulation in computing power extraction from the beam, his results were not valid in case of severe electron slowdown and/or turn-around.

Various other workers have devised digital computer programs to study klystron behavior, most notably Rowe[8] at the University of Michigan, and Sun and Dalman[9] at Cornell University. Both of these formulations utilize the distance-stepping formulation throughout the entire calculation and therefore they also should not be expected to be accurate under highly efficient power extraction conditions in the output gap.

In 1963, Mihran and Branch developed a computer program for multicavity klystrons which combined distance-stepping with time-stepping in order to improve the accuracy of the simulation at very large signal levels. The program now is able to predict large signal efficiency and gain to within 5 percent of the measured values.

Simulation of the electronic interactions in linear-beam tubes with the aid of computers has progressed to the point where both the basic interaction efficiency and the electron trajectories in the collector region can be determined. Prior optimization studies have also shown that klystron amplifiers with efficiency significantly greater than 50 percent are feasible. This report covers the use of these analytic methods in the design optimization of klystrons in both AM and FM television broadcast applications.

Additional constraints are placed on the klystron designs by the intended operation of these tubes in a satellite. Devices of this power level have not yet been orbited and such problems as power supply design and heat rejection systems also require attention. The heat pipe concept appears to be the most desirable way to remove the wasted energy to an appropriate radiator; hence, the application of these principles to the klystron designs also represents a portion of the study effort. Corollary to these problem areas was consideration of fabrication techniques to achieve the desired electrical performance in a device having mechanical strength sufficient to survive the expected environmental factors of shock, vibration, and temperature.

Section III

DESCRIPTION OF KLYSTRON ANALYSIS METHODS

KLYSTRON SIMULATION PROGRAMS

History of Development of G.E. Klystron Simulation Program

The contributions of the General Electric Company to klystron development began in 1939 with Hahn's parallel invention and demonstration of the klystron.[10] The pioneering space-charge wave approach of Hahn and Ramo[11, 12] forms the basis for present-day small-signal theories of multicavity klystron performance. Later, Branch and Mihran[13] recognized the practical importance of plasma frequency reduction factors for microwave tube design, and they derived working relationships for this factor. The large-signal interaction computation was programmed by Webber[14] in 1957 using the disk-electron model. In later papers, he extended this work to multicavity klystron bunching[7] and to an approximate calculation of the large-signal energy extraction process in the output gap.[15] Webber[14] and Mihran[16] then established a rigorous basis for reducing final and penultimate drift lengths below a quarter plasma wavelength to optimize efficiency. Mihran[17, 18] has recently found that small diameter beams are harmful to power conversion efficiency, contrary to previous understanding. His work takes into account the effect of velocity distribution on power conversion efficiency in a more accurate way than Webber had done.

Finally, a recent investigation[19] by Branch, Mihran, Neugebauer, and Pohl has shown how to obtain effective beam diameter for RF interaction calculations from a measurement of the magnetic field which collimates the klystron beam.

Before the present study was undertaken, this background knowledge had been utilized to develop two computer programs which permit very accurate modeling of the small-signal and large-signal interactions in "O" type devices, including the multicavity klystron amplifier. Both programs give identical results at small-signal levels, but the more complex disk-model program is required to accurately simulate the large-signal performance of the amplifier.

Small-Signal Space-Charge Wave Program

The small-signal space-charge wave klystron analysis program uses analytic equations to describe the klystron bunching process in a modulated electron beam. The program is permanently stored in the memory disk file of a GE-235 time-shared computer, to which there is immediate access via a teletype link. The program can be called out and the small-signal performance of a multi-cavity klystron can be computed in less than a minute. Because a large number of design variations can be quickly analyzed, the small-signal program proves very useful in the initial development of a klystron design. By comparing subsequent large-signal computations with the small-signal results, one can, with experience, anticipate fairly well the result of a large-signal analysis of a given design derived with the small-signal program.

Hahn's linear space-charge wave theory is used in the computation of the magnitude and phase of the fundamental component of RF current at each gap as a function of frequency. The basic space-charge wave equation, as given by Beck,[20] for example, is:

$$I_{i,j}/I_o = 2J_1\left[\frac{\mu_j \alpha_j}{M_r(M_r+1)}\ \frac{\omega}{\omega_q}\ \sin\beta_q \ell_{i,j}\right] \qquad (1)$$

where $I_{i,j}$ is the fundamental RF component of the modulated current at klystron interaction gap i produced by a voltage modulation index α_j at a distance $\ell_{i,j}$ from gap j. J_1 is the ordinary Bessel function of order 1 and I_o is the DC beam current. M_r is the relativistic mass ratio of the beam electrons moving at a velocity u_o and is given by:

$$M_r = \left[1 - (u_o/c)^2\right]^{-1/2} \qquad (2)$$

The quantity μ_j is the small-signal gap coupling coefficient given by:

$$\mu = \left[I_o^2(\gamma b) - I_1^2(\gamma b)\right]^{1/2}/I_o(\gamma a) \cdot \sin\theta/\theta, \qquad (3)$$

where γ is the radial propagation constant given by:

$$\gamma = \omega/(M_r u_o) \qquad (4)$$

and θ is the gap half-transit angle $\omega d/2u_o$ for a gap length d. In this equation, I_o and I_1 are Bessel functions of the second kind, order 0 and 1, respectively. This expression applies for beams of radius b in a drift tunnel of radius a, and is adequate for computing the velocity modulation applied to a beam in bunching gaps even in large-signal computations, since even at large-signal levels, the voltage index rarely rises above 0.5 or 0.6.

In Eq. (1) the quantity β_q is the plasma wave propagation constant computed from the average of the fast and slow space-charge wave propagation constants, which are found by solving a transcendental boundary condition equation.[13]

The current modulation index at each gap is computed by summing the current indices as given by Eq. (1) for all the previous gaps. At each gap, the voltage modulation induced in the cavity may be computed by multiplying the total current index times the effective cavity impedance as determined from its R/Q parameter, the small-signal beam coupling coefficient, and the beam-loaded Q of the cavity. The voltage modulation index at the input gap is computed from the effective gap impedance and the drive power. All impedances, voltages, and currents are treated as complex quantities, and complex arithmetic is used for carrying out all operations. From the real and imaginary parts of the output circuit voltage, the phase angle and hence the phase shift of the output signal with respect to the input signal can be computed.

The small-signal program is useful for computing the small-signal gain and phase characteristics of a multi-cavity broadband klystron. While some insight into the large-signal performance can be derived from this computation, no accurate estimate can be made of output power and efficiency. For this purpose the large-signal disk-model program was developed in a previous independent research effort to simulate accurately the amplifier under saturation drive conditions. At each gap in the bunching portion of the klystron, beam-loading susceptance and conductance as well as gap impedance are computed as in the small-signal program; instead of computing the subsequent bunching action from space-charge wave theory, however, an integration of the equations of motion of disks representing the beam is used.

Large-Signal Disk-Model Program

The large-signal disk-electron program is run on the large capacity, high-speed GE-635 computer. This program uses the disk-electron model

in a two-stage calculation, as shown in Figure 1. In the bunching stages, a distance-stepping calculation is used between gaps. At each gap the characteristics of the external circuits are introduced using appropriate coupling coefficients.[21] As pointed out by Webber[14, 15] a distance-stepping calculation in the output region can lead to significant error, because it does not accurately allow for large electron velocity reduction and reflection by the strong RF fields in the output gap. A reformulation of the output gap interaction by using a time-stepping rather than a distance-stepping calculation has overcome this limitation. Thus, the advantages of the disk-electron formulation (allowing overtaking, and including space charge) are preserved in the output gap region; in addition, electron velocity reduction and reflection are handled correctly. The two stages of the calculation, bunching and output gap interaction, are appropriately matched in such a way that the computer makes the transition automatically, quickly, and accurately.

Other program features applicable to the study of high-efficiency klystrons are:

(1) Provision for multiple-tuned resonators at all interaction gaps.

(2) Provision for the variation of magnetic field along the tube, including the possibility of cathode flux, with the consequent depression of beam potential.

(3) Provision for voltage stepping along the beam in an extended-interaction output region.

(4) Computation of approximate space-charge forces from a summation of the forces between disks representing sections of the beam.

(5) Improvement in the method of computing power extraction in the output circuit using Ramo's theorem for induced current.

(6) Allowance for gridless interaction gaps, using analytic approximations to the exact fringing field distributions.

(7) Extension of output circuit calculation to include extended-interaction multiple gaps with standing or traveling waves.

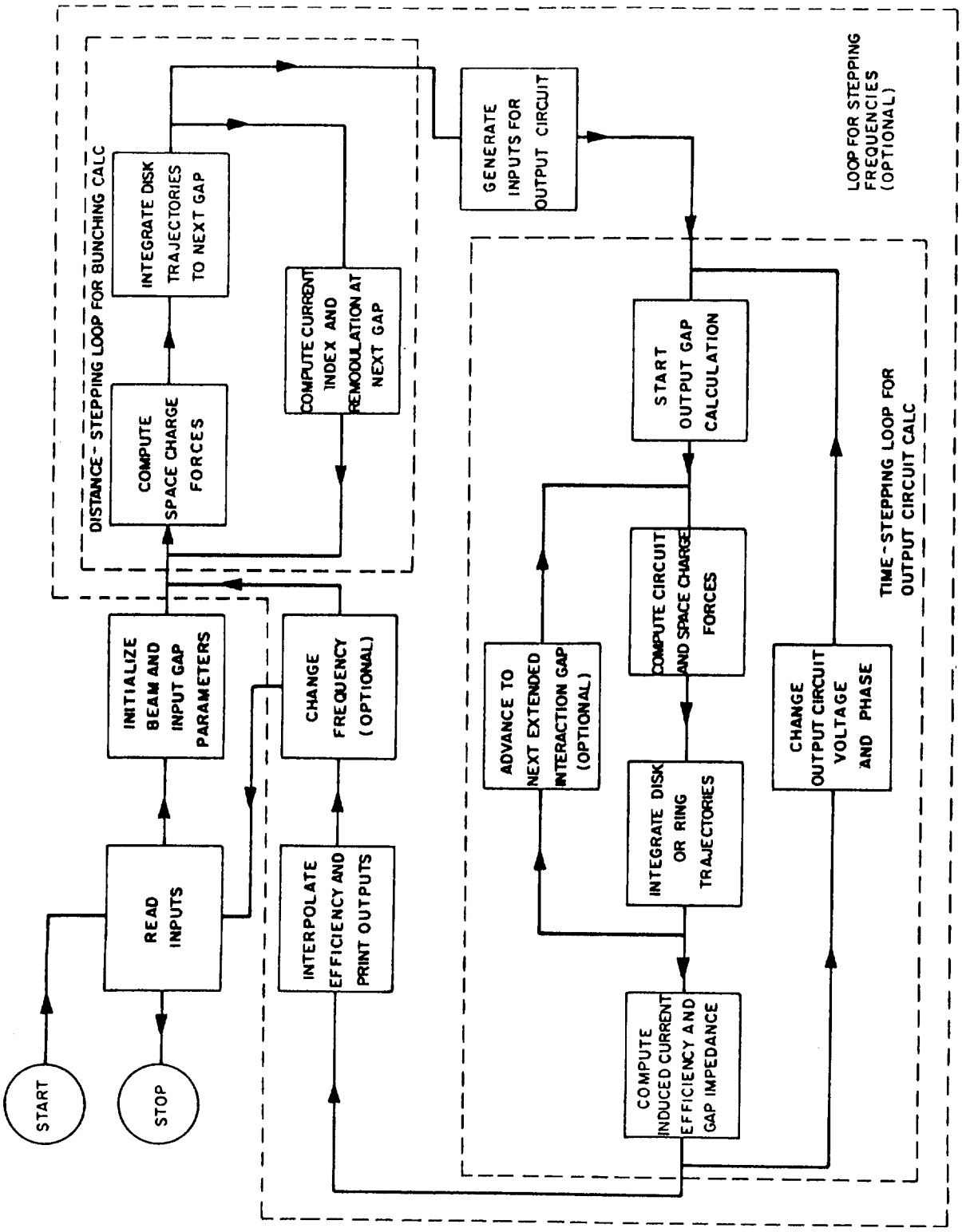

Figure 1 - Block Diagram of Large-Signal Disk-Electron Klystron Program

The important outputs of the large-signal computer program are:

(1) Power conversion efficiency at the fundamental frequency.

(2) Current modulation ratios (amplitude and phase) of the fundamental, second, and third harmonics.

(3) Phase shift between input and output signals.

(4) Power gain between output and input signals.

(5) Phase positions and velocities of all electrons as a function of distance, up through the output gap.

(6) Electron-disk positions and velocities as a function of time in the output gap or gaps, including the spent beam spectrum.

The first four outputs give the overall performance characteristics of the klystron, which can be optimized and compared with experiment, whereas outputs (5) and (6) are used to gain an understanding of the physical processes that lead to good performance, as well as aiding in the design of the collector.

For the disk model, one electrical wavelength of the electron beam is divided into a number of disks of equal length, as illustrated in Figure 2. Usually there are 20 disks, although this number can be increased at the expense of longer computation time and greater cost. Greater accuracy is achieved when the number of disks per wavelength is increased, but experience has shown that 20 disks per wavelength is an adequate number for most klystron analyses.

For dynamical calculations, the motion of an electron at the radius of gyration (RMS radius) of the disk is assumed to give a good representation of the motion of all the electrons included in the disk. The dynamical equation of motion of an electron is given by the Lorentz force equation:

$$\frac{d\bar{p}}{dt} = e\,(\bar{E} + \bar{v} \times \bar{B}) \qquad (5)$$

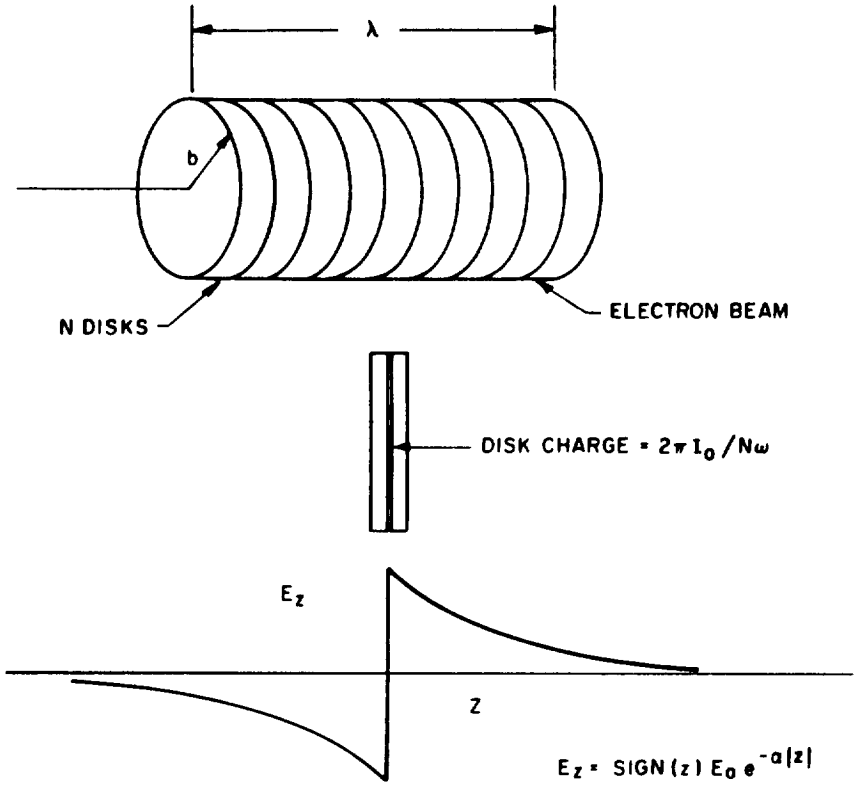

Figure 2 - Disk Model of Electron Beam (Division of One Wavelength into N Disks and Sketch of Axial Field Variation of Single Disk.)

where $\bar{E}$ is the total electric field (space-charge field created by the other disks and the circuit field, if the disk is in an interaction gap), $\bar{B}$ is the vector sum of the collimating magnetic field and the self-induced field created by the beam, $\bar{p}$ is the vector linear momentum having both axial, radial, and circumferential components, and $\bar{v}$ is the vector velocity also having 3 components. In terms of the vector velocity $\bar{v}$, the vector $\bar{p}$ is given by the relativistic equation:

$$\bar{p} = m_o \bar{v} / \sqrt{1 - \bar{v} \cdot \bar{v}/c^2} \tag{6}$$

Only two components of $\bar{p}$, p_z and p_r need be computed by step-wise integration (using a Runge-Kutta method), and the third component p_θ can be directly evaluated by using a development of Busch's Theorem as follows:

$$p_\theta = e(zB_r - rB_z/2 + r_c^2 B_c/2r) \tag{7}$$

where r_c is the radius on the cathode where the electron originated, and B_c is the axial magnetic field strength at the cathode.

If the radius of the beam were of infinite extent, there would be no decay of the axial electric field of a disk, and the field to the right of the disk would be given simply by Gauss's Law as follows:

$$E_z = E_1 = I_o/N\omega\epsilon_o b^2 \tag{8}$$

where I_o is the current included in a tube of radius b, N is the number of disks per wavelength at the angular frequency ω, and ϵ_o is the permittivity of free space. In the same infinite beam, the plasma frequency would be the unreduced plasma frequency ω_p. In a finite beam of radius b enclosed within a drift tunnel of radius a, however, the field lines from a given disk would terminate partly on induced positive charges in the tunnel wall, thus reducing the plasma frequency to a value ω_q and causing the axial field to decay with an attenuation constant α.

Various approximations to the disk space charge field attenuation constant have been given by Tien, Walker and Wolontis,[22] who used a Green's Function approach in evaluating the axial field of charged disks in a cylinder. At a distance z from the disk in the moving frame of reference, the field of a single disk is given by:

$$E_z = \text{sign}(z)\, E_1\, e^{-\alpha|z|} \tag{9}$$

where E_1 is defined in Eq. (8), and α is given approximately by

$$\alpha = 2/b \tag{10}$$

The plasma frequency reduction factor ω_q/ω_p has previously been given[13] as:

$$\omega_q/\omega_p = 1/\sqrt{1 + (T/\gamma)^2} \tag{11}$$

The concept of a reduced plasma frequency and of a related disk-field attenuation constant permits the three-dimensional motion of the electrons in a beam under both magnetic and RF influences to be treated as a one-dimensional problem if radial motions are not allowed, i.e., if a strongly-confined electron beam is assumed.

During the bunching calculation, the phase of arrival at successive planes (usually 10) between each of the klystron buncher gaps of all the disks is computed from the integration of the equations of motion. The current modulation is derived from a Fourier analysis made of the phase positions at each step. Figure 3 includes a polar plot of the phases of 20 disks as the beam progresses from the inner circle corresponding to the midplane of the input-cavity interaction gap to the outer circle corresponding to the midplane of the output gap. Note that the phases of the 20 disks are uniformly distributed in the beginning, but as the bunching process proceeds all the disks tend to concentrate toward the lower left portion of the diagram. The diagram corresponds to the bunching computed for the 2000-MHz FM Klystron (Design No. 3B) to be discussed later. At a drive level of 0.2 watt at the input gap, the computed current modulation index at each of the successive gaps (2 through 6) was 0.0556, 0.1547, 0.6365, 1.1692, and 1.7324. The final current modulation index of 1.7324, approaching closely the theoretical limit of 2 for a perfectly bunched beam, has a phase angle of 69.9 degrees with respect to the RF voltage of the initial gap. This phase is computed from the Fourier analysis of the phases of the negative electron disks. The polar plot demonstrates that the electron disks are clustering about a phase diametrically opposite from the location of the positive current phase, as expected. The effect of space charge in altering the converging pattern of the disks is clearly seen in the curved paths shown on the polar plot.

Power extraction in the output gap and the accompanying internal conversion efficiency is computed by integrating the motion of all the disks through the radial and axial fields of the output interaction circuit. The

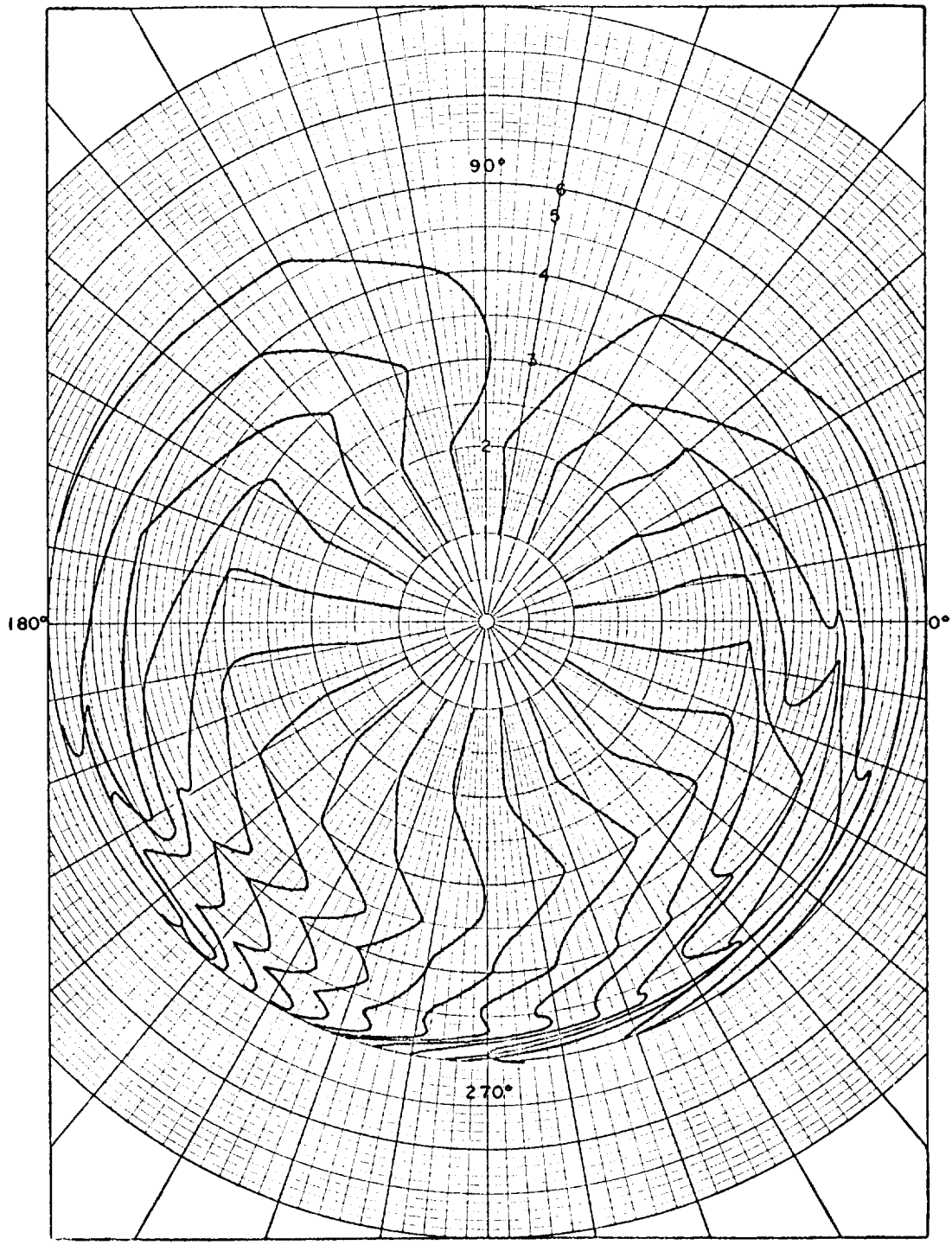

Figure 3 - Polar Phase Plot of 20 Electron Disks Advancing from the Input Cavity (Inner Ring) to the Output Cavity (Outer Ring)

instantaneously induced current in the output circuit is then calculated by Ramo's Theorem. Since the induced current, and hence the induced voltage, in the output circuit is not known in advance for a given circuit impedance, as determined by the R/Q and loaded Q of the output circuit, a series of 3 or 4 values of the output voltage modulation index and voltage phase are assumed, and the motion of all the disks in the corresponding circuit fields and the accompanying space-charge fields is computed. The ratio of the assumed voltage to the corresponding computed induced current gives a corresponding impedance amplitude, and the difference of their phases gives the corresponding impedance angle. From an interpolation of the plots of efficiencies versus impedance angle and magnitude, the computer program finds the efficiency corresponding to the known output circuit impedance.

The process by which the electron disks in the output gap give up their kinetic energy to generate output RF power can be seen graphically in Figures 4 and 5. Plotted in these figures are the normalized kinetic energies of each of the 20 disks as they traverse the interaction gap, or gaps, of the output interaction circuit. Figure 4 is a plot of the 2000-MHz FM Klystron (Design No. 3) with a conventional single interaction gap, in which the modulation index is 1.2. At a drive level of 0.2 watt, the current modulation index at the entrance to the output-gap field interaction region is 1.690 which, in the absence of output gap fields, would have developed to 1.733 at the midplane of the interaction gap. The computed internal conversion efficiency under these conditions was found to be 73.5 percent. Figure 5 is plotted for the same Klystron (Design No. 3), except that the single-gap output circuit has been replaced by a π-mode double-gap extended-interaction output circuit. Here the energy transfer takes place in two roughly equal cascades. The same total voltage modulation is applied, one half to each interaction gap. The resulting internal conversion efficiency is computed to be 70.7 percent.

Comparison of Computed and Measured Efficiency

The validity of the disk model of the klystron beam and the accuracy of the computer program has been established by correlation of computed and measured performance on several different klystron designs.

Three different categories of existing tubes have been investigated:

(1) Broadband klystrons, with 30 to 50 percent efficiency.

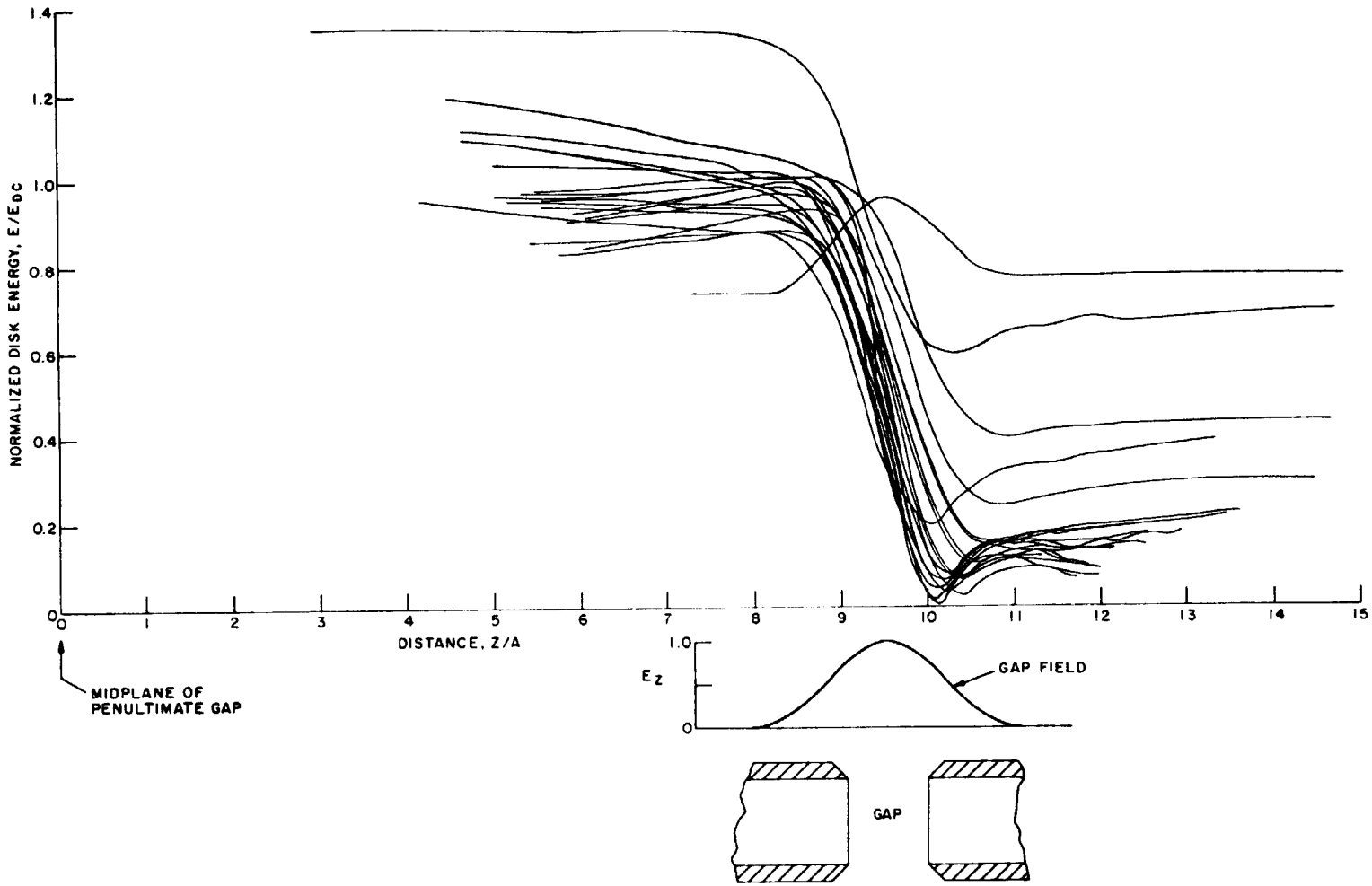

Figure 4 - "Waterfall Diagram" Showing Computed Decrease in Kinetic Energy of Bunched Electrons as they Traverse a Single Output Gap in a High-Efficiency Klystron

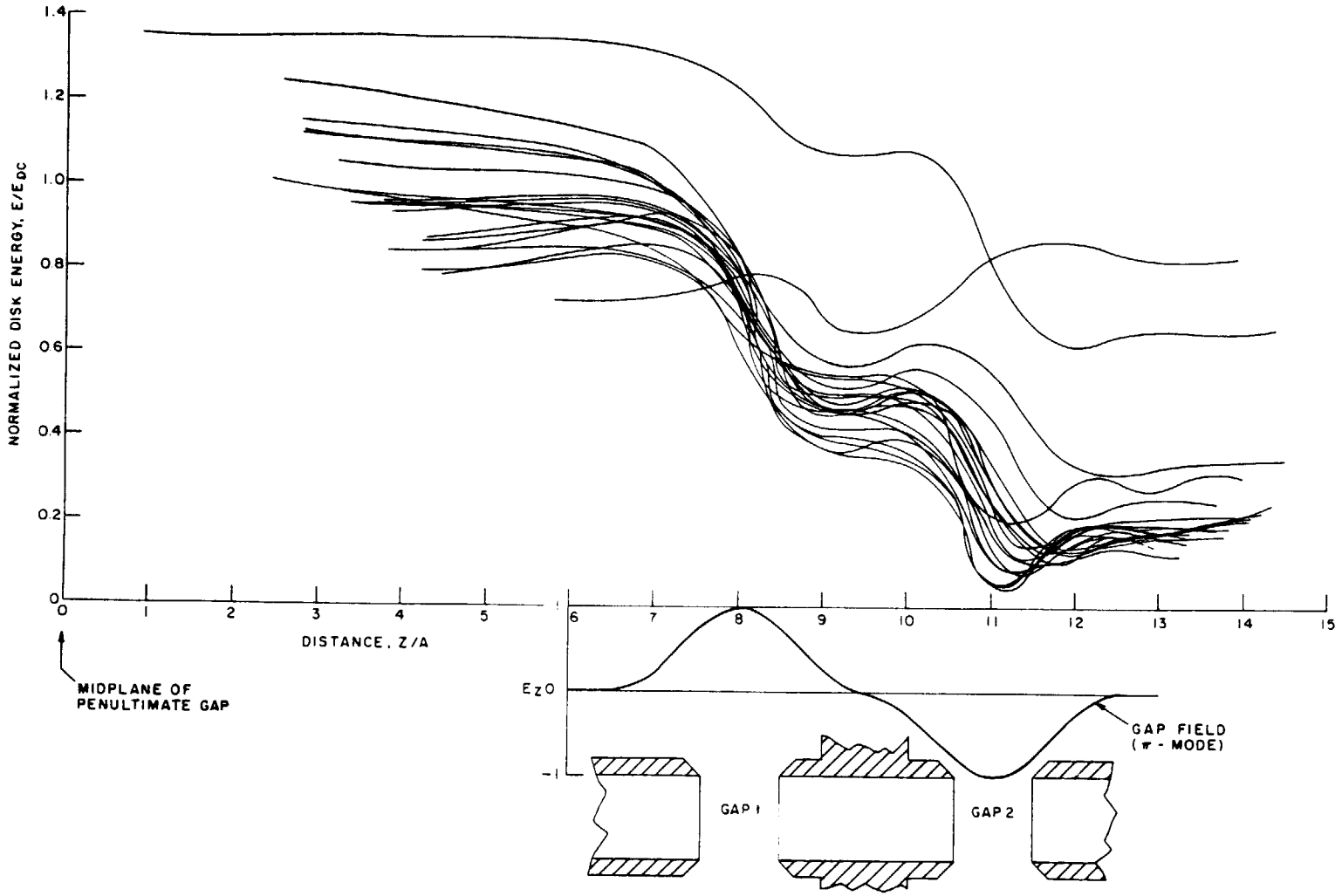

Figure 5 - "Waterfall Diagram" Showing Computed Cascaded Decrease in Kinetic Energy of Bunched Electrons as they Traverse the Two Interaction Gaps in a π -Mode Double-Gap Cavity in a High-Efficiency Klystron

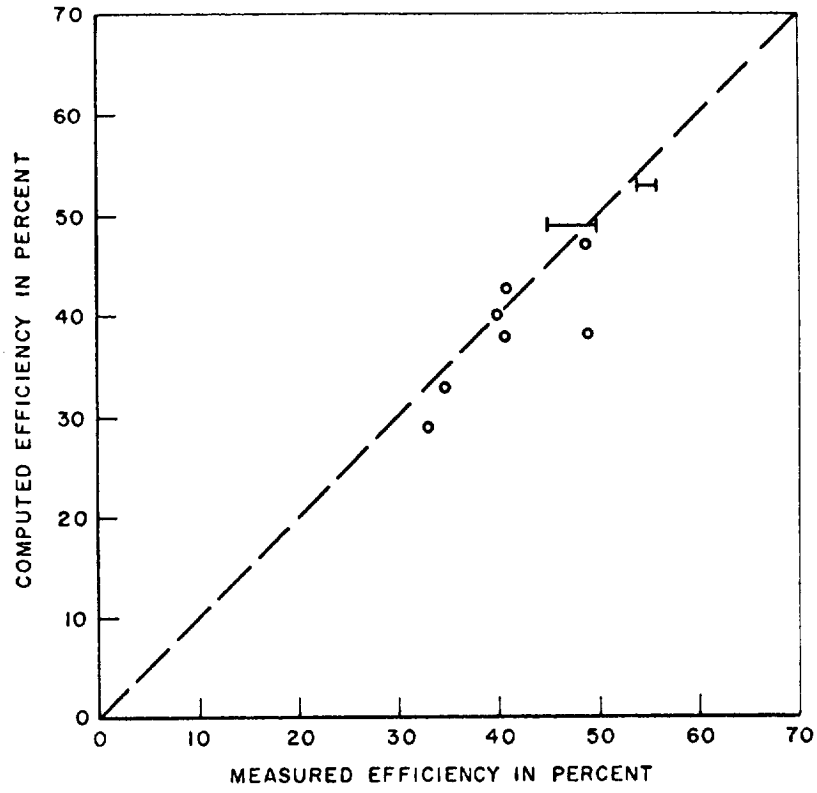

Figure 6 - Comparison of Computed and Measured Efficiency for a Variety of Klystrons Investigated

(2) Tunable klystrons, with 45 to 60 percent efficiency.

(3) Narrowband klystrons, with 40 to 60 percent efficiency.

The results of these comparisons are summarized in Figure 6. In this figure the computed efficiency for each of the tubes considered is plotted versus the corresponding measured efficiency. The points lie near the 45-degree line, indicating excellent correlation. The broadband tubes have the lowest efficiencies, in general, because of the compromises that must be made to obtain reasonable penultimate and output impedances across the band.

Since the digital computer program correctly computes the efficiency of existing klystrons and reveals in detail the effect of various parameter changes in a given design, it is considered to be reliable in determining the characteristics of new designs. Some of the new designs for fixed frequency klystrons analyzed with the computer simulation program in this study are computed to have efficiencies in excess of 70 percent.

OPTIMIZATION PROCEDURES

The large-signal digital computer program allows rapid, systematic optimization of a klystron design for a given application. However, so many parameters must be optimized in a typical multicavity klystron that a complete computer investigation of all combinations of parameters would be prohibitively costly and time-comsuming. To minimize duplication and to obtain results of the most generality, a series of prototype klystron designs have been established in previous independent research activities. This prototype series has been used to find optimum values for a number of design parameters such as (1) beam perveance, (2) cavity tuning, (3) output-gap transit angle, and (4) output-cavity impedance. Pertinent results of these investigations will now be summarized:

Effect of Beam Perveance on Efficiency

The prototype series assumes a circuit efficiency of 100 percent, as would be approximately true for tubes with a power output of the order of 10 kilowatts or more. For the lower power levels considered in the present study, circuit efficiency may be as low as 90 to 95 percent at the higher frequencies. However, optimization of the internal conversion efficiency as a function of perveance still should provide a satisfactory criterion for these designs.

Optimum internal power conversion efficiency for the prototype series is approximately 80 percent at a perveance of 0.5×10^{-6}. Prototype efficiency is found to drop 10 and 20 points from its optimum value of 80 percent for beams of perveance 1.0×10^{-6} and 2.0×10^{-6}, respectively. These losses of efficiency are greater than the increase in efficiency due to improved circuit efficiency at the higher perveances. On the other hand, a reduction of perveance below 0.5×10^{-6} is found to give no increase in internal power conversion efficiency but does lead to reduced circuit efficiency. This trade-off suggests 0.5×10^{-6} as the optimum beam perveance at all frequencies.

Effect of Cavity Tuning on Efficiency

It has long been known that detuning of the penultimate resonator in a klystron to produce an inductive reactance enhances the electron bunching and hence improves the efficiency by 10 to 20 percentage points. Computer simulation studies have shown a further enhancement of efficiency if the resonator next preceding the penultimate (pre-penultimate) also is tuned to an inductive phase. Another 10 percentage points in efficiency may thus be achieved.

The reduction in resonator impedance associated with detuning results in a gain trade-off (decrease) of approximately 15 dB, but this is easily recovered by the addition of one more resonator to the tube. Tuning of the other resonators is set by bandwidth considerations and has little effect on efficiency.

Effect of Output Cavity Parameters on Efficiency

An output impedance that is too low provides insufficient voltage swing for optimum efficiency, while an output impedance that is too high turns electrons around in the output gap, again reducing efficiency. Previous investigations have shown that for a 0.5-radian gap the optimum output impedance is close to 0.8 R_o, where R_o is DC beam resistance. If the gap is increased to 1.0 radian, the optimum value of Z/R_o is 1.0; however, 5.3 points of efficiency are lost at the longer transit angle. In this study, designs were originally carried out using $Z/R_o = 0.8$, but in the final designs this value was increased to 1.0 for one of two reasons. First, in the case of the AM tubes, an investigation of amplitude linearity showed that a value of Z/R_o equal to 1.0 is better than a value of 0.8. In the 8 and 11-GHz tubes, a 1-radian output gap was employed to offset the reduction in impedance caused by the relatively thick tunnel walls dictated by thermal design considerations.

KLYSTRON CAVITY STUDIES

Analytic Estimates of Doubly-Reentrant Ungridded Cavity R/Q and Q_u

Klystron design and the computation of gain and efficiency depend critically on the bandwidth-impedance parameter R/Q of the microwave cavities in the device. Because no systematic study of doubly-reentrant ungridded klystron cavities has been published, the early studies of Hansen[23] and Ginzton and Nalos,[24] on singly-reentrant gridded cavities were reexamined. The Hansen computations were based on two types of equivalent circuits, while the Ginzton and Nalos studies covered a net-point solution of field distributions, as well as confirming experimental measurements. The latter authors considered only "square" singly-reentrant gridded cavities, in which the internal height is equal to the difference of the cavity radius and the tunnel radius, as sketched in Figure 7.

The curves in Figure 8 show the product of gap shunt resistance and skin depth-to-wavelength ratio, δ/λ, as a function of gap length d, tunnel

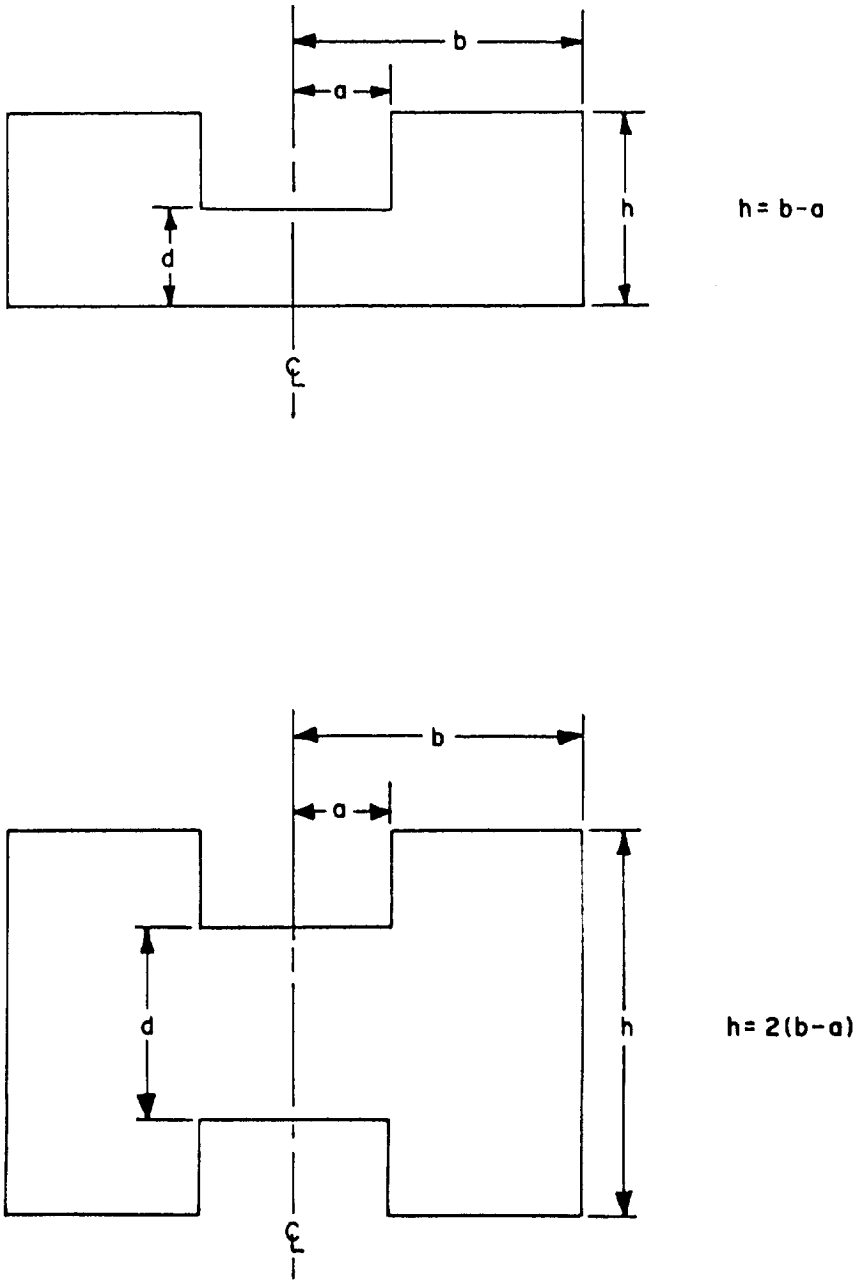

Figure 7 - Singly-Reentrant "Square" Klystron Cavity and Doubly-Reentrant "Double-Square" Klystron Cavity, with Tunnel Outer Radius, a, and Cavity Inner Radius, b ("Square" cavities have internal height equal to b-a. "Double-square" cavities have height, h, equal to 2 (b-a).)

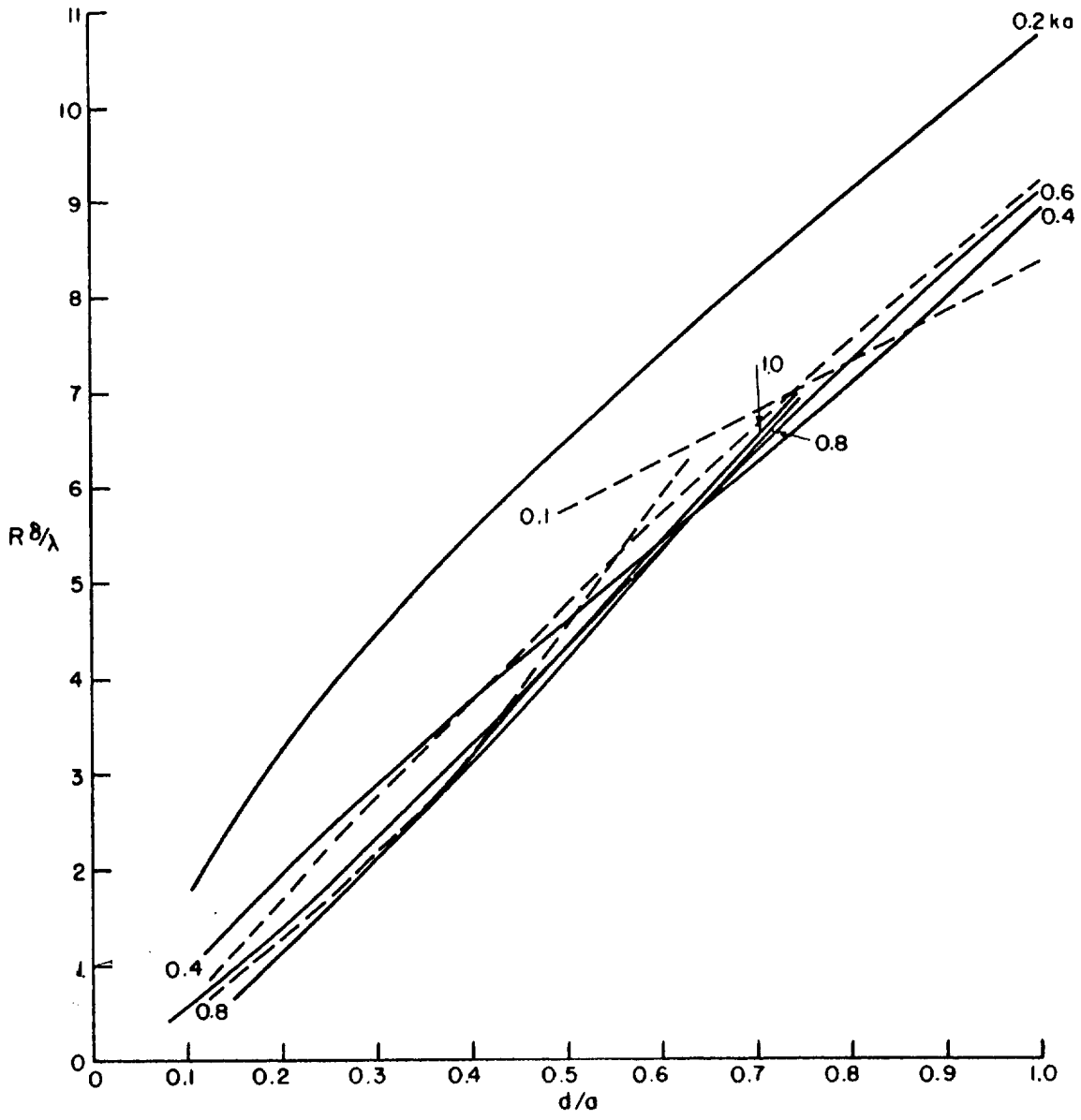

Figure 8 - Normalized Shunt Resistance of "Square" Singly-Reentrant Gridded Cavities versus Gap Aspect Ratio d/a

radius a, and frequency parameter k ($k = \omega/c$. Except for a discrepancy at $ka = 0.2$, all of the curves derived from either Hansen or Ginzton and Nalos fall near the line

$$R_{sh}\,\delta/\lambda = 9.0\,d/a \tag{12}$$

Since a doubly-reentrant cavity, as sketched in Figure 7, can be considered to be approximately equivalent to the juxtaposition of a singly-reentrant cavity, and its mirror image reflected in its flat face, with the intervening surface subsequently removed, the same formula for $R_{sh}\,\delta/\lambda$ should give a lower limit to the values expected for doubly-reentrant cavities, where d is again interpreted as the total gap length. This hypothetically constructed double cavity has the same field distribution, field amplitudes, and stored energy in each of its halves as the prototype singly-reentrant cavity, but its impedance and Q should be relatively higher because the power loss in the flat face is eliminated.

From the ratio δ/λ for copper[25]

$$\delta/\lambda = 2.20 \times 10^{-10}\sqrt{f} \tag{13}$$

one may deduce that the unloaded Q for doubly-reentrant cavities is given by:

$$Q_u = R_{sh}/(R/Q) = 4.09\,d/a \times 10^{10}/(\sqrt{f} \times R/Q) \tag{14}$$

Figure 9 illustrates the computed values of R/Q given by Ginzton and Nalos for singly-reentrant cavities. The curves in Figure 9 show the variation of a deduced analytic approximation to the Ginzton and Nalos values, the approximation being computed from:

$$R/Q = 120\,d/a\,(0.267/\sqrt{d/a} + 0.625\,ka - 0.2)/ka \tag{15}$$

The correlation between this analytic approximation and both the computed and the measured values of Ginzton and Nalos is shown in Figure 10, where the Ginzton and Nalos values of R/Q are plotted versus the corresponding value computed from the analytic approximation. Perfect correlation would be demonstrated in a plot in which all points lie on the 45-degree diagonal.

For doubly-reentrant gridded klystron cavities, Eq. (15) may be considered applicable if d/a is replaced by d/2a and if the right-hand side is

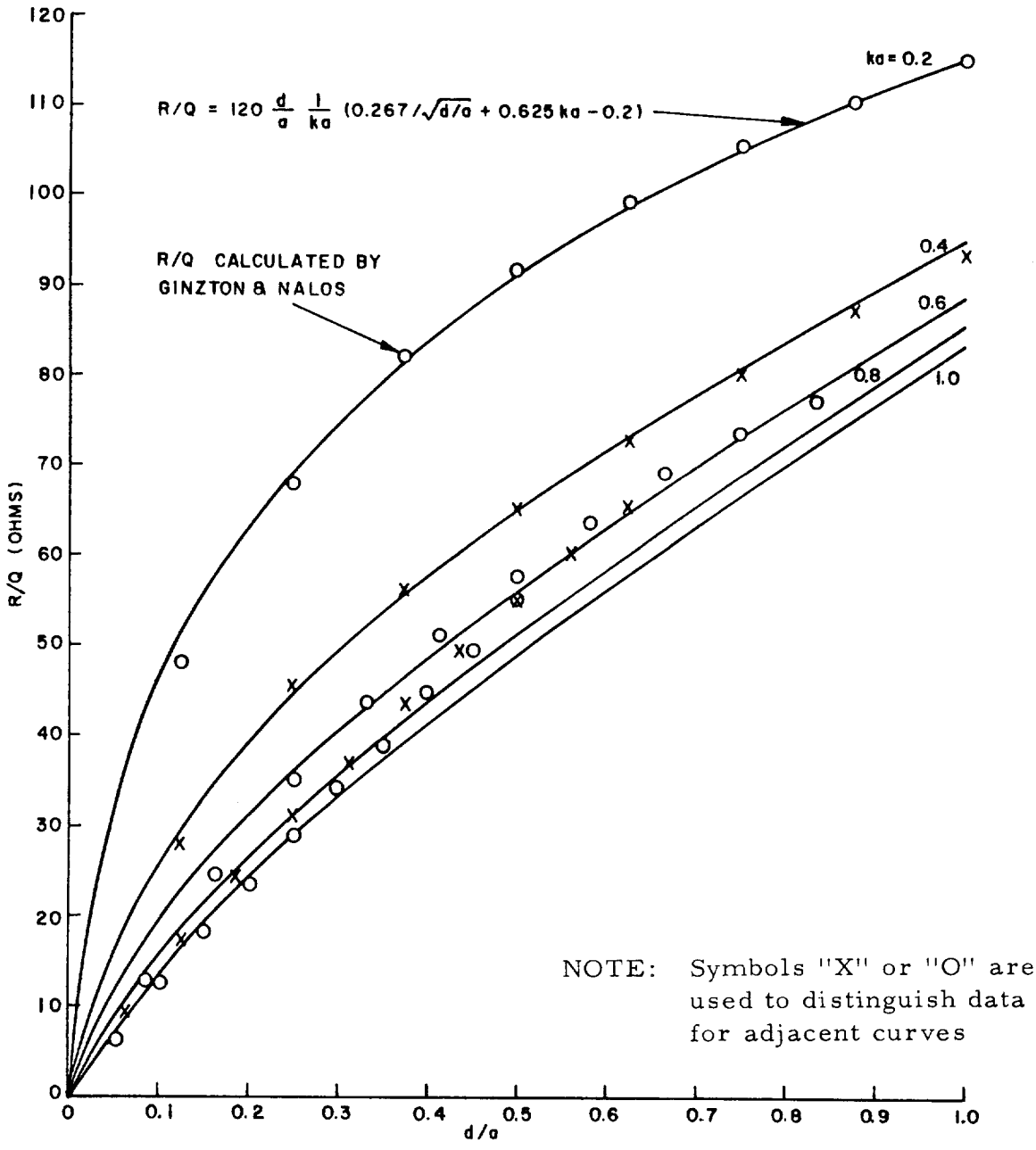

Figure 9 - Analytic Curve Approximation to "Square" Singly-Reentrant Cavity R/Q

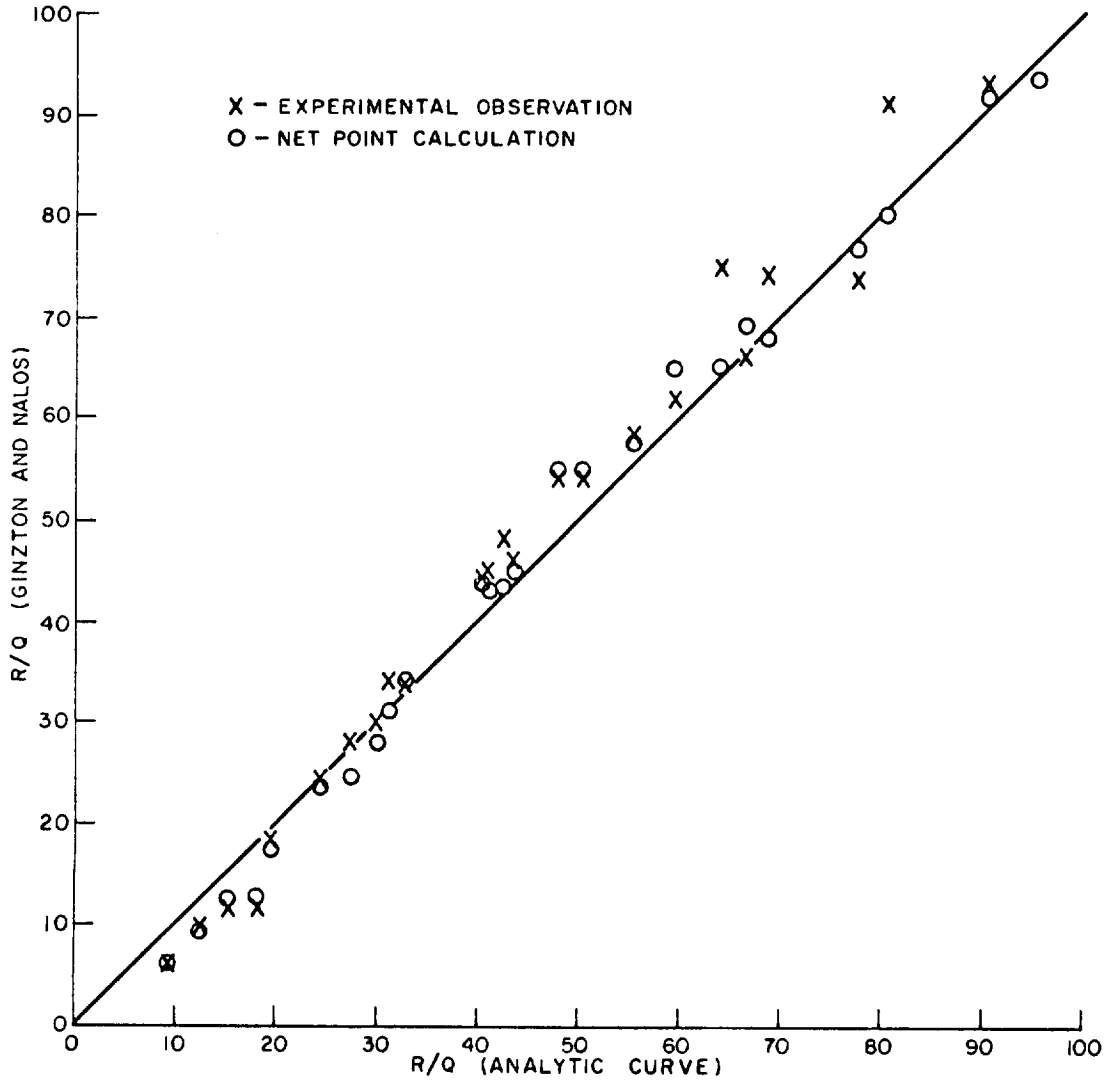

Figure 10 - Correlation Between Both Computed and Measured R/Q Values of Singly-Reentrant Cavities with Fitted Analytic Curve for R/Q

multiplied by a factor of 2, yielding the following equation for gridded doubly-reentrant cavities:

$$R/Q = 120\ d/a\ (0.378/\sqrt{d/a} + 0.625\ ka - 0.2)/ka \qquad (16)$$

In the case of gridless doubly-reentrant cavities, it may be expected that Eq. (16) might apply if an additional frequency-dependent factor were included to account for the variation of the fringing fields. From the comparison of Eq. (16) with the measured values of R/Q in a number of ungridded doubly-reentrant cavities (many of which were not "double-square" but were of relatively greater height and of smaller diameter), the following analytic approximation was derived for ungridded doubly-reentrant cavities:

$$R/Q = 120\ d/a\ (0.461/\sqrt{d/a} + 0.762\ ka - 0.244)(1 - 0.36\ ka)/ka \qquad (17)$$

The correlation between values computed from this formula and the measured values is shown in Figure 11. Included among the data are the measured points (A, B, and C) for three scaled-up versions of low-ka cavities of the type under consideration in the present klystron design study. The measured parameters for cavities A, B, and C are given in Table I.

- - - - - - -

Table I - Measurement of Cavity R/Q

Parameter		Cavity A	Cavity B	Cavity C
ka		0.197	0.160	0.206
Tunnel O.D., 2a	(in.)	1.530	1.530	1.530
Tunnel I.D.	(in.)	1.030	1.030	1.030
Cavity Height	(in.)	8.396	9.430	7.953
Cavity I.D., 2b	(in.)	7.000	7.000	4.750
b/a		4.58	4.58	3.10
Gap Length	(in.)	0.660	0.330	0.330
R/Q	(ohms)	193	177	143
Resonance Frequency	(MHz)	484	392	507

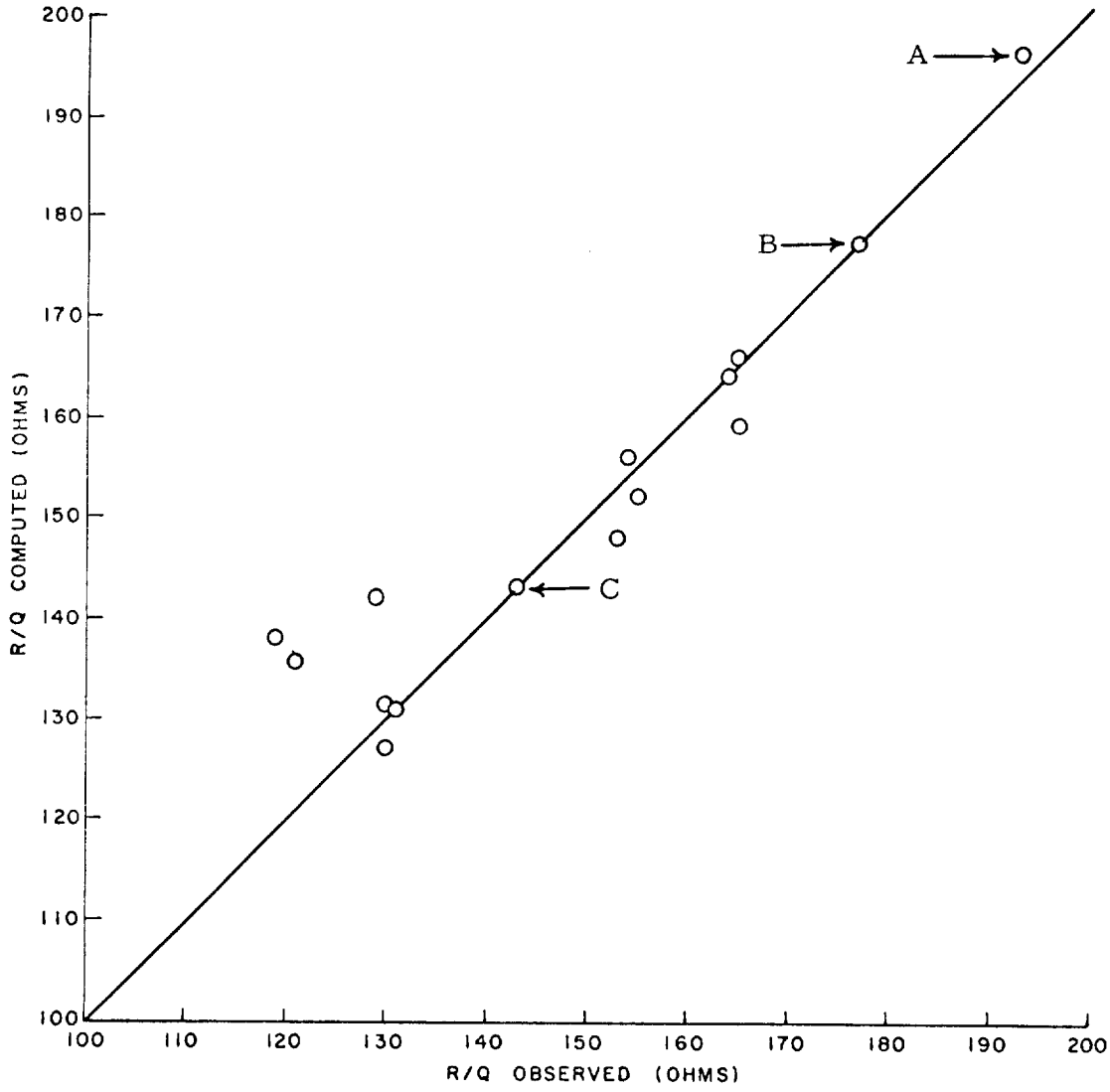

Figure 11 - Correlation Between Analytic Function for R/Q and Measured R/Q for Ungridded Doubly-Reentrant Cavities. A, B, and C are Data for Three Cavities Measured for this Klystron Study

Because of the good correlation between the computed curve and the measurements, (Eq. (17) is useful for predicting R/Q values of ungridded doubly-reentrant klystron cavities to an accuracy of about ± 5 percent, provided the shape of the cavity is reasonably good. Values of R/Q obtained from Eq. (17) may then be substituted in Eq. (14) to yield conservative values of Q_u expected for these cavities. During the development phase of an amplifier, models of the proposed resonators would be measured to correct the values used in the initial designs.

An examination of the Ginzton and Nalos data also shows that for singly-reentrant cavities the ratio of the internal cavity height, h, to the tunnel outer radius, a, is given to a good approximation by:

$$h/a = (\sqrt{2d/a} - 0.24\ d/a)/ka, \tag{18}$$

as shown in Figure 12.

Accordingly, for "double-square" doubly-reentrant cavities one may write:

$$h/a = (2\sqrt{d/a} - 0.24\ d/a)/ka \tag{19}$$

In terms of the height ratio, h/a, and the tunnel outer radius, a, the cavity inner radius, b, is given by:

$$b/a = (h/a)/2 - 1 \tag{20}$$

It will also prove useful to modify Eq. (15) for ungridded singly-reentrant cavities by introducing the ungridded factor from Eq. (17) as follows:

$$R/Q = 120\ d/a\ (0.326/\sqrt{d/a} + 0.762\ ka - 0.244)(1 - 0.36\ ka)/da \tag{21}$$

Optimum Design of RF Cavities Meeting Thermal Requirements

The analytic formulas for doubly-reentrant cavity R/Q and unloaded Q indicate that for a given tunnel I.D. the thinner the tunnel wall is, the higher the R/Q and the unloaded Q values become. However, as the wall thickness is reduced, a higher temperature drop will occur between the reentrant tunnel tip and the cavity end wall. The most severe heat load will occur in the output interaction circuit where from 1/2 to 2 percent of the beam power may be intercepted because of RF defocusing. An additional

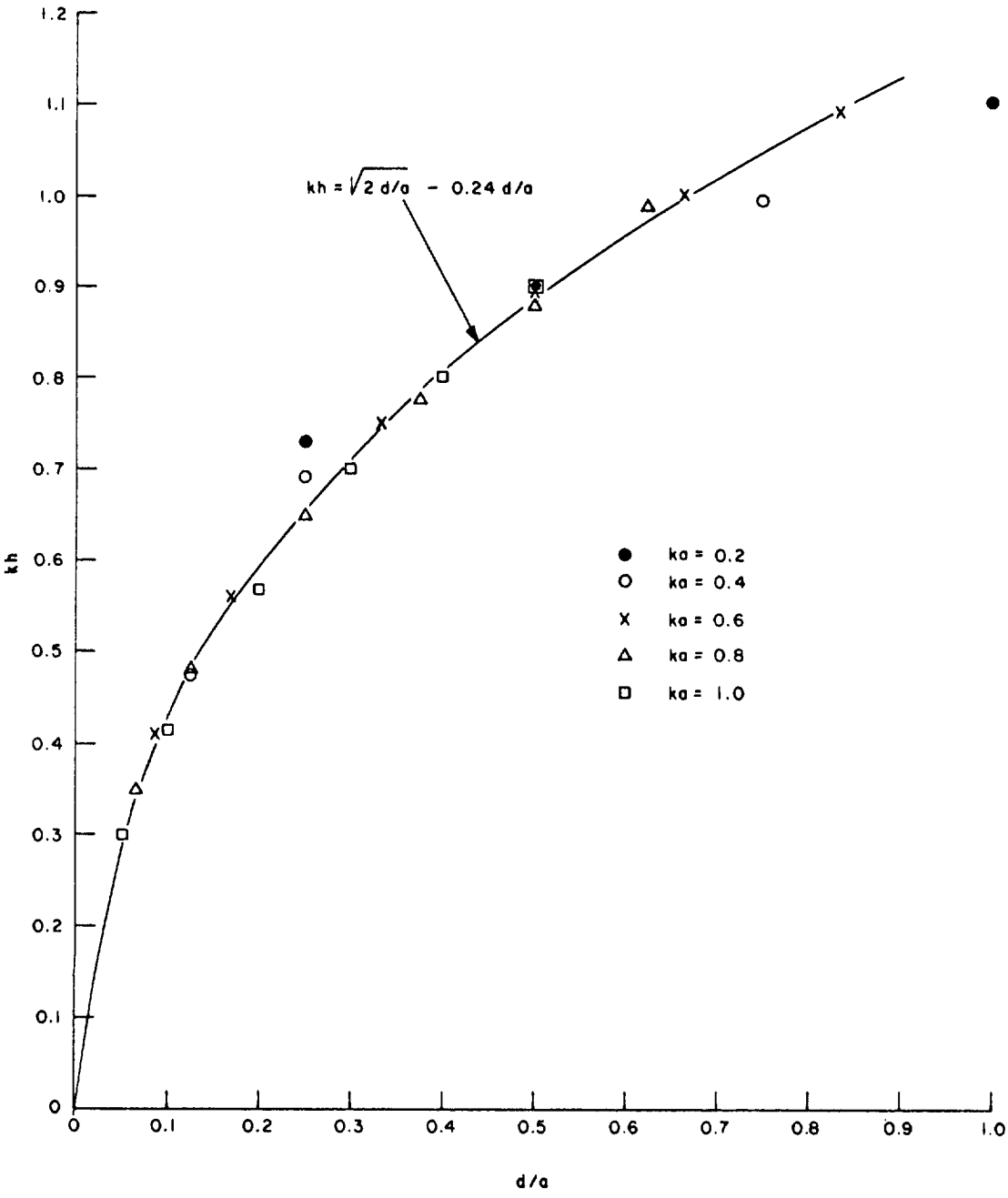

Figure 12 - Normalized Cavity Height kh versus Gap Aspect Ratio d/a for Several Values of ka in "Square" Singly-Reentrant Gridded Cavities, Where $k = 2\pi f/c$

source of heat in the cavity results from ohmic heating in the cavity walls by the RF cavity currents induced in the cavity. A sketch of a doubly-reentrant cavity with heat sources is given in Figure 13.

On the conservative assumption that a maximum of 1 percent of the beam power would be intercepted on the tip of the output-cavity tunnel in the 850-MHz and 2000-MHz klystrons, and 2 percent would be intercepted in the 8000-MHz and 11,000-MHz klystrons, and that one-third of the total internal RF heat in the output cavity is generated at one of the tunnel tips, a Time-Sharing Computer Basic Program was written for computing both the thermal and RF properties of cavities as a function of gap length, tunnel O.D. and tunnel I.D. A listing of the program is given in Appendix A.

Assuming that the cavity walls will be maintained at an operating temperature of 150°C by a water heat pipe cooling system, the maximum temperature rise in the tunnel that can be tolerated is 250°C if the tunnel tips are to be kept lower in temperature than 400°C, a safe level for long-term mechanical stability. From a sequence of computations made for a given gap length and tunnel I.D., as specified by the basic electrical design of the klystron, the minimum tunnel O.D. yielding the highest value of R/Q and the highest value of Q_u consistent with a maximum temperature drop of about 250°C was chosen. A sample plot of the computed characteristics for the 8000-MHz klystron is given in Figure 14.

ELECTRON BEAM OPTICS COMPUTATIONS

Analog Computer and Resistor Network Simulation Method

Initial design studies of the electron guns and the reflex depressed collector to be described below were carried out on electrical models set up on a precision resistor network integrated with a PACE 231R Analog Computer and an array of current sources for the simulation of space charge. A photograph of this facility is shown in Figure 15, while Figure 16 shows the resistor network and probe assembly. In operation, the metallic boundaries of a given electrode system are defined by interconnecting appropriate nodes of the network, and a 100-volt potential is applied between the cathode and anode. The four-point probe, which is servo-controlled by the computer, reads the potential and potential gradient at a given point in the region between electrodes, and the electron trajectories are computed and plotted on an X-Y recorder. A stepping voltage generated in the computation moves the probe assembly from one resistor cell to the next in the direction of the trajectory. After an initial run to

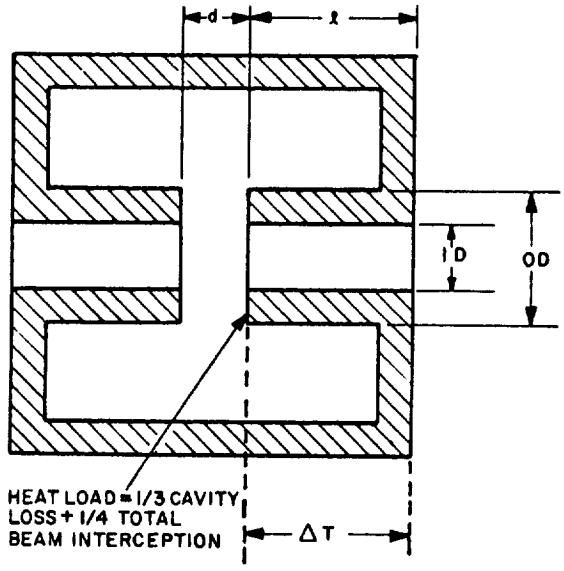

Figure 13 - Sketch of Heat Sources in an Idealized Doubly-Reentrant Klystron Cavity

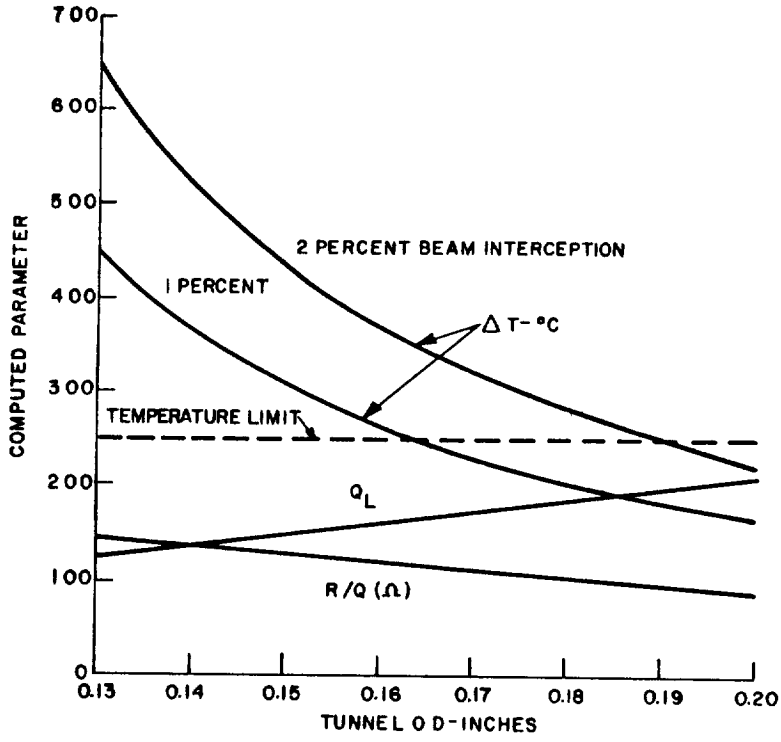

Figure 14 - Compute R/Q, $Q\ell$ and Tunnel Tip Temperature Drop for 8000-MHz Klystron Output Cavity with 1-Radian Interaction Gap

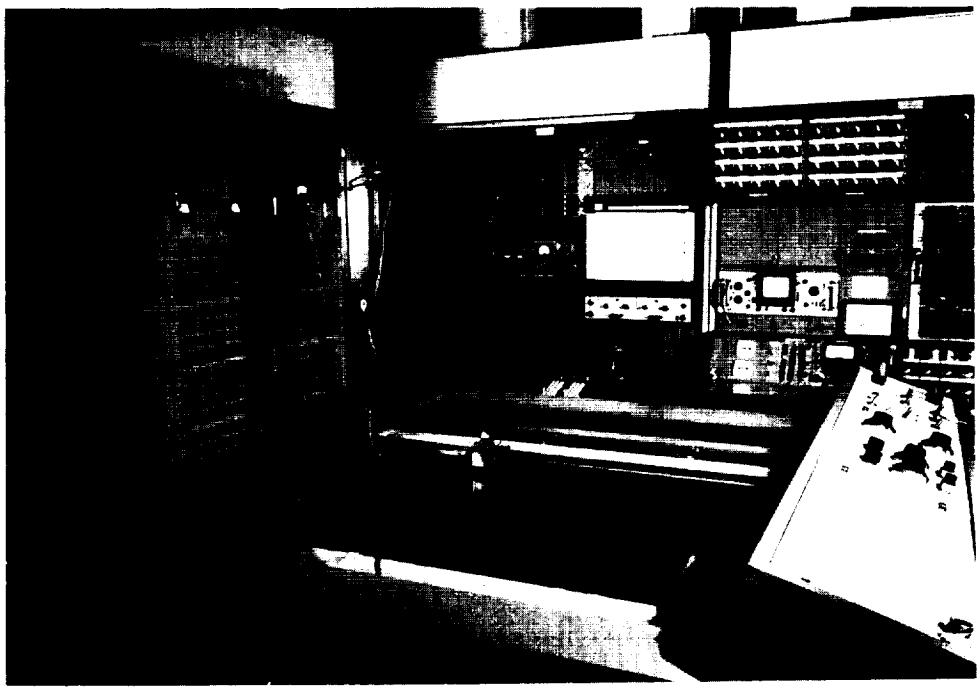

Figure 15 - General View of Analog Computer Beam Optics Facility

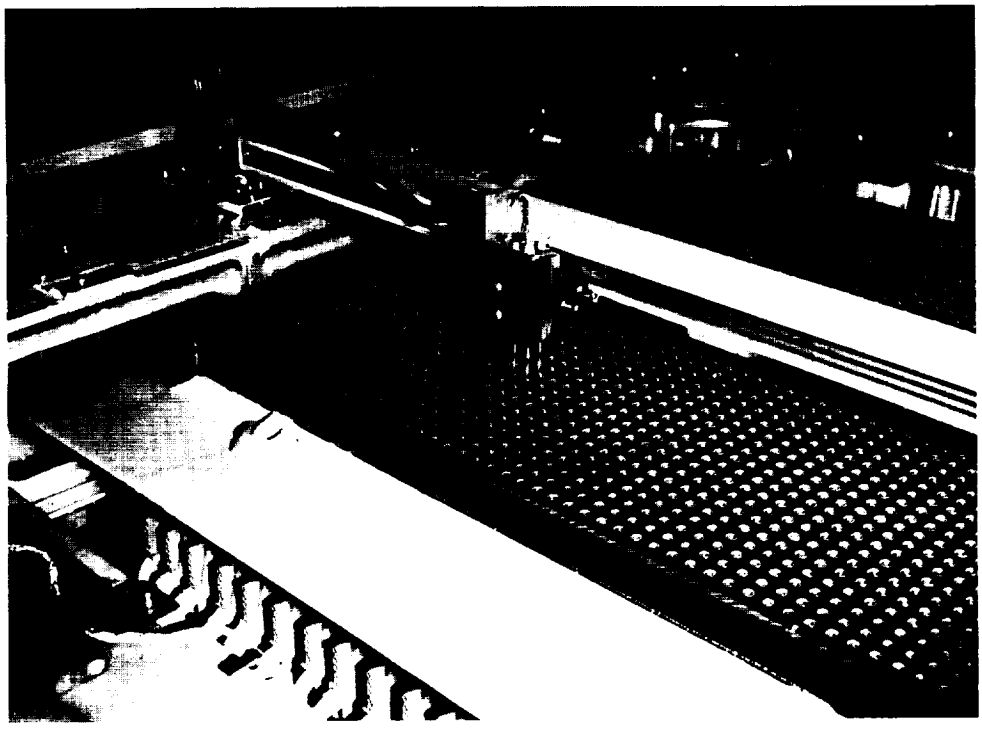

Figure 16 - Resistor Network and Potential Probes

solve the space-charge free problem, the current sources may be used to simulate space charge by injecting appropriate currents at the resistor nodes. For exploratory studies, it is usually sufficient to approximate the space charge rather crudely, and depend on later more-detailed computations made with the digital computer.

Digital Computer Program for Electron Gun Analysis

For the precise solution of Poisson's equation with complicated boundary conditions, including a thermionically emitting cathode surface, a digital computer program is used on a large-capacity GE-635 machine. This program, which was developed on an independent research effort, makes use of expandable arrays in solving field distributions by the relaxation method, with as many as 100,000 memory locations available if needed. It is an outgrowth of an earlier program which was developed under NASA sponsorship for the analysis of ion engines.[27,28,29] Correct conditions are ensured at cathode emitting surfaces by the use of analytic extensions based on the early work of Langmuir and Blodgett.[26]

A diagram of the loading map of the program for an available memory allocation of 32,000 words is shown in Figure 17. A vertical line drawn from the horizontal time axis at any time intersects the portions or links of the program that are loaded into the computer and available for use at that time. At later times, links to the right will overlay links to the left. The principal control program PRINCE determines whether secondary control shall be given to the branching sub-program BRANCH, which controls the sub-programs for carrying out the relaxation solution of Poisson's equation, or to the electron trajectory calculator program TRACK, or the space-charge distribution calculator RHOCAL. Relaxation solutions can be made over grids of up to 100 horizontal lines and up to 100 vertical lines. One of the features of the program is that the spacing between lines can be made variable so that close spacing can be used in critical areas and coarse spacing in other areas, thus yielding an accuracy about an order of magnitude higher in some cases than could be achieved with a uniformly spaced mesh with the same number of nodes.

Self-consistent solutions of the computed beam perveance, the electron trajectory pattern, and the resulting space-charge distribution are computed in a method employing successive iterations. Usually four to six cycles are sufficient to obtain convergence to a fixed solution. Figure 18 illustrates the convergence of the computed perveance of a planar diode to its known theoretical perveance. Faster convergence can be achieved by using space-charge averaging between iterations.

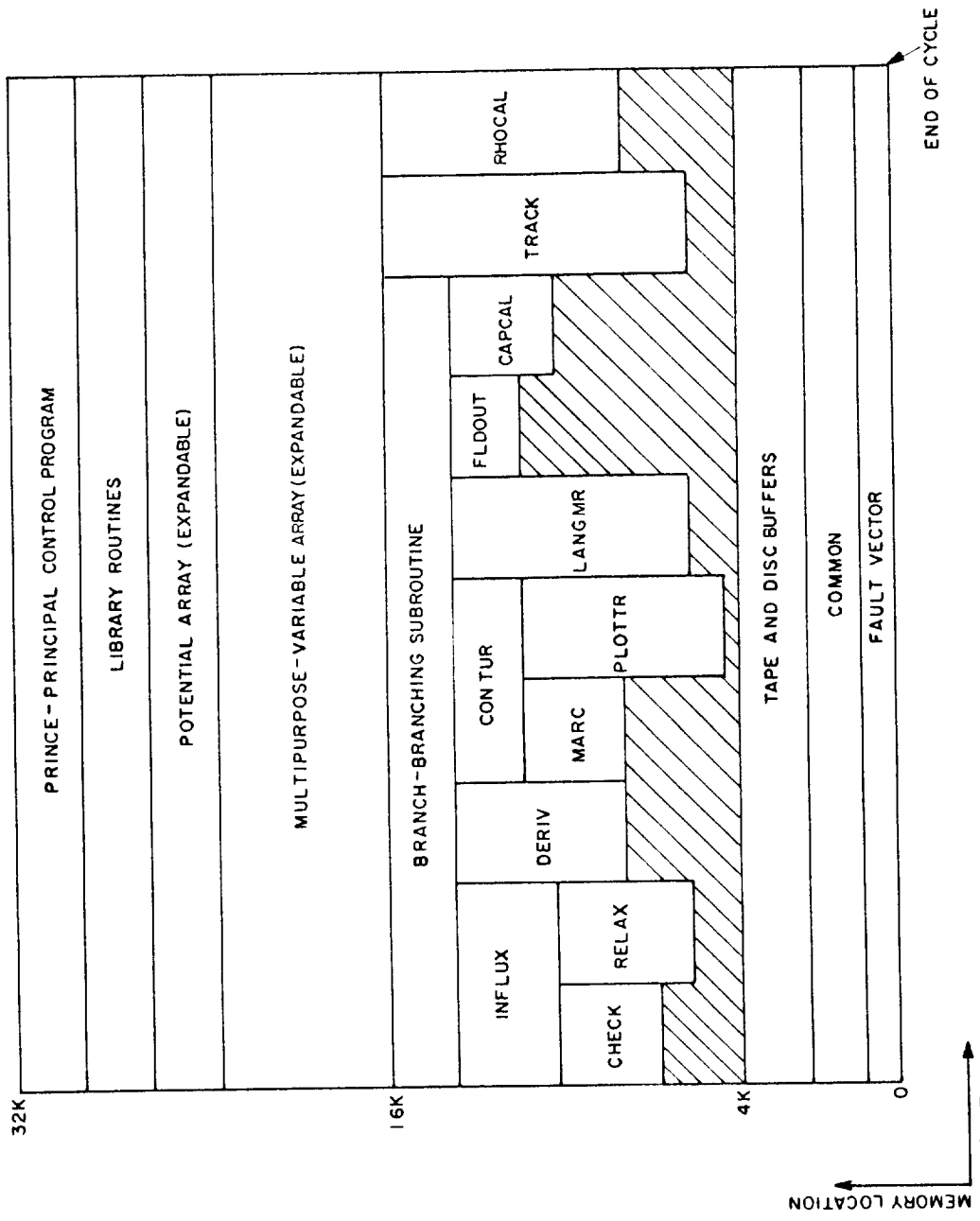

Figure 17 - Loading Map for GE Electron Gun Analysis Program

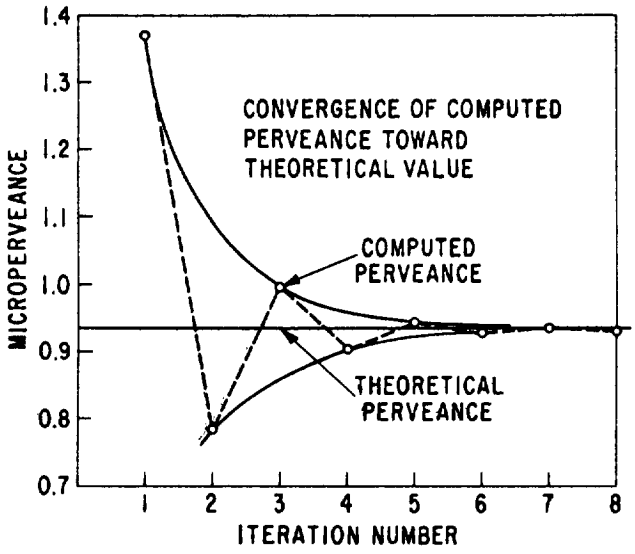

Figure 18 - Computed Perveance of a Planar Diode Converging to the Known Theoretical Value During Successive Iterations

Collimating Magnetic Field Computations

Standard handbook design methods are employed in the design of both the solenoidal electromagnets and the permanent magnets considered in this study.[30, 31] The following basic equations apply in the case of solenoids wound with foil of thickness h and lateral width d_1, to provide a magnetic field of B teslas over a length ℓ_1 when carrying a current of I amperes:

$$\ell_2 = (4.10 \times 10^{-8})(B/I)\ell_1 d_o + (8.26 \times 10^{-12})(B/I)^2 h d_1/k \quad (22)$$

$$W_1 = h d_1 \ell_2 \delta \quad (23)$$

$$R = \rho \ell_2/(h d_1) \quad (24)$$

$$d_2 = d_o + (2.61 \times 10^{-8})(B/I) h d_1/k \quad (25)$$

$$P = I^2 R/1000 \quad (26)$$

$$W_2 = 45.4 \quad (27)$$

$$W_3 = W_1 + W_2 \quad (28)$$

where

ℓ_2 = length of foil conductor (m)

d_o = inner diameter of solenoid (m)

d_2 = outer diameter of solenoid (m)

δ = density of conductor (kg/m^3)

k = conductor filling factor (usually 0.7 to 0.9)

ρ = volume resistivity of foil (ohm-meters)

W_1 = solenoid weight (kg)

W_2 = weight of solenoid power supply computed at 45.4 kg/kW

W_3 = combined weight of solenoid and its power supply (kg)

R = solenoid resistance (ohms)

P = ohmic heating of coil (kW)

Equations (22) through (28) were programmed in English units in BASIC for computation on the GE-235 digital time-sharing computer. The program is listed in Appendix B.

The design of permanent magnet field structures for klystrons is based on the relationship of the coercive force, H_r, and retentivity, B_r, of the magnet material as published.[31] While the design principles are straightforward, it is difficult to compute the total magnetic field furnished by the magnet because of the generally complex pattern of the leakage field. In the designs which are presented, those for the 850- and 2000-MHz klystrons employ ellipsoidal magnets which have a relatively well defined field pattern. In the design of the horn magnet systems for the 8000- and 11,000-MHz tubes, leakage field factors derived from experience with magnetron magnets were employed. The designs were therefore based on a total leakage flux 5 to 10 times that in the RF interaction region of the device.

Section IV
DEVELOPMENT AND EVALUATION OF KLYSTRON DESIGNS

In the initial stages of the project, a set of R/Q and unloaded Q_u values were assumed in order to establish preliminary designs of tubes for all frequencies. These designs were based on the narrowband prototype designs discussed previously in Section III under "Optimization Procedures". These designs were modified by stagger-tuning the resonant frequencies and adjusting the Q's of the first two cavities to give good current bunching and relatively flat small-signal gain over the desired bandwidth. The total number of cavities for each tube was chosen to meet the 40-dB gain specification. This trade-off resulted in the choice of a six-cavity tube for 2000-MHz FM service and five-cavity tubes for all other bands and services. These numbers of cavities remained unchanged as the designs developed through their interim and final stages.

When a more rigorous theoretical basis for R/Q and Q_u was established, as outlined earlier in Section III under "Klystron Cavity Studies", the preliminary designs were replaced by a set of interim designs in which thermal limitations on tunnel wall thicknesses were used to establish optimum cavity designs. A trade-off of thermal considerations with efficiency led to the choice of 1-radian output gaps in the 8000- and 11,000-MHz tubes, rather than the 0.5 radian used at 850-MHz and the 0.5 or 0.7 radian used at 2000 MHz. The interim designs met all specifications except phase deviation.

In order to meet the phase deviation specification, a third and final set of designs was developed. In general, the first two cavities had to be loaded more heavily and separated further in frequency in order to meet the phase specification. This reduced the saturation gain below its specification value, but in most cases the gain could be increased to above 40 dB again by decreasing the tunnel wall thickness of the buncher gaps, thus raising their R/Q. This could be done because the thermal loading of the buncher gaps is much lower than that of the output gap.

PRELIMINARY DESIGN CONSIDERATIONS AND EXPLORATORY CALCULATIONS

The initial development of designs for the various bands and types of service proceeded as follows:

On the basis of previous computations, the internal conversion efficiency of the NASA klystrons was anticipated to range from 70 to 80 percent, depending upon the choice of output transit angle. However, it was known that a number of factors such as circuit efficiency and linearity considerations would reduce efficiency to the 60 to 70 percent range before collector depression. Assuming an efficiency of 65 percent, tentative DC beam power requirements were established. The perveance was chosen to be 0.5×10^{-6} a/$V^{3/2}$ for all designs on the basis of previous investigations. The knowledge of the DC power input and this choice of perveance determined DC beam voltage and DC beam current. The next step was the choice of a normalized tunnel radius γa of approximately 0.75 radian and a beam filling factor b/a of 0.6, giving the normalized beam radius γb as approximately 0.45 radian. The choice of this value of γb represents a trade-off between loss of efficiency at small γb due to non-uniform reduction in plasma frequency on the one hand, and electron beam circuit decoupling at large γb on the other hand.

The procedure given above established the inner diameter of the drift tube. The gap spacing was chosen to be 1.0 radian in all gaps except the output gap. In the output cavity the gap spacing was reduced to 0.5 radian for the two AM designs. In the three FM designs at 2000, 8000, and 11,000 MHz, the output gap was increased to 0.7, 1.0, and 1.0 radian, respectively, in order to increase R/Q and to prevent the necessity of adding another bunching cavity. Thermal problems were also relieved by increasing the output gap length in the FM tubes.

Drift lengths in terms of the developed effective plasma angle $\beta_q \ell$ were chosen as follows:

(1) Final drift: $\beta_q \ell = \pi/6$ radians

(2) Penultimate drift: $\beta_q \ell = \pi/3$ radians

(3) All other drifts: $\beta_q \ell = \pi/2$ radians

Previous computations and experimental observations have demonstrated that these numbers are near optimum.

In the initial designs of this study, R/Q and unloaded Q_u values were assumed for buncher and output cavities on the basis of measured values for existing klystrons. The cavity resonant frequency placement was as follows:

(1) Input cavity:	slightly below upper band edge
(2) Second cavity:	slightly above lower band edge
(3) Third and fourth cavities:	detuned to high side
(4) Output cavity:	tuned slightly above band center

On the 2000-MHz FM tube, the additional cavity was placed slightly below band center. The design optimization consisted, in part, of varying the tuning pattern and observing the effect on amplifier characteristics.

The loaded Q of the input cavity was chosen to be approximately one-half the beam-loaded Q. For the output cavity the loaded Q was chosen such that the normalized output impedance, Z/R_Q, at band center was unity in all cases. In the case of the AM tubes, this represented a trade-off to achieve linearity at a higher power level than is achieved when $Z/R_Q = 0.8$, the condition for optimum saturated power output. This trade-off is illustrated in Figure 19 which shows power output as a function of power input for a variety of normalized output impedances. The dashed line is the locus of points where the gain falls one-half dB below the small-signal gain. Note that the locus attains its maximum value near $Z/R_Q = 1$. In the 8000- and 11,000-MHz FM tubes, this output impedance could be achieved at band center in a single-tuned circuit whose 70-percent points were outside the band edges. In the 2000-MHz FM tube, it was necessary to use a double-tuned output circuit, as discussed below.

The performance of the initial designs was satisfactory from the point of view of gain and efficiency. In the meantime, however, the cavity analysis presented in Section III under "Optimization Procedures" was completed, showing that the assumed initial R/Q values were pessimistic. On the basis of the new values of R/Q, all tubes were redesigned. The interim redesigns had more gain as a result of the higher R/Q values, which turned out to be fortunate because in the final set of designs, gain had to be traded-off to achieve the desired phase characteristics.

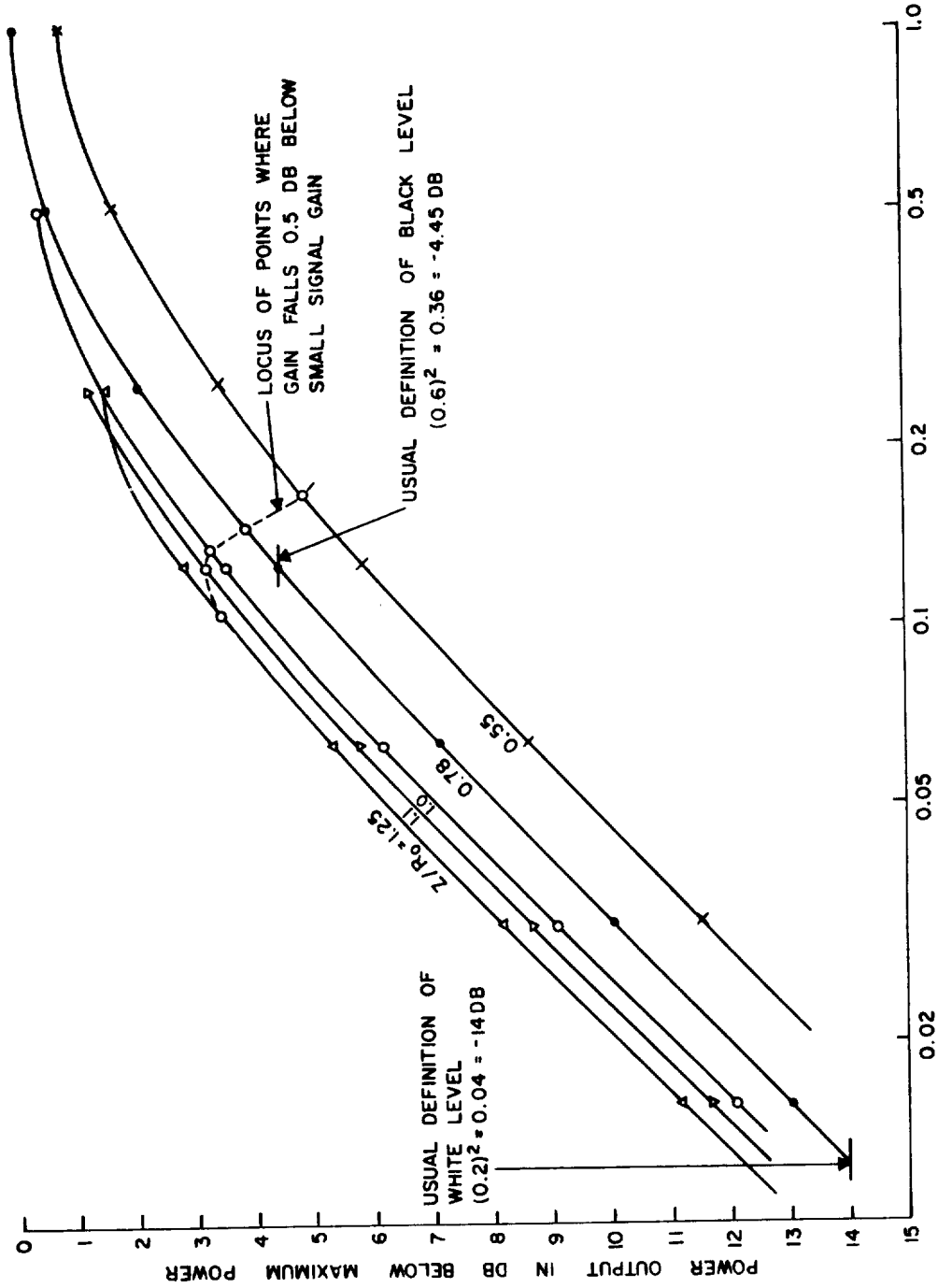

Figure 19 - Computed Power Output versus Power Input as a Function of the Output Gap Normalized Impedance

DEVELOPMENT OF INTERIM DESIGNS

In this section, the various trade-offs that led to the interim cavity designs are discussed, along with the establishment and evaluation of the resulting interim klystron designs, which met essentially all of the specifications.

Optimum Design of Cavities

Final optimum cavity parameters were computed following the completion of the analytic methods of computing the cavity dimensions and temperature drops described previously in Section III under "Klystron Cavity Studies". From the desired values of tunnel diameter and gap transit angles for both buncher and output cavities, the dimensions and values of R/Q and Q_u were computed and the results tabulated in Table II. For each of the output gaps, the temperature rise computed for one of the output cavity tunnel tips is also given for both an assumed 1-percent and an assumed 2-percent beam interception in the output cavity. It is expected that the total beam interception in the output cavity of the 850-MHz and 2000-MHz klystrons will be less than 1 percent, and that the interception in the 8000-MHz and 11,000-MHz klystrons will be less than 2 percent, so that in all cases the maximum temperature rise will be less than 250°C.

Interim Design of Klystrons

The amplitude and phase characteristics of the 850-MHz, 2000-MHz (AM), and 8000-MHz designs are shown in Figure 20. These interim designs were established with the small-signal program. In all cases, the gain specification is easily met but the phase linearity and the second derivative of the phase characteristic exceed the desired limits. This is indicated by the shaded areas in the figure.

To bring the phase response within the specification, the Q values of the first two resonators were reduced and their resonant frequencies were separated to provide the greater linearity. The final designs thus established are discussed later in this section under "Development and Performance of Final Designs".

Table II - Basic Cavity Parameters for Final Designs

Service	Type	Cavity I. D. (Inches)	Cavity Length (Inches)	Tunnel I. D. (Inches)	Tunnel O. D. (Inches)	Gap Length (Inches)	R/Q (Ohms)	Q_u	ΔT (°C) Interception (1%)	ΔT (°C) Interception (2%)
850-MHz AM	Buncher	4.96	3.92	0.815	1.040	0.530	186	7670	~0	~0
850-MHz AM	Output	3.92	2.88	0.815	1.040	0.265	138	5170	99	166
2000-MHz AM, FM	Buncher	2.06	1.67	0.300	0.420	0.200	203	4630	~0	~0
2000-MHz AM	Output	1.62	1.23	0.300	0.390	0.100	153	3065	203	316
2000-MHz FM	Output	1.82	1.43	0.300	0.390	0.140	176	3730	207	334
8000-MHz FM	Buncher	0.496	0.346	0.075	0.150	0.050	125	2440	~0	~0
8000-MHz FM	Output	0.501	0.311	0.076	0.190	0.050	93	2580	181	246
11000-MHz FM	Buncher	0.360	0.240	0.055	0.120	0.036	111	2110	~0	~0
11000-MHz FM	Output	0.377	0.202	0.055	0.175	0.036	68	2360	202	256

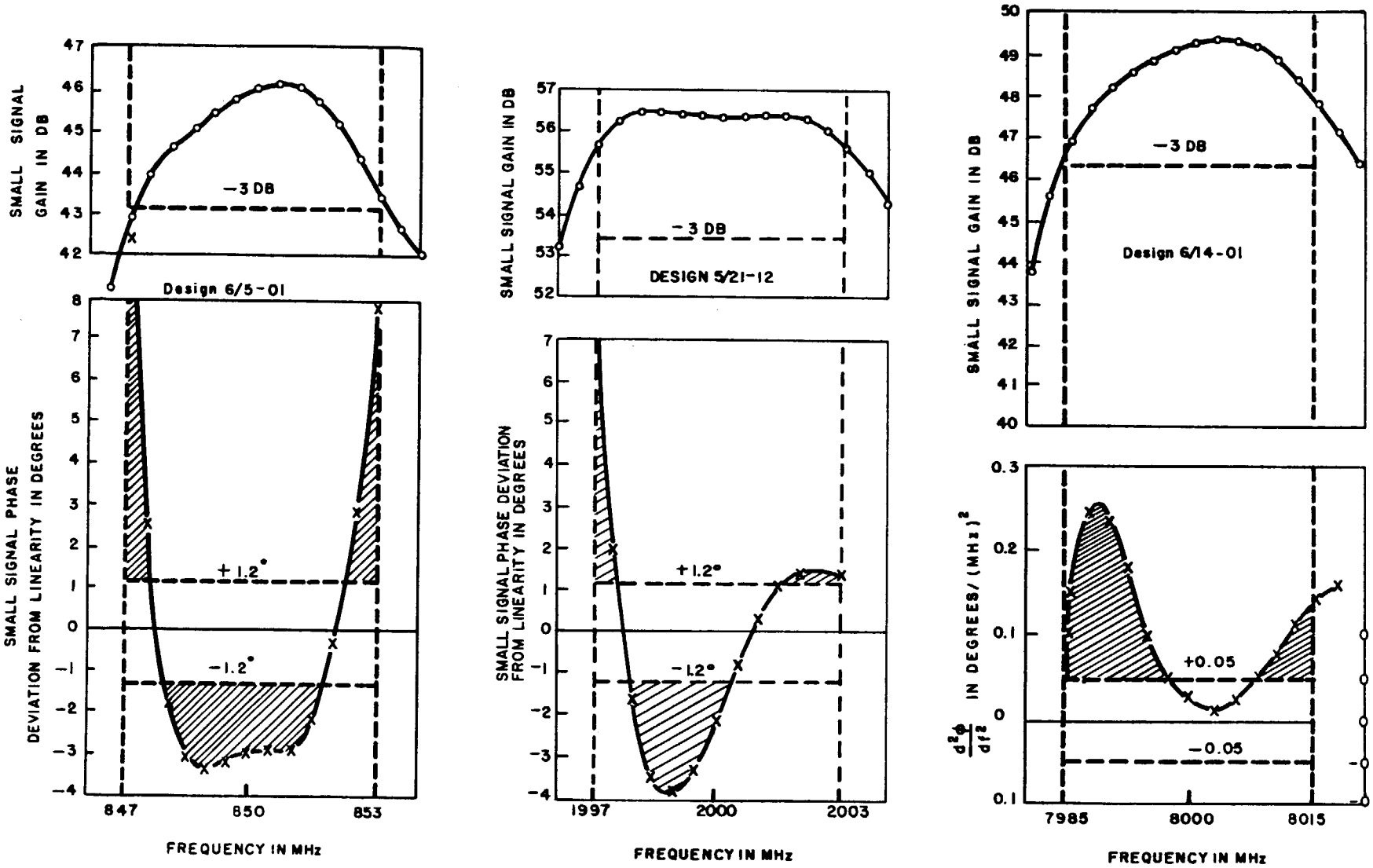

Figure 20 - Small-Signal Amplitude and Phase Characteristics of the Interim Designs of Three Klystrons

BROADBANDING STUDIES AT 2000 MHz

Of the five klystrons considered for AM or FM service in the range of frequencies from 850 MHz to 11,000 MHz, the 2000-MHz FM tube requires the largest percentage bandwidth. In klystron design the principal limitation to bandwidth is not in the bunching portion of the klystron but in the output power extraction circuit. Design studies were thus made to obtain high interaction efficiency with broadband output circuits.

One method of broadbanding a conventional single-gap doubly-reentrant output cavity is to establish a multiply-tuned response with additional tuned circuits in the output waveguide adjacent to the output cavity. Multiple tuning, in effect, removes impedance from the skirts of the cavity response curve and places it within a given band to increase the impedance within the desired band. Offsetting disadvantages of multiple tuning are the increased construction complexity and the increase of circuit losses due to the energy stored in the additional resonators. For example, the losses in a double-tuned circuit are approximately 50 percent greater than those in a single resonator of equal center band impedance.

The computed value of R/Q for a thermally feasible output cavity with a gap transit angle of 0.7 radian is 176 ohms. For the desired 30-MHz bandwidth at a center frequency of 2000 MHz, an output-circuit loaded Q of about 67 is indicated. The resulting cavity impedance at this value of Q is only 12,800 ohms, meaning $Z/R_o = 0.7$ for $R_o = 18,250$ ohms. Consequently, the interaction efficiency and linearity would be degraded (see Figure 19). As shown in Figure 21, double-tuning the cavity can bring the impedance close to, but somewhat short of, the beam impedance at which good efficiency is expected. Two double-tuned curves are shown: one is for a 0.7-radian gap with an R/Q of 176, a primary Q of 94, and a secondary Q of 47; the other is for a 1-radian gap with an R/Q of 203, a primary Q of 88, and a secondary Q of 44. Even though the longer gap has a higher R/Q than the shorter one, the large-signal interaction in the long gap proved to be not as efficient; further, greater overall efficiency is achieved with the shorter gap.

An alternate approach to high impedance and broad bandwidth in the output region is the multiple-gap (extended-interaction) output circuit. These circuits have the advantage of high impedance - bandwidth products but do involve increased size and construction complexity. Also, the

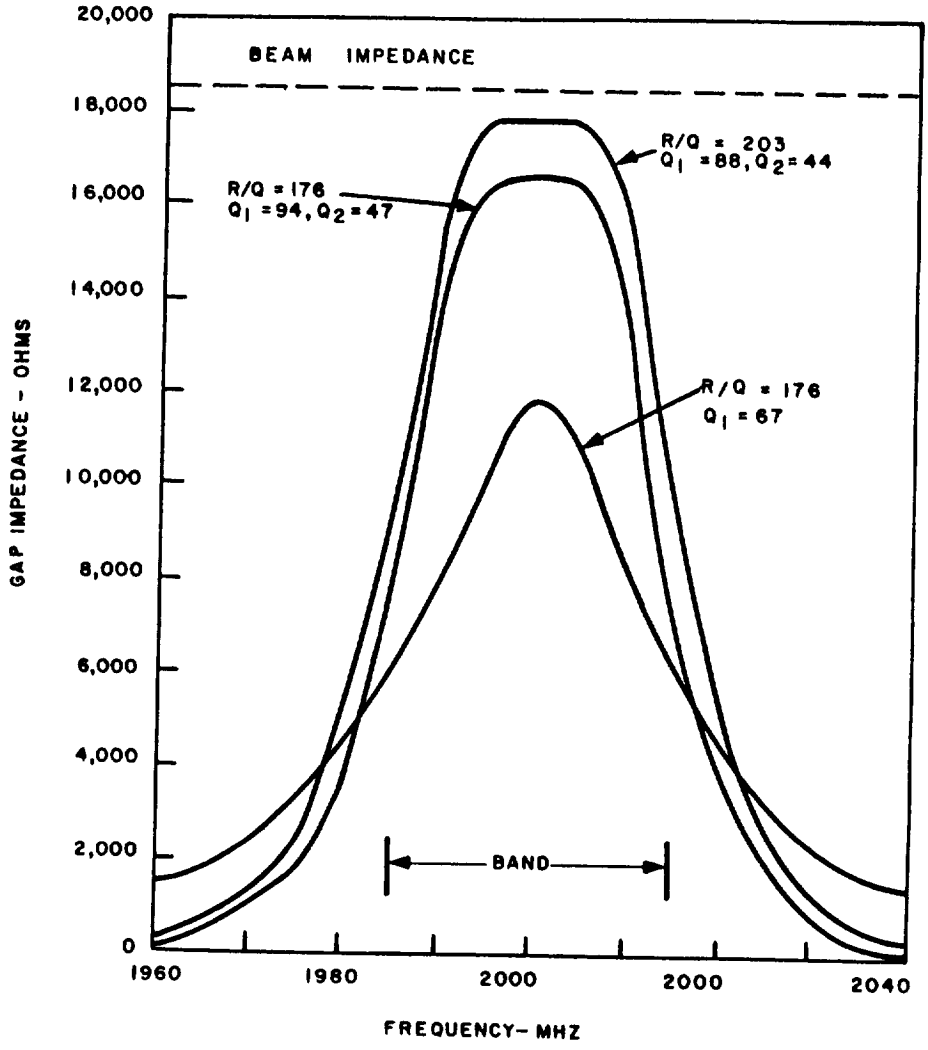

Figure 21 - Impedance of Singly-Tuned and Doubly-Tuned Output Cavities for 2000-MHz FM Klystrons

practical realization of multiple-gap resonators involves consideration of complex coupling to the external load and avoidance of higher-order-mode oscillations.

The 2000-MHz FM klystron was analyzed with a two-gap extended-interaction output circuit as shown in Figure 22. The two gaps each have a 0.7-radian transit angle, and the π-mode of resonance is employed. The spacing between the gaps was optimized by a series of computations of the effective impedance parameter $\mu^2 R/Q$. Parameters which were varied were the ratio d/a (ratio of gap length to drift tube radius) and the ratio w/a (where w is the total interaction distance from the first edge of the first gap to the second edge of the second gap).

For the range of cavity dimensions considered, the R/Q of the double-gap cavity in π-mode was taken as the value computed by Eq. (21). The beam coupling coefficient was obtained by the published expression for the appropriate field distribution.[21] The series of impedance curves shown in Figure 23 were computed on the time-sharing digital computer. From the

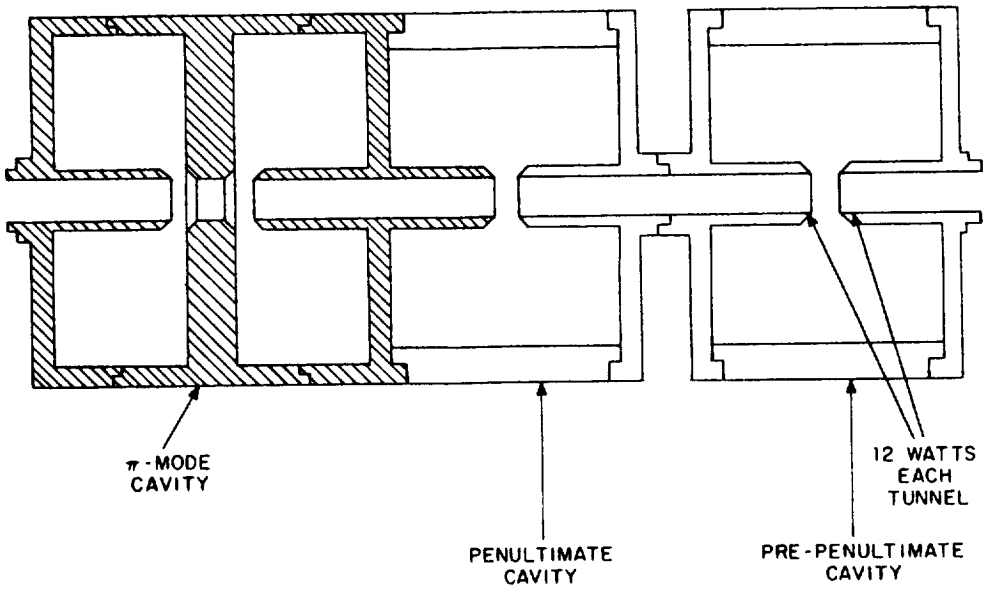

Figure 22 - Sketch of Output Portion of 2000-MHz FM Klystron Showing Single-Gap Pre-Penultimate and Penultimate Cavities and Double-Gap π-Mode Output Cavity

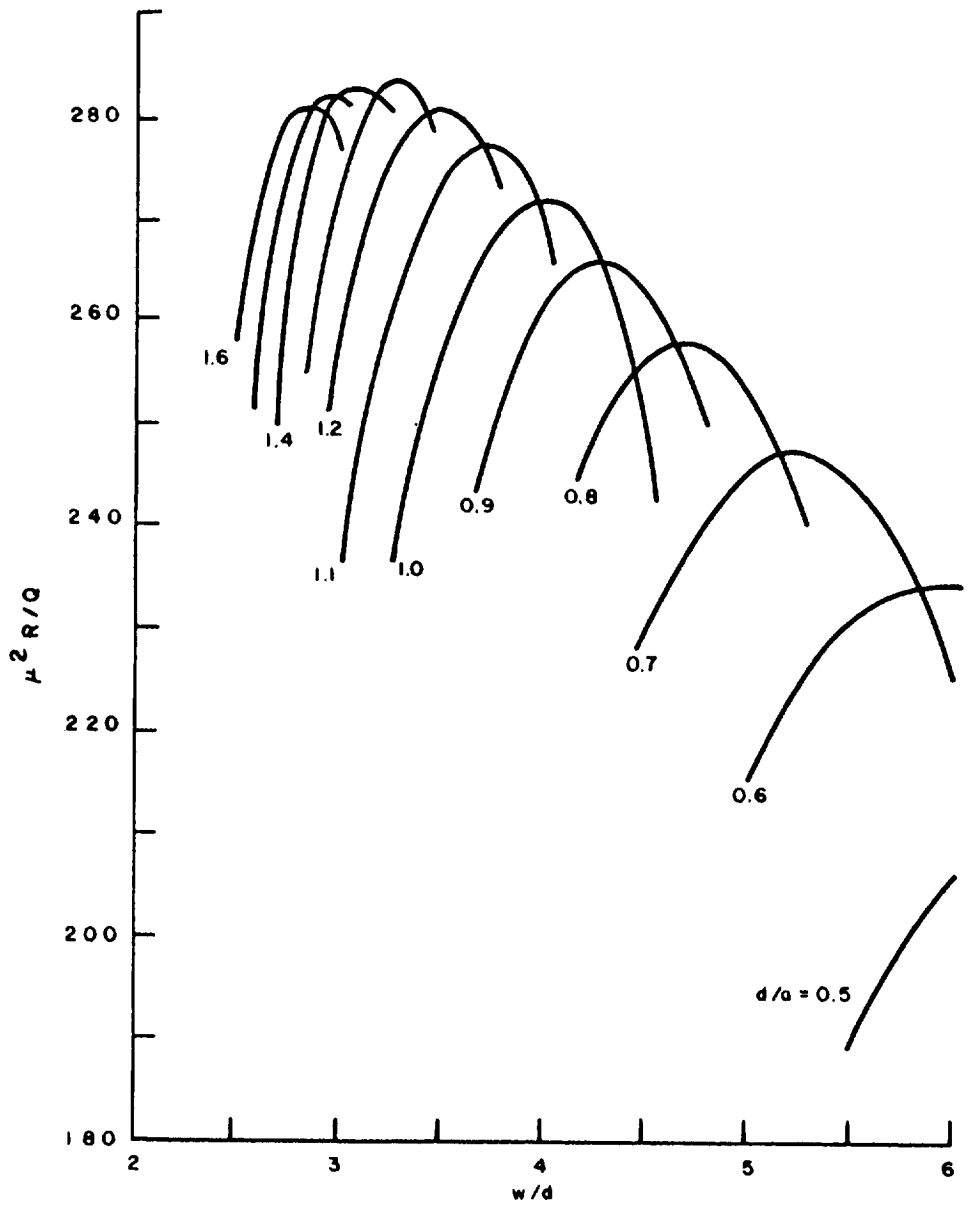

Figure 23 - Small-Signal Effective Impedance Parameter versus Interaction Region Width in π -Mode Cavity

envelope of the peaks of the curves, the optimum value of the gap interaction width, w/d, was read from each value of the normalized gap length, d/a, and the corresponding value of w/a was deduced and plotted in Figure 24. The points thus obtained graphically fall close to the straight line w/a = d/a + 3, which equation may be used to give the optimum length, w, for a given gap length, d. In Designs No. 3 and No. 3C which are discussed below, double-gap cavities with an optimum gap spacing as determined by the above considerations were analyzed.

Six basic designs were developed as a result of small-signal optimization calculations, but only Design No. 3 and two of its variations were studied in depth. Parameters for the various designs are given in Table III.

Design No. 1 was a preliminary computation with an assumed R/Q of 100 and a beam of 1×10^{-6} perveance. It was not pursued after an analysis of cavity R/Q showed higher values to be possible. Similarly, Design No. 2 was based on a higher, but still assumed, R/Q of 165 and a perveance of 0.5×10^{-6}.

The parameters of Design No. 3 were obtained from cavity analysis based on the development discussed in Section III under "Klystron Cavity Studies". The R/Q values are now 185 ohms, and cavities 4 and 5 in the interaction stack have been detuned slightly higher than they were in

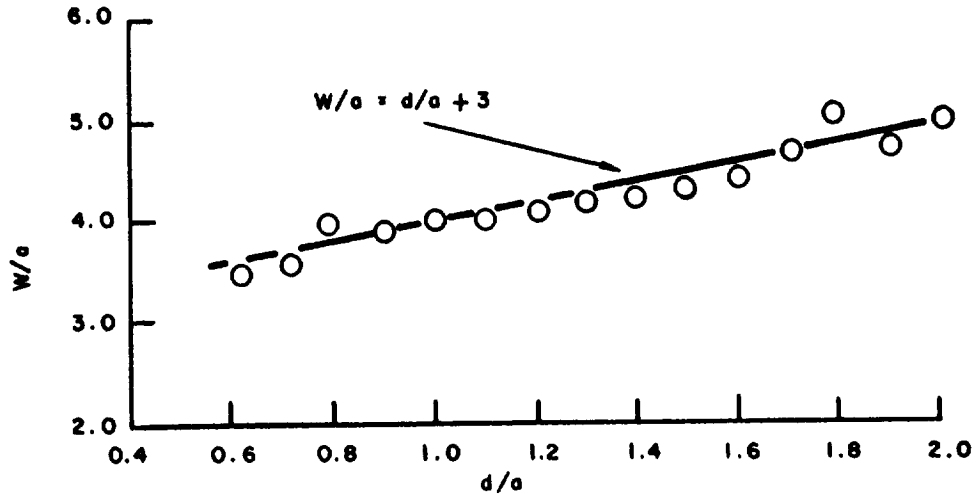

Figure 24 - Optimum Normalized Interaction Width w/a versus Gap Aspect Ratio d/a for π-Mode Double-Gap Cavities

Table III - Summary of 2000-MHz FM Klystron Designs

Parameter	Design Case 1	2	3	3A	3B	3C	3D	4	4A	5	6
f_1 (MHz)	2015	2010	2010	2010	2010	2000	2000	2000	2000	2000	2000
f_2 "	1998	1985	1985	1985	1982	1982	1982	1980	1980	1985	1985
f_3 "	1986	1998	1998	1998	1998	1998	1998	2000	1985	2000	1998
f_4 "	2030	2025	2028	2028	2028	2028	2028	2030	2025	2030	2028
f_5 "	2030	2025	2028	2028	2028	2028	2028	2030	2025	2030	2028
f_6 "	20000	2000	{2000* 2000	2000	2000	{2000* 2000	{2000* 2000	2000		2000	{1999* 2000
Q_1	220	60	60	60	60	66.7	66.7	50	50	66.7	66.7
Q_2	175	250	250	240	240	240	240	250	250	200	205
Q_3	1000	125	125	120	100	100	100	50	50	66.7	90
Q_4	4000	4000	4630	4630	4630	4630	4630	4630	4630	6750	4630
Q_5	4000	4000	4630	4630	4630	4630	4630	4630	4630	6750	4630
Q_6	66.7	66.7	{88* 44	{88* 44	{88* 44	{88* 44	{80* 48	{88* 44	{88* 44	{88* 44	{80* 48
ℓ_1 (in.)	2.00	4.30	4.30	4.30	4.30	4.30	4.30	4.30	4.30	4.30	4.30
ℓ_2 "	2.00	4.30	4.30	4.30	4.30	4.30	4.30	4.30	4.30	4.30	4.30
ℓ_3 "	2.00	4.30	4.30	4.30	4.30	4.30	4.30	4.30	4.30	4.30	4.30
ℓ_4 "	1.30	2.87	2.87	2.87	2.87	2.87	2.15	2.87	2.87	2.87	2.87
ℓ_5 "	0.70	1.43	1.43	1.43	1.43	1.43	2.15	1.43	1.43	1.43	1.43
R/Q_b (ohms)	100	165	185	203		203	203	203		230	203
R/Q_o "	100	165	203	203		203	203	203		203	203

*Double-tuned

Note: R/Q_b applies to the buncher resonators
R/Q_o applies to the output resonator

Design No. 2. Extensive large-signal computations were made, both with a conventional single-gap output cavity and with a double-gap π-mode cavity. Subsequently, a scale drawing revealed that the proposed extended interaction cavity had a physical length that was excessive for the bunching design because portions of the penultimate cavity would partially overlap the output cavity. The results still have significance, however, because they give a direct comparison between the interaction of a double gap and a single gap with the same highly developed klystron bunch.

The internal conversion efficiency as computed for both the single-gaps and double-gap cavities is plotted across the band in Figure 25. The "waterfall" diagrams showing the loss of energy as the electrons traverse the two types of output-cavity interaction regions were given previously in Figures 4 and 5. Although the double-gap interaction produces a somewhat broader bandwidth than the single gap, the interaction efficiency is not as high as in the single-gap case.

Design Nos. 3A through 3D, were considered because Design No. 3 was slightly deficient in bandwidth. The cavity R/Q values were increased to 203 ohms by thinning the walls of the reentrant tunnels. Small-signal computations indicated that no significant bandwidth improvement resulted, and therefore a series of design changes were considered, leading to Design No. 3B. No large-signal computations were made for Design No. 3A.

For Design No. 3B, the current modulation index at the midplane of the output gap was computed across the band at drive levels of 0.1, 0.2, and 0.4 watt. At the optimum drive level of 0.2 watt, the efficiency computed at the lower band edge and at band center was 34.4 and 69.4 percent, respectively. These again indicated a bandwidth that was slightly too narrow and a low midband efficiency. Consequently, additional parameter modifications were investigated with the small-signal computer program to produce Design No. 3C. This design differs from No. 3B in that cavity 1 is now tuned to band center rather than 10 MHz above band center and the Q of cavity 1 has been raised from 60 to 66.7. Large-signal computations were made at 0.1 and 0.2 watt, with the 0.1-watt drive yielding the optimum efficiencies shown in Figure 26. The impedance characteristics of the output interaction are shown in Figure 27. Superimposed on the computed constant efficiency contours for various complex impedances is the actual impedance characteristic of the double-tuned output resonator.

Design No. 3D is a modification of Design No. 3C, to test an extended interaction output cavity in a physically realizable klystron design.

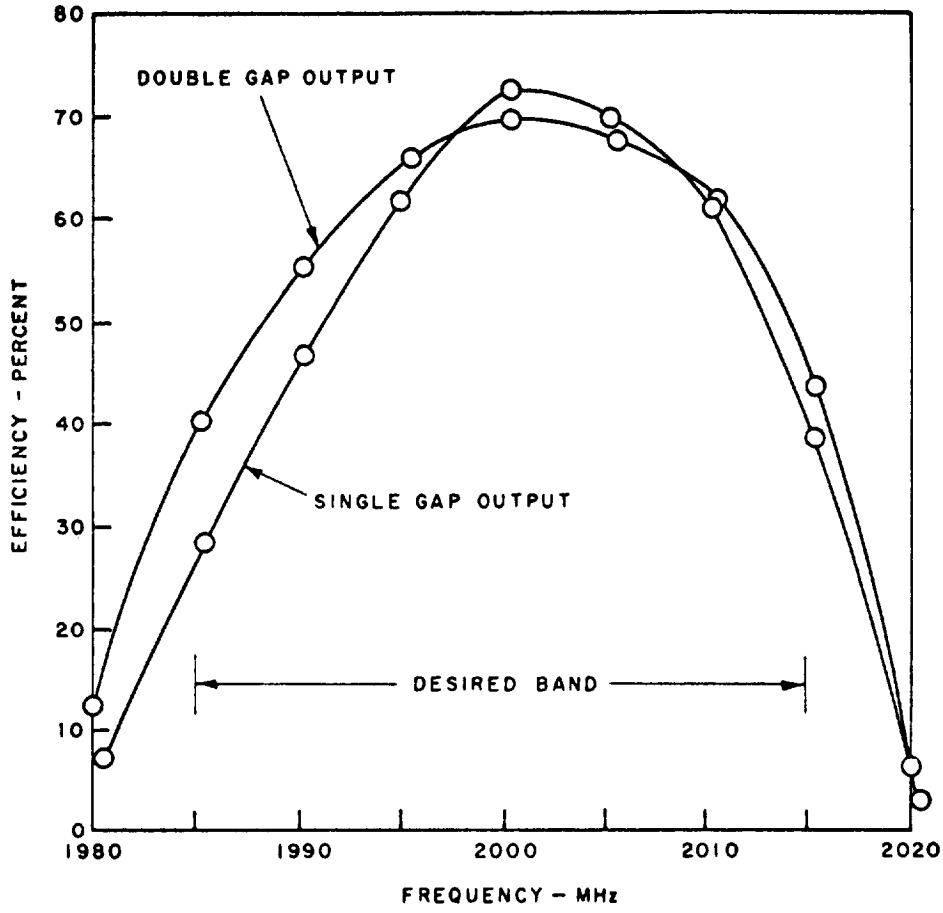

Figure 25 - Efficiency Conversion in Single-Gap and Double-Gap Output Circuits for Identical Current Modulation in Beam Entering Output Interaction Region (2000-MHz FM Klystron Design No. 3)

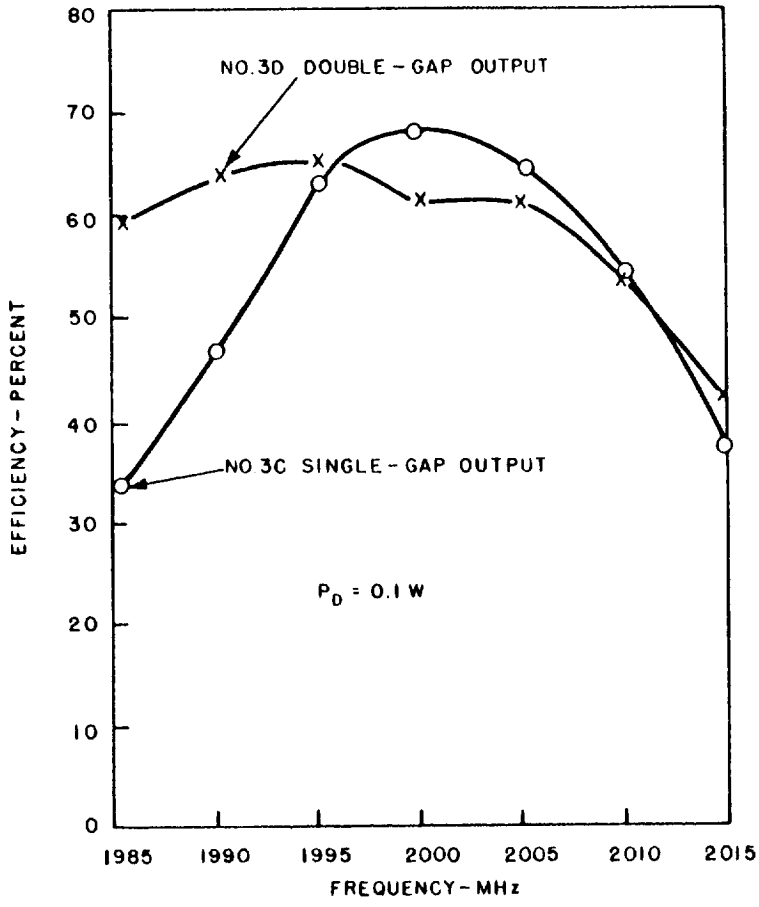

Figure 26 - Computed Internal Conversion Efficiencies Across the Desired 30-MHz Band in Single-Gap (3C) and Double-Gap (3D) 2000-MHz FM Klystrons

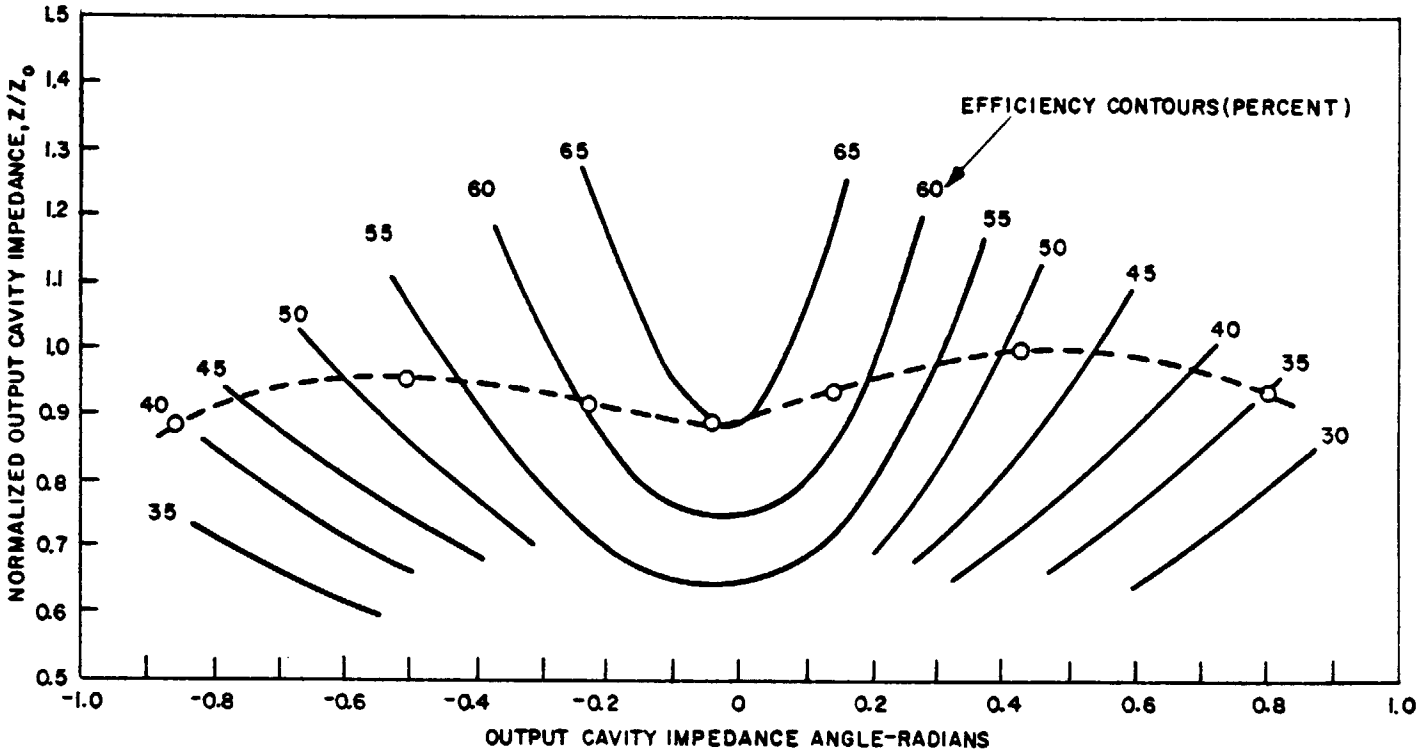

Figure 27 - Computed Constant Efficiency Contours on the Output Circuit Impedance Plane (The dashed line through the circles from right to left traces the actual impedance of the double-tuned single-gap output cavity employed in Design No. 3C.)

The penultimate cavity was moved 0.62 inch toward the pre-penultimate cavity in order to make room for the double-gap cavity previously considered in Design No. 3. The computed internal conversion efficiency across the band is also given in Figure 26.

A comparison of the efficiency curves for design Nos. 3C and 3D reveals that in this case the double-gap output cavity has broader bandwidth than the single-gap circuit. The midband efficiency is lower than the efficiency of the single-gap, but it is possible that further modifications in buncher design could improve this factor. Since the single-gap circuit was computed to have higher efficiency, and also has adequate bandwidth, the double-gap klystron design was not further developed. However, the double-gap circuit does merit further study.

Design No. 4 was originated to determine whether a broadband bunching design could best be developed on the criterion of maximum flatness in the small-signal current modulation index computed at the midplane of the output gap. From a series of small-signal runs, in which the cavity tuning and cavity Q's were varied systematically, the design parameters given in Table III were developed for Design No. 4. As shown in Figure 28, the small-signal current modulation index at a drive level of 0.004 watt is

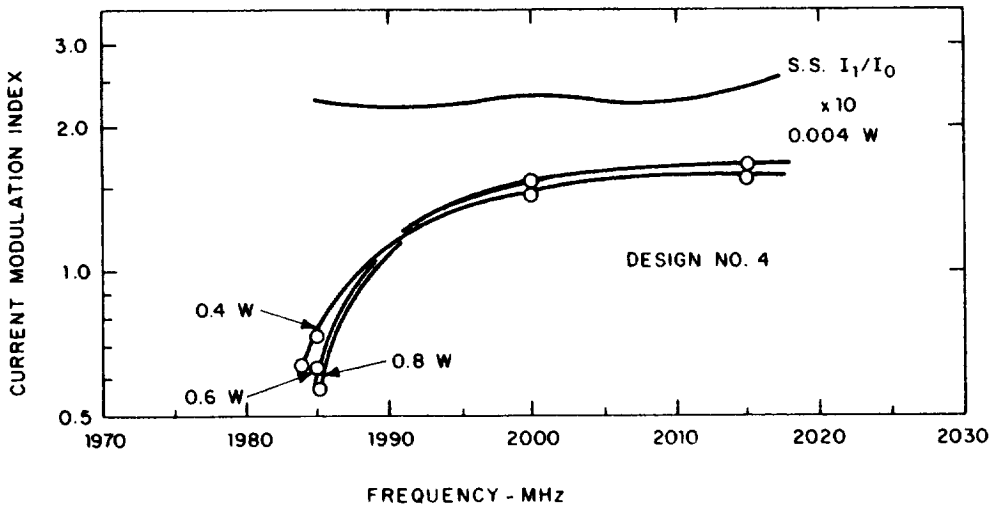

Figure 28 - Small-Signal and Large-Signal Current Modulation in a Klystron with Flat Small-Signal Bunching Characteristics (2000-MHz FM Klystron Design No. 4)

remarkably constant, having a maximum value of 0.23 and a minimum value of 0.22 within the desired 30-MHz bandwidth. The large-signal computations, however, show that at drive levels of 0.4, 0.6, and 0.8 watt, very poor bunching is achieved at the lower edge of the band. The reason for this appears to be that at small-signal levels the relatively large current index is achieved by feed-through currents from gap 3, since gaps 4 and 5 are tuned far above the band and provide very little interaction impedance to the beam at the lower band edge. At large-signal levels, the beam becomes badly overdriven at gap 3 and low current modulation is developed at the output gap.

Design No. 4A represents an attempt to trade some of the good bunching at the upper band edge for improved bunching at the lower band edge. It was assumed that the low RF currents being developed at the bottom edge of the band in Design No. 4 were due to insufficient gain in the three bunching cavities nearer the input end of the klystron. Accordingly, cavity 3 was tuned to the bottom edge of the band to allow the resonance frequency of cavities 4 and 5 to be moved nearer to the desired band so that they could exhibit somewhat higher impedance at the lower band edge. The large-signal results, as shown in Figure 29, are not as good as those achieved with Design No. 3C, and this design approach was dropped.

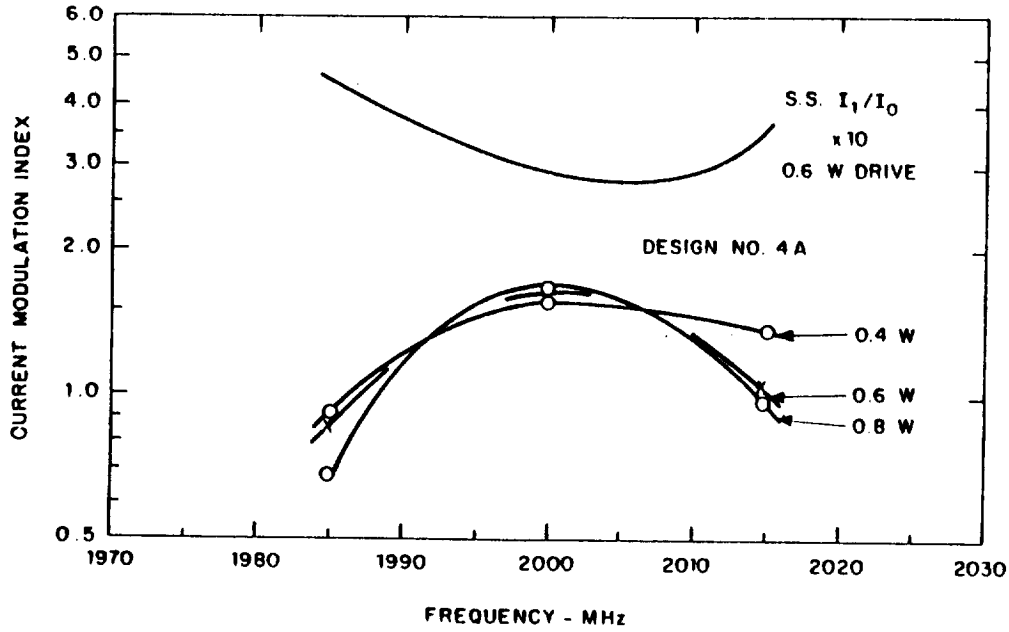

Figure 29 - Small-Signal and Large-Signal Current Modulation in a Klystron with Supposedly Compensated Small-Signal Bunching Characteristics (2000-MHz FM Klystron Design No. 4A)

The purpose of the development of Design No. 5 was to evaluate the advantage, if any, of achieving higher R/Q in the interaction cavities by increasing the gap lengths. In this instance, when the gap lengths are increased from 0.2 inch to 0.28 inch, the gap transit angle increased from 1 radian to 1.4 radians and the R/Q increases from 203 ohms to 230 ohms. A series of small-signal runs, in which the cavity tuning and loading parameters were systematically varied, yielded the optimum design parameters given in Table III. Large-signal computations were made only at band center, indicating that at a drive level of 0.2 watt, the internal conversion efficiency is only 64.8 percent. Because no outstanding increase in efficiency seems obvious, and because cavities with long gaps are not expected to have good gap coupling coefficients at large gap voltages (as developed in cavity 5 and the output gap), it was concluded that the investigation should be limited to cavities with transit angles of 1 radian or less. Thus, Design No. 5 was not analyzed to any greater extent.

The purpose behind the development of Design No. 6 was to evaluate the effect of employing values of Q as low as possible in order to more readily achieve large bandwidths, such as required for the 2000-MHz FM klystron. As shown in Table III, Design No. 6 is essentially the same as Design No. 3C, except that the Q's of cavities 2 and 3 have been lowered and cavity 2 has been moved from 1982 MHz to 1985 MHz for purposes of compensation. Also, in order to enhance the output gap interaction at the lower band edge, the output cavity was double-tuned asymmetrically in order to present a higher impedance at 1985 MHz than at 2015 MHz. The computed conversion efficiency at three drive levels is shown in Figure 30. Again, no improvement in performance over that achieved in Design No. 3C is noted.

It may be concluded from these studies that a double-gap output interaction circuit is not required to achieve the desired bandwidth, although such a circuit might be desirable for achieving flatter response across a given band. Accordingly, the design adopted for the 2000-MHz FM service is Design No. 3C.

DEVELOPMENT AND PERFORMANCE OF FINAL DESIGNS

The modification of the interim designs to meet the phase specifications resulted in a decrease of gain below 40 dB. To increase the gain it was necessary to redesign the buncher cavities with thinner tunnel walls, thus giving a higher R/Q. This could safely be done because the thermal loading of the buncher cavities should be an order of magnitude less than the thermal loading of the output cavity.

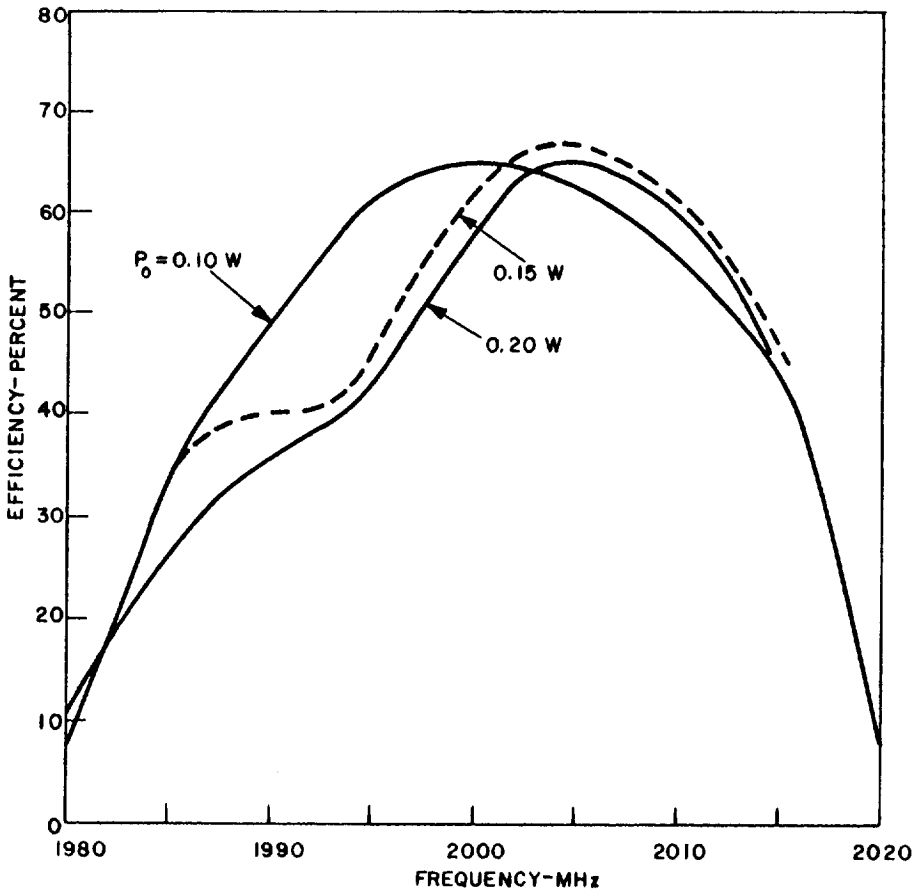

Figure 30 - Internal Conversion Efficiency at 3 Drive Levels in a Low-Q Broadband Klystron (2000-MHz FM Klystron Design No. 6)

The final design parameters for all tubes are given in Table IV. The computed performance of these tubes will now be discussed.

850-MHz AM Service

The performance characteristics of this tube are depicted in Figures 31 and 32(a)(b)(c). An important restriction on the performance of this tube is the specification on amplitude linearity. In the upper graph of Figure 31, a curve of power output is shown as a function of power input. It will be noted that constant gain loci are given by the dashed lines fanning out from the origin. The small-signal gain is 42 dB. As drive is increased, the efficiency rises and the gain falls. This behavior is directly plotted in the lower graph of Figure 31. From this plot it is evident that the deviation from small-signal gain exceeds 0.5 dB at an efficiency of about 32 percent. This point must occur at half the saturation output of the tube, according to the amplitude linearity specification. This sets the efficiency at the peak synchronizing pulse at 64 percent, even though the efficiency at saturation could exceed this value. Since a feasible AM transmitter using a klystron requires some form of collector depression, the final RF design was chosen to have a peak efficiency of 60 percent while meeting all other specifications for power gain, amplitude linearity, and phase linearity.

As shown in Figure 31, at the small-signal drive power of 0.16 to 0.19 watt yielding a power output of 2.6 to 3.0 kW at the average picture level, the deviation from linearity is approximately 0.1 dB, and the efficiency is approximately 20 percent. This figure for efficiency is so low that it is essential to consider methods of increasing it. This is done in Section VII, where the reflex collector is shown to increase the average signal efficiency to the 55 to 80 percent range, depending on the energy margin that can be stably achieved.

In Figure 32(a), the internal power conversion efficiency at 1-watt drive is plotted across the band. It is evident that the -3 dB gain specification at the band edges is easily met. The lower plots in Figure 32(a) show the normalized RF current at each gap. The solid lines give the large-signal current at 1-watt drive as computed by the disk model. The dashed lines are the small-signal current at 0.01-watt drive. Note that these values have been multiplied by ten to facilitate comparison with the large-signal currents. The large-signal current index at the output gap ranges from 1.3 to 1.6 over the band. These figures are lower than the corresponding figures in the FM cases because of the amplitude linearity specification.

Table IV - Summary of Tube Design Parameters

1.	Frequency (GHz)	0.85 (AM)	2.0 (AM)	2.0 (FM)	8.0 (FM)	11.0 (FM)
2.	Bandwidth (MHz)	6	6	30	30	30
3.	Power Input (KW)	15.0	9.63	7.9	7.9	7.9
4.	Beam Voltage (KV)	15.5	13.0	12.0	12.0	12.0
5.	Beam Current (Amp)	0.965	0.741	0.657	0.657	0.657
6.	Perveance (x 10^{-6})	0.5	0.5	0.5	0.5	0.5
7.	Cathode Dia (CM)	1.5	0.7	0.7	0.35	0.255
8.	Cathode Loading (Amp/cm^2)	0.1	0.3	0.3	1.4	2.7
9.	Beam Area Convergence	9.4	15.1	15.1	60	60
10.	Number of Cavities	5	5	6	5	5
11.	(R/Q) Buncher (Ohm)	186	203	203	142	111
12.	(R/Q) Output (Ohm)	138	153	176	93	68
13.	(Q_u) Buncher	7670	4630	4630	2390	2110
14.	(Q_u) Output	5170	3065	3730	2580	2360
15.	Buncher Gap (Inch)	0.53	0.2	0.2	0.05	0.036
16.	Output Gap (Inch)	0.265	0.1	0.14	0.05	0.036
17.	Tunnel ID (Inch)	0.815	0.3	0.3	0.075	0.055
18.	Tunnel ID (Inch) - Buncher	1.040	0.390	0.390	0.150	0.120
	- Output	1.040	0.390	0.390	0.190	0.175
19.	γa_i (rad)	0.75	0.71	0.74	0.74	0.74
20.	b/a_i	0.6	0.6	0.6	0.6	0.6
21.	Tunnel Wall (Inch)	0.112	0.06	0.06	0.0525	0.0375
22.	Cavity ID (inch) - Buncher	4.96	2.06	2.06	0.498	0.360
	- Output	3.92	1.62	1.82	0.501	0.377
23.	Cavity Ht (Inch) - Buncher	3.92	1.67	1.67	0.363	0.240
	- Output	2.88	1.23	1.43	0.311	0.202
24.	Drift Lengths (Inch)	11.60	4.3	4.3	1.075	0.78
		11.60	4.3	4.3	1.075	0.78
		7.77	2.87	4.3	0.716	0.52
		4.27	1.43	2.87	0.358	0.285
				1.43		
25.	Cavity Tuning (MHz)	855	2005	2000	8020	11,024
		845	1995	1985	7984.5	10,977
		863.5	2027.5	1998	8080	11,090
		863.5	2027.5	2028	8080	11,090
		850.25	2001	2028	8000	11,000
				2000/2000		
26.	Q_{input}	125	250	66.7	275	270
27.	$Q_{intermediate}$	400	800	240	300	450
		7670	4630	100	2390	2110
		7670	4630	4630	2390	2110
				4630		
28.	Q - Output	118	120	88/44	196	268
29.	Brillouin Field (Tesla)	117.5	293	282	1127	1550
30.	3x Brillouin Field (Tesla)	353	880	846	3381	4650
31.	η-ckt (%)	97.7	96.1	96.5	91.8	88.6
32.	η-int (at f_o) (%)	62.1	62.7	68.6	67.2	62.9
33.	η-ext (at f_o) (%)	60.7	60.3	66.2	61.7	55.7
34.	P_{out} (KW)	9.1	5.8	5.2	4.9	4.4
35.	P_{drive} (W)	1.0	0.065	0.10	0.5	0.7
36.	Gain - sat (dB)	39.5	49.7	47.2	40.2	38.4
37.	Output Cavity Type	Single-Tuned	Single-Tuned	Double-Tuned	Single-Tuned	Single-Tuned

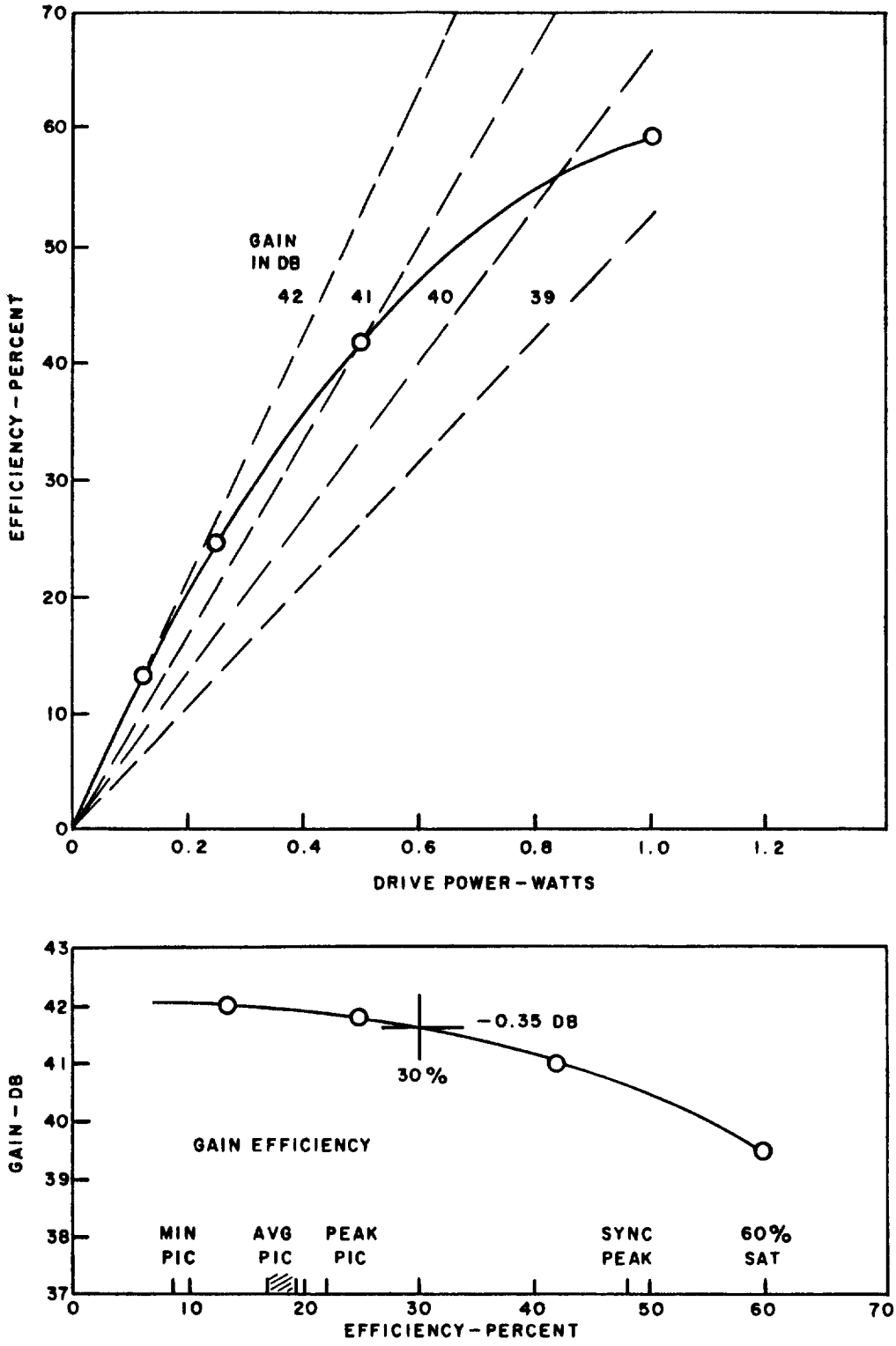

Figure 31 - Large-Signal Characteristics of 850-MHz AM Klystron at Various Signal Levels at Midband

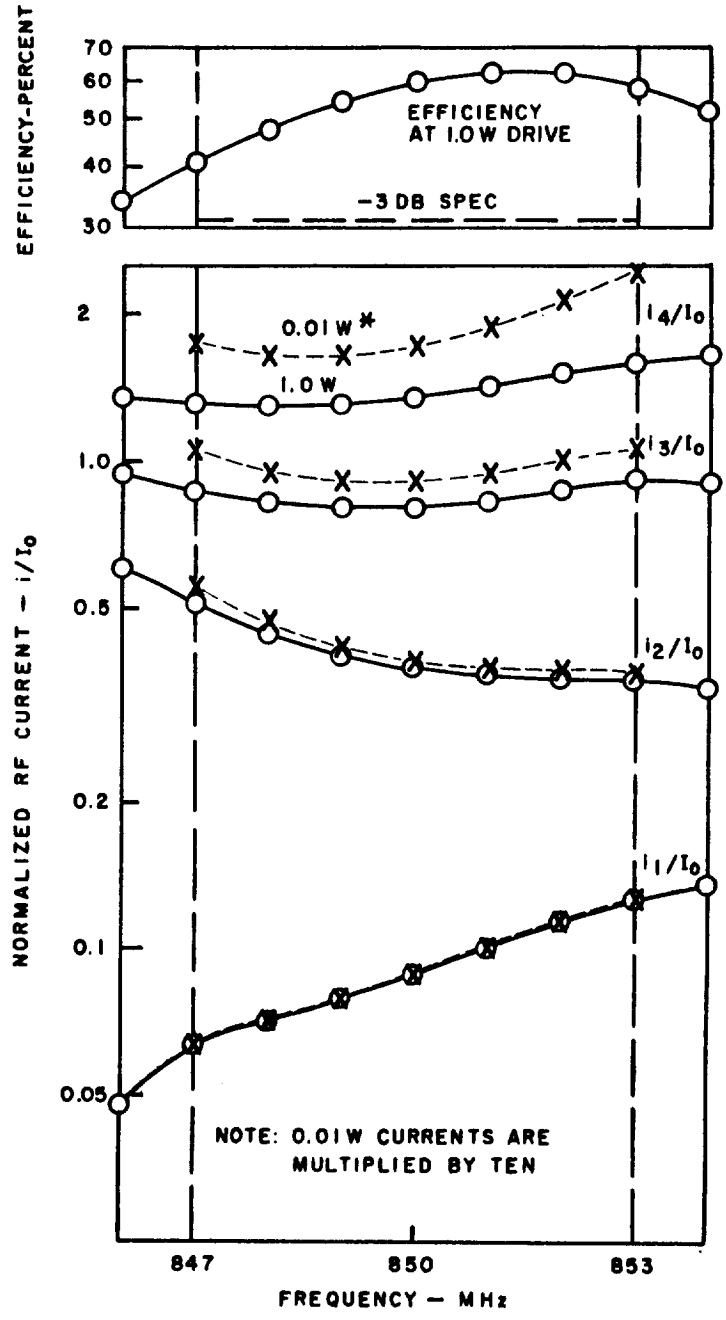

Figure 32(a) - Internal Power Conversion Efficiency and Development of Current Modulation Across the Band in the 850-MHz AM Klystron

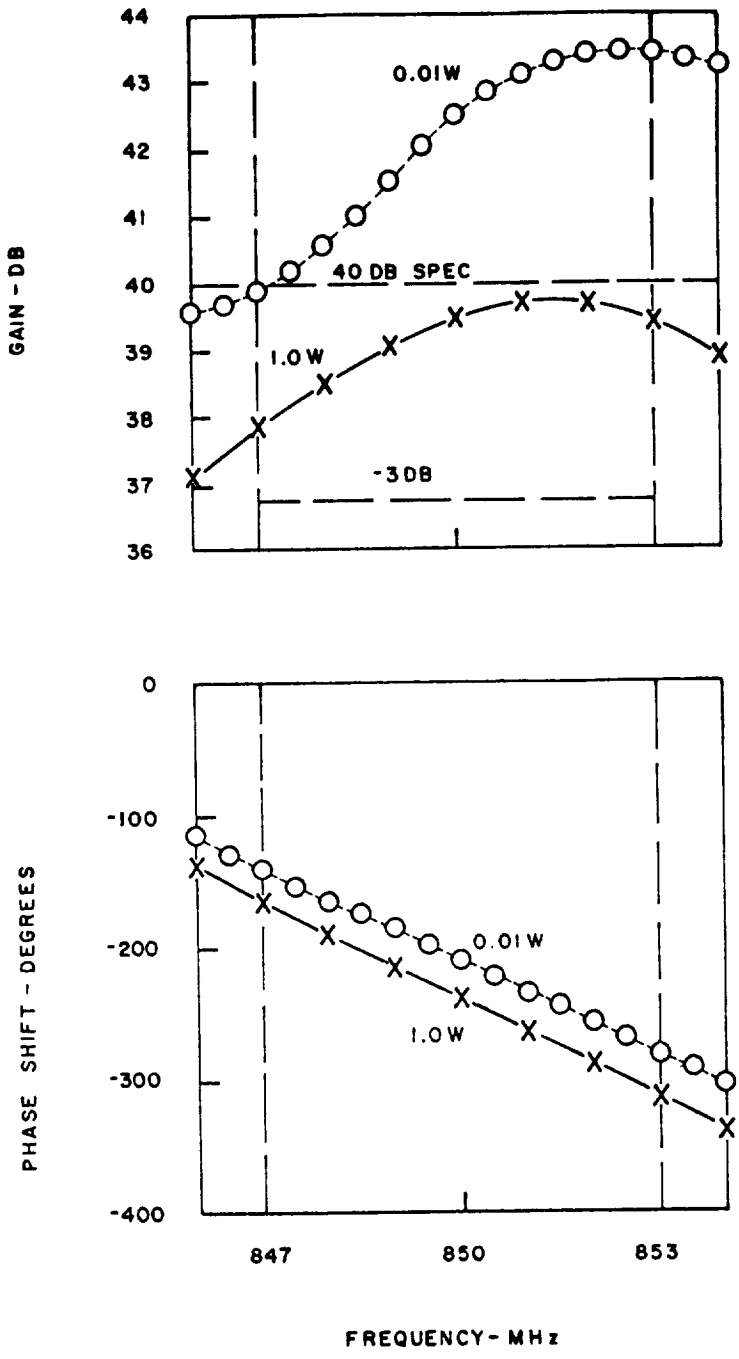

Figure 32(b) - Gain and Phase Shift Characteristics of 850-MHz AM Klystron

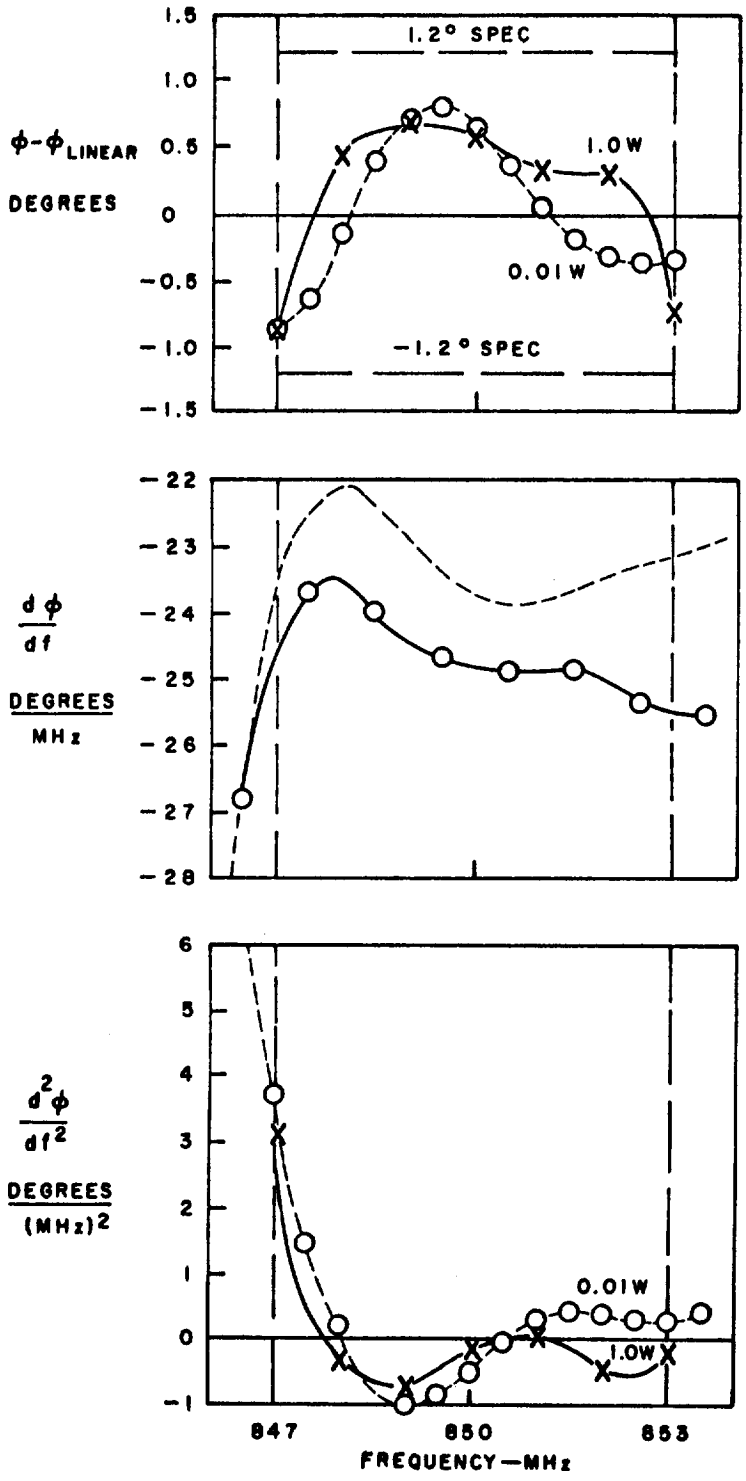

Figure 32(c) - Phase Linearity Characteristics of 850-MHz AM Klystron

The gain and phase shift of the output voltage is shown in the upper and lower plots of Figure 32(b), respectively. Small-signal results are given by the dashed lines, and large-signal results are given by the solid line as computed at the points shown. As the lower plots illustrate, the phase shift in the final designs is extremely linear. To achieve this, it was found necessary to distort the gain characteristic from that shown in the upper left of Figure 20 to that shown in the upper plot in Figure 32(b). The large-signal gain shows a 2-dB sag at the low frequency end, and the small-signal gain shows a 3.5-dB rise as frequency is increased across the band. The underlying physical reason that makes it necessary to distort the gain characteristic to achieve phase linearity has not been investigated, but it is related to the use of the non-symmetrically tuned penultimate and pre-penultimate cavities.

The difference between small-signal and large-signal phase shift has been resolved. It is due to two distinctly different mechanisms: (1) an additional small-signal phase shift proportional to $(\omega_q/\omega)^2$, representing the fact that the average of the slow and fast wave velocities is somewhat slower than the DC beam velocity, an effect not considered by the small-signal program; and (2) an additional phase shift due to the large voltage index in the penultimate cavity at large-signal levels. When these two phase shifts are considered, the small-signal and large-signal phase shifts are found to agree within 3 degrees.

A detailed analysis of phase shift at both small- and large-signal levels is shown in Figure 32(c). The uppermost plots represent the deviation from linear phase shift as established by fitting a straight line through phase shift points equally-spaced throughout the band. The ± 1.2-degree specification for deviation of phase shift from linearity is given by the horizontal dashed lines. In contrast to the phase deviation shown for the interim design in the lower left-hand plot of Figure 20, the final design easily meets the phase specification over the entire band at both small- and large-signal levels. The plots of the first and second derivative of phase shift are included for completeness in Figure 32(c), but are not of concern in AM service.

Thus, the amplitude linearity, gain, and phase specifications have all been satisfactorily achieved in the 850-MHz AM tube.

2000-MHz AM Service

The performance of the 2000-MHz AM tube is considerably flatter across the band than its 850-MHz counterpart because of the reduced percentage bandwidth at the higher frequency. Plots of efficiency as a function of drive power, and gain as a function of efficiency are shown in Figure 33. These plots closely resemble those shown in Figure 31 for the 850-MHz tube. The saturation efficiency is 62.4 percent, and 3 dB down from this level the gain is 0.55 dB below the small-signal gain.

From the upper plot in Figure 34(a), it is evident that the efficiency is extremely flat across the band. The lower plots in this figure show that the large-signal current index builds up to a value of about 1.4 at the output gap. In Figure 34(b), the deviation in both small-signal and large-signal gain across the band are shown to be less than 0.3 dB. The lower plot in this figure again shows extremely linear phase shift characteristics at both small- and large-signal levels. The deviation of these phase shift plots from linearity is examined in more detail in Figure 34(c). The upper plot shows that the ± 1.2-degree phase linearity specification is comfortably met with a factor of two to spare. The remarkable agreement exhibited by the two derivative plots in Figure 34(c) gives confidence that the large-signal disk-electron simulation model is a highly accurate representation of the RF behavior of electron beams.

Knowledge of the energy distribution of the spent beam is important in depressed-collector design. The spent beam energy distribution is set primarily by the voltage swing in the output gap. In Figure 35, spent beam energy distributions are shown for four signal levels, corresponding roughly to minimum picture, peak picture, sync peak, and saturation power output. The normalized output voltage swings in these cases are 0.5, 0.7, 1.0, and 1.2, respectively. Since these voltage swings are reduced somewhat by the large-signal coupling coefficient, μ, in the output gap it is evident that the edges of the energy distributions in Figure 35 appear at roughly $1 \pm \mu\alpha_{out}$. At the highest drive level, the bulk of the electrons have energies less than 0.4 V_o, as shown by the dashed line. The efficiency corresponding to this case is 62 percent. The efficiencies corresponding to the remaining cases are 46.1, 24.4, and 12.0 percent, respectively.

All specifications -- amplitude linearity, gain, and phase linearity -- are met by this final 2000-MHz design. Note that the gain of this tube is approximately 50 dB.

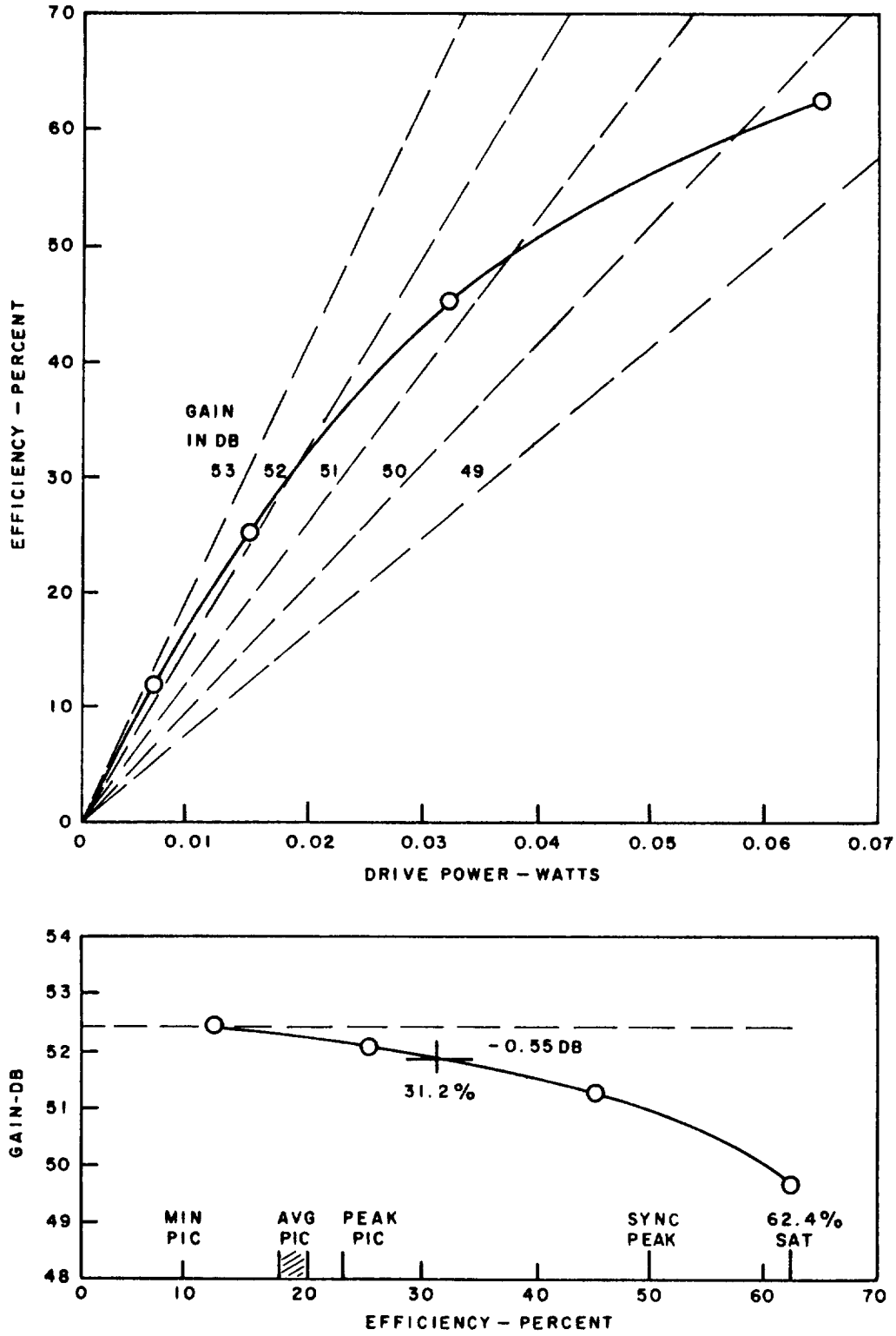

Figure 33 - Large-Signal Characteristics of 2000-MHz AM Klystron at Various Signal Levels at Midband

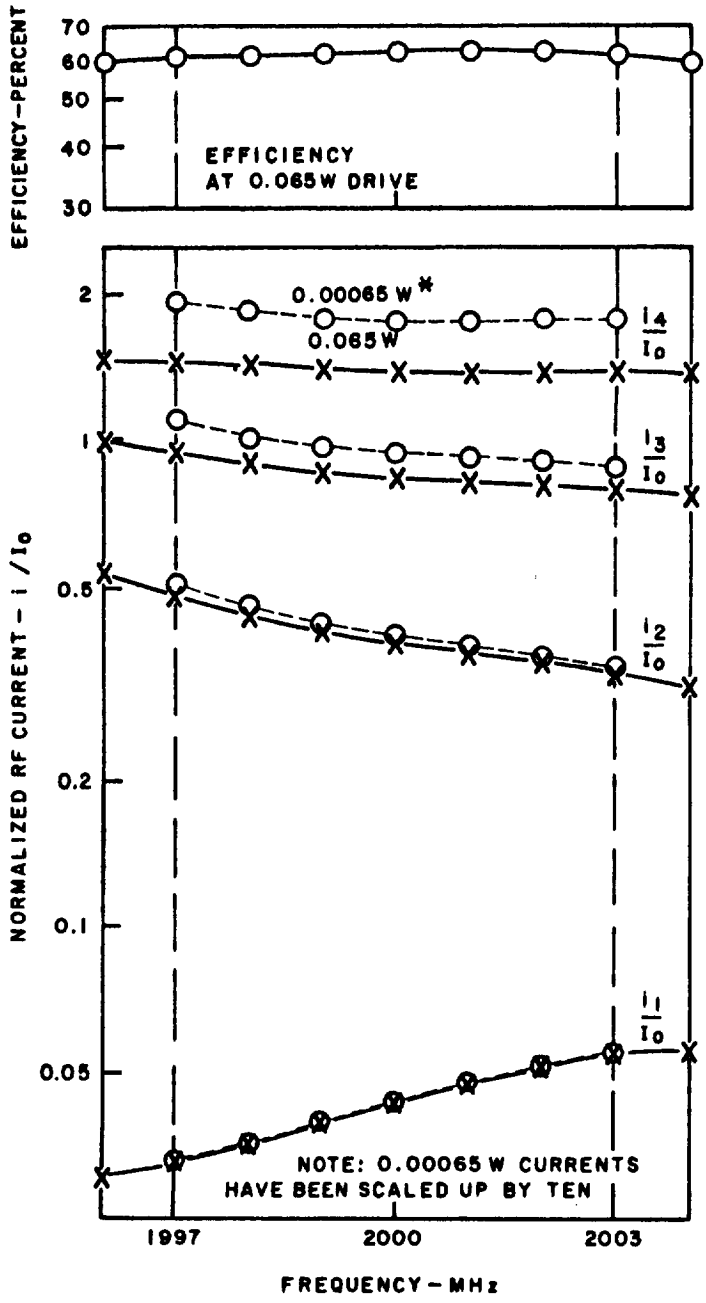

Figure 34(a) - Internal Power Conversion Efficiency and Development of Current Modulation Across the Band in the 2000-MHz AM Klystron

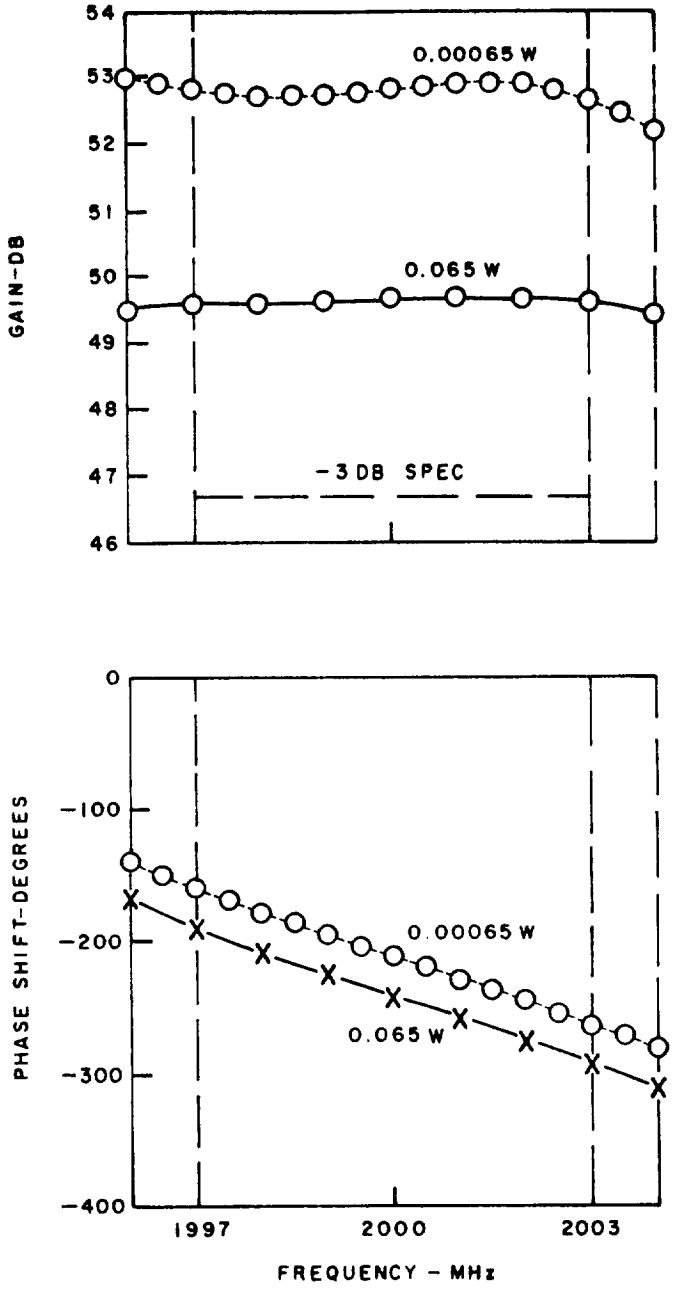

Figure 34(b) - Gain and Phase Shift Characteristics of 2000-MHz AM Klystron

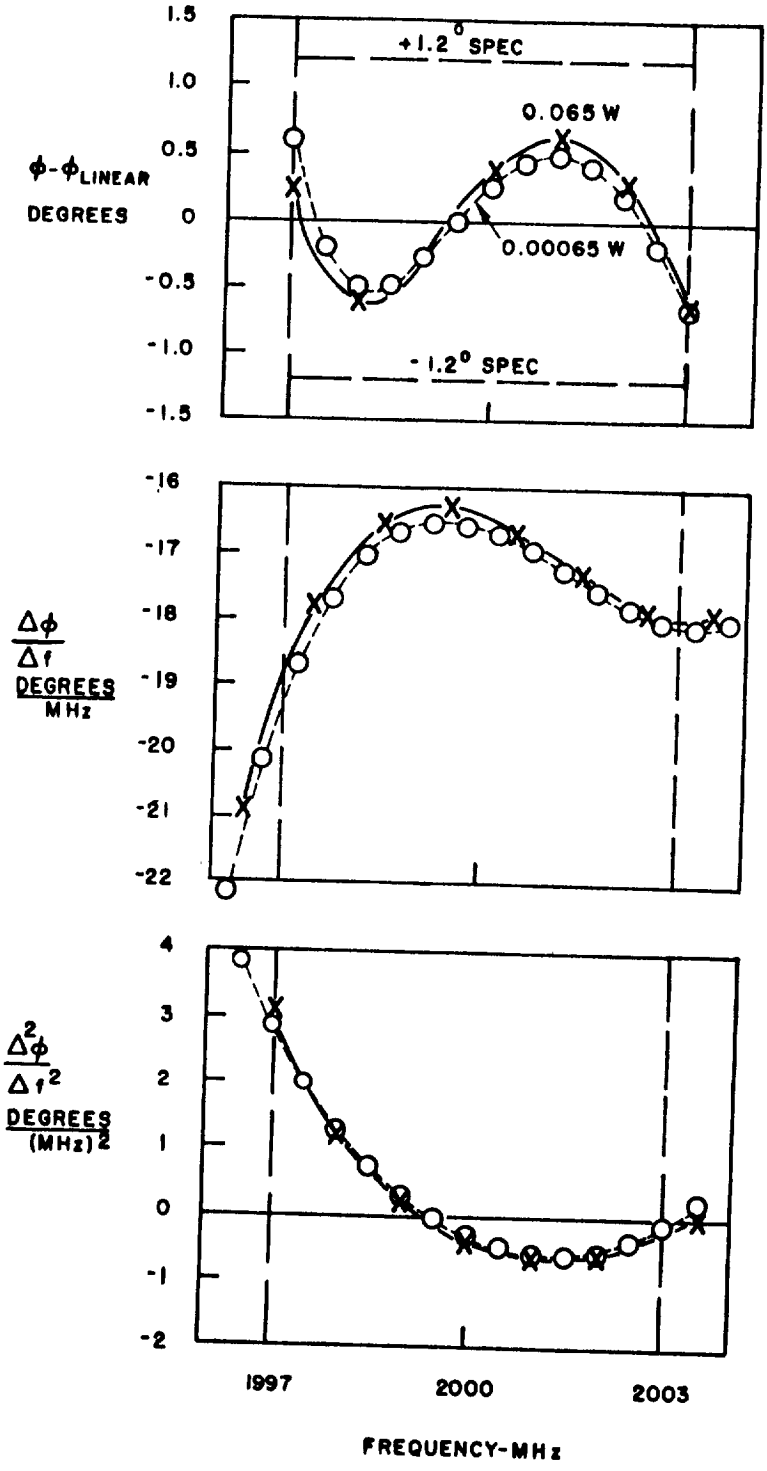

Figure 34(c) - Gain and Phase Shift Characteristics of 2000-MHz AM Klystron

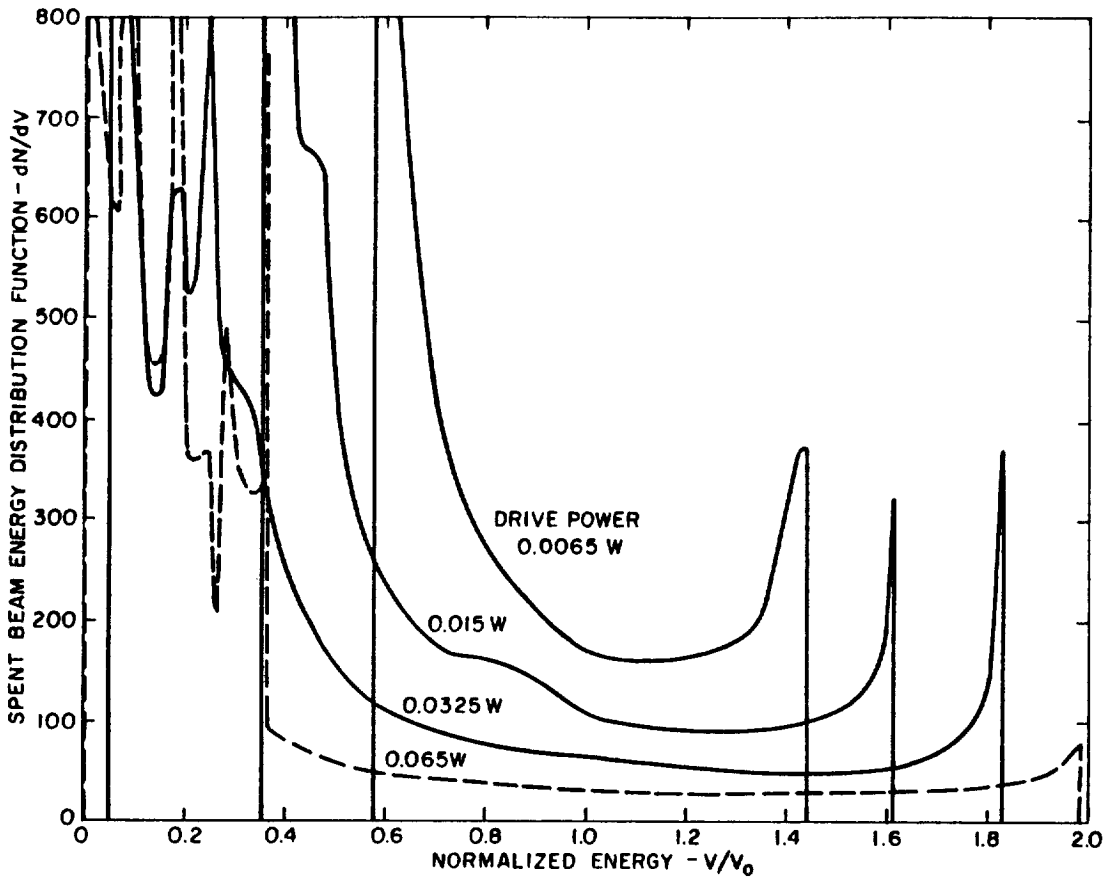

Figure 35 - Spent-Beam Spectrum of 2000-MHz AM Klystron as Function of Drive Level

2000-MHz FM Service

The final design of this klystron is essentially that given as Design No. 3C in the interim series. The primary task in this case was to achieve sufficient bandwidth with high efficiency. Performance of this design is summarized by the curves in Figures 36(a), (b), and (c). By using a 0.7-radian single-output interaction gap and double tuning, the bandwidth is achieved with a midband-interval conversion efficiency of 68.6 percent and large-signal gain of 47 dB. Amplitudes of the fundamental current component of the beam at the various interaction gaps is also shown in Figure 36(a). The solid curves are for full 0.1-watt drive, while the dashed curves show the small-signal values (0.01-watt drive). It is again evident that small-signal computations are valid only in the range where I_1/I_o is less than 0.3, although useful data in the form of trends can be obtained at higher levels.

The phase delay and phase linearity characteristics shown in Figures 36(b) and 36(c) show a slope $\Delta\phi/\Delta f$ which would be satisfactory for AM service, but the second derivative reaches 0.5 degree per MHz^2 compared with the desired 0.05 degree per MHz^2. This characteristic could be improved by the technique of lowering cavity Q and changing resonant frequency as was done in the 850-MHz design. However, this optimization could not be completed within the present study program.

8000-MHz FM Service

The performance of this tube is summarized in Figures 37(a), (b), and (c). The upper plot in Figure 37(a) shows a peak efficiency of 67 percent, corresponding to a large-signal output gap RF current index of 1.5 to 1.7. In Figure 37(b), the lower plots show the phase shift to be extremely linear. As in the case of the 850-MHz tube, this linear phase characteristic is accompanied by a tilted gain characteristic, as shown in the upper plots of Figure 37(b). The large-signal gain is 40 dB and the loss of gain at the lower band edge is less than 2 dB at the saturation drive of 0.5 watt.

The phase shift is examined in more detail in Figure 37(c). The specification for the FM tubes is that the second derivative of the phase shift shall not exceed ± 0.05 degree/MHz^2. This specification is met at small-signal levels, as evidenced by the dashed line in the bottom plot. At large-signal levels, the phase shift takes on an undulating character and apparently exceeds the specification by a factor of three. However,

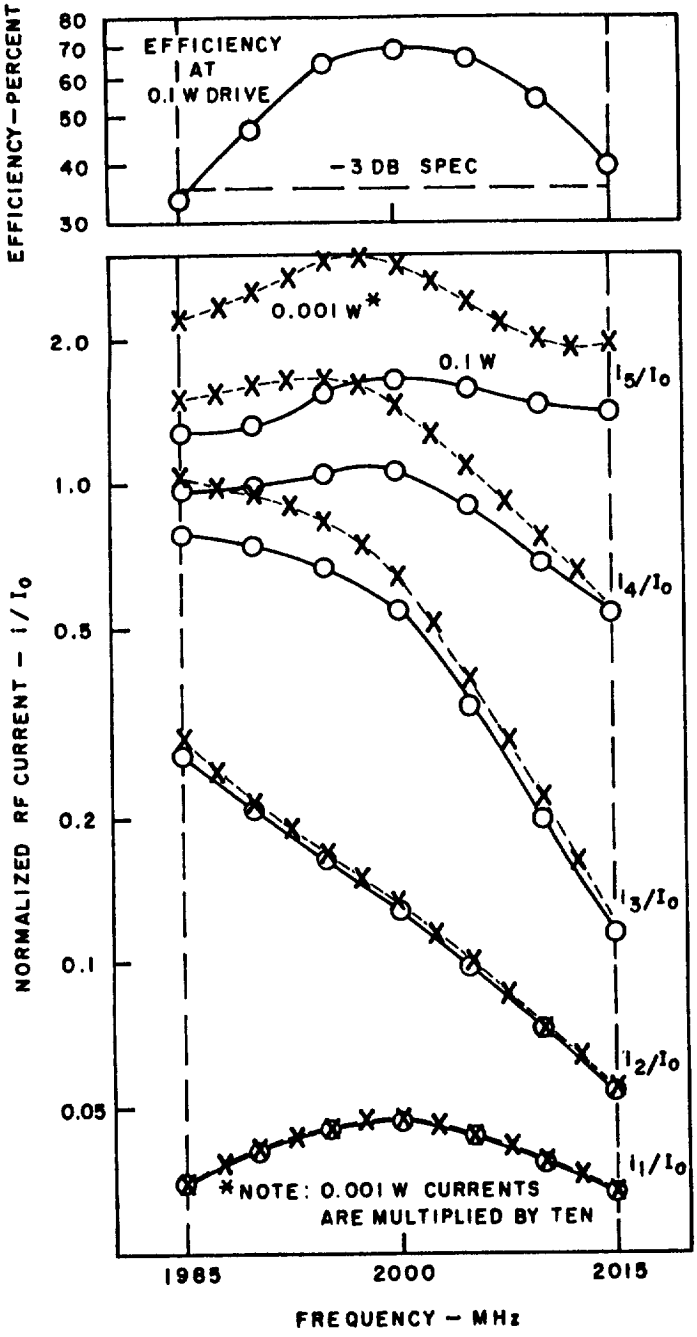

Figure 36(a) - Internal Power Conversion Efficiency and Development of Current Modulation Across the Band in the 2000-MHz FM Klystron (Design No. 3C)

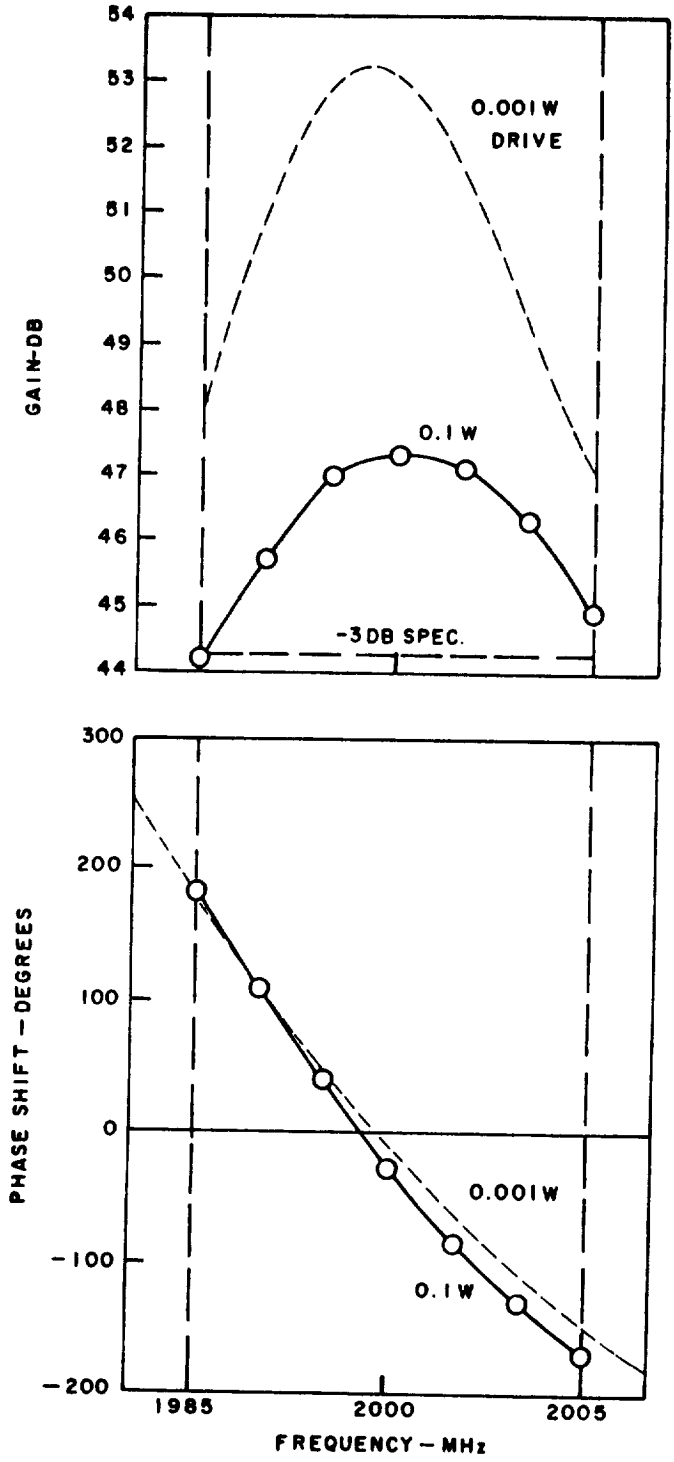

Figure 36(b) - Gain and Phase Shift Characteristics of 2000-MHz FM Klystron (Design No. 3C)

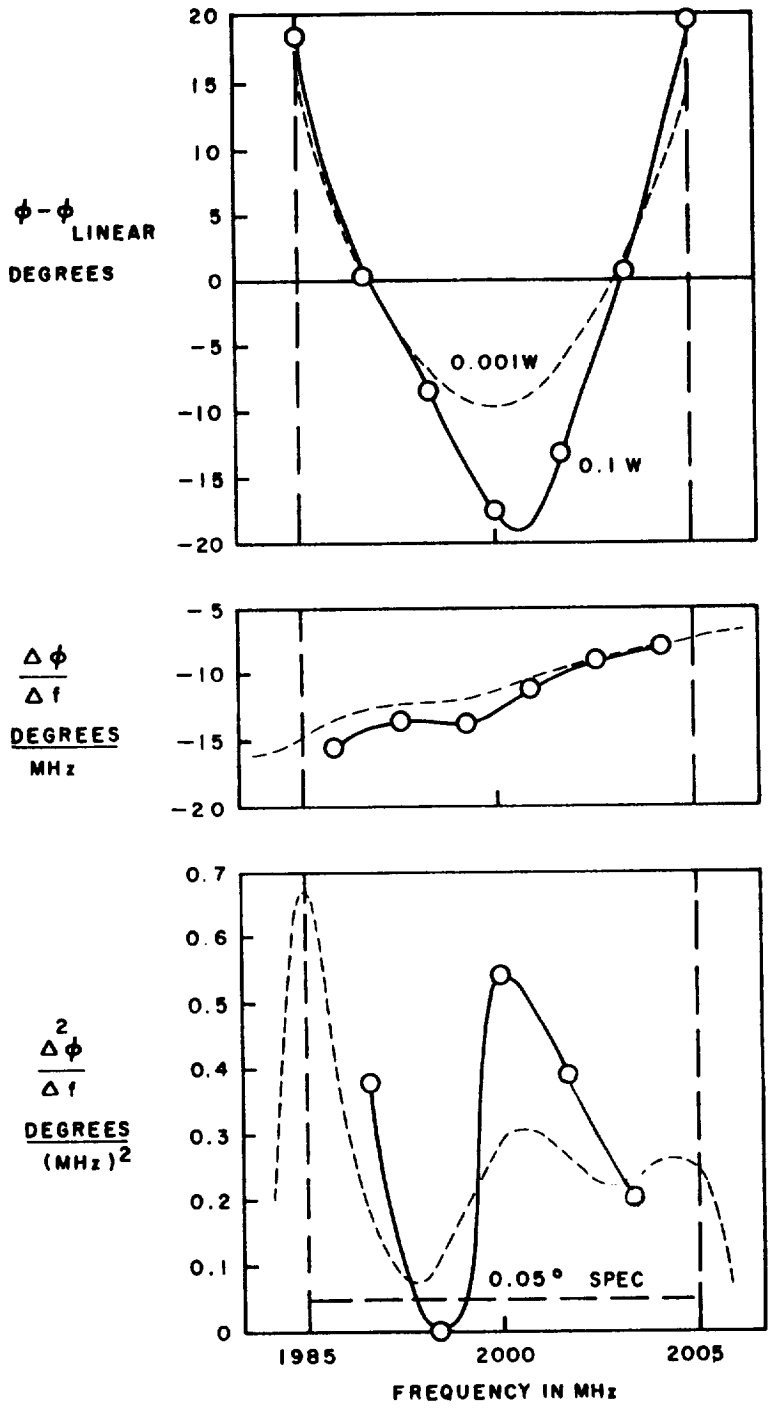

Figure 36(c) - Phase Linearity Characteristics of 2000-MHz FM Klystron (Design No. 3C)

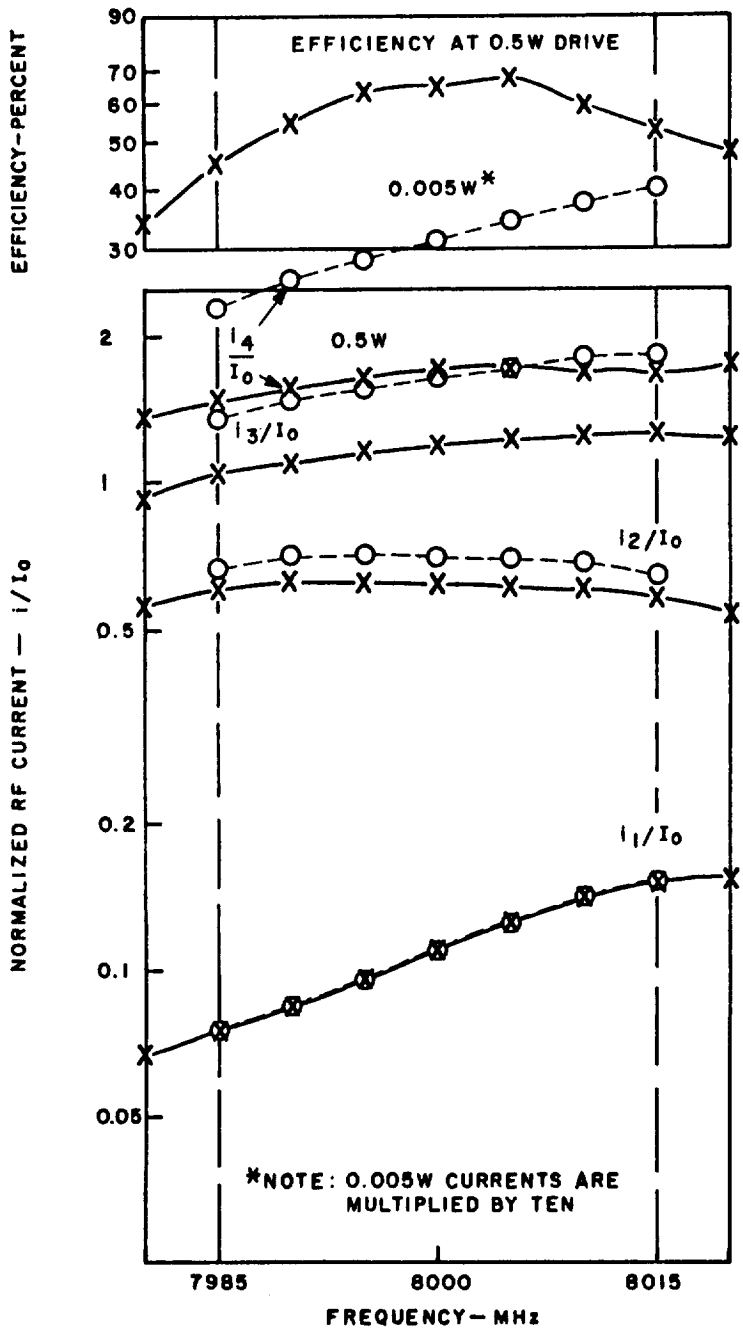

Figure 37(a) - Internal Power Conversion Efficiency and Development of Current Modulation Across the Band in the 8000-MHz FM Klystron

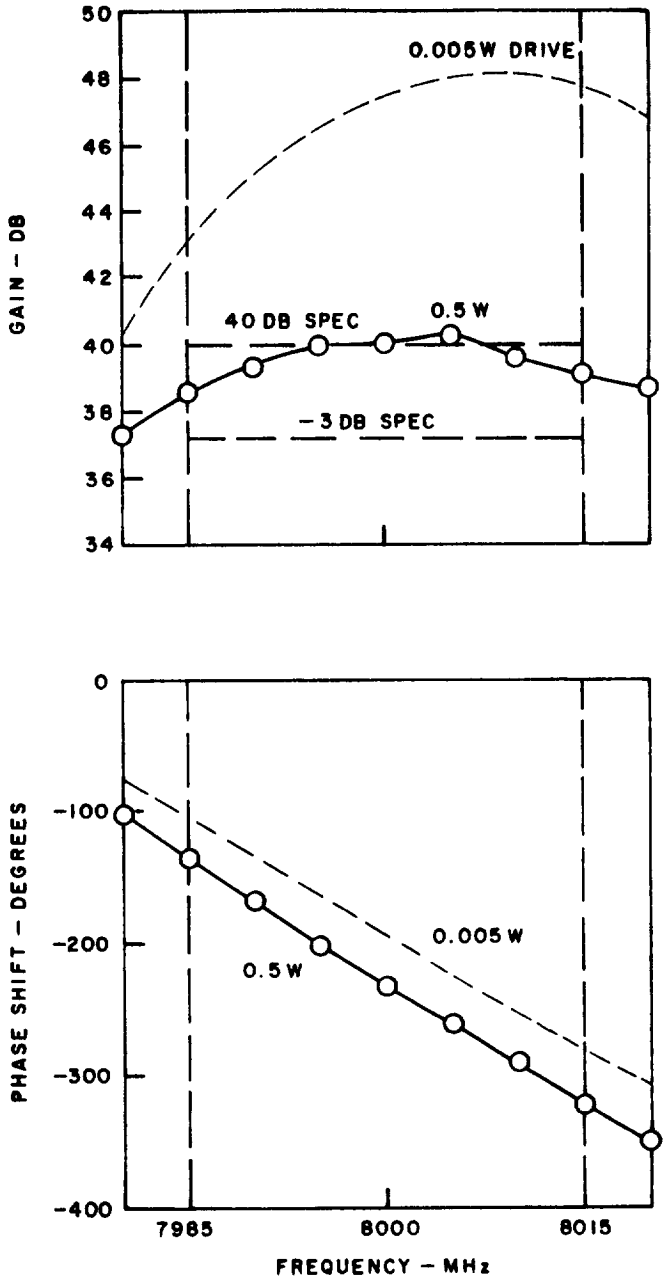

Figure 37(b) - Gain and Phase Shift Characteristics of 8000-MHz FM Klystron

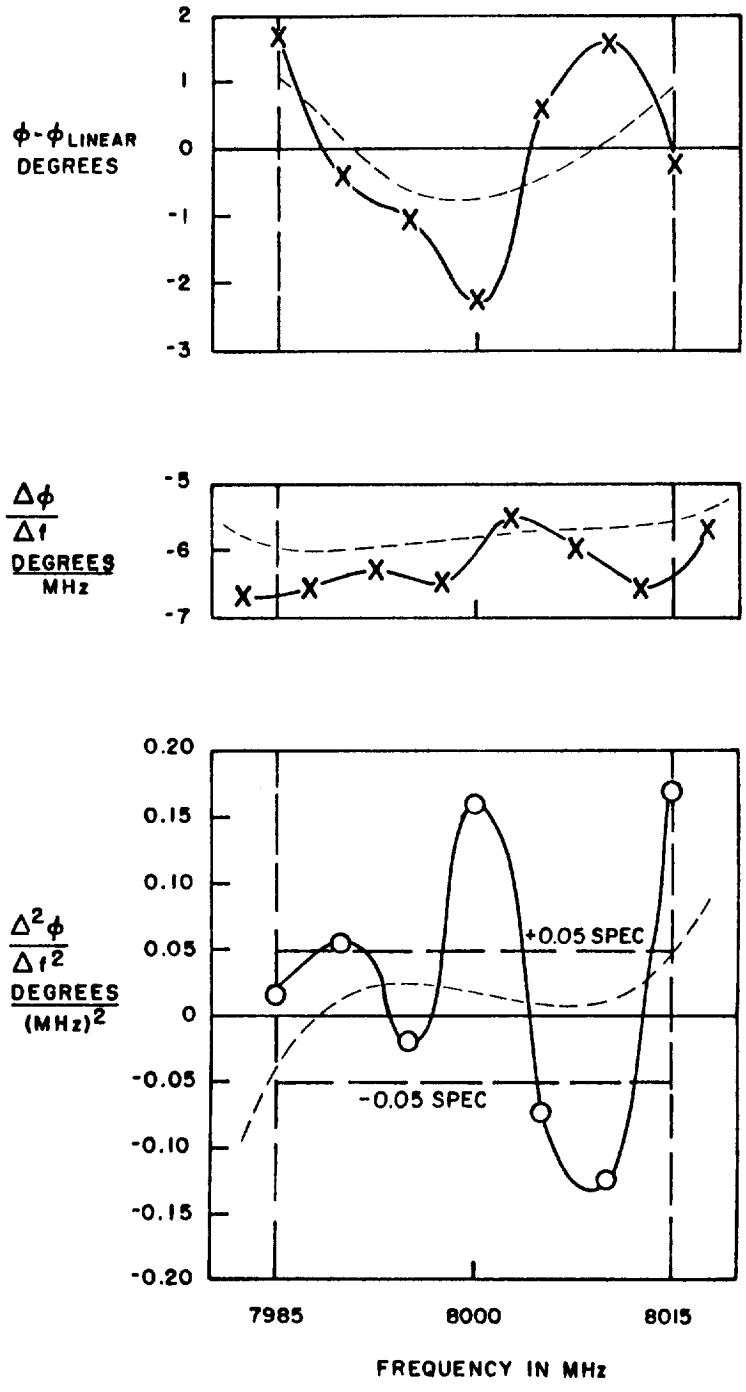

Figure 37(c) - Phase Linearity Characteristics of 8000-MHz FM Klystron

this undulation is believed to be spurious, as discussed in Appendix C. It is most likely due to the sensitive nature of the phase calculation regarding the choice of disk number under high-efficiency bunching conditions. The same effect is probably responsible for the small ripple evident in the large-signal efficiency and gain calculations in Figures 37(a) and 37(b). It would be possible to reduce the size of these undulations by increasing the number of disks in the computer simulation, but this is not practical from an economic standpoint. There is no physical reason why such undulations should appear at large-signal levels other than the granularity of the disk-electron model. Thus, the undulations are ascribed to an artifact of the model and would not appear in an experimental measurement.

11,000-MHz FM Service

The performance of the tube for 11,000-MHz FM service is given in Figures 38(a), (b), and (c). Its performance is similar in most respects to that of the 8000-MHz design. The efficiency, shown in Figure 38(a), exhibits a flatter top than that noted at 8000 MHz. This is again believed to be due to the granularity of the 20-disk computation model. The same granularity is believed to be responsible for the undulation in the second derivative of the phase shift, as shown in the lowermost solid line plot in Figure 38(c). The small-signal second derivative as given by the dashed line meets the 0.05 degree/MHz^2 specification, and it is believed that the large-signal second derivative would also meet this specification if the number of disks could be made to approach one hundred.

In Figure 39, the energy distribution of the spent beam in the 11,000-MHz klystron is shown at band center and at 5 MHz outside the two band edges. It is evident that the bulk of the electron energies fall below 0.5 V_o in the upper two graphs in this figure, whereas in the bottom graph the electron energies are more or less uniformly spread from 0.1 V_o to 1.2 V_o. The resolution of the location of the upper edge of the distribution function again depends on the number of electron disks used in the digital calculation. With 20 disks the location of the upper edge is probably not determined to better than ±25-percent accuracy because the antibunch electrons which comprise this most energetic group are spread out in phase an order of magnitude more than they were originally at the klystron input gap before the development of the density modulation. More disks are needed in the digital calculation if more accurate knowledge of the detailed spent beam energy spectrum is desired.

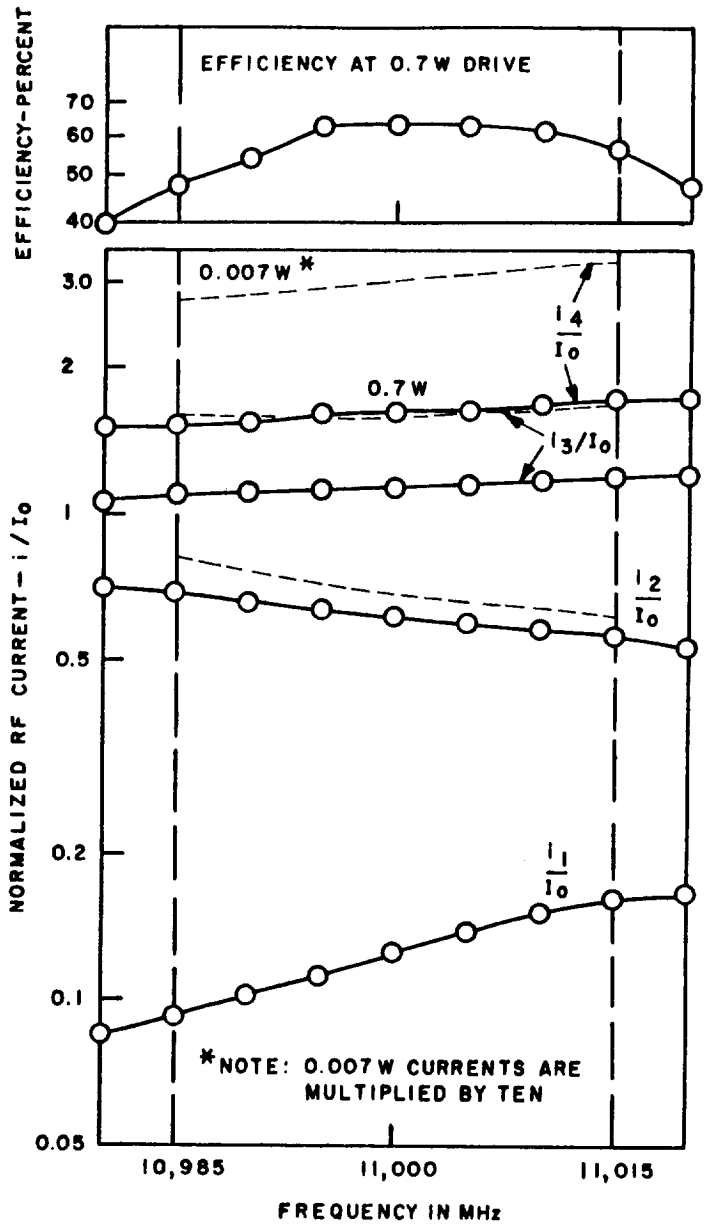

Figure 38(a) - Internal Power Conversion Efficiency and Development of Current Modulation Across the Band in the 11,000-MHz FM Klystron

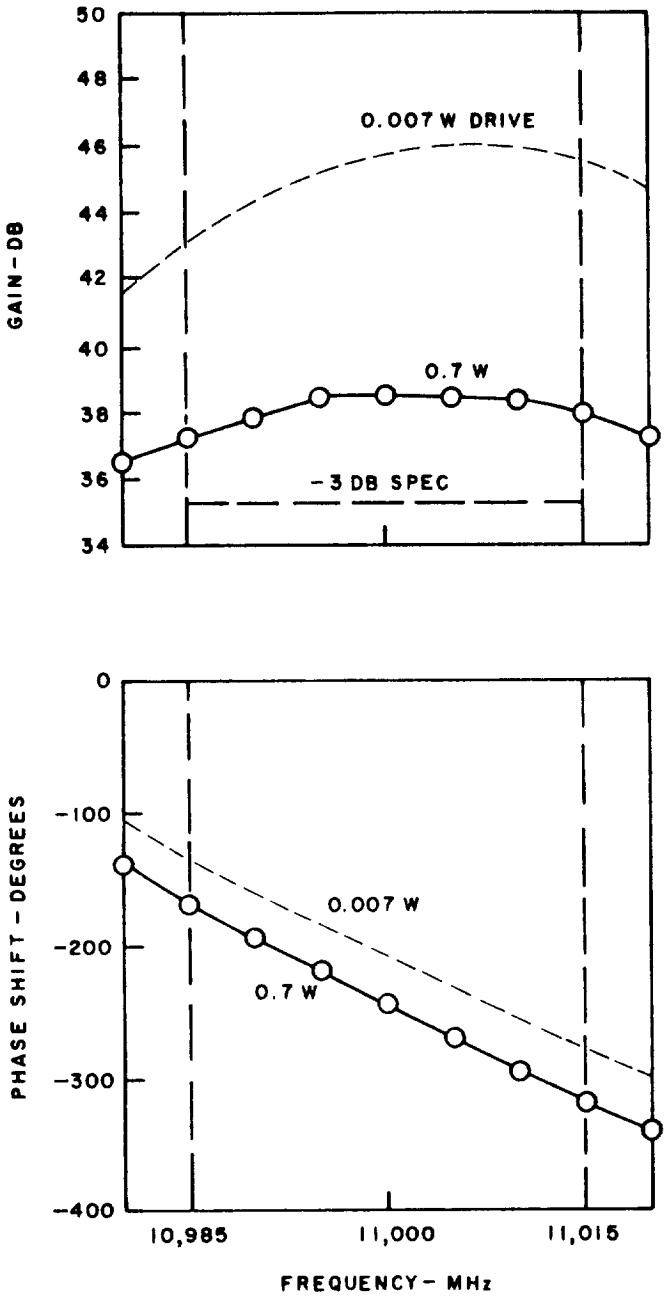

Figure 38(b) - Gain and Phase Shift Characteristics of 11,000-MHz FM Klystron

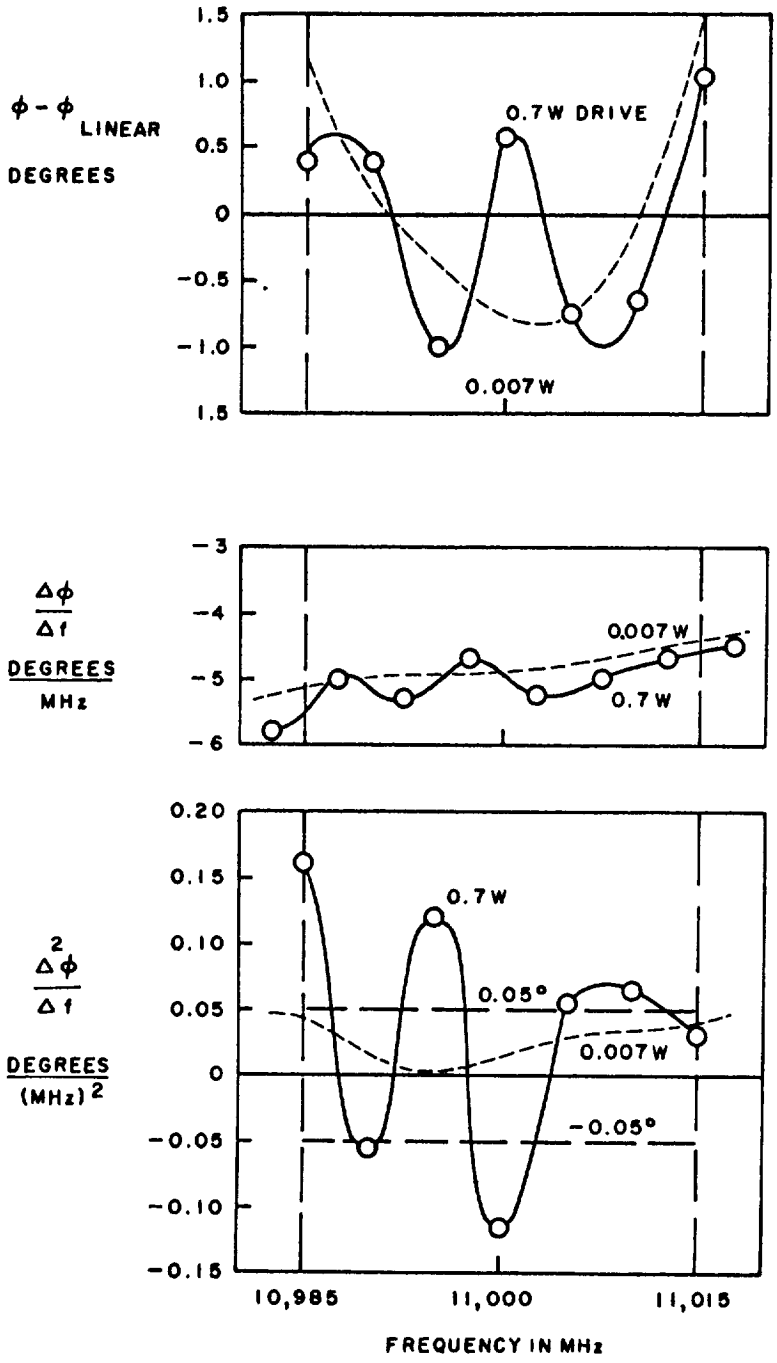

Figure 38(c) - Phase Linearity Characteristics of 11,000-MHz FM Klystron

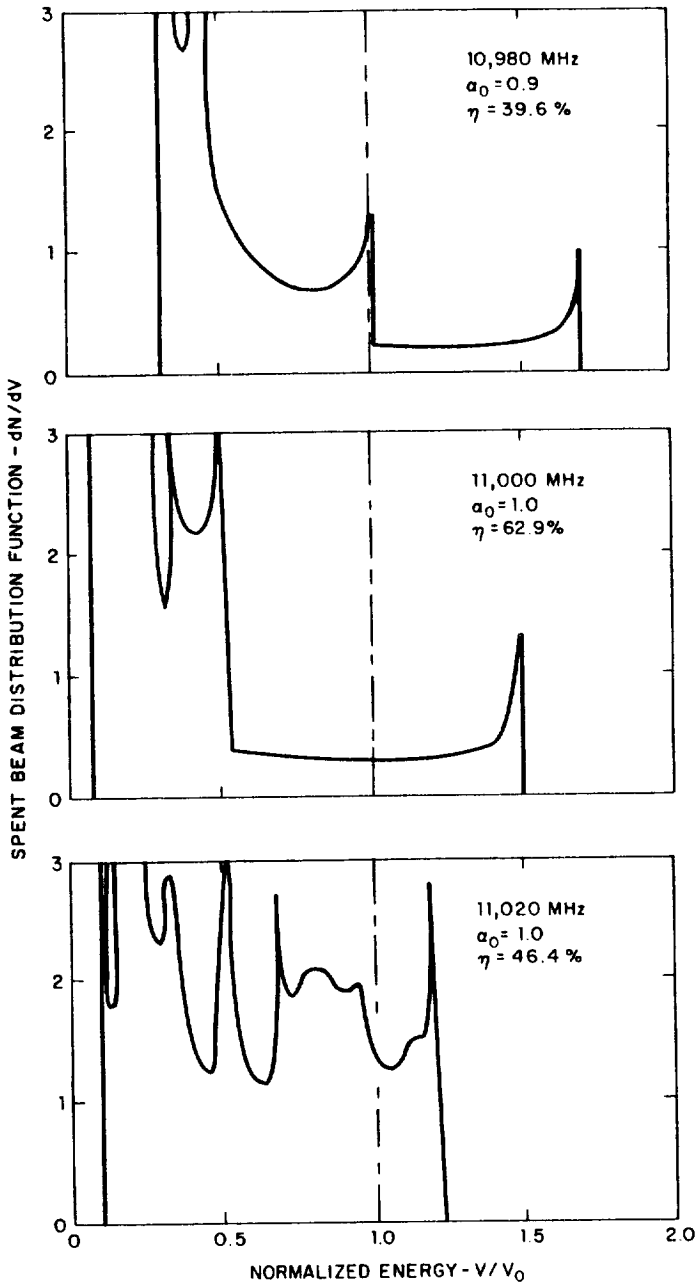

Figure 39 - Spent-Beam Energy Spectrum at Three Frequencies in 11,000-MHz FM Klystron

While the large-signal gain of this 11,000-MHz design is approximately 1.5 dB below the specified 40 dB, the actual drive power required is still less than 1 watt; hence no additional design effort was expended to attempt to reach the 40 dB value.

Section V
ELECTRON GUN DESIGNS FOR LONG LIFE AND RELIABILITY

The klystron designs developed in the preceding chapter are postulated on the feasibility of long-lived electron guns capable of producing the required electron beams. The perveance was fixed at 0.5 microamperes/(volt)$^{1.5}$ for high efficiency and the beam voltage was subsequently set to yield the required DC beam power to supply the RF power specified at an anticipated efficiency. Gun analyses were carried out to the extent necessary to show that the required electron guns are indeed feasible.

SELECTION OF CATHODE EMITTERS FOR LONG LIFE

By its very nature, the thermionic cathode is a continually depleting component of the klystron amplifier. However, by appropriate choice of materials and by optimum electron beam design, the life can well exceed the 20,000-hour minimum required for an orbiting transmitter.

The classical emitter for which the most experience is available is the barium-strontium (Ba-Sr) system in which BaO and SrO are formed from the carbonates which are spread in a thin layer on a nickel or nickel-alloy substrate. Life data on this cathode system are illustrated in Figure 40. These data are for operation in the 10^{-7} to 10^{-9} Torr pressure range. Since the low work function of this cathode is due to a monolayer or partial layer of Ba and Sr atoms resulting from the reduction of the oxides, the emission activity of cathodes with "A" nickel substrate is less than that of those with the 0.1 percent zirconium in nickel alloy. The "A" nickel is very pure and reacts very little with the oxides, whereas the zirconium in the alloy substrate is an effective reducing agent. It is noted that the desired life can be achieved if the required cathode current density can be held below 0.4 Amp/cm^2. In the topic which follows in this section, the design considerations for electron guns are presented with cathode current density requirements which can be met by the Ba-Sr system for three of the amplifiers. These are the 850-MHz and 2000-MHz designs and their operating points are indicated in Figure 40.

When current density greater than 0.4 Amp/cm^2 is required, other cathode systems must be employed. A barium-strontium system in which the oxides are embedded in a matrix of porous tungsten is often used when

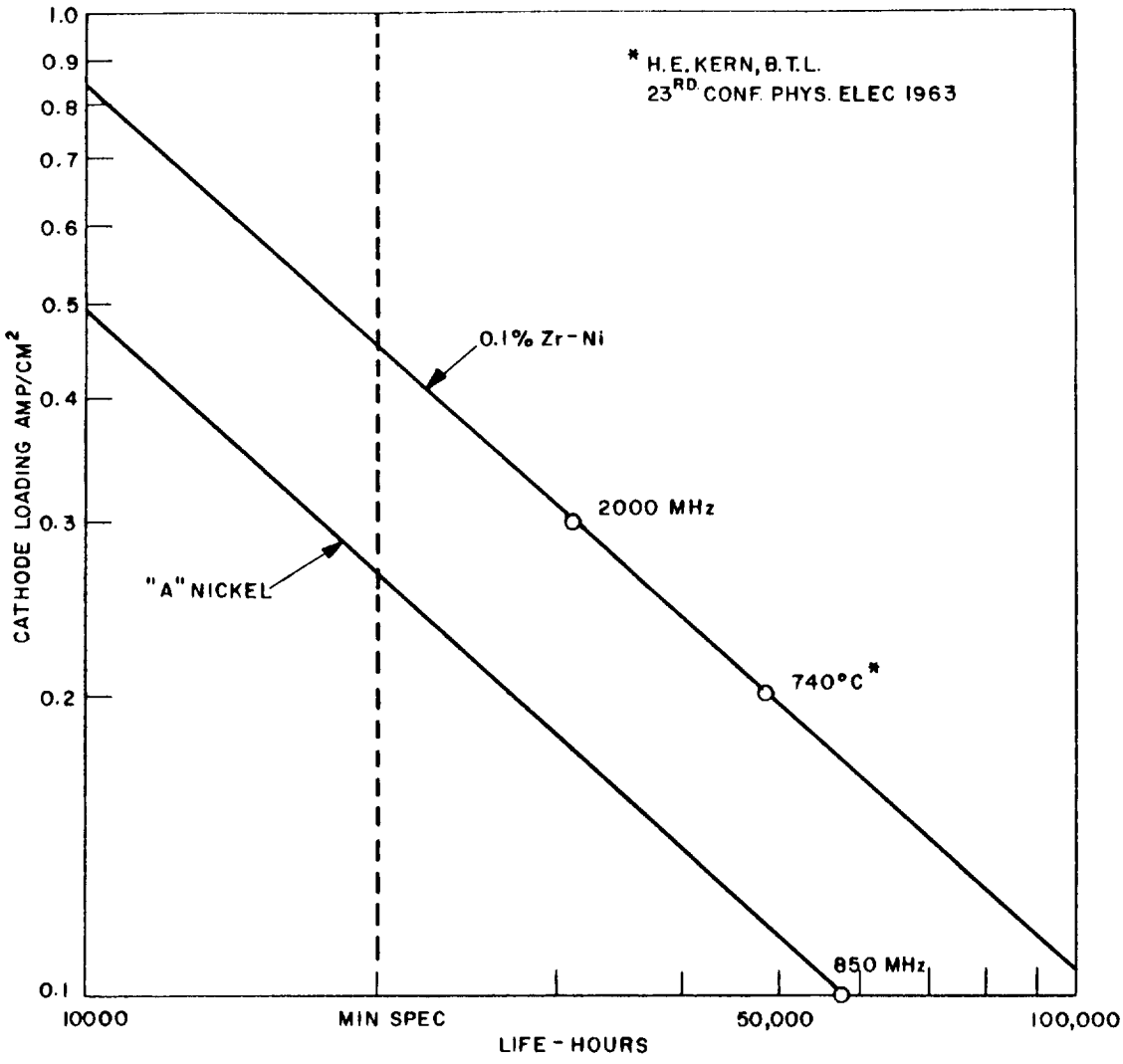

Figure 40 - Life Capability of Ba-Sr Cathode System

the emission required is in the 0.4 to 2 Amp/cm^2 range. However, its depletion rate is approximately two orders of magnitude greater than that of the Ba-Sr system on nickel, and this tends to negate the advantage of the larger mass of emitting material present in the matrix. A newer cathode system consisting of barium and calcium tungstate in a tungsten matrix has both high emission capability and low evaporation rate. These properties are illustrated in Figure 41 where the evaporation rate is related to the emission density available. Emitter temperature is not specifically indicated since it is less relevant than the evaporation rate in determining life. Note that the tungstate cathode has a depletion rate which is less than one order of magnitude greater than that of the Ba-Sr system with the lowest available rate. It should be explained that the high current densities shown for the Ba-Sr cathode are not available on a continuous basis, but are only useful for short pulses because of another property of the oxide coating; it is a semiconductor and therefore will be unstable at high average currents and may actually fail physically by cracking or flaking from the nickel substrate.

For the higher emission densities required by the 8000- and 11,000-MHz designs, a matrix cathode is indicated in order to enable the design of a feasible electron gun. While life statistics on these cathodes in power tubes are not as extensive as in the Ba-Sr oxide case, there is ample evidence that these cathodes will perform well in the klystron application. Life data on several test diodes with the tungstate cathodes are summarized in Figure 42. These data show that the desired 20,000-hour minimum life should be achieved at a temperature between 900°C and 925°C and an emission density between 2 and 3 Amp/cm^2.

All of the life data cited in this section are based on operation in vacua of the 10^{-7} to 10^{-9} Torr range. At higher pressures, cathode deactivation can be serious due to chemical reactions between the residual gas and the cathode material. This can be avoided by care in processing and fabricating the tube components. It is often desirable to attach permanently a small appendage pump to the tube to remove gas continuously that may be evolved during operation. An unanswered question concerns the merits of venting the tube envelope to the environment external to the spacecraft where pressures in the 10^{-12} to 10^{-14} Torr range have reportedly been measured. Since the cathode emission capability depends on the reduction of oxides or tungstates to form free barium or strontium, it is not known how the activity may be affected by a very low pressure environment. For the present designs, it is assumed that the tube is not vented to the space environment.

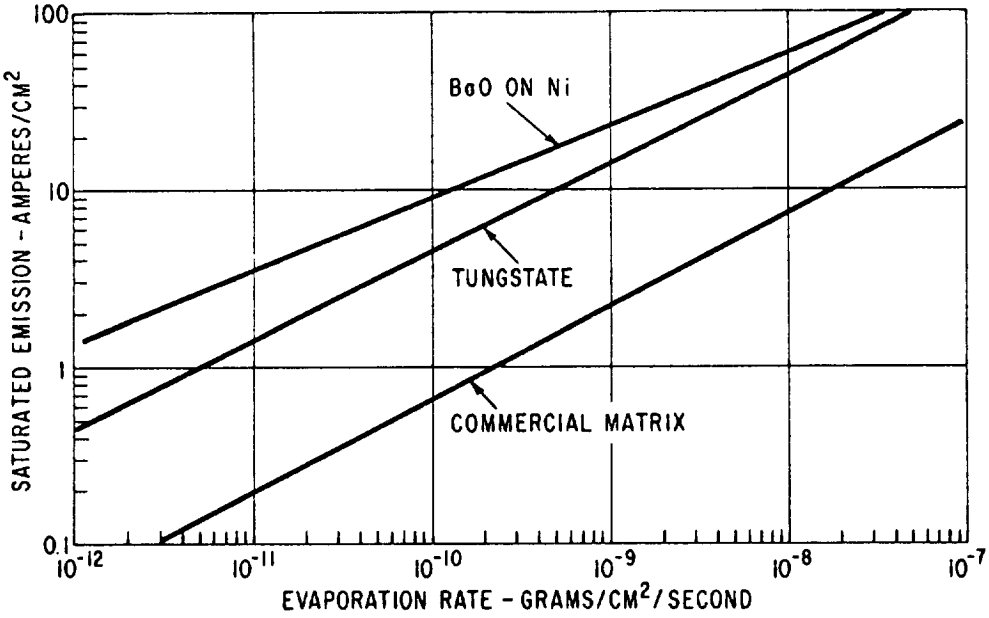

Figure 41*- Saturation Emission Capability of Three Cathodes as Function of Evaporation Rate

*Data derived from Contract AF 19(628)-279, entitled "Investigation of Various Activator Refractory Substrate Combinations" and Contract DA 28-043 AMC-02289(E), entitled "High-Current Density Cathodes"

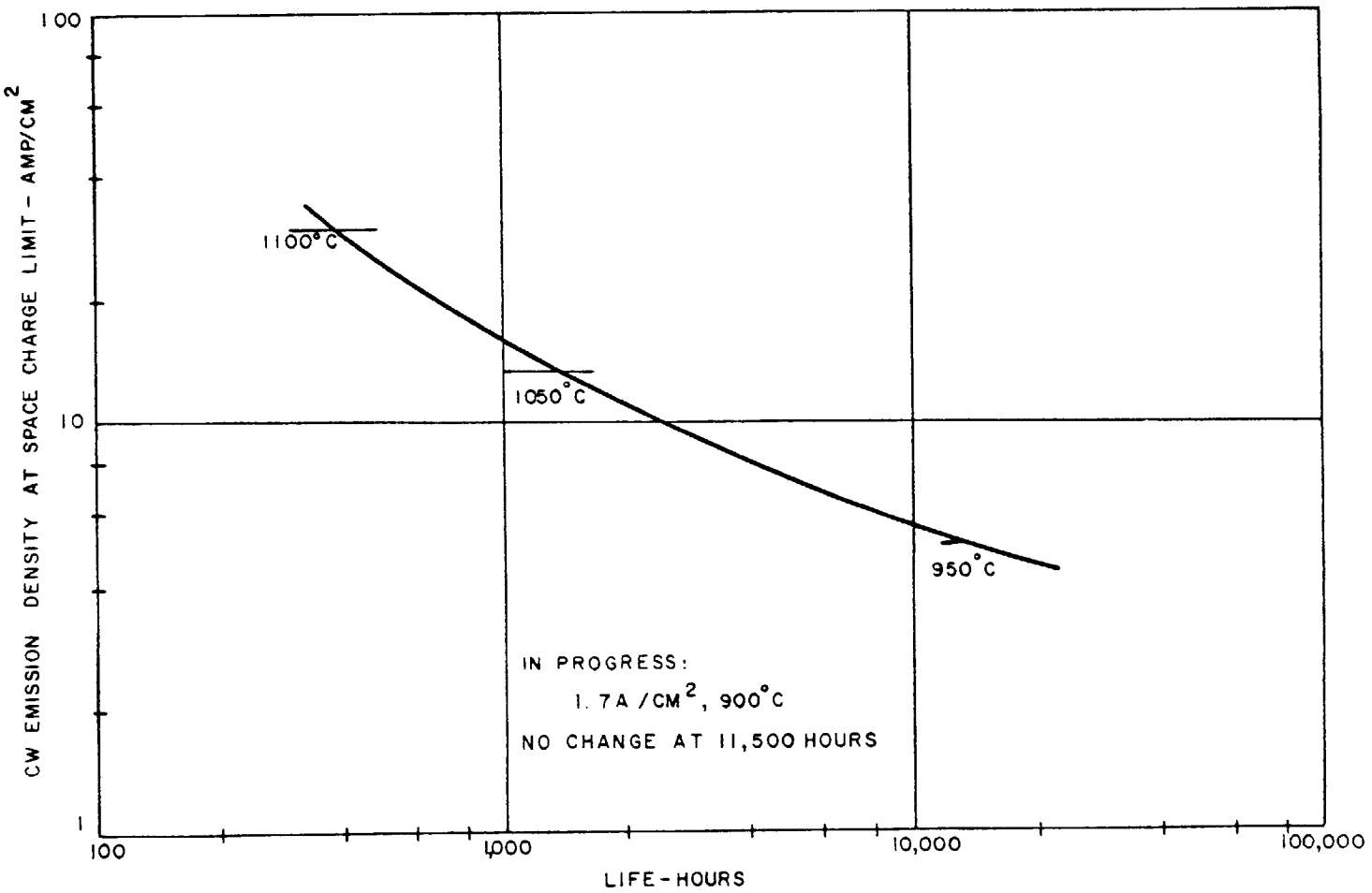

Figure 42*- Tungstate Cathode Life Test Results

*Data derived from Contract DA 28-043 AMC-02289(E), entitled "High-Current Density Cathodes"

Feasibility of Required Electron Gun Designs

Beam parameters for each of the five klystrons designed above are listed in Table V. With the beam diameter, current, and voltage given by the klystron design, the one independent parameter remaining to be determined by the gun designer is the cathode diameter. The greater the cathode diameter becomes, the less stringent are the current emission density requirements on the cathode thermionic surface, but the more difficult is the development of a gun design with uniform cathode emission density and good electron trajectory laminarity. The result of many trade-off analyses is that, in general, the cathode diameter should be made as small as possible without exceeding cathode emission densities consistent with long life. Proposed cathode diameters and corresponding beam convergence ratios are also given in Table V. The required current emission densities are all compatible with long life, using the available cathode system previously discussed.

The area convergence for the 850-MHz and 2000-MHz klystron guns is low and the required design is well within the current state-of-the-art for 0.5-microperveance guns using the Ba-Sr oxide cathode on a nickel substrate. The 8000-MHz and 11,000-MHz klystron guns, on the other hand, require an area convergence of 60, along with a change to the matrix type cathode. In order to demonstrate the feasibility of these two guns, a detailed design of the electrode configuration for the 8000-MHz klystron gun was developed and analyzed with the digital computer analysis program, described in Section III. The computed electron trajectories and equipotentials as plotted by the computer are shown in Figure 43. This preliminary design shows good convergence and laminarity at the required perveance and beam diameter. It is considered to be a feasible design for the 8000-MHz case and also a good prototype for the 11,000-MHz design.

Figure 43 also shows the effect of thermal velocities on the beam profile. The trajectory marked with "x's" is the computed beam edge profile, within which 99 percent of electrons will pass. The beam profile shown is that computed for the electrostatic gun in the absence of a magnetic field. With proper shaping of the magnetic flux threading the cathode in order to produce the desired beam stiffness, the shape of the beam down to the beam diameter minimum at about 0.7 inch from the cathode would be essentially unaltered.

Table V - NASA Klystron Gun Designs

Frequency (MHz)	850	2000	2000	8000	11,000
Modulation	AM	AM	FM	FM	FM
Anode Voltage (kV)	15.5	13.0	12.0	12.0	12.0
Current (A)	0.965	0.741	0.657	0.657	0.657
μ Perv	0.5	0.5	0.5	0.5	0.5
Cathode Diameter (In.)	1.5	0.7	0.7	0.35	0.255
Drift Tube Diameter (In.)	0.815	0.3	0.3	0.075	0.055
Cathode Magnetic Field (Gauss)	35.4	54.8	52.7	52.7	72.8
Main Field (Gauss)	353	880	846	3382	4612
b/a	0.6	0.6	0.6	0.6	0.6
Immersion (%)	94	94	94	94	94
Area Convergence	9.41	15.1	15.1	60	60
Axial Velocity Dispersion (%)	0.37	0.37	0.37	0.37	0.37
Cathode Loading					
At Edge (A/cm^2)	0.1	0.31	0.3	1.42	2.68
At Center (A/cm^2)	0.1	0.21	0.2	0.78	1.48
B/Brillouin Field	3	3	3	3	3
Heater Power (Watts)	100	60	60	30	20

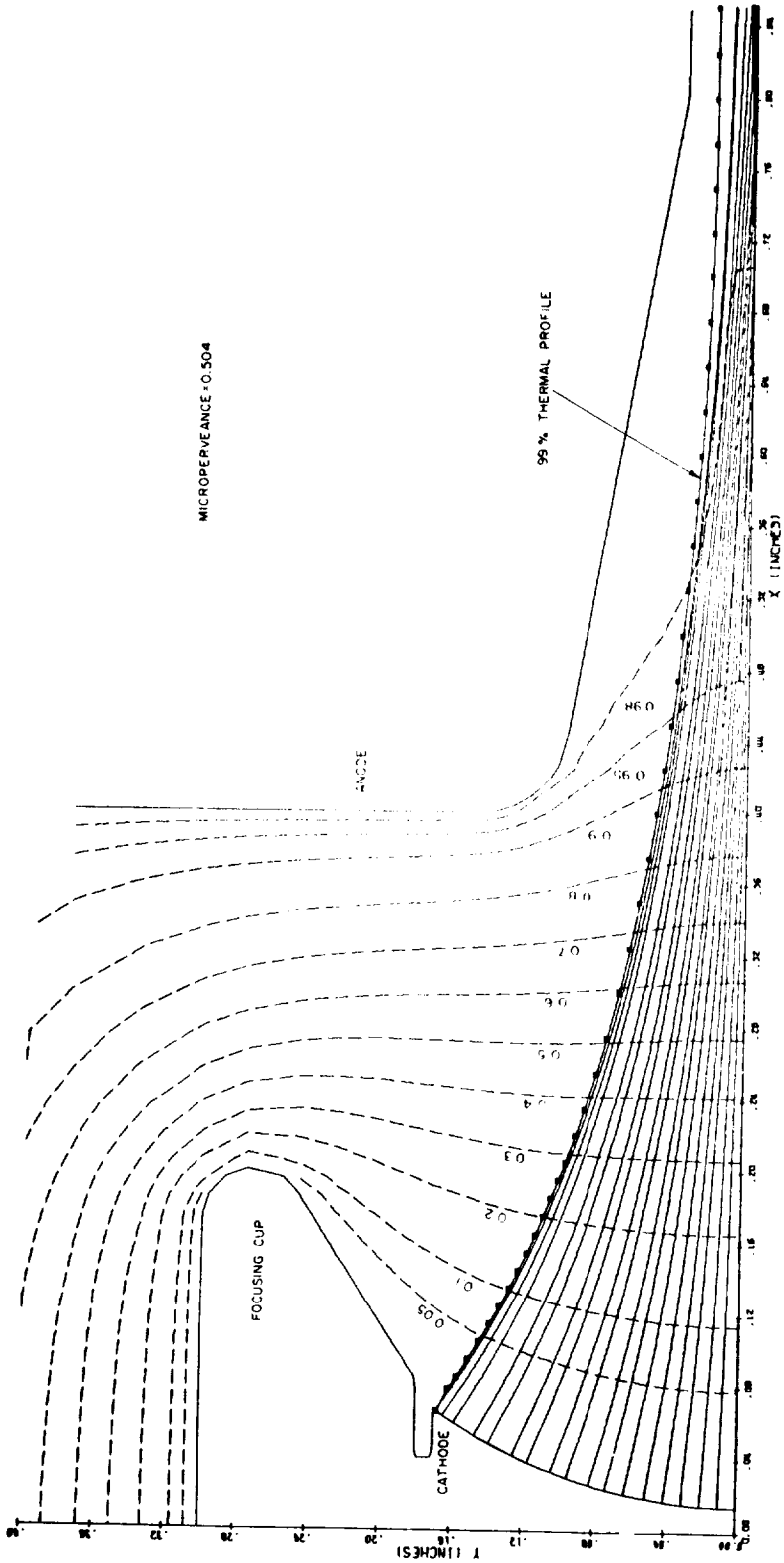

Figure 43 - High-Convergence 0.5-Microperveance Electron Gun for 8000-MHz and 11,000-MHz Klystrons

The electron trajectory calculations that were made indicate that feasible gun designs are available for all five of the klystrons. The design work was not carried beyond the feasibility stage, since this would involve construction and testing of diodes, which was beyond the scope of the present study. A generalized construction for the guns is given in Figure 44 and is shown again in the tube cross-sections depicted in a subsequent section of this report. The size and shape of the gun support structure and high-voltage bushing will ultimately be set by mechanical design considerations, particularly with respect to survival under shock and vibration. Also, in the case of PM focusing design, it will be necessary to reduce the size of the cathode housing to the minimum value in order to optimize the design of a magnetic shield for the gun and to minimize the weight of the magnet.

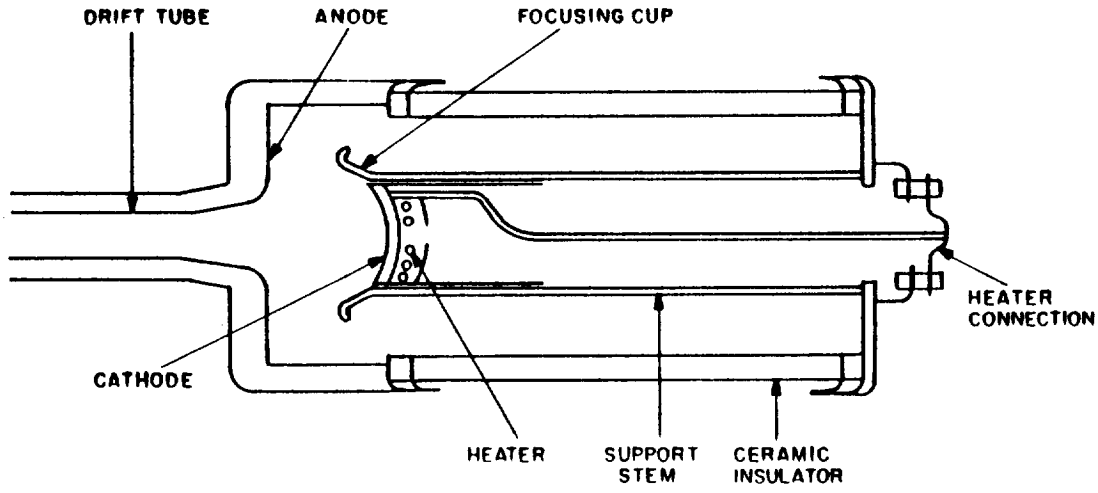

Figure 44 - Sketch of Physical Embodiment of Electron Guns for Space-Borne Klystrons

Section VI
MAGNETIC COLLIMATION OF ELECTRON BEAMS

OPTIMUM ELECTROMAGNETIC DESIGNS AND TRADE-OFFS

An optimization of magnetic field coil parameters was made keeping the total weight of the coil and its required power supply to a minimum. An arbitrary value of 100 pounds per kilowatt of coil supply power was used for this optimization. The solenoid current was fixed at 10 amperes which, for the range of solenoid powers of between 100 and 700 watts, corresponds to reasonable current and voltage levels for solar array power supplies. In accordance with good construction practice, the thickness of the foil conductor was restricted generally to the range of 0.005 to 0.006 inch, and the width was adjusted to be an integral sub-multiple of the overall solenoid length to place the impedance of the coil in the desired range. Both aluminum and copper foils were considered, and the optimum material giving the lightest total weight for each klystron was found. The foil insulation was fixed at one-half mil in thickness, and the insulator material was assumed to be either bonded Mylar*, Kapton*, or Alkanex.**

Optimum solenoids were designed not only for the postulated operating temperature of 150°C, but also for lower temperatures. The lower temperature designs require less power and are lighter in weight. However, the size and weight of the low-temperature cooling system is increased. Trade-off studies of these parameters were made.

These designs were made on the assumption that high efficiency in the klystron amplifier would require a relatively stiff beam focused with a magnetic field three times the Brillouin value of a beam of the same diameter originating from a shielded cathode. Solenoids were also designed for one and two times the Brillouin value so that estimates of the weight and power saving could be made in case experiment or more detailed analyses should prove that a less stiff beam could provide good RF performance at high efficiency.

---

* E.I. duPont de Nemours & Co., Inc.

**General Electric Company

Solenoid weights and total weights including the solenoid power supply for both aluminum and copper foil, are given in Table VI. The table indicates that aluminum is the preferred material for a minimum-weight solenoid and power supply for the 850-MHz and 2000-MHz klystrons, and that copper is preferred for the 8000-MHz and 11,000-MHz klystrons. These solenoid weights correspond to a design operating temperature of 150°C and to a design magnetic field of three times the Brillouin value. As such, they represent upper limits of magnet weights. Outline sketches of the klystrons in the focusing solenoids are shown drawn to scale on Figures 45 through 49.

The reduction in total weight of the coil and its power supply as the solenoid temperature is reduced is illustrated in Table VII. For the case of the 2000-MHz AM klystron solenoid considered, the reduction in weight as the operating temperature is decreased from 150°C to 100°C is approximately 5 pounds. This would be offset by the increased weight of the larger radiator required at the lower temperature.

The reduction in solenoid and power supply weight, if a field strength of less than three times the Brillouin value can be used, is shown in Table VIII, again for the case of the 2000-MHz AM klystron. Both the power required and the weights are seen to be approximately linearly proportional to the required magnetic field strength.

PERMANENT MAGNET DESIGNS

The electromagnet designs just described have the advantage of being adjustable so that beam transmission can be optimized. In state-of-the-art tubes, it frequently is desired to shape the field for optimum performance by control of coil currents. However, the electromagnet requires a power supply, controls, and heat removal. Although permanent magnets do not require auxiliary equipment, they do entail a greater weight and have large leakage fields, particularly in those forms which are adaptable to the large air gap geometry required by the klystron. It is necessary to magnetically shield both the gun and collector regions of the klystron when permanent magnets are used, and it may be necessary to shield the entire magnetic structure if the leakage flux will interfere with the performance of the spacecraft.

Table VI - Solenoid Weights

Klystron	Aluminum Winding		Copper Winding	
	Sol. Wt. (lbs.)	Total Wt.* (lbs.)	Sol. Wt. (lbs.)	Total Wt.* (lbs.)
850-MHz AM	66.6	133.5	90.5	181.4
2000-MHz AM	29.0	60.8	38.9	80.1
2000-MHz FM	37.6	78.1	50.9	103.6
8000-MHz FM	18.1	71.5	21.5	65.0
11,000-MHz FM	22.8	109.2	26.3	91.7

*Includes weight of solenoid power supply at 100 lbs/kW

Coil Current:	10 Amperes
Operating Temperature:	150°C
Foil Insulation:	0.0005" Mylar, Kapton, or Alkanex

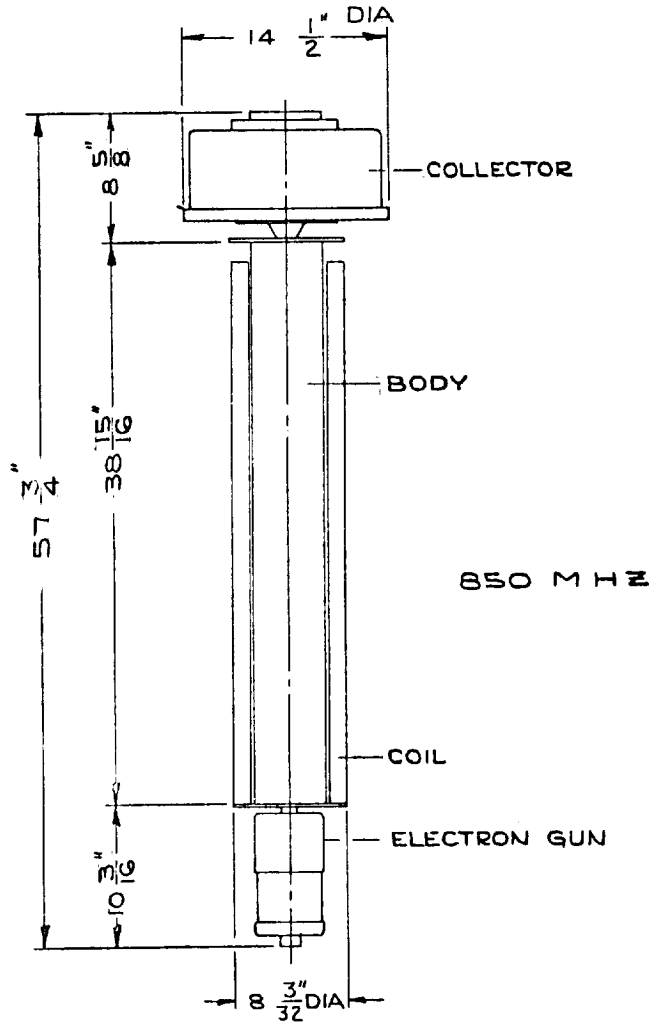

Figure 45 - Outline Sketch of 850-MHz AM Klystron in its Solenoid

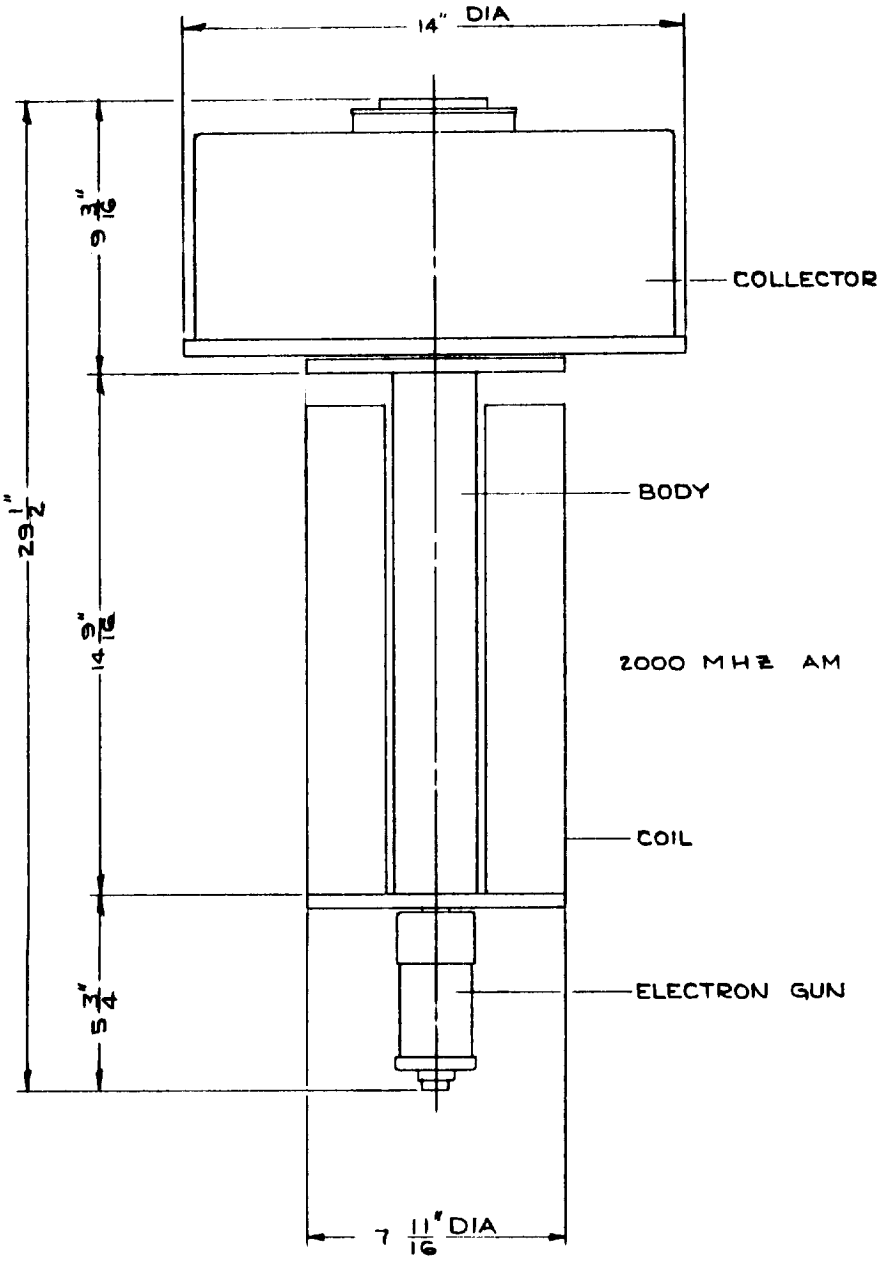

Figure 46 - Outline Sketch of 2000-MHz AM Klystron and Solenoid Assembly

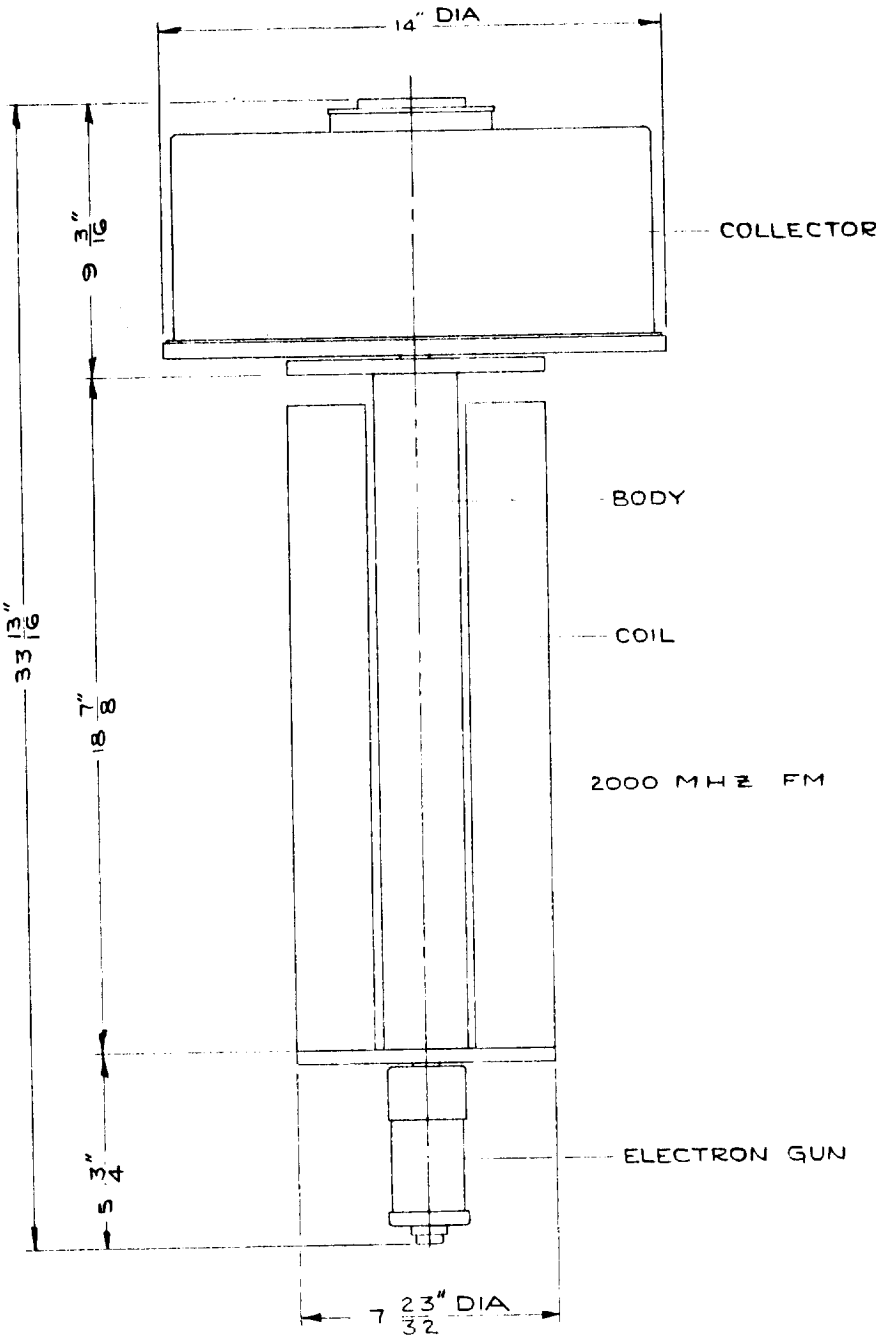

Figure 47 - Outline Sketch of 2000-MHz FM Klystron and Solenoid Assembly

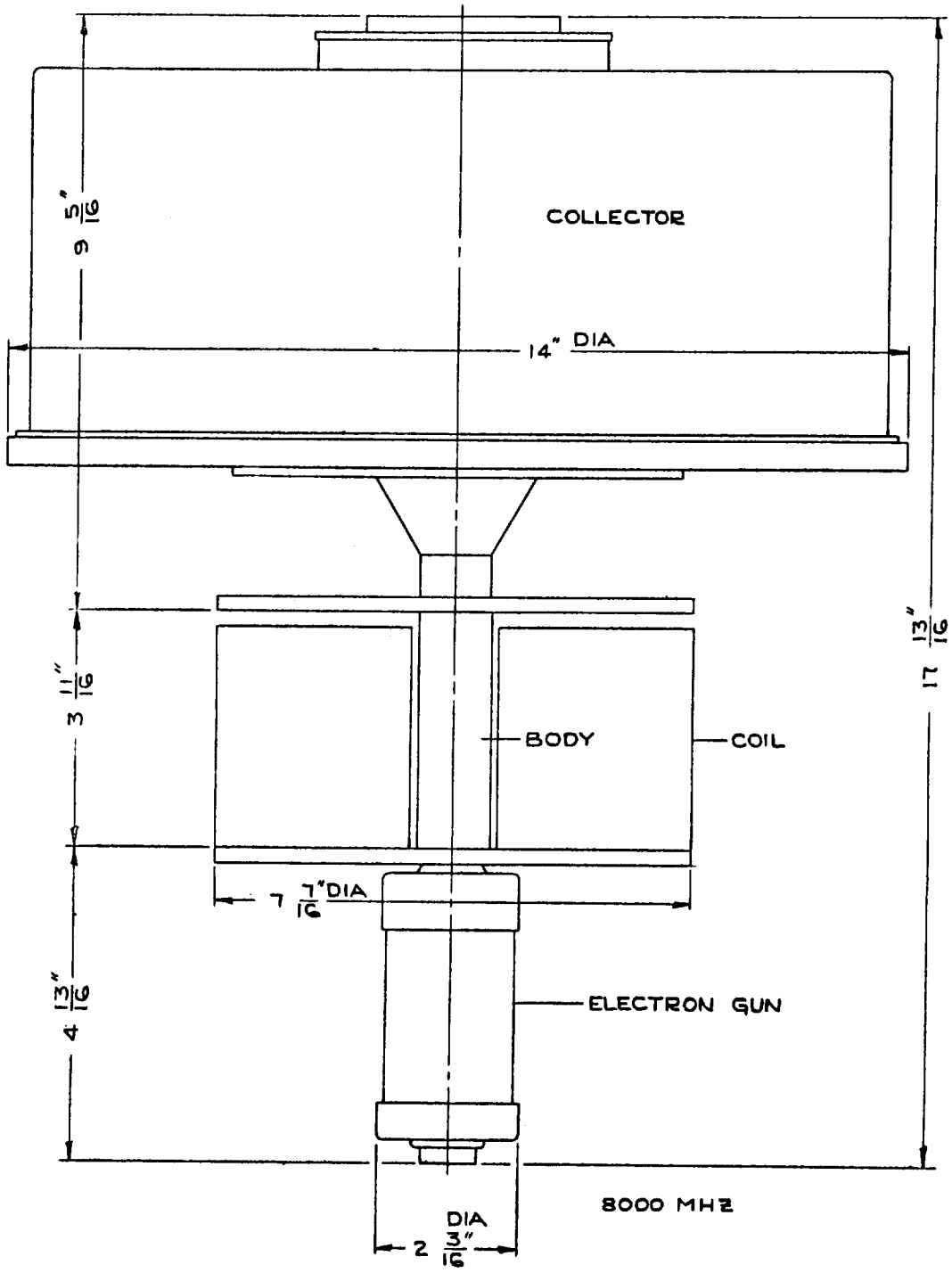

Figure 48 - Outline Sketch of 8000-MHz FM Klystron and Solenoid Assembly

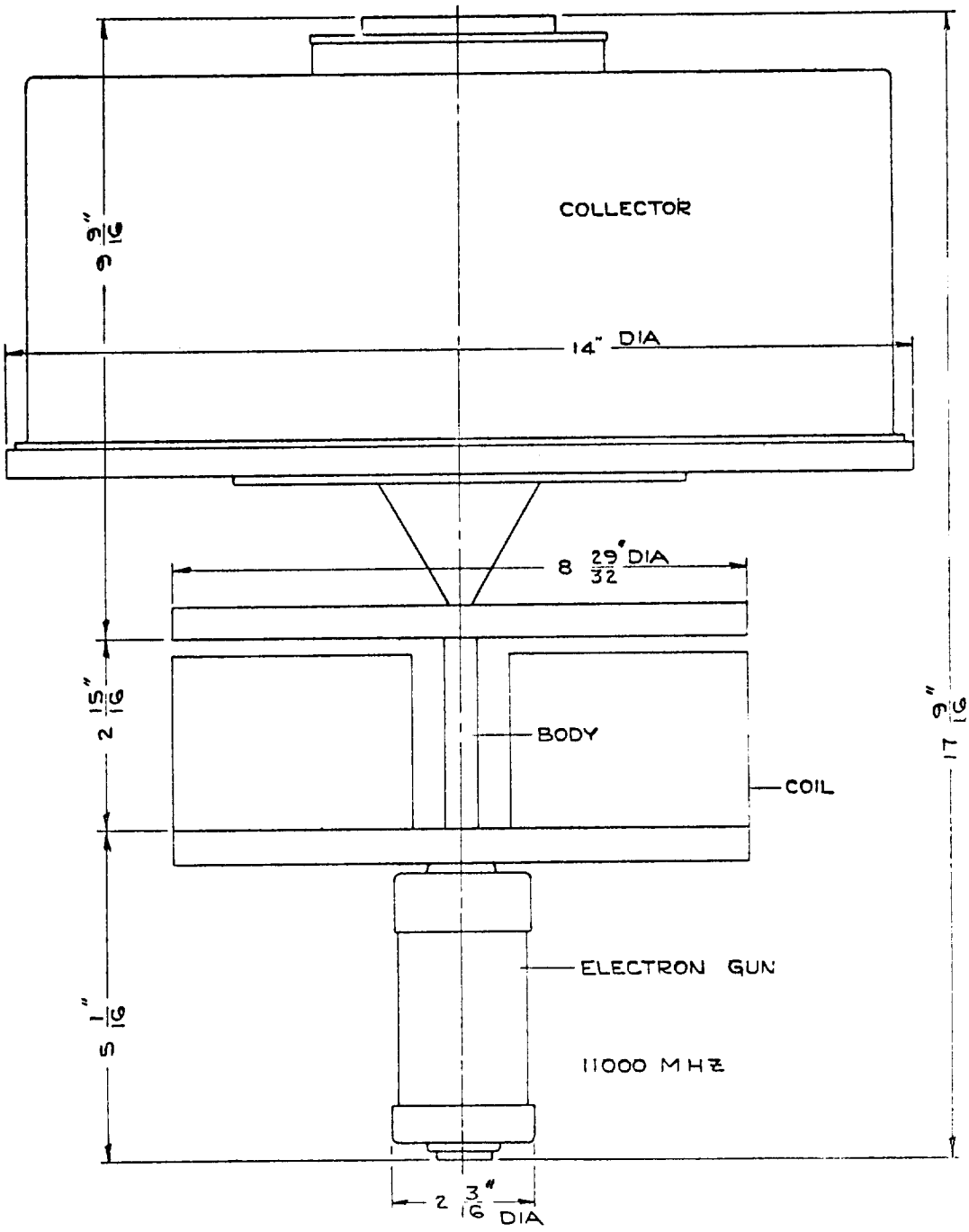

Figure 49 - Outline Sketch of 11,000-MHz FM Klystron and Solenoid Assembly

Table VII - Solenoid Parameters as Affected by Temperature (2000-MHz AM Klystron)

Solenoid Temp.	Power (KW)	Sol. Wt. (lbs.)	Total Wt. (lbs.)
0°C	0.231	21.4	44.5
50°C	0.263	24.2	50.4
100°C	0.291	26.8	55.9
150°C	0.319	29.0	60.8

- - - - - - -

Table VIII - Solenoid Parameters as Function of Required Magnetic Field Strength (2000-MHz AM Klystron)

Magnetic Field (Normalized to Brillouin Field)	Power (KW)	Sol. Wt. (lbs.)	Total Wt. (lbs.)
1	0.099	9.6	19.5
2	0.205	19.3	39.7
3	0.319	29.0	60.8

Because a stiffened beam, in which a properly shaped magnetic field threads the cathode, is considered necessary for high interaction efficiency, it is not possible to utilize magnetic structures with field reversals. Such periodic fields do have the advantage of much lower leakage field.

Permanent magnet designs were carried out for the five klystrons and the weights were computed, including such auxiliary steel pole-pieces as might be required. Parameters are given in Table IX. For the 850-MHz and 2000-MHz designs, ellipsoïdal magnets were designed, since sufficient magnetomotive force can be developed in the length of the RF structure with available magnet materials (Alnico 5 or 8). Even though the ellipsoidal shape minimizes leakage field and weight, these low frequency tubes are large, and the magnet weight is much larger than the weight of the solenoid plus its power supply. In addition, it will be shown in Section VIII that heat rejection from the solenoid is a relatively easy problem.

In the high-frequency cases, the required mmf cannot be achieved within the length of the tube structure, and a magnet structure of extended length is required. In order to achieve the magnet length, and also shield the electron gun and collector from stray fields, the structures shown in Figures 50 and 51 were devised. Here two "horn" magnets composed of Alnico 8 are mounted on the magnetic-shield disk of the collector, and the electron gun is enclosed in a steel shell. In order to minimize the weight of the magnetic material, the gun structure has been reduced in size as much as practical while still maintaining good electrical and mechanical properties. A disk of steel is located just below the collector to shield it from the field.

The major unknown in the specification of the magnet size is the amount of leakage flux in a given design. Because of the large air gap and constraints at the gun and collector, the leakage flux will be high. In the designs shown in Figures 50 and 51, the leakage factor, F, used in standard magnet design texts[31] was taken as 15. Alnico 8 was chosen as the magnetic material because of its high coercive force. A much lighter weight magnet could be obtained with a platinum-cobalt alloy magnet, but the weight of this material required would make the cost very high. Also, a significant portion of the weight of the magnetic structure is in the steel pole-pieces which will not change much with different magnet materials.

Table IX - Solenoid and Permanent Magnet Parameters

Klystron	Tube Wt. (lbs.)	Perm. Mag. Wt. (lbs.)	Solenoid & Power Supply Wt. (lbs.)	Solenoid Wt. (lbs.)	Solenoid Length (In.)	Solenoid O.D. (In.)	Solenoid Power (KW)	Foil Parameters
850-MHz FM	35.8	3400	133.5	66.6	37.33	8.094	0.669	.0055" x 2.49" Al
2000-MHz AM	28.2	405	60.8	29.0	14.26	7.683	0.319	.0055" x 2.38" Al
2000-MHz FM	36.6	655	78.1	37.6	18.56	7.725	0.405	.0057" x 2.32" Al
8000-MHz FM	8.7	81	65.0	21.5	3.466	7.436	0.435	.0046" x .866" Cu
11,000-MHz FM	8.6	257	91.7	26.3	2.711	8.885	0.654	.0053" x .678" Cu

Coil Current: 10 Amperes

Foil Insulation: 0.0005" Mylar, Kapton, or Alkanex

Operating Temperature: 150°C

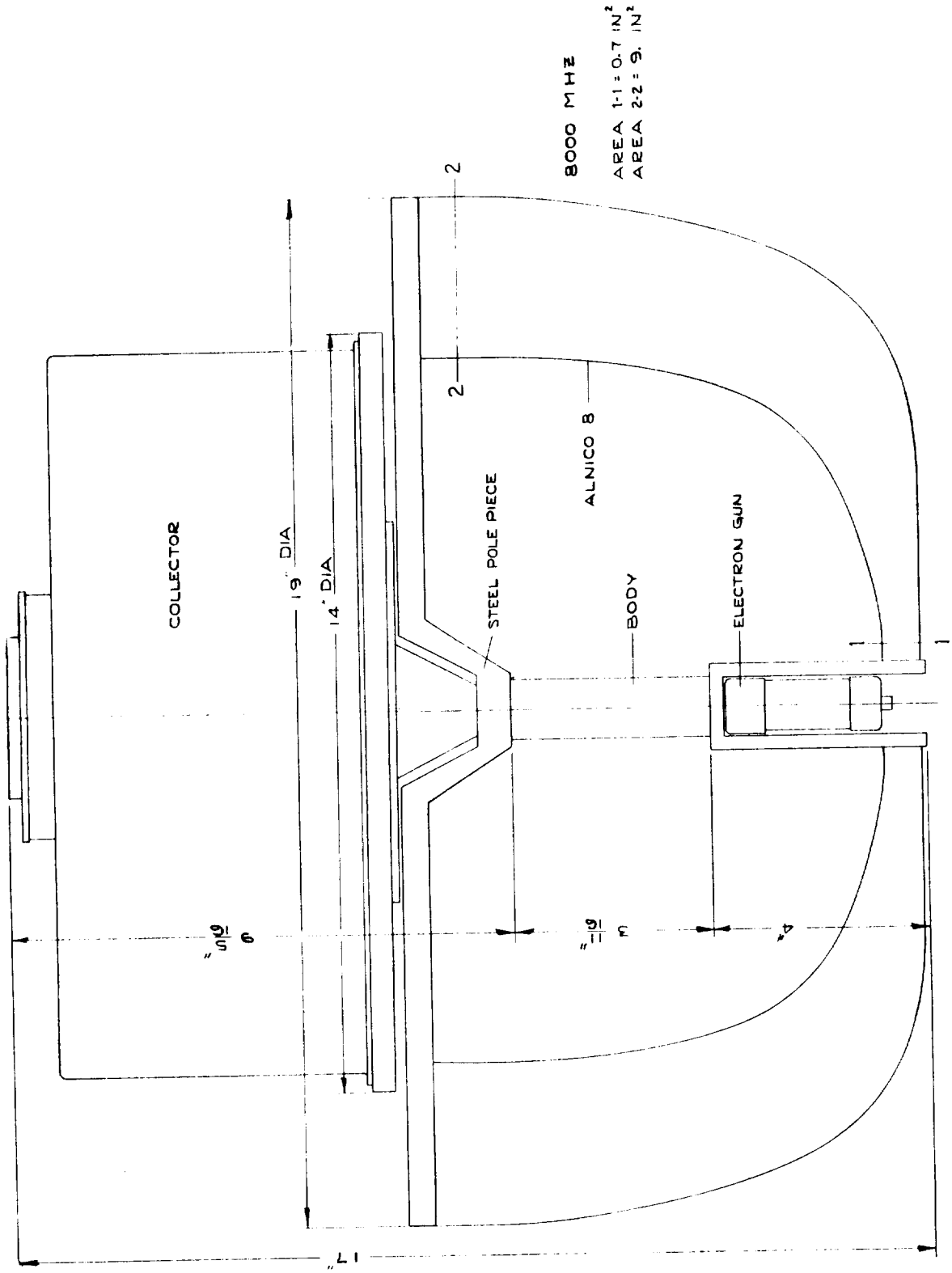

Figure 50 - Outline Sketch of 8000-MHz FM Klystron and Permanent Magnet Assembly

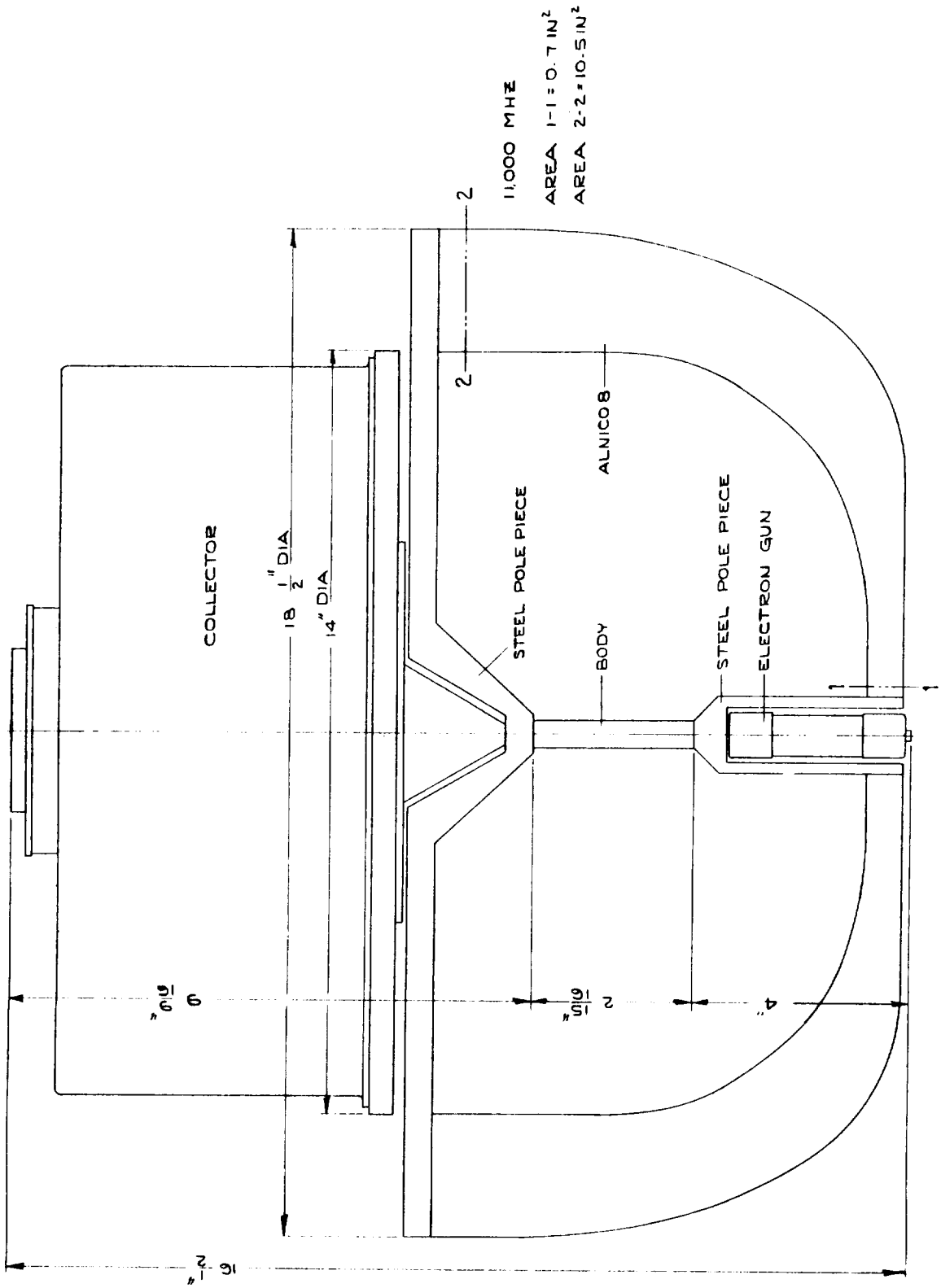

Figure 51 - Cutline Sketch of 11,000-MHz FM Klystron and Permanent Magnet Assembly

A summary of both solenoid and permanent magnet parameters is given in Table IX. The permanent magnet focusing system appears feasible for the two highest frequency klystrons, but the advantage over a solenoid system is not outstanding.

Section VII
REFLEX DEPRESSED-COLLECTOR STUDIES

The wide dynamic range of an amplitude modulated TV signal makes it imperative that some scheme be devised for enhancing the efficiency over the entire video range. A number of methods were considered, some superficially and some in detail. The final choice was the utilization of the principle of depression of potential at the collector to recover a portion of the unused kinetic energy of the beam. The idea of a velocity-sorting depressed collector has been tried several times in the past and has been found to lead to incipient instability due to electrons traveling backwards through the drift tube.[6] The depressed-collector scheme below was discovered during this study and should reduce the returned-electron problem by an order of magnitude. To distinguish it from conventional depressed-collector schemes, it has been given the name "reflex collection".

In this section, various means of enhancing AM klystron efficiency will be discussed. These will be followed by a description of the principle of reflex collection and the improvement in efficiency that results from application of this principle.

EFFICIENCY-ENHANCEMENT SCHEMES

In Table X, specified powers for various amplitude modulation levels are listed for the 850-MHz and 2000-MHz tubes. The most significant feature of this table is the relatively low power level (hence, low internal conversion efficiency) at which the tubes operate under "average picture" conditions.

Perhaps the simplest way to enhance efficiency at the average signal level is to achieve a more linear amplitude characteristic so that the entire saturated output of the tube can be utilized at the sync peak level. However, even if the characteristic could be made perfectly linear, and assuming the saturation efficiency could be made 100 percent, the efficiency under average picture conditions would range from 35 to 40 percent. This represents a limiting figure for any linearity enhancement method, and all practical schemes would fall short of this. Thus, perhaps 30 percent is a reasonable upper boundry for efficiency based on linearity enhancement scheme. This low figure does not offer much incentive for following this course of action.

Table X - AM Klystron Power Specifications

Signal	Power Level (KW) 850 MHz	2000 MHz
Saturated Output	9.5	6.25
Sync Peak	7.5	5.0
Peak Picture	3.5	2.3
Average Picture	2.6-3.0	1.7-2.0
Minimum Picture	1.3	0.9

- - - - - - -

The sync peak power is roughly twice the peak picture power and three times the average signal power (see Table X). This suggests that a two-tube scheme could be devised, with one tube operating to its full power capability in handling just that portion of the signal which carries the signal, and the second tube being switched in to generate the additional power required for the sync peak power burst. This scheme has two requirements which make it appear prohibitively difficult: (1) the signal tube must be extremely linear all the way up to its peak power output, and (2) appropriate circuitry must be developed to synchronize the output of the second tube with that of the first during the sync peak pulse. The first of these requirements appears to be impossible to achieve with a simple klystron because of the Bessel function nature of the current bunching process. Perhaps feedback schemes could be devised to linearize the amplitude characteristic, but very little is known about this type of operation. While the successful realization of this system would increase the average efficiency, the improvement would not be as great as that which might be achieved by a good depressed collector.

A third idea for efficiency enhancement was investigated in a fair amount of detail. This method involved the development of a control grid capable of modulating the beam current of a klystron at video frequencies. A constant RF drive signal would be fed into the input cavity, and the DC beam current would be modulated at a video rate. An early version of the 850-MHz tube was investigated using the small-signal program to determine the dependence of output power on DC beam current. This characteristic turned out to be very non-linear; hence, it would require development of a

video compensating network. A further difficulty was noted in that the frequency response of the tube varied with DC beam current, and hence with modulating level. To correct this variation, the cavities would require heavy external loading, thus making the beam loading a negligible fraction of the total loading. This is undesirable since it would require an increase in the number of bunching cavities and; hence, an increase in tube length.

Thus, the development of a video-grid driven klystron involves three difficult problems: (1) development of a close-spaced control grid capable of operating at video frequencies, (2) development of a network for amplitude linearity compensation, and (3) use of heavily loaded cavities, leading to longer tubes. The difficulty of solving each of these problems constitutes a strong argument against the use of this approach to enhance efficiency.

A fourth scheme that was briefly considered was efficiency enhancement with voltage jumps as observed by Walder.[2] Since the major effect of the voltage jumps appeared to be to correct the effective drift lengths from non-optimum values, it appeared that little would be gained in a klystron with its parameters previously optimized by computer analysis.

Of the various opportunities for enhancing efficiency, the depressed collector was considered to have the greatest potential. Effort was therefore concentrated on re-examining the problems which have prevented success in the earlier work.

THE REFLEX COLLECTION PRINCIPLE

The most serious problem in the design of a depressed collector is backstreaming primary and secondary electrons. These electrons carry small amounts of RF energy toward the input end of the tube and lead to instability of reflex klystron action. The higher the gain, the more effectively backstreaming must be suppressed in order to prevent instability. Even if these is not enough feedback to cause actual oscillation, the amplitude and phase characteristic of the klystron are distorted as the phase of the RF energy carried by the backstreaming electrons alternately interferes constructively and destructively with the input energy.

Thus, the most important requirement in the design of a depressed collector is virtually complete suppression of all primary and secondary electron backstreaming. To get an overall look at this problem our first approach was to run a series of trajectory plots on an analog computer for a variety of input energies. The use of the analog computer greatly speeds

up data acquisition and analysis compared to a digital computer, and hence a large variety of electrode shapes could be evaluated quickly. The main difficulty with using the analog computer is that space charge must be simulated by current injection throughout a two-dimensional array in a time-consuming process. With a view toward minimizing the error resulting from neglect of space charge, an electrode shape was chosen which created an electrostatic electric field that was large compared to the electric field due to the space charge of the electrons. This was done so that the electron trajectories would be altered only slightly when space charge was included in the calculation. That this indeed is the case was demonstrated by a digital computer run of the final design, as will be shown below.

Preliminary analog computer runs quickly showed the need for a needle-shaped electrode placed on the axis of the beam to disperse the beam radially into various velocity classes. The most satisfactory electrode shape found in preliminary runs is shown in Figure 52. The beam-dispersing electrode and the outer housing are operated at cathode potential and the drift tube, with its end plate, is V_o volts above cathode potential. The equipotentials with this arrangement of electrodes and potentials are shown by the dashed lines in Figure 52.

Under these conditions electrons were injected into the analog computation at a beam radius equal to 0.6a, where a is the drift tube radius, with energies equal to 0.5 V_o, 0.75 V_o, 0.90 V_o, and V_o. Electrons with energies greater than this initial DC value were not considered since the spectrum computed for very high efficiency klystrons exhibit few fast electrons. In less optimally-operating klystrons the outer shell of the collector should be operated at a sufficiently negative potential to retard any electron with excessive velocities. Their trajectories as determined by the analog computer are shown as solid lines in Figure 52. In viewing these trajectories, it is evident that each electron could be collected by an electrode placed at the point of deepest penetration of the trajectory, in which case nearly all of the energy of the electrons could be extracted. More specifically, the 100-percent energy particle in Figure 52 could be collected by an electrode at roughly 0.04 V_o, the 90-percent electron on a 0.14 V_o electrode, the 75-percent electron on a 0.29 electrode, and the 50-percent electron on a 0.54 electrode. Note that in all cases the particle is collected at a kinetic energy of 0.04 V_o. This energy appears as heat at the various collector electrodes, and represents the degree to which operation of the collector is not perfect. Thus, the electrode configuration shown in Figure 52 would extract all but 4 percent of the energy of all electrons injected into it, providing as many collector electrodes were used as there

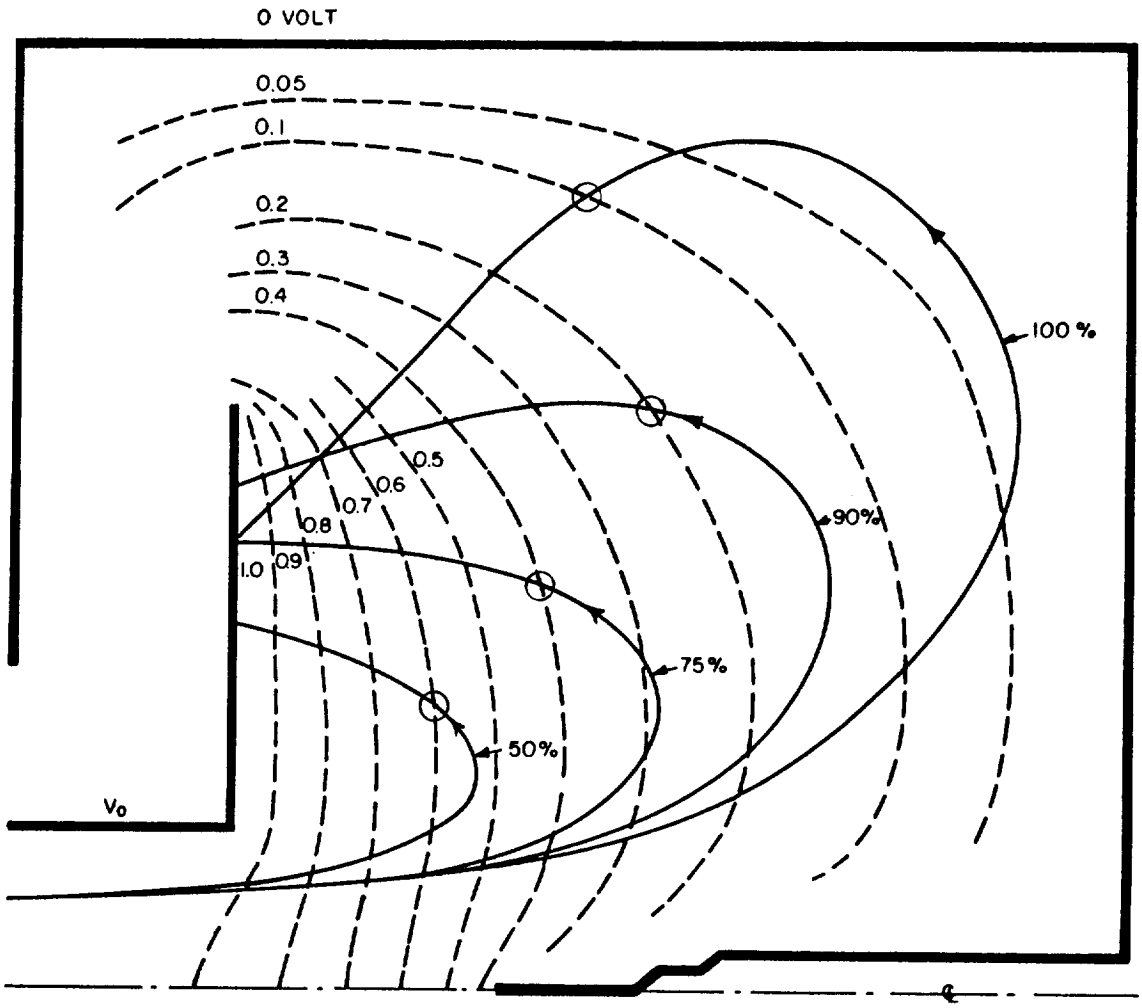

Figure 52 - Electron Trajectories and Equipotentials as Plotted by Analog Computer for Reflex Collector Simulated on Resistance Network

were electron classes injected. The fact that the excess energy of collection, 0.04 V_o, may be a coincidence for the electron configuration studied, but the larger the number of electrodes, the smaller should be the excess collection energy. In a practical case, a continuum of velocity classes is present, of course. If a finite number of collector segments are used -- for example, ten -- a given electron might just miss reaching its proper electrode and continue upward and to the left in Figure 52, traveling between the collector vanes, and be accelerated as it approaches and strikes the next higher potential electrode. This represents a gain of about 0.1 V_o in energy that is not recovered, but lost as heat.

With ten electrodes, for example, some electrons will strike their intended collector electrode perfectly, while others will just miss and go to the next electrode. These represent the two extremes; most electrons will fall somewhere in between. Thus with N electrodes, the average unrecoverable energy due to missing the proper electrode is roughly $V_o/2N$ -- e.g. 0.05 V_o for ten electrodes. If this energy is added to the 0.04 V_o energy loss described earlier, it is evident that 0.09 V_o is lost on the average in a ten-electrode collection system. This figure increases to 0.14 V_o for a five-electrode collection system. Thus, a 14-percent energy margin appears to be a reasonable figure for a five-electrode collector system. The corresponding figure for a ten-electrode system is a 9-percent margin. With a large number of electrodes, the limit appears to be a 4-percent margin with the electrode system shown in Figure 52.

The energy margin established by a given collector design affects efficiency in a very simple way. If a klystron has an efficiency η_o, the RF power output is $\eta_o P_o$, where P_o is the undepressed DC power input. With a depressed collector whose energy margin per electron is mV_o, the total energy margin for a beam current of current I_o is $mI_o V_o$. The total DC input to the tube is the sum of the RF output power and the energy margin, namely $\eta_o P_o + m P_o$. Thus, the efficiency with collector depression is simply:

$$\eta = \frac{\text{RF Output}}{\text{DC Input}} = \frac{\eta_o P_o}{\eta_o P_o + m P_o} = \frac{\eta_o}{\eta_o + m} \qquad (29)$$

This equation shows the remarkable improvement in efficiency that can be achieved with reasonable margins. For instance, a collector operating with a 10-percent margin would increase the efficiency of a 20-percent klystron to 67 percent!

The parameter m is seen to represent the unrecoverable fraction of the remaining energy in the spent electron spectrum. It is useful to define a reflex collector energy recovery efficiency as:

$$\eta_{rc} = 1 - m \tag{30}$$

Let us now turn our attention to the all-important backstreaming problem. This problem has two sources: reflected primaries, and secondary electrons. If primary electrons approach an electrode which is at a lower potential than that required to stop them, the electrons will be reflected and may return back down the beam. However, this problem is greatly affected by the choice of collector electrode configuration. A desirable shape follows the equipotential contours shown in Figure 52. These electrodes will begin at the upper left hand corner of the configuration shown in Figure 52, at which point they will be supported and insulated from one another. They will extend into the collector space along the equipotentials to a point just under the midpoint of the trajectory of the electron they are intended to collect. (A practical embodiment amenable to heat-pipe cooling is shown later in Figure 70.) In general, the primary electrons will approach their intended electrode at an angle between 45 degrees and grazing incidence. A little thought shows that with this electrode configuration, no electron can approach an electrode of higher potential that can stop it; hence the primary electron reflection problem should be reduced by several orders of magnitude. Primaries which are elastically reflected from the electrode surface should come off at an angle equal to the angle of incidence, thus elastically-reflected primaries will proceed deeper into the electrode structure (up and to the left in Figure 52) and therefore should not be a source of trouble.

Perhaps the most important feature of the depressed collector as visualized is the highly effective suppression of low-velocity secondary electrons. This comes about because with the electrode shapes described above, the primary electrons are not collected at the apex of their trajectories, but are <u>reaccelerated</u> a small amount before collection. Points of impact of electrons of various energies on typical electrodes designed to capture them are denoted by the circles in Figure 52. It is very significant to note that secondary electrons released at the surface of these electrodes see a <u>decelerating</u> field and are automatically and quickly returned to the electrode from which they emerged. Again, this suppression of secondary electrons occurs because the approaching primary electrons are not collected at the apex of their trajectory, but are actually accelerated somewhat before collection. Since the primary electrons are actually <u>reflected</u> before they

are collected, this scheme has been given the name "reflex collection". It is important to note that reflex collection involves a small additional loss of energy, typically 0.05 V_o, and this must be included when calculating overall tube efficiency. This small additional loss of energy may be considered as an investment to ensure the complete stability of the collector against returning secondaries to the klystron interaction region.

Thusfar, only four electron trajectories have been considered in establishing collector design. Analog computer runs for the same four classes shown in Figure 52 were made for a variety of input radii from 0.1a to 0.8a, and for injection angles of ±6 degrees (10-percent radial velocity). A highly significant characteristic was observed under these conditions -- namely, upon reflection, essentially all primary electrons of a given energy class focus at points in the vicinity of the circles shown in Figure 52. This is in contrast to the location of the apexes of their trajectories which are found to span several of the equipotentials shown in Figure 52. This focusing action means that the efficiency of electron collection can be high even with an electron beam of finite diameter and radial velocity components.

The variety of radial injection positions may cause some electrons to strike on the bottom, rather than the top, of the electrode which they are intended to hit. Low-energy secondaries released from the bottom side of the collector see a strong electric field accelerating them toward the left in Figure 52 due to the adjacent higher voltage electrode; hence, they again are not returned back down the beam but are immediately removed. Thus, it is expected that backstreaming of secondaries will virtually be eliminated in the reflex collector. The forward edges of the collector electrodes and the point of the needle should be made as sharp as possible, within the limits set by thermal considerations, in order to minimize the generation of secondaries. Depending upon the sharpness of the electrodes, the number of such reflected electrons should be several orders of magnitude below that of a conventional, non-segmented, forward-collecting electrode structure. Also, special coatings, such as lamp black, may be applied to these surfaces to diminish the generation of secondaries.

To make sure the essential features of the reflex collector are not altered by space charge, a digital computer run was made for a DC beam of perveance 0.5×10^{-6} injected from a cathode and passed through an anode aperture and a short drift tube into a reflex collector containing a beam-dispersing electrode but no inner electrodes. The resulting trajectories of the beam-edge electrons (shown in Figure 53) may be compared directly

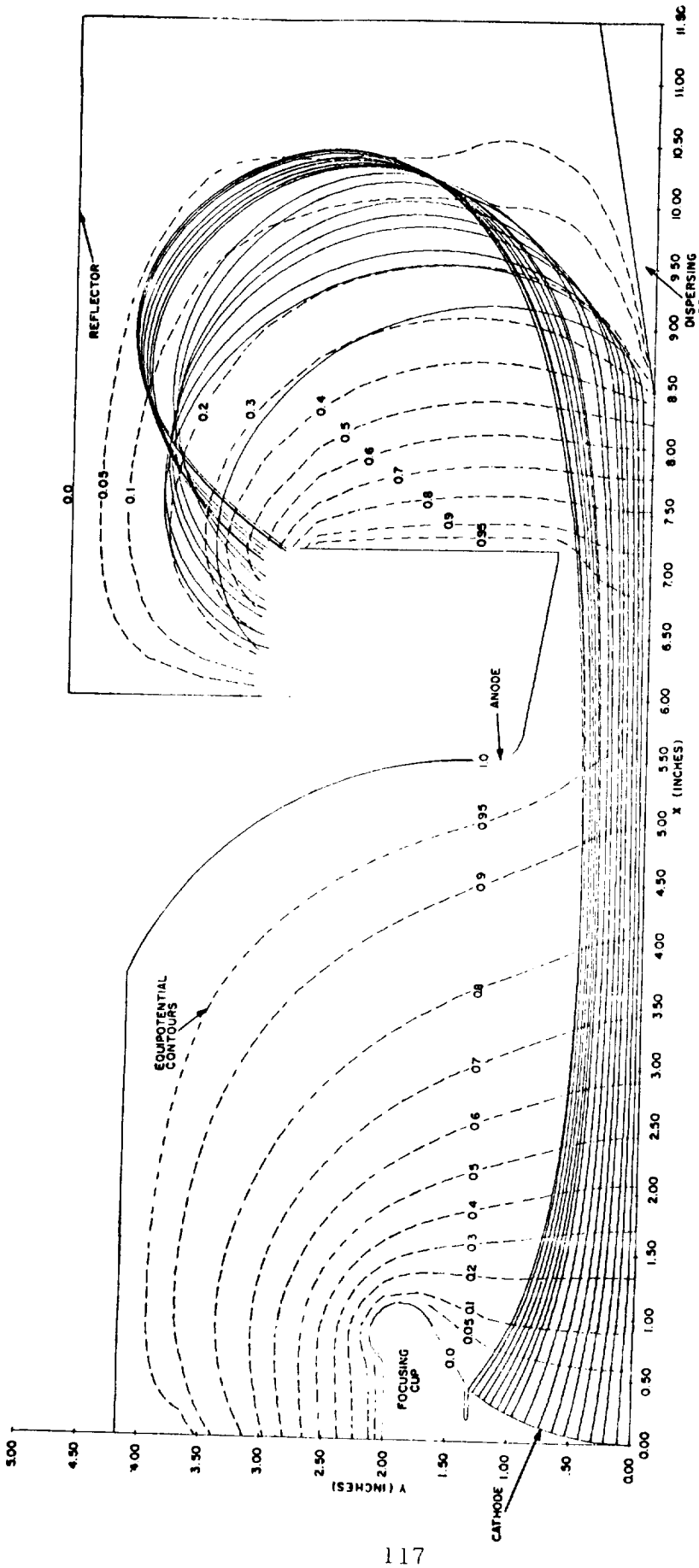

Figure 53 - Digital Computer Calculation and Plot of Trajectories and Equipotentials in Presence of Space Charge in Reflex Collector with Beam Injected from an Electron Gun

with the non-space-charge trajectories of Figure 52. It is evident that there is only slight distortion of the equipotentials, and the trajectories are virtually the same in the two cases. Thus the presence of space charge will influence the collector only slightly. (Note that the phenomenon of reflection-focusing is clearly evident in Figure 52.)

The reflex collector has another advantage which deserves mention. In a magnetically-focused klystron, the electron beam is collimated by a longitudinal magnetic field which is usually removed just before the collector by means of an apertured magnetic plate. It is difficult to eliminate small stray magnetic fields in the collector, however. Since the reflex collector described above is axially symmetric, the presence of a stray magnetic field will simply cause a small angular rotation of the electron trajectories, which should not interfere in any way with the operation of the collector. This is in contrast to schemes in which a transverse magnetic field is used to sort the beam in the collector. An extremely careful magnetic shielding job is required in this case to eliminate interaction between the sorting field and the main field, since the former is transverse and the latter is longitudinal.

Section VIII
THERMAL ENVIRONMENT CONTROL

REQUIREMENTS FOR THERMAL CONTROL SYSTEM

For the purpose of thermal control, the klystron is made up of five major elements, each having different requirements. Specific limits for these elements are as follows:

(1) Collector: The depressed collector, shown in Figure 54, has two heat sources -- the beam disperser (350 watts) and the collector elements (2250 watts). The metallic portions of both the beam disperser and the collector must be maintained below 1000°C, and metal-to-ceramic seals cannot exceed 700°C.

(2) Output Cavity: The power dissipated in the output cavity is considerably higher than for the buncher cavities and thus must be considered separately. Cooling must be adequate to maintain the tunnel tips below 400°C.

(3) Input and Buncher Cavities: Input and buncher cavity power dissipation is low and can be removed either individually or in conjunction with the output cavity. The temperature limit is 400°C on the tunnel tips.

(4) Electron Gun: Thermal control of the electron gun is primarily concerned with preventing thermal interaction with other portions of the klystron or the spacecraft.

(5) Field Magnet: Power dissipated by field coils must be radiated at a temperature low enough that the inside surface of the coil does not exceed 150°C. Permanent magnets must be maintained below 200°C.

In addition to the above limits, deviation from design temperature will cause bandpass distortion. Figure 55 shows the maximum temperature deviation allowable for a klystron with 20 percent excess bandwidth. This represents a "worst case" condition. Values shown for expected excursion can be brought to almost any desired limit using louvers, phase change materials, or a coating with a strongly temperature-dependent emissivity.

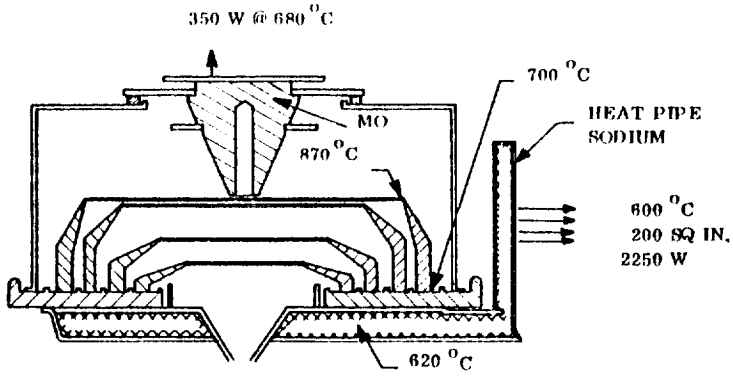

Figure 54 - Heat Pipe Cooling System for Multi-Potential Reflex Collector

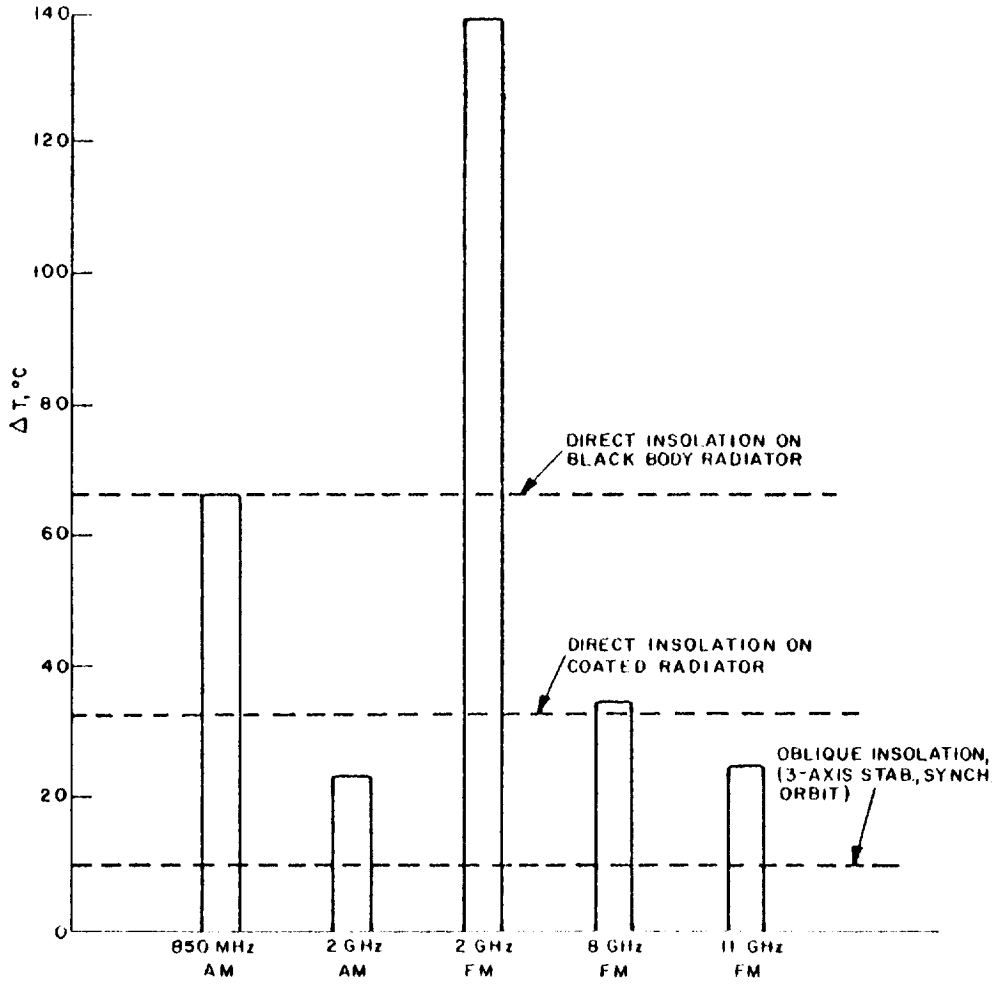

Figure 55 - Maximum Allowable Temperature Excursion for Klystron Constructed with Copper Cavities and Having 20 Percent Excess Bandwidth

THERMAL CONTROL TECHNIQUES

The design of high-power transmitter output devices intended for use in space vehicles must include consideration of certain thermal problems peculiar to space operation. Since radiation is the only practical long-term means of rejecting power dissipated by these components, a radiating surface must be provided. Heat flow paths must then be included to move the heat from the output device to the radiator. Due to limitations on geometry and the magnitude of the dissipation, excessive temperature differentials are caused by conduction even through materials having the highest thermal conductivity. Thus, some type of thermal transport system -- an active liquid loop or a heat pipe -- must be used. Since the active loop requires electrical power to run the pump and is heavier than a heat pipe system, it will not be considered in detail in this report. The merits associated with each of the cooling methods considered are discussed in the paragraphs which follow:

Active Thermal Control

An active thermal control system consists of a fluid pumped through a closed loop. At one point the fluid absorbs heat from the source. The fluid then flows through a radiator where the heat is rejected to space. Trade-off studies must be made for specific design parameters in order to optimize a system. Higher liquid flow rates provide higher heat transfer coefficients between the fluid and pipe wall and reduce the fluid temperature rise required to move a given amount of heat. They also, however, require more pump power. Optimization may be based on weight, pump power, or volume, whichever is considered most important for a given application. Systems design for Bios and Apollo indicate that the pump power requirement is from 3 to 6 percent of the cooling load. Radiator weight for an active system is approximately the same as the weight of a heat pipe radiator, but the pump weight and solar array weight make the total higher. The higher weight plus the relatively low reliability of the pump make the heat pipe by far the best cooling technique for high-power thermal systems.

Heat Pipes

The heat pipe is a device which uses the phase change of a fluid and capillary action to provide an extremely efficient heat flow path. Heat added to the evaporator surface causes liquid to vaporize. This, in turn, causes a pressure gradient which forces vapor from the evaporator to the condenser, resulting in a vapor density in excess of equilibrium conditions. The excess

vapor condenses, thus transporting an amount of heat equal to the product of the mass transferred and the latent heat of vaporization of the fluid. Condensate is returned to the evaporator by means of a wick.

The design of a heat pipe is dependent on several parameters. First, the working fluid is chosen on the basis of its saturation pressure and performance characteristics at the operating temperature, and on the basis of compatibility with the container and wick. Figure 56 shows the saturation pressure, and Figure 57 the computed performance characteristics for several selected fluids over a range of temperatures. The fluid should have a maximum wicking parameter and a pressure which makes it easy to contain. The freezing point of the fluid should be below the lowest temperature that would be encountered, either operating or non-operating. The vapor density should be high enough that the vapor velocity is considerably below choke flow velocity.

The temperature drop in a heat pipe is the total of several individual drops, of which the most significant are due to conduction through the wall and wick in the evaporator and condenser, and the liquid-vapor drop in the evaporator.

Heat pipe capacity is determined by the cross-sections of the vapor and liquid channels and the power density in the evaporator and condenser. Since the condenser is considerably larger than the evaporator in cooling configurations, condenser limitations are unimportant for the purpose of this study. The required heat pipe cross-section for low thermal conductivity fluids can be estimated from the semi-empirical equation:

$$Q_{max} = 6 \frac{A \sigma \lambda}{L} \qquad (31)$$

where:
- A = cross sectional area (m^2)
- σ = surface tension (kg/m)
- λ = latent heat of vaporization (Joules/kg)
- L = heat pipe length (m)
- Q_{max} = maximum heat transfer (kW)

Because of the danger of local liquid burnout, the power density in the evaporator should not exceed 50 W/cm^2 unless a larger limit is experimentally demonstrated.

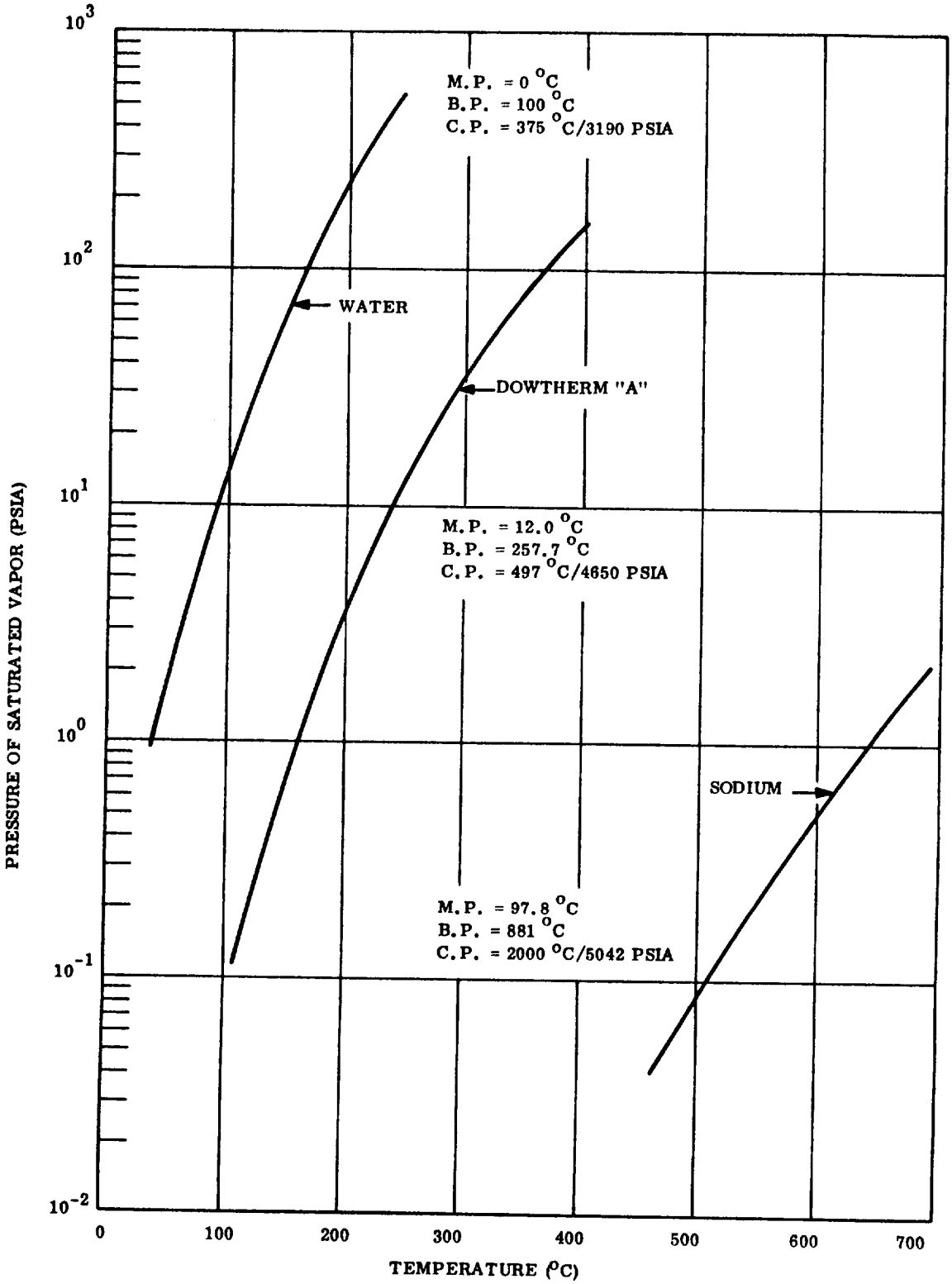

Figure 56 - Vapor Pressure versus Temperature Characteristics for Several Heat Pipe Fluids

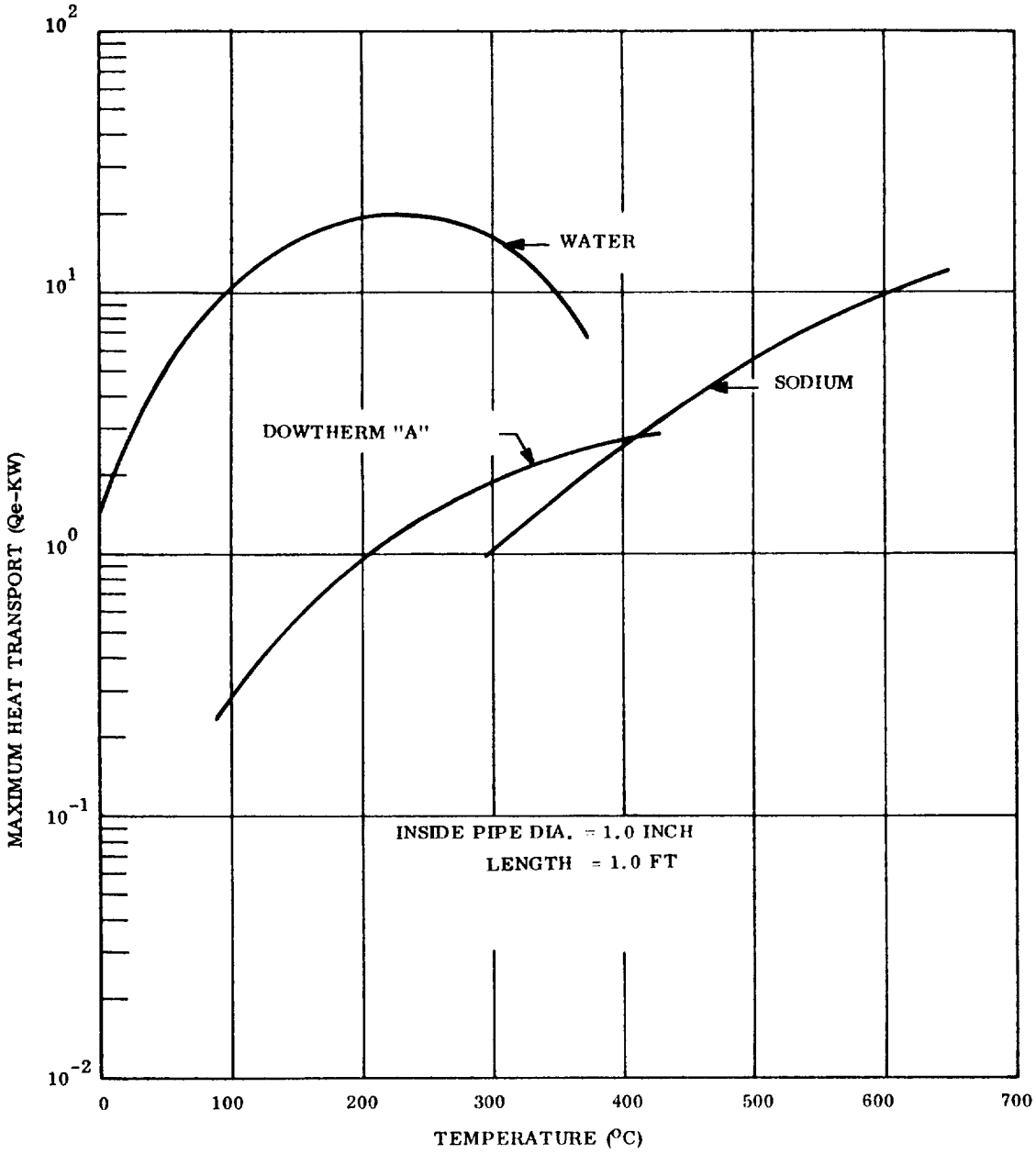

Figure 57 - Maximum Heat Pipe Capacity versus Temperature for Several Fluids

The heat pipe is an extremely reliable device. The probability of continued operation for long time periods can be placed at almost any desired level by adjusting the wall thickness or providing shielding to protect against meteorid penetration.

Heat Conduction

Conduction of large quantities of heat from the heat source to the radiator causes large temperature differences. The larger the difference is, the lower the radiating temperature must be to maintain the component below its maximum temperature limit. Under some conditions, conduction alone is inadequate to transfer the required amount of heat without requiring an unattainable radiator temperature. Here there is no choice but to use heat pipes or an active loop. In some instances, however, the use of conduction paths and their increased weight must be traded against the increased complexity, reliability, and cost of other devices.

Radiators

Some of the radiation devices used to cool the klystrons in this study are direct radiators or direct condensing vapor fins, and thus the radiated power simply follows the fourth power of the temperature. Where conduction fins are used, however, the drop in temperature as distance from the heat source increases causes a reduction in the quantity of heat radiated per unit area. In this study, all fin calculations were made by a GE-605 computer program using published[32, 33] analyses. The fin is optimized to minimize weight. A summary of area and weight requirements of a weight-optimized heat pipe fin system is given in Figure 58. The values are given for heat pipes attached parallel to each other and equally spaced. No consideration is given to the means of conducting heat from the heat source to the heat pipes on the radiator, since this is a function of the geometry and other restraints imposed by the particular klystron being cooled.

Coatings having a high emissivity and low solar absorptivity are used on the radiator surface to maximize radiation and minimize the temperature excursion caused by solar impingement. A means of controlling temperature during periods when the klystron is not operating will also have to be selected -- heaters, a heat storage material, thermally actuated shutters, a temperature control heat pipe, or a temperature dependent emissivity coating. Since the selection of a temperature control device will depend on several parameters other than the heat source, a description of each is given below to briefly outline their capabilities:

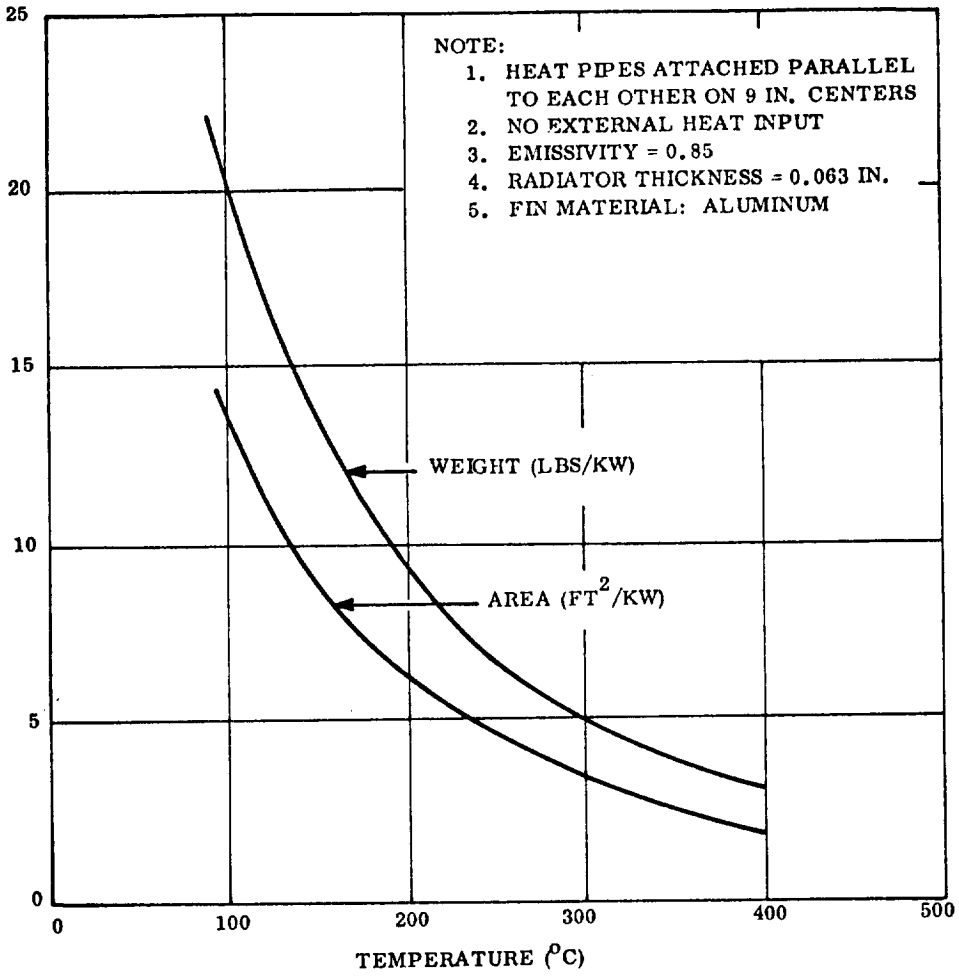

Figure 58 - Heat Pipe Radiator Requirements, Weight and Area versus Temperature

(1) Heaters: When the klystron is not operating, heat is supplied to the radiators to maintain some minimum temperature imposed by the klystron itself or by the temperature control system (e.g., the freezing point of a heat pipe fluid).

(2) Heat Storage Material: A heat storage material absorbs heat while the klystron is operating and releases it when needed to maintain some minimum temperature. To minimize the weight of such a system, a phase change material can be used which absorbs heat equal to the latent heat of fusion at its melting temperature. Such systems, however, are heavier than other temperature control devices.

(3) Shutters: A shutter or louver system exposes more or less of the radiator to vary the emittance of the system. The shutters can be actuated by electrical or mechanical devices with either a step or proportional response to temperature. A 6-to-1 change in emissivity can be achieved from the full-open to full-closed positions.

(4) Temperature Control Heat Pipe: This device is a heat pipe with a large-volume (relative to the volume of the heat pipe) container attached to the condenser end and filled with an inert gas. Diffusion of the heat pipe vapor forces the inert gas toward the condenser end. The interface between the vapor and the inert gas is quite sharp, thus causing an abrupt drop in temperature at some point along the heat pipe. If more heat is fed into the evaporator, the interface is moved farther along the pipe, thus heating more of the pipe. By attaching a fin to the heat pipe, temperature control is maintained because more or less of the fin is heated, depending on the power input. The degree of temperature control is a function of the ratio of the inert gas container volume to the volume of the heat pipe condenser. Temperatures can be controlled to a few degrees over very wide power levels using such a system.

(5) Temperature Dependent Emissivity Coatings: Due to the shift in the black body curve with temperature and the spectral reflectance characteristics of some coatings, a strong change in emissivity is exhibited as a function of temperature. Over the wide range of temperature limits, between operating and non-operating conditions, a change of up to 3 to 1 in emissivity appears

to be feasible by the proper selection of coating materials. This method of temperature control has the advantage that it does not add weight to the existing radiator.

(6) Combination of Temperature Control Methods: A combination of two or more of the above devices can be used to provide the lightest, most efficient thermal control system.

SPECIFIC THERMAL DESIGNS FOR KLYSTRONS

Except for the collector and electron gun, the geometry of the klystron depends on the frequency involved to the extent that separate consideration must be given to the device designed for each of the four frequencies studied. The collector and electron gun, however, are almost identical for all klystrons considered in this study and thus will be considered only once.

Collector

The four collector elements are made of a refractory metal such as molybdenum or tungsten and brazed to a ceramic disk. The maximum service temperature for reliably brazing such joints is 700°C. Thus, taking this as the design temperature, the "worst case" temperature at the tip of a collector element is 830°C for tungsten or molybdenum. The outside surface of the ceramic (BeO) would be 650°C for the case where almost all of the beam is intercepted by a single collector element, and 680°C for a more evenly distributed beam interception. Maximum power density at the outside ceramic surface is well below 25 W/cm^2, making the surface ideal for attachment of a heat pipe evaporator. The temperature drop through the wall of the evaporator and due to evaporation yields a minimum vapor temperature of 610°C. While sodium, potassium or cesium can be used as a working fluid at this temperature, sodium has several advantages which make it the most attractive choice. Most important, sodium has a surface tension high enough to permit more thorough testing under 1 "g" conditions. The heat pipe-radiator configuration shown in Figure 54 is the most straightforward means of cooling the collector. Its advantage, besides being compact, is that in the event the sodium freezes in the condenser, enough heat can be carried by conduction and radiation to melt the fluid and continue operation.

The remaining heat-producing element of the collector is the beam disperser. Since this element may possibly operate at a high electrical potential with respect to the spacecraft frame, it is most easily cooled by direct radiation. A 16 square inch (100 cm^2) radiator at 680°C coated with a 0.7 emissivity material is required to prevent the metal-ceramic seals from exceeding 700°C.

The geometry of the collector with the heat rejection elements, shown in Figure 54, applies to all klystrons included in this study, since there are only minor differences among the several designs.

Electron Gun

The electron gun should be thermally insulated to be as efficient as possible and to prevent overheating of adjacent components. Ten to fifteen layers of highly polished 1-mil-thick stainless-steel foil separated by either alumina or stainless-steel wire would constitute a good insulating system.

Solenoid Thermal Control

The magnetic field required by the klystron may be produced by an electromagnetic coil. The coil is made up of concentrically wound copper or aluminum foil with a layer of insulator between each wrap. The equivalent thermal conductivity is 10 joules/m sec°C for copper foil in the circumferential and axial directions. For a hollow cylinder with uniform internal generation, where the inside and outside surface temperatures are equal and fixed, the temperature distribution is given as:

$$t - T_o = \frac{q}{4K}(r_o^2 - r^2)\left[1 + \frac{\ln(r_i/r_o)}{\ln(r_o/r_i)}\right] \qquad (32)$$

and the maximum temperature can be shown to occur at:

$$r = \sqrt{\frac{1/2(r_o^2 - r_i^2}{\ln(r_o/r_i)}} \qquad (33)$$

where: T = Temperature at r surface

t = Temperature at r

q = Volumetric heat generation

K = Thermal conductivity

r_i = Inner radius

r_o = Outer radius

Using this relationship, the maximum internal temperature of each solenoid was computed. Data used in the computation and the results are given on Table XI. Aluminum foil is used in the solenoids for the 850-MHz AM, 2000-MHz AM and 2000-MHz FM klystrons, while copper foil is used in the remaining two.

The solenoids considered in this study have several alternate means of thermal control. For the 850-MHz klystron, the most simple method is to allow the outer surface of the solenoid to radiate directly to space. At the 144°C temperature from Table XI, 490 square inches of surface area are required to radiate the heat generated in the solenoid, assuming a 0.85 emissivity. One half of the circumference of the solenoid has an area of 520 square inches, of which approximately 300 square inches is blocked by radiators used to cool the cavities. Thus, the addition of two small fins as shown in Figure 59 will provide sufficient radiating area. Inclusion of a heat pipe at the base of each fin will even out temperature differentials along the axial length of the solenoid caused by blockage by other radiators.

Alternately, if the klystron cannot be positioned so the solenoid can radiate directly, a heat pipe radiator can be used. The evaporator of one or more heat pipes is mechanically attached to the outer surface of the solenoid. From here, the heat is transferred to fins where it is radiated to space. Heat pipes must be spaced so that the temperature of the solenoid is maintained below 150°C to avoid degradation of the insulation.

Cooling of the solenoid for the 2000-MHz AM and FM klystrons will be accomplished by winding the foil directly on the outside of the heat pipe used to cool the cavities. While this method decreases the temperature at which the heat from the cavities can be radiated (the maximum operating temperature of the solenoid is lower than that of the cavities), the resulting increase in radiator area and weight is small (an increase of less than 3.2 square feet and 5 pounds), and the mechanical arrangement is greatly simplified. Further cooling can be accomplished by fastening the solenoid to the radiator. Due to the high circumferential conductivity, this will introduce a circumferential temperature differential of less than 6°C. Figure 60 depicts the details of the configuration.

Using the inner and outer surfaces of the solenoid of the 8000-MHz FM and 11,000-MHz FM klystrons results in far too low a radiating temperature. Therefore, heat must be removed from the coil edge to take advantage of the high axial thermal conductivity. For a uniformly heated body

Table XI - Solenoid Thermal Characteristics

Klystron	Solenoid Dimensions: Inside Diameter (Inches)	Solenoid Dimensions: Outside Diameter (Inches)	Solenoid Dimensions: Length (Inches)	Radius of Max. Temp. (Inches)	Power (Watts)	Maximum Allowable* Outside Surface Temperature (°C)
850-MHz AM	5.962	8.094	37.33	----	669	144
2000-MHz AM	2.815	7.683	14.26	2.54	319	132
2000-MHz FM	2.815	7.725	18.56	2.53	405	132
8000-MHz FM	1.4	7.436	3.466	1.99	435	44
11,000-MHz FM	1.5	8.885	2.711	3.02	654	-11

*Required to maintain 150°C inside temperature

NOTE: All solenoids have 1/2-mil thick insulation between layers

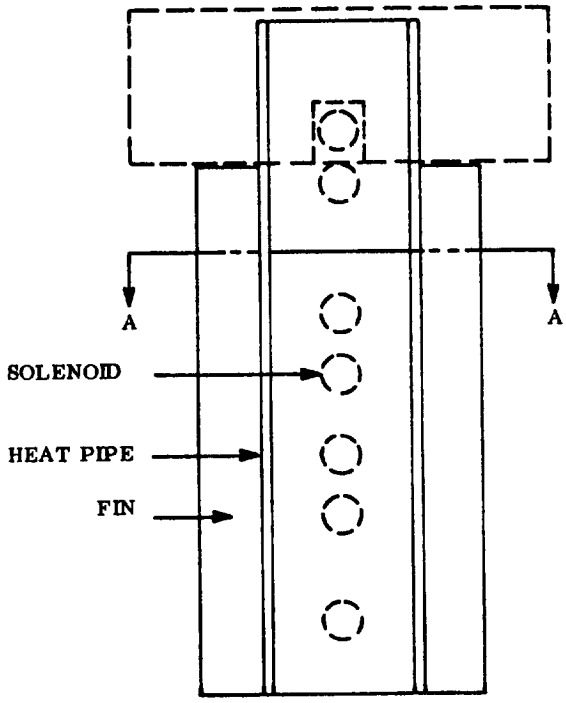

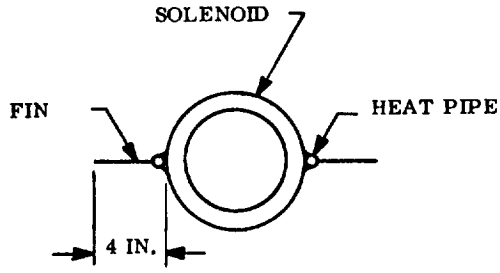

NOTE: 1. DASHED LINES INDICATE OTHER RADIATING SURFACES

2. AXIAL HEAT PIPES ARE REQUIRED DUE TO DISCONTINUITIES IN THE FOIL WHICH PREVENT AXIAL CONDUCTION (DISCONTINUITIES ARE DUE TO ELECTRICAL CONSIDERATIONS)

Figure 59 - Thermal Control System for 850-MHz AM Klystron Solenoid

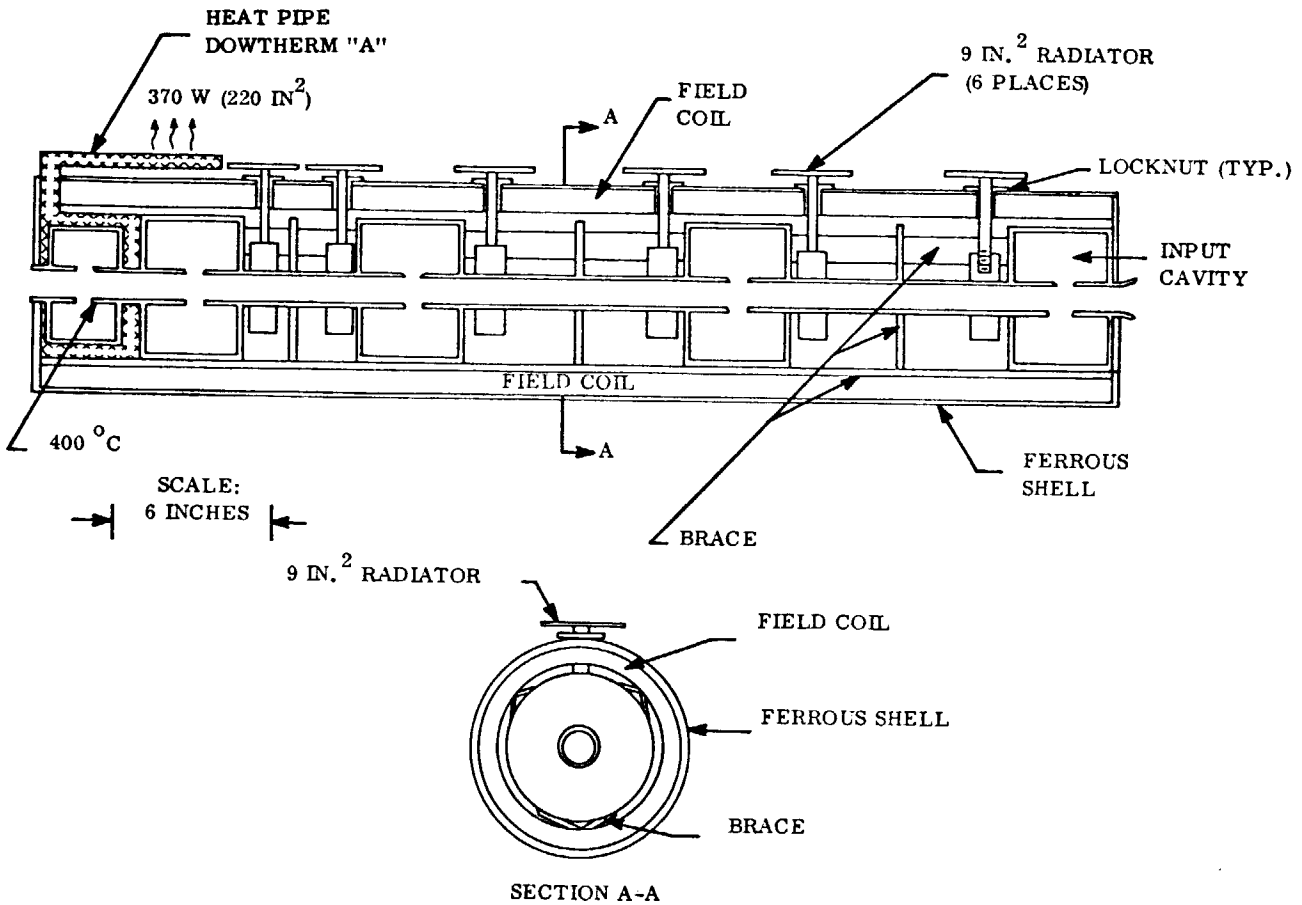

Figure 60 - Thermal Control System for 850-MHz AM Klystron

of constant cross-section, with one end at constant temperature, the maximum temperature is given as:

$$t - T_o = \frac{q}{2K} L^2 \qquad (34)$$

where L is the length of the solenoid and the remaining symbols have been previously defined. The temperature rise for either solenoid is found to be less than 3°C. The temperature drop through the electrical insulation between the end of the solenoid and the heat pipe evaporator is approximately 15°C for both coils. Thus, the heat rejection temperature is 132°C at the evaporator. Integration of this evaporator into the cavity heat pipe is described later.

Permanent Magnets

Permanent magnets may be used in the 8000- and 11,000-MHz klystrons in place of the solenoids (see Figures 50 and 51). These elements do not dissipate heat and can operate satisfactorily at 200 to 225°C. They should present no thermal problems. Since the surface of the klystron body will not exceed the maximum magnet temperature, thermal control will be maintained by insulating the magnets from the collector and electron gun, and mechanically fastening them to the mounting surface.

Cavity Thermal Control

Table XII shows the power dissipation and temperature drops from the tunnel tip to the surface where the heat can be removed for the cavities of each klystron considered. The maximum temperature at the heat transfer interface, shown as T_{max}, is based on a 400°C maximum on the tunnel tip. In addition to the beam and RF power dissipated on the tunnels of the output cavity, some additional RF in the amounts shown is dissipated over the inside surface of this cavity. This does not affect the heat rejection temperature, but must be provided for in the thermal design. The total power dissipated in the output cavity is therefore the summation of cavity-wall losses plus losses on tunnel tips. Due to geometry and dissipation differences, thermal control of the cavities of each device must be considered separately.

(1) 850-MHz AM Klystron: Heat from the buncher cavities can be removed directly at the outside surface of the cavity at a temperature of 389°C. While this heat can be conducted to the solenoid and there radiated, the temperature would have to be reduced

Table XII - Cavity Thermal Characteristics

Klystron	Buncher Cavity			Output Cavity				
	Tunnel-Tip Dissipation (Watts)	ΔT^* (^oC)	T_{max}** (^oC)	Tunnel-Tip Dissipation (Watts)	ΔT^* (^oC)	T_{max}** (^oC)	Cavity Dissipation (Watts)	Total Dissipation (Watts)
850-MHz AM	19	11	389	150	65	335	70	370
2000-MHz AM	18	29	371	135	170	230	60	330
2000-MHz FM	12	20	380	95	155	245	36	226
8000-MHz FM	20	36	364	221	226	174	142	584
11,000-MHz FM	25	31	369	311	129	271	212	834

*From tunnel tip to cavity wall

**Based on a maximum of 400^{o}C at the tunnel tip

to below 150°C to avoid overheating the inside surface of the solenoid. This reduces the black body emissive power from 10.9 to 1.36 kW/m^2, requiring an eight-fold increase in radiating area. By providing a conduction path through the solenoid to a small radiator, the radiating area can be minimized. A half-inch (1.25 cm) diameter copper rod 4 inches (10 cm) long, attached as shown in Figure 60, provides a radiator with a root temperature of 345°C. Taking aluminum as a fin material, the required area is 9 square inches (58 cm^2).

The output cavity dissipates too much heat to use conduction alone. The most simple means of control, therefore, is a heat pipe. The outside portion of the output cavity is completely covered with a wick and used as an evaporator. Figure 60 shows the configuration. Since the operating temperature is too high to use water as the working fluid and too low for liquid metal, Dowtherm A is the best choice. By placing the radiator as shown in Figure 60, the problem of the working fluid freezing in the condenser can be overcome. In the event that restarting becomes a problem, heat radiated and conducted from the solenoid to the condenser can melt the fluid.

(2) 2,000-MHz AM and FM Klystrons: Heat generated at the tunnel tips of the 2,000-MHz klystrons must be conducted radially from the base of the tunnel to the cylindrical surface of the cavity, causing a temperature drop of approximately 35°C. This lowers the maximum heat rejection temperature for the output cavity to 195 and 210°C for the AM and FM klystrons, respectively. The outside cylindrical surface of the output cavity is covered with a wick as in the 850-MHz klystron. A total of 348 watts must be removed over a 7.5-$in.^2$ (48 cm^2) surface, yielding a power density of 46.4 W/$in.^2$ (7.2 W/cm^2), a small fraction of the evaporator capacity. Thermal control of the buncher cavity tunnel tips can be maintained by continuing the heat pipe from the output cavity over the entire length of the klystron. In addition to cooling the cavities, the outer surface of this heat pipe can be used to cool the solenoid as was described previously. The disadvantage of this design is that the radiating temperature is decreased from the limit for the output cavity to 132°C, the solenoid limit. The total power which must be removed by the heat pipe now is the total of all of the cavities plus the solenoid power. This amounts to 793 watts for the AM design and 751 watts for

the FM. Allowing 25°C for heat pipe and interface temperature drops, from the data of Figure 58 the 2000-MHz AM klystron requires an 8.3-ft.^{2} (0.8 m^2) radiator weighing 13.2 pounds (6 kg) and the 2000-MHz FM klystron requires a 7.9-ft.^{2} (0.7 m^2) radiator which weighs 12.5 pounds (5.7 kg). The configuration is shown in Figure 61.

(3) 8,000-MHz FM Klystron: Table XII shows the power and temperature requirements for the cavities of the 8,000-MHz FM klystron. The cylindrical wall of the output cavity is used as an evaporator and requires a minimum wall thickness of 0.1 inch (0.25 cm). The power density at the evaporator, 320 W/in.^{2} (50 W/cm^2), is somewhat marginal but can be taken care of, if necessary, by increasing the surface area by either increasing the wall thickness or convoluting the surface.

The temperature limit shown in Table XII for the output cavity is in excess of the maximum solenoid temperature, and therefore the heat pipe will operate at the lower limit, 132°C. Allowing 25°C for heat pipe and interface temperature drops, the radiator will operate at 107°C and require 13.7 ft.^{2} (1.27 m^2) of area to radiate 1179 watts. Radiator weight is 21 pounds (9.5 kg). Figure 62 shows a cross-section of the 8000-MHz FM klystron, with the heat pipe integrated into the design.

If the klystron beam is focused with permanent magnets instead of an electromagnet (see Figure 50), the thermal design is made easier both because the heat of the solenoid is eliminated and heat removal from the klystron cavities is facilitated by the open path between the magnet "horns". The cross-section shown in Figure 63 depicts a design wherein a wick-lined heat pipe surrounds the klystron and transports heat to a condenser at an appropriate outer surface of the spacecraft.

(4) 11,000-MHz FM Klystron: Cooling for the 11,000-MHz FM klystron is accomplished with the same approach as used for the 8,000-MHz design. The output cavity is the primary problem in that little surface area is available for evaporation. A total of 859 watts is dissipated and can be rejected at a maximum temperature of 236°C (271°C at the tunnel less 35°C radial drop).

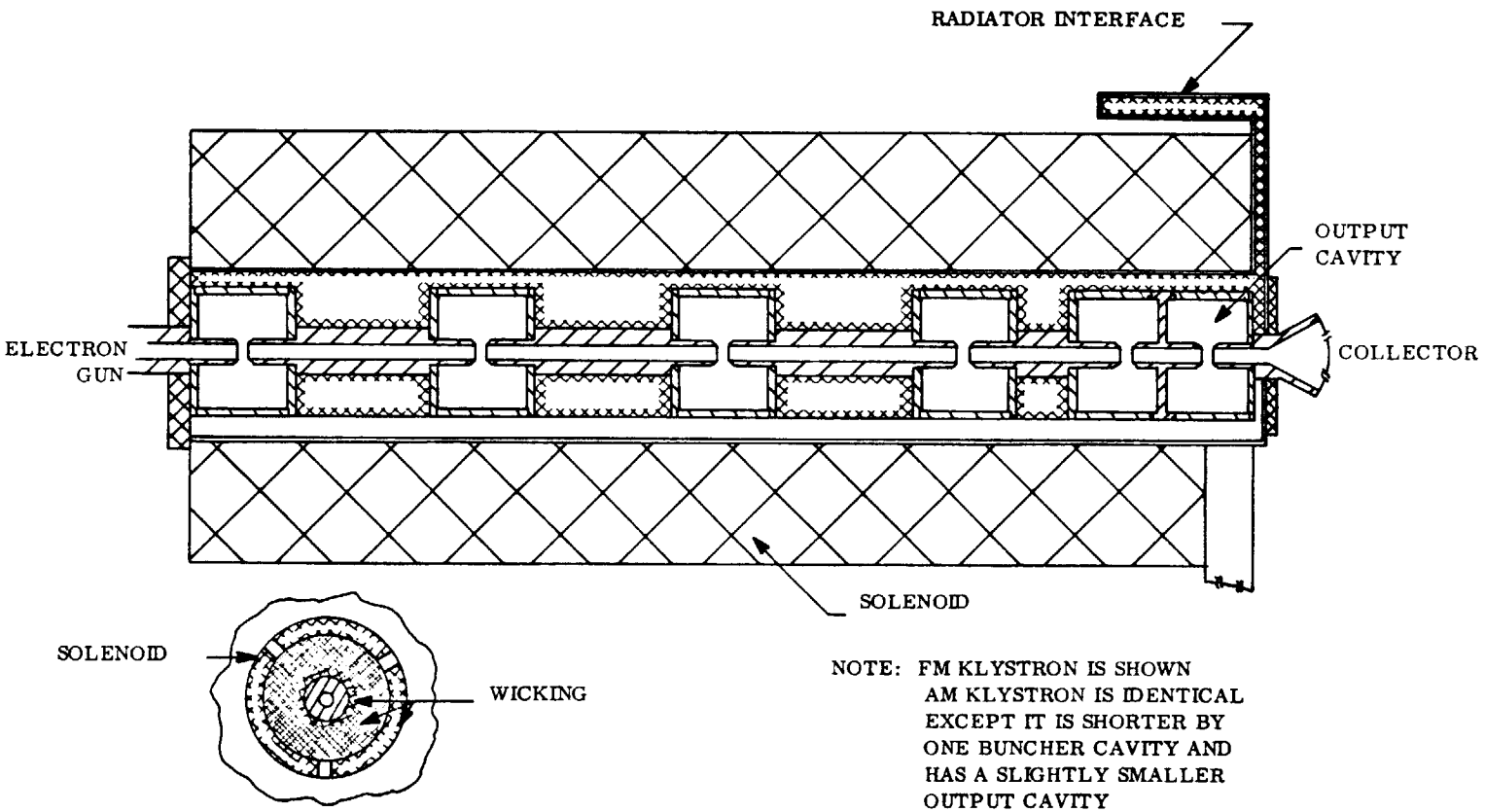

Figure 61 - Thermal Control System for 2000-MHz Klystrons

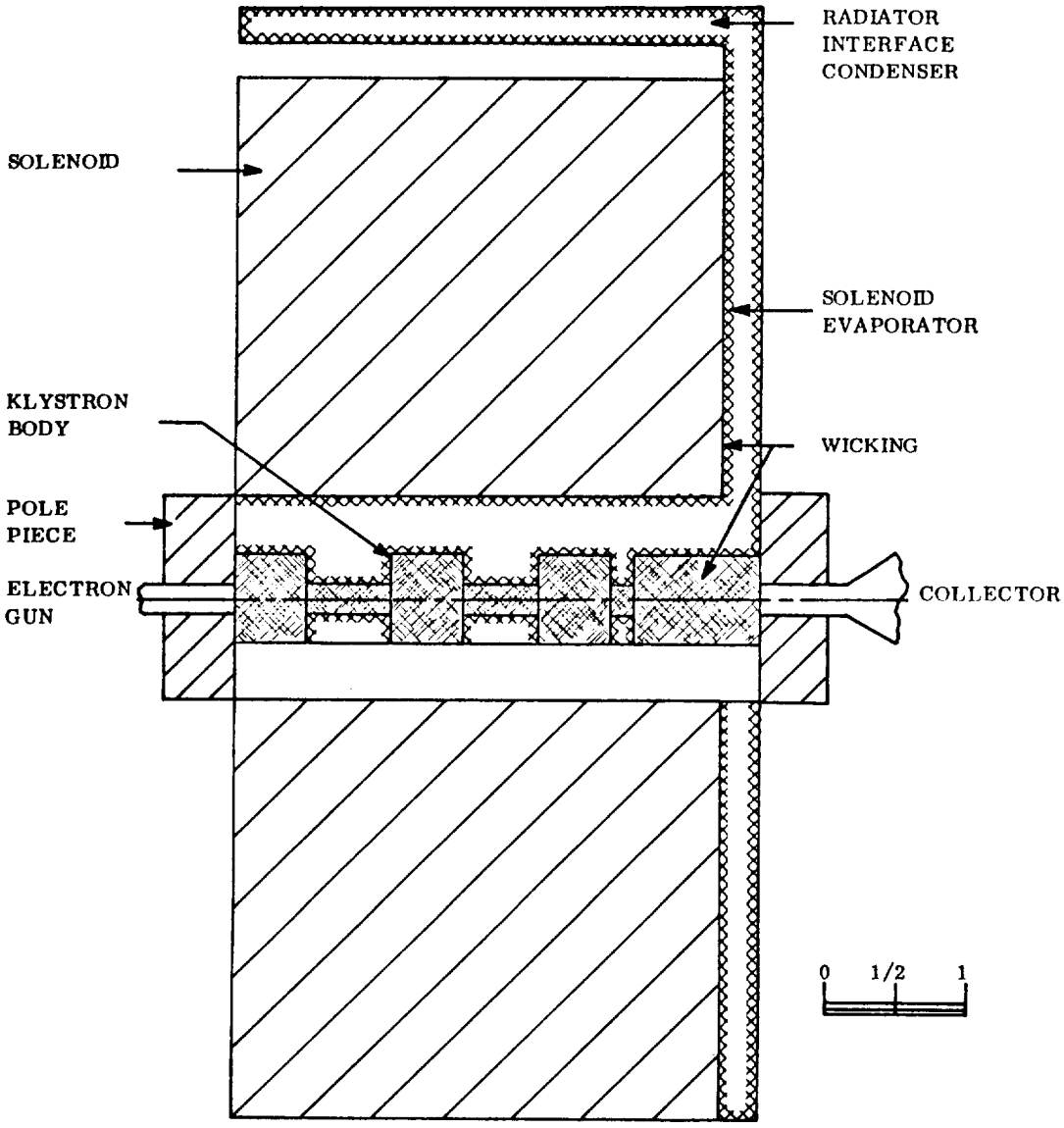

Figure 62 - Thermal Control System for 8000-MHz Klystron with Solenoid

Since the physical size of the 11,000-MHz klystron makes inclusion of separate heat pipes difficult, a single chamber is used as shown in Figure 64. Also shown is the location of the solenoid cooling evaporator. As for the 8000-MHz klystron, the solenoid must be end-cooled due to the excessive radial drop, as shown on Table XI. The total heat which must be rejected by the radiator is 1688 watts which, using the solenoid temperature limit, requires an area of 19.7 ft.^{2} (1.8 m^2) weighing 30 pounds (13.6 kg).

Where permanent magnets are used, the configuration is similar to the 8000-MHz klystron shown in Figure 63. The radiator area required is 12.1 ft.^{2} (1.1 m^2) at a weight of 18.4 pounds (8.3 kg).

Summary of Radiator Requirements

A table of radiator weights, areas, and radiating temperature for each of the heat sources in the AM and FM klystrons is given in Table XIII. The size of the radiator for the collector has been adjusted to correspond to the heat load computed for the conversion efficiencies listed for each of the klystrons, as given in Tables XIX through XXIII in Section XI.

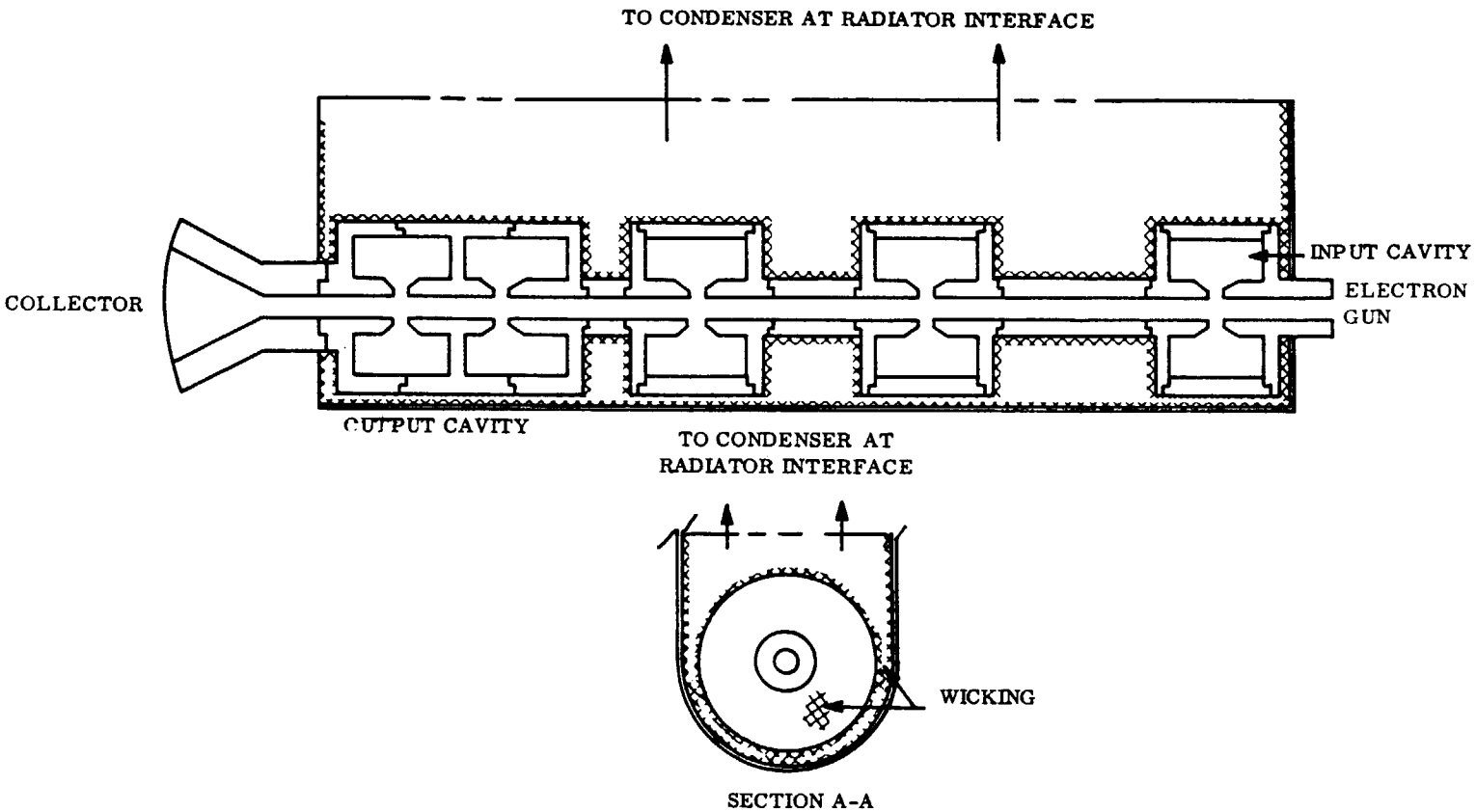

Figure 63 - Thermal Control System for 8000-MHz Klystron with Permanent Magnet

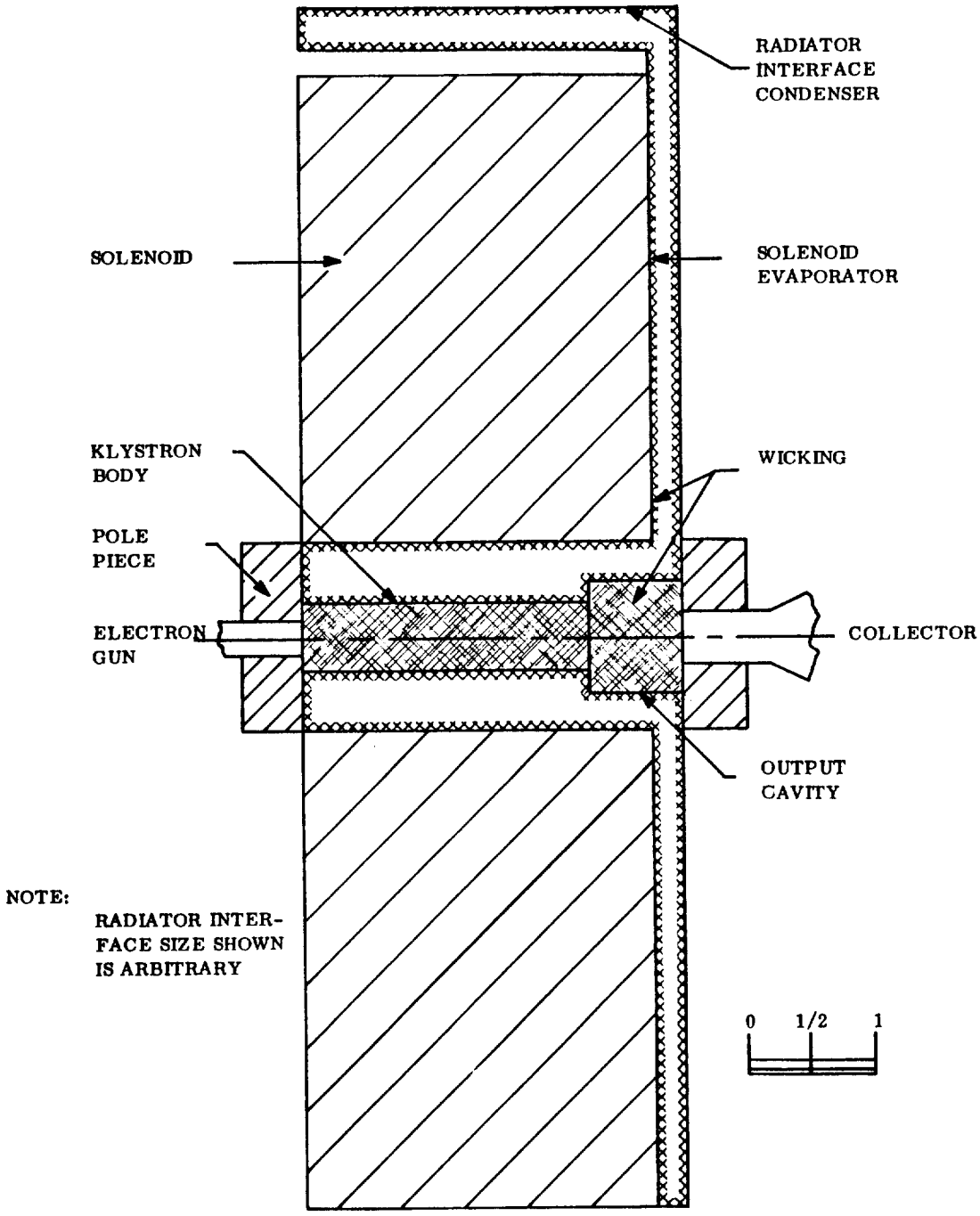

Figure 64 - Thermal Control System for 11,000-MHz Klystron with Solenoid

Table XIII - Radiator Parameters

Klystron	Heat Source	Radiator Weight (lbs.)	Radiator Area (Sq. Ft.)	Radiator Temperature (°C)
850-MHz AM	Solenoid	3.6	1.9	144
	Body	5.8	1.4	214
	Collector	6.2	1.5	600
2000-MHz AM	Solenoid	13.2	8.3	107
	Body			
	Collector	4.9	1.1	600
2000-MHz FM	Solenoid	12.5	7.9	107
	Body			
	Collector	3.4	0.5	600
8000-MHz FM (With PM)	Body	13.2	8.7	107
	Collector	4.0	0.7	600
8000-MHz FM (With Solenoid)	Solenoid	21.0	13.7	107
	Body			
	Collector	4.0	0.7	600
11,000-MHz FM (With PM)	Body	10.4	12.1	107
	Collector	4.8	1.0	600
11,000-MHz FM (With Solenoid)	Solenoid	30.0	19.7	107
	Body			
	Collector	4.8	1.0	600

Section IX

POWER SUPPLIES FOR SPACE-BORNE KLYSTRONS

DESCRIPTION OF POWER REQUIREMENTS

The nominal power supply requirements for the five spaceborne klystrons are given in Table XIV. In addition, in Tables XV, XVI, and XVII, the high-voltage DC power requirements are separately listed for the 850-MHz AM klystron, the 2000-MHz AM klystron, and the FM klystrons, respectively. The efficiencies appearing in the tables are estimates made before the final values were available, but the supplies as designed have sufficient reserve to accommodate the final specifications. Two values of the reflex collector potential margin -- 5 percent and 15 percent -- have been considered, the latter value considered a feasible immediate objective and the former an ultimate objective.

A diagram of the required power supplies is given in Figure 65. The beam dispenser electrode is shown as connected to a negative bias supply, but later analysis has shown that it may be feasible to connect this electrode to the negative terminal of the main beam supply.

Although the EIA standard for hum and noise in a broadcast television signal is 50 dB below signal, a 10 dB degradation in this parameter is generally experienced in relating the beam voltage noise and hum to RF output hum and noise in klystron transmitters. The 10 dB discrepancy is explained by the non-linear nature of the klystron voltage-current characteristic. The desired signal to noise ratio S/N in dB is given by:

$$S/N = 20 \log (V_{sig}/V_{hum}) = 50 \text{ dB} \qquad (35)$$

Solving for the ratio V_{hum}/V_{sig}, one finds that

$$V_{hum}/V_{sig} = 0.32\%$$

In a klystron employing an electron gun with a given perveance, the beam power and hence the output signal power is proportional to the 5/2 power of the beam voltage. Hence, the signal voltage is proportional to the 5/4 power of the beam voltage. To achieve a 50 dB signal-to-hum and noise ratio in the output the deviation allowed on the beam voltage is

Table XIV - Power Supply Requirements for Klystrons

Klystron	V_b	I_b	V_1	V_2	V_3	V_4	I	P_{c1}	P_{c2}	V_f	I_f	V_h	I_h
850-MHz AM	15.5	0.02	11	6.2	4.6	2.6	0.9	1.75	2.0	67	10	20	5
2000-MHz AM	13.0	0.025	9.1	5.2	3.9	1.3	0.7	1.1	1.3	32	10	20	3
2000-MHz FM	12.0	0.02	8.4	4.8	3.6	1.2	0.6	0.35	0.35	41	10	20	3
8000-MHz FM	12.0	0.03	8.4	4.8	3.6	1.2	0.6	0.35	0.35	44	10	20	1.5
11000-MHz FM	12.0	0.035	8.4	4.8	3.6	1.2	0.6	0.35	0.35	65	10	20	1

V_b = Beam accelerator voltage - kV (Tolerance = ±0.05%)

I_b = Current furnished by V_b - Amp

V_1-V_4 = Collector segment voltages (Tolerance = ±1%)

I = Collector segment current - Amp. Each supply V_1-V_4 must be able to furnish this much current on demand.

P_{c1} = Total average power furnished by collector power supply - kW

P_{c2} = Peak power into collector - kW

V_f = Field coil voltage - volts (Tolerance = ±2%)

I_f = Field coil current - Amp.

V_h = Cathode heater voltage - volts (Tolerance = ±5%)

I_h = Cathode heater current - Amp.

Table XV - Depressed Collector Power Requirements of 850-MHz AM Klystron

		5% Margin		15% Margin	
		Eff.	P Input	Eff.	P Input
Saturated Power Output (kW)	9.5	92.6	10.25	80.7	11.80
Synch Power (kW)	7.5	90.9	8.25	76.9	9.75
Black Picture (kW)	3.5	82.4	4.25	60.5	5.80
Average Picture (kW)	3.0	80.0	3.75	57.1	5.25
White Picture (kW)	1.3	57.1	2.28	37.5	3.46

Maximum current to any collector tap: 0.77 ampere

Current to 15.5 KV supply: 0.20 ampere

- - - - - - -

Table XVI - Depressed Collector Power Requirements of 2000-MHz AM Klystron

		5% Margin		15% Margin	
		Eff.	P Input	Eff.	P Input
Saturated Power Output (kW)	6.25	92.6	6.75	80.7	7.75
Synch Power (kW)	5.0	90.9	5.41	76.9	6.40
Black Picture (kW)	2.3	82.4	2.80	60.5	3.82
Average Picture (kW)	2.0	80.0	2.46	57.1	3.45
White Picture (kW)	0.9	57.1	1.50	37.5	2.28

Maximum Current to any collector tap: 0.59 ampere

Current to 13 KV supply: 0.022 ampere

Table XVII - Depressed Collector Power Requirements of FM Klystron

Beam Power (kW)	7.89
Beam Voltage (kV)	12
Saturation Efficiency (%)	65
Overall Efficiency (5% Margin)	92.8
Overall Efficiency (15% Margin)	72.3
For 5 kW Power Out:	
Input Power (5% Margin) (kW)	5/92.8 = 5.4
(15% Margin) (kW)	5/72.3 = 6.9
Maximum Current at any Collector Tap (A)	0.525
Currents at 12 kV	
Current to 12 kV Supply:	
0.03 A (8000 MHz)	
0.035A (11000 MHz)	

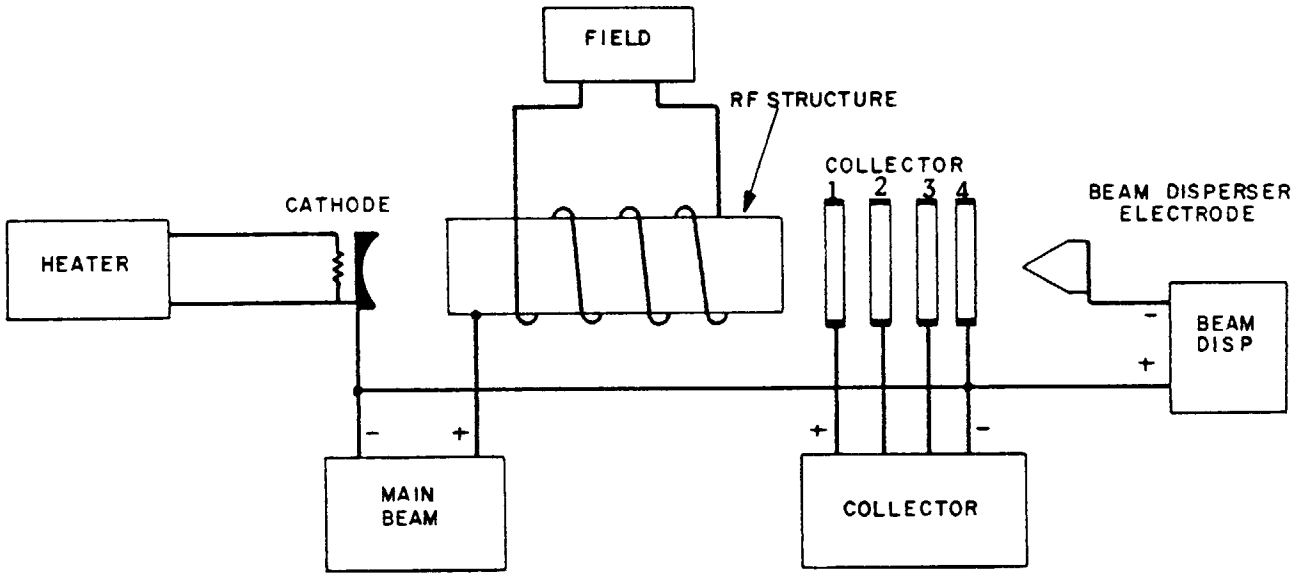

Figure 65 - Schematic Diagram of Power Supplies Required for Operation of Magnetically-Focused Klystrons with Solenoid and Reflex Collector

$$S/N = 50\ dB = 20 \times 4/5 \log (V_o/V_{hum}) \qquad (36)$$

corresponding to a 0.1 percent peak-to-peak deviation on the DC beam voltage. Here it is assumed that hum is the only significant part of the total beam noise.

The main beam power supply must be well regulated and have low hum and noise but it need furnish only the small current intercepted by the drift tube walls. The total rms hum and noise voltage should be less than 0.1 percent peak-to-peak of the given beam voltage.

The solenoid power is furnished at relatively low impedance since foil-wound coils are used to minimize size and weight. The tolerance on field voltage is tentatively set at 2 percent in order to preserve a high beam transmission.

Heater power can be developed over a range of voltages, although the most practical heater designs for long life will fall in the range 5 to 20 volts for all tubes. Specific choice of voltage is left to the power supply designer. A DC heater supply with 5 percent or less ripple is desired.

The collector power supply presents the greatest challenge. There will be a number of collector segments each operating at a different potential. In the AM cases, the amount of current collected by any one segment will depend on the modulation depth which varies with scene brightness. Thus a near-black scene will result in a larger proportion of the total beam current incident on the V_1 and V_2 taps whereas a near-white scene will put the current predominantly on the V_3 - V_4 taps. For the FM cases the current will vary only slightly with modulation since the klystron will be operating at near saturated amplitude conditions at all times. However, the current will not be equally distributed among the various taps.

Because of the variable current demand on the collector power sources, it would appear to be impractical to utilize the direct output from a large array of solar cells since the peak current capacity at any one tap will need to be essentially full beam current while the average current will be much lower. It also seems impractical to use energy storage in capacitors to integrate the current demand because a given picture scene may remain black or white for a second or longer.

OPTIMUM POWER SUPPLY DESIGNS

The power subsystem diagram, presented in Figure 66, indicates two converters to supply the required voltages for the klystron amplifier. The heater, solenoid, and beam are relatively constant loads and are all supplied from a single pulse-width-modulation (PWM) regulated converter (Figure 67).

Since the solenoid requires close regulation, the solenoid voltage is sensed and compared against a fixed reference voltage by the control circuits for the pulse-width modulator. The control signal from the comparator is used by the pulse-width modulator to determine the conduction angle of the transistor amplifier, and thereby to hold the solenoid voltage constant. The heater and beam voltages, which are derived from the same transformer as the solenoid supply, will also be held constant against changes in the supply voltage. Since all loads on the converter are relatively constant, all of the voltages will thus be well regulated.

Additional regulation is used to hold the beam voltage to the close accuracy needed. Since this supply is at low power, high-voltage shunt regulation may be used without a significant loss of efficiency for the overall system.

Protection for the converter and the klystron is provided by a circuit breaker in series with the converter. Additional protection for the klystron is provided by a triggered gap which is fired by its control circuit whenever the beam current exceeds a preset level.

The various voltages required for the collectors may be provided by either the single PWM regulated converter of Figure 68 or the modular approach of Figure 69.

In the circuit of Figure 68, the required voltages are derived from multiple windings on the single transformer of the converter. The lowest voltage is sensed and the pulse width controlled to maintain this voltage constant. The other voltages will follow to a degree, depending on the variations in currents to the collectors. It is assumed that the minimum load on the supply to any of the collectors will be 10 percent of the maximum value.

This approach will require a large number of transistors to be paralleled in the converter if currently available transistors are utilized. The

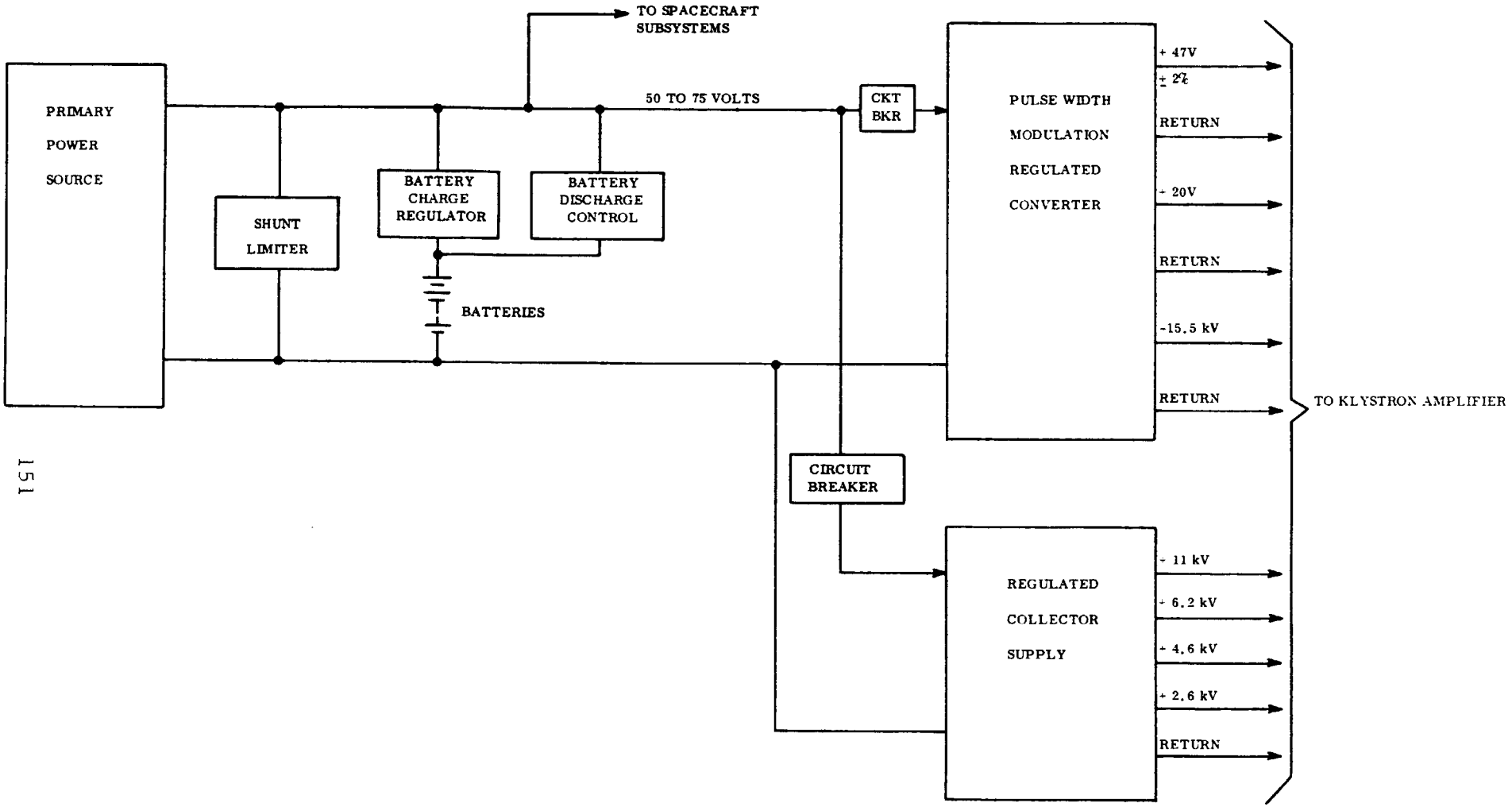

Figure 66 - Space-Borne Magnetically-Focused Klystron Power Subsystem

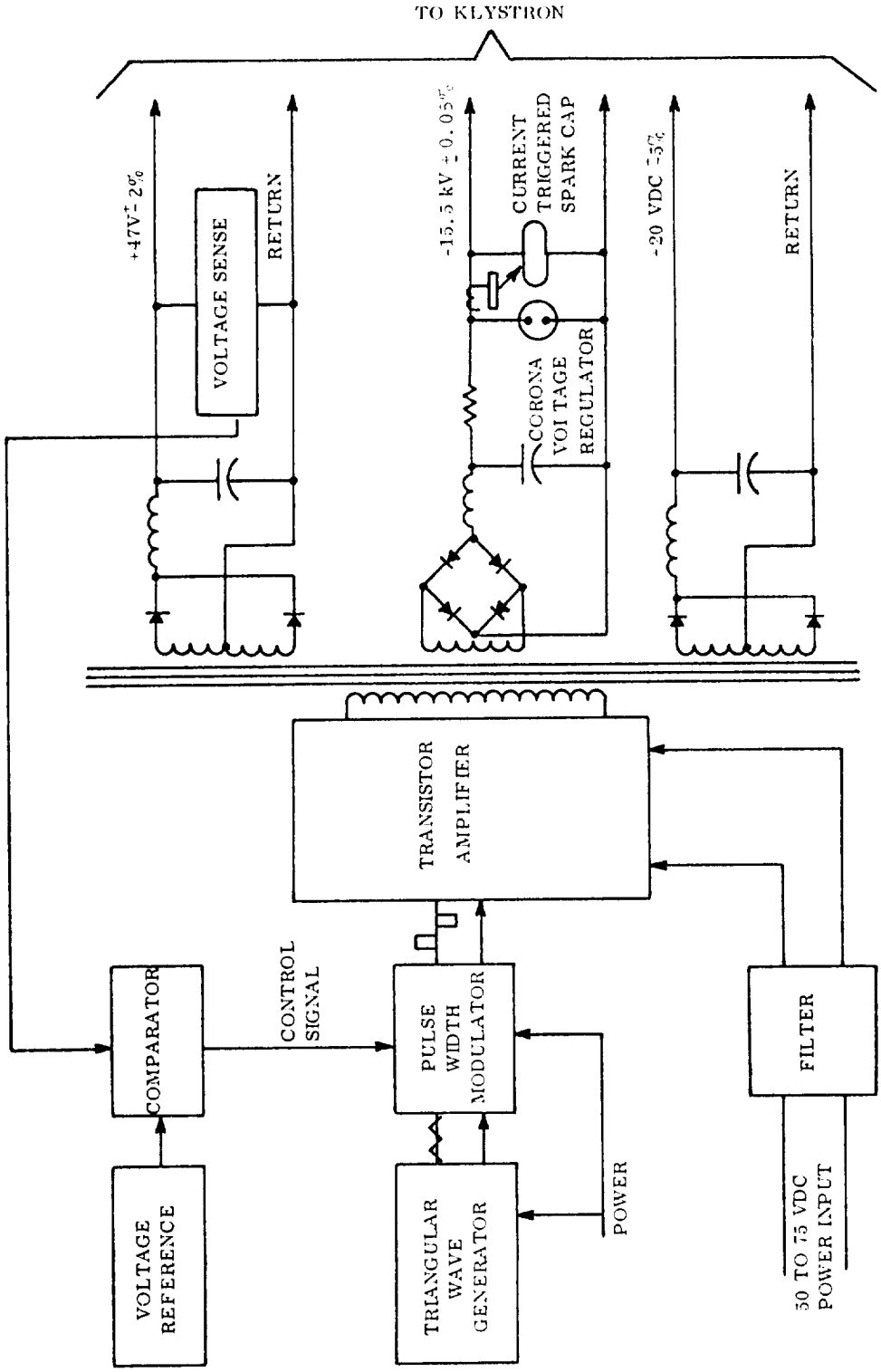

Figure 67 - Pulse-Width Modulation Regulated Converter for Solenoid, Beam and Electron Gun Cathode Heater Supplies

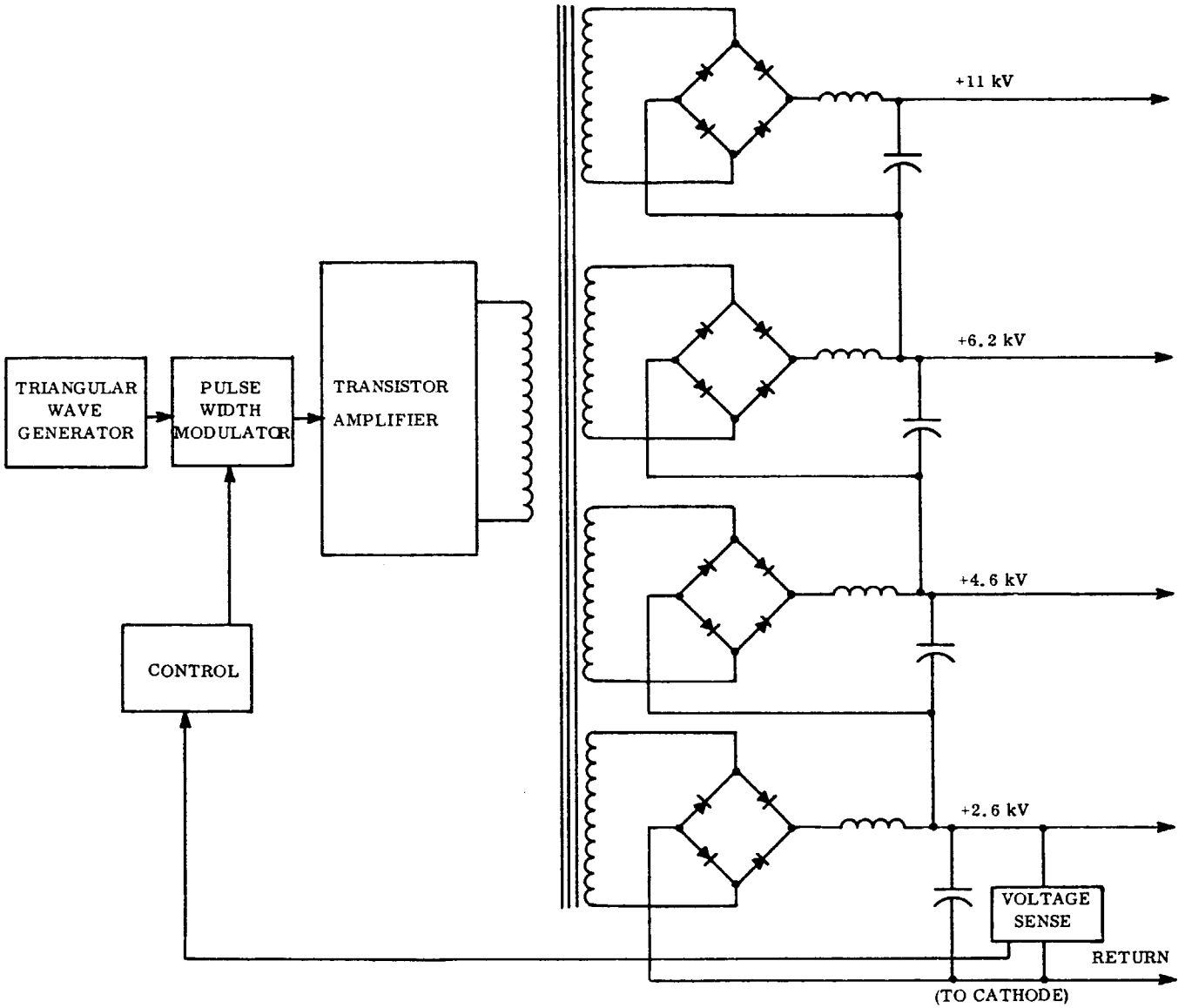

Figure 68 - Single PWM Regulated Converter for Reflex Collector Voltages

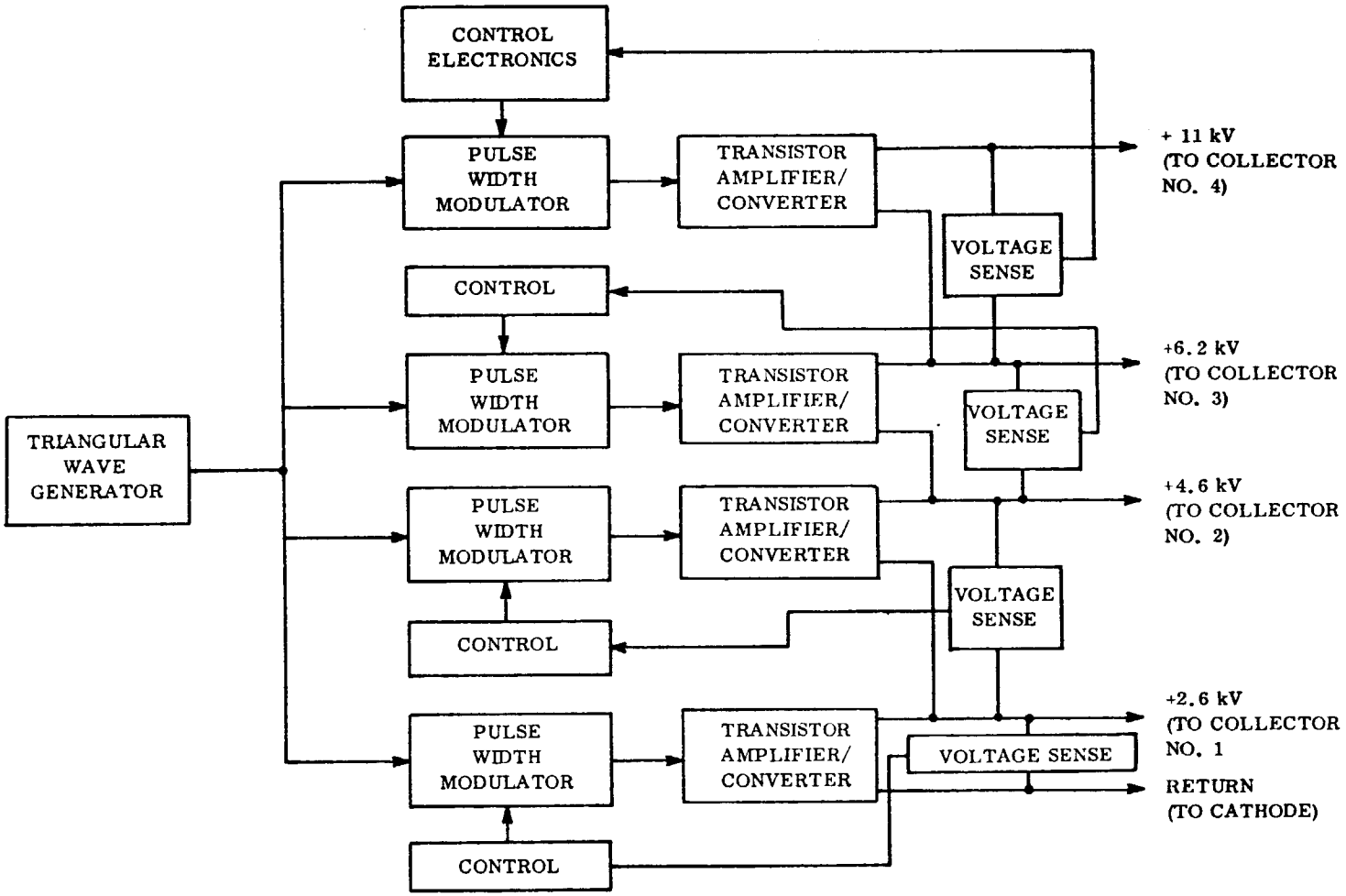

Figure 69 - Alternate Modular Power Supply for Magnetically-Focused Klystrons

converter must be designed to supply at least the power level required for a black picture, which will be 5.8 kW for the 850-MHz transmitter. (Peak synch and vertical blanking power can be provided by the filter capacitors on the output of the supply.) At the lowest input voltage, and assuming a transformer efficiency of 95 percent, the transistors will be required to supply an average current of 130 amperes; because of the variable conduction angle, the peak transistor current will probably be 40 percent higher. Currently available transistors rated at 200 volts are also rated for 20 amperes continuous current, which means that approximately 10 transistors would be required to drive each half of the push-pull transformer, and current sharing would become a problem.

A second approach for the collector supply is presented in Figure 69. Four separate converters provide voltage increments so that when the outputs are connected in series, the required collector voltages are available at the connections between converter outputs. Each converter output can be regulated separately and the voltages more accurately controlled.

Referring again to Figure 66, the protection for the klystron and the collector supply is provided by a circuit breaker. Since the collectors will be able to withstand the discharge of the stored energy in the filters and transformer, no "crowbar" circuit, such as that used for the main beam supply, is provided.

Calculations, substantiated by tests, have shown that the peak synch and vertical pulses can be supplied by energy-storage circuits with a time constant of 50 milliseconds. The primary power source may be selected to supply only the picture power, with the peak power being supplied by the converter output filter capacitors. A further improvement in primary power requirements may be realized by supplying short-term black level demands from batteries and adding control circuits to reduce the overall transmitter power output during extended periods of dark scenes.

Section X
MECHANICAL EMBODIMENT AND LAYOUT

DESIGN FACTORS

Klystrons are readily adaptable to the space environment because of their structural simplicity and basically rigid construction. Magnetically focused klystrons are single-potential, self-shielding RF structures of brazed, solid metal. Moreover, modern ceramic-metal sealing techniques are available for constructing the electron gun and multi-segment collector. The relatively simple configuration of klystron cavities and drift tunnels makes heat-pipe cooling methods relatively straightforward and simple. Also, in some cases, klystrons can be cooled by direct radiation.

Since the high-efficiency klystron designs prepared in this study do not employ voltage jumps, all RF circuits are at the same potential, which can be the same as the frame of the spacecraft. The cathode and the various collector electrodes which are operated at potentials other than the RF body are amenable to good high-voltage seal designs.

Space Environment

The operation of klystrons in the space environment is essentially the same as in a ground environment as long as the thermal environment is controlled as described in Section VIII. The evolution of klystron technology, over many years, has enabled klystrons with the proper processing to maintain their own internal space environment for long-lived operation. It is not known whether the hard vacuum to be realized in the vicinity of a satellite after degassing of the vehicle would be helpful in prolonging the life of the electron guns in klystrons. Undoubtedly, however, the gases present in the early hours following launch would have a deleterious effect on the cathode. Because long life has been achieved in sealed-off klystrons, it would appear desirable to continue to isolate the interior of the klystron from the satellite and to depend on a small appendage ion pump to maintain the proper pressure in case a gas burst should develop in the klystron.

Mechanical Rigidity and Strength

The most severe environmental requirements for the klystrons are the vibrational specifications of 20-400 Hz at 5.0 g, and 400-3000 Hz at

15.0 g. The mechanical design will require considerable analysis and vibrational testing to eliminate or damp resonances in these frequency ranges. Since the klystron and magnetic circuit, particularly for the lower frequency tubes, are relatively large structures, they will be supported by and firmly attached to the spacecraft frame. In such an arrangement, the total package structure would have to be analyzed on environmental equipment to determine compliance with the required specifications. Since large klystrons have been successfully designed and constructed to meet the acceleration specifications required for mobile military equipment, it is anticipated that present construction techniques can be modified to meet the specifications for space qualification.

KLYSTRON MATERIALS AND FABRICATION TECHNIQUES

The following materials and techniques are appropriate for constructing the klystron designs discussed herein.

Cavities and Drift Tubes

Oxygen-free high-conductivity copper of controlled impurity levels is chosen for the basic cavity and drift tube material. This material will provide good thermal conductivity for the drift tube tips, and ensure high cavity Q. Copper-gold brazing alloys are used to join the various cavity and drift tube combinations, with the brazing accomplished in hydrogen atmospheres at elevated temperatures. The RF conducting copper surface of the output cavity may have to receive special treatment to decrease the surface RF resistance, since the Q of this cavity contributes a great amount to the overall performance.

Ceramic and Ceramic-Seal Materials

High density, low-loss, alumina ceramics are used for the cathode bushing, RF input seal, and RF output seal. The main collector seal is made of high thermal conductivity beryllia oxide to conduct the heat generated by electron interception on the various electrodes to the heat pipe system for rejection.

The metal-seal portion will, in most cases, be Ceramvar*, an iron-nickel-cobalt alloy which has been used extensively for high-alumina

*Wilbur B. Driver Co.

ceramic vacuum seals. This material closely matches the thermal expansion characteristics of the alumina-oxide ceramic in the sealing and brazing temperature ranges. While most of the ceramic-metal joints utilize a copper-gold braze alloy, the high-temperature seals in the collector would be made with a palladium-cobalt alloy.

Cathode and Heater Structure

Structural material for the cathode, heater, and focus electrode include electronic-tube grades of nickel, tungsten, and stainless steel. The emitting surfaces will vary according to the emission demands of the various designs. The more common barium-strontium oxide cathode would be used for the 850-MHz klystron. The emission density required (0.1 A/cm^2) would yield a cathode life in excess of 50,000 hours. This cathode system might also be suitable for the 2000-MHz klystrons (emission density of 0.2 A/cm^2 required) if the cathode operating temperature could be kept as low as 740°C, where again a life of 50,000 hours could be expected. For the higher emission densities of 1.42 A/cm^2 and 2.68 A/cm^2 associated with the 8000-MHz and 11,000-MHz klystron designs, the tungstate cathode system presently under evaluation should yield life expectancies of over 20,000 hours at an operating temperature of 900°C. At present, a life test of a tungstate cathode at 1.7 A/cm^2 and 900°C has exceeded 15,000 hours of operation with no change in characteristics.

Of all the component parts of a klystron, the cathode support structure is the most vulnerable to damage by shock and vibration. For the spaceborne klystrons, an electron-gun structure more rugged than is usually employed will be possible, because there will be less heat loss to the space environment with the absence of convection cooling of the outer surface of the cathode seal.

Structural Members

In the 850-MHz klystrons support members of stainless steel are used to tie the resonators, drift tubes, and magnetic pole-pieces into a unified structure. For the higher frequency tubes, structural support is provided by the integration of tube body, heat pipe, and electromagnet, as shown in Figures 61, 62, and 63.

Processing

All parts that comprise the vacuum envelope are cleaned to remove all surface contamination, and fired in either vacuum or a controlled

hydrogen atmosphere to remove surface gases. After parts and subassemblies are completed, the final assembly is welded in an inert arc process and the klystron put in a dual vacuum oven for final outgassing and cathode activation. This bakeout at 550°C for periods of 12 to 20 hours is essential in assuring that all internal klystron surfaces are outgassed prior to cathode activation.

Preliminary cross-section drawings for magnetically-focused klystrons are presented in Figures 70 through 75. While these serve to illustrate some of the construction techniques which have been discussed, they are not intended to be final designs. In particular, the final integration of electrical, mechanical, and thermal designs will result in modification of some of the details in these figures.

OPERATING PROCEDURES

Start-Up and Shutdown

After installation of the klystron in the magnetic field coil and socket environment, and connection of the necessary power supply leads, start-up under normal conditions would consist of the following:

(1) Apply and adjust magnetic field supplies. This enables the klystron body to absorb the heat generated by the magnetic field supplies and to approach the ambient temperature experienced during operation. In some cases this will also serve to melt the heat pipe working fluid.

(2) Apply ion pump supply voltage. This enables the ion pump to remove any residual gas left in the klystron after its previous operation. While it might be desirable to open the klystron up to the space environment after the required orbit has been obtained, further information about the residual gases given off by associated components during operation would be required before such a step is recommended.

(3) Apply heater voltage. A fast-heating filament and cathode structure could be designed for this application; however, since a five-minute restarting time is adequate, a more reliable heater design having a longer time constant is contemplated.

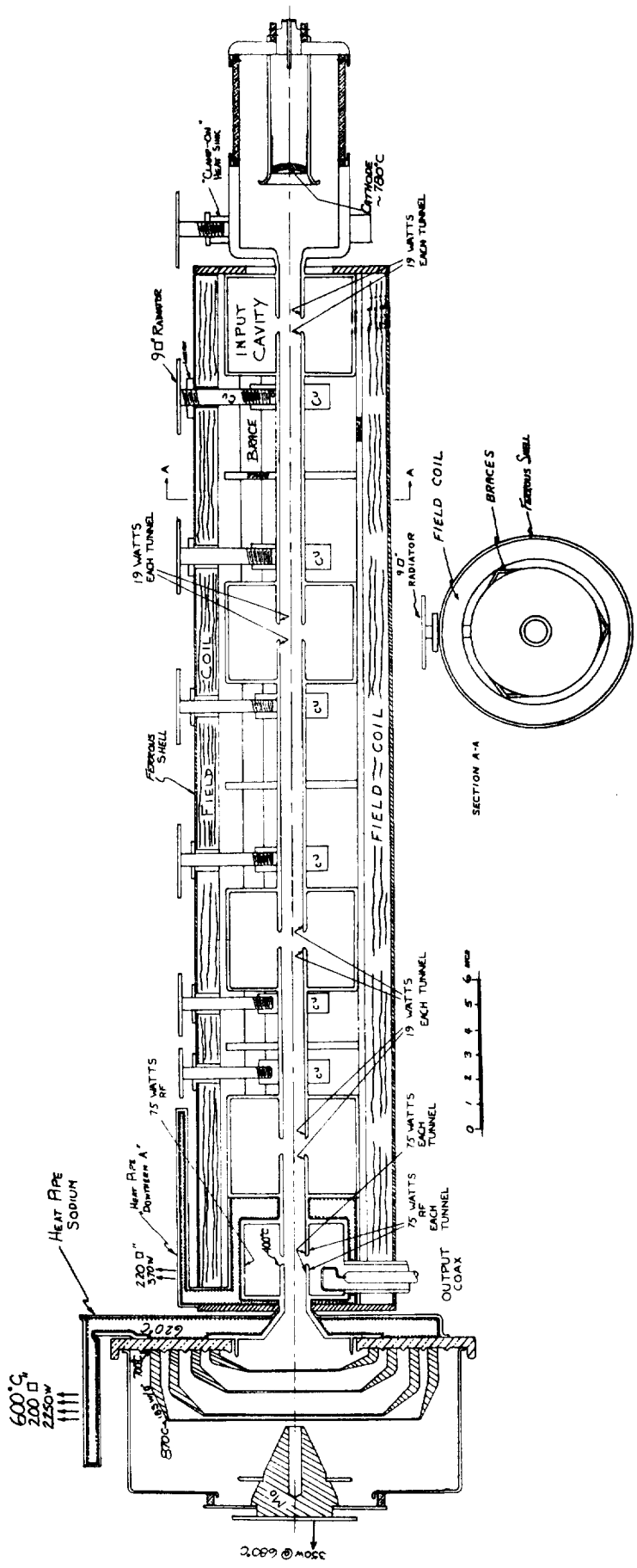

Figure 70 - Layout Sketch of 850-MHz AM Klystron

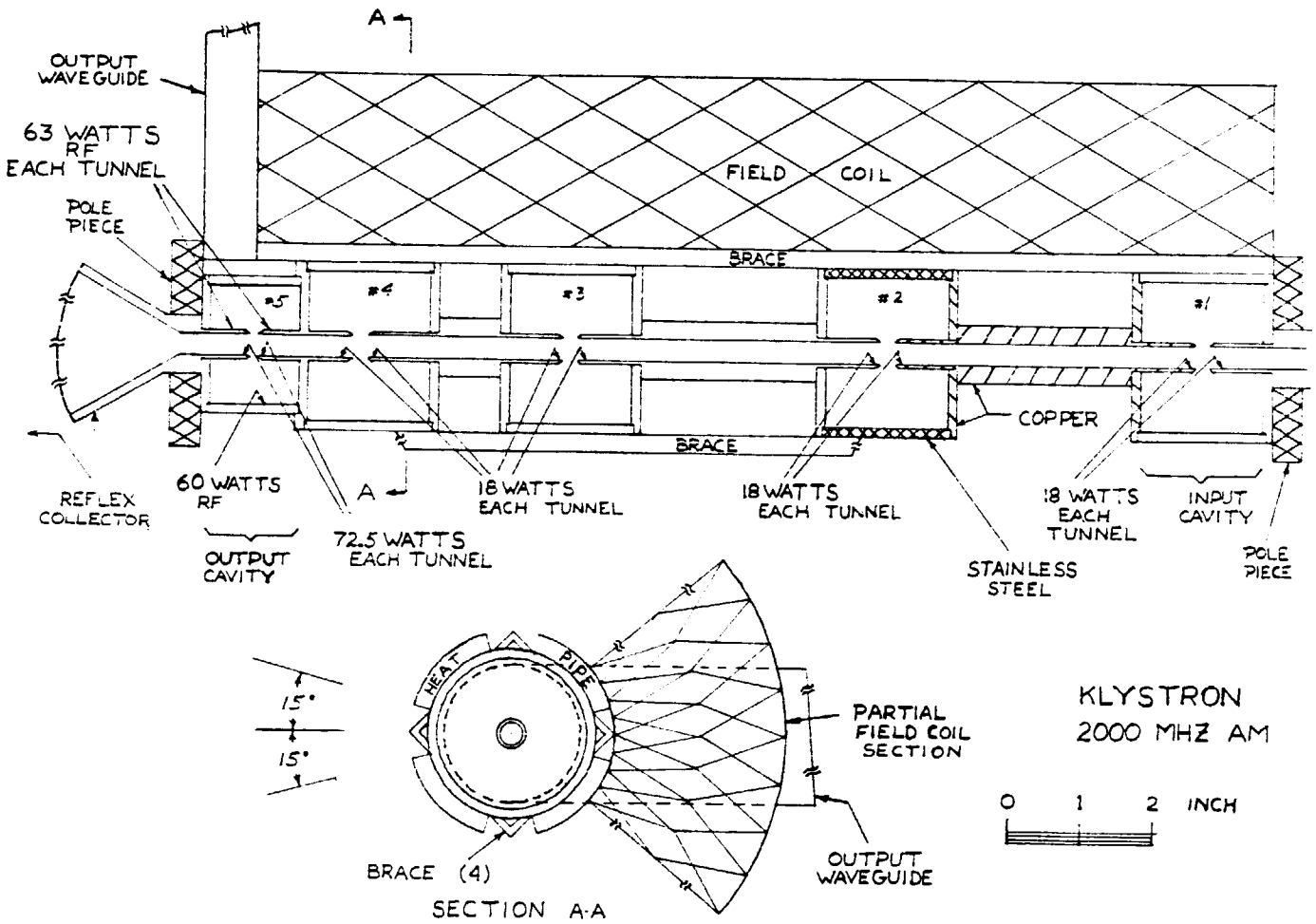

Figure 71 - Layout Sketch of Main Body of 2000-MHz AM Klystron

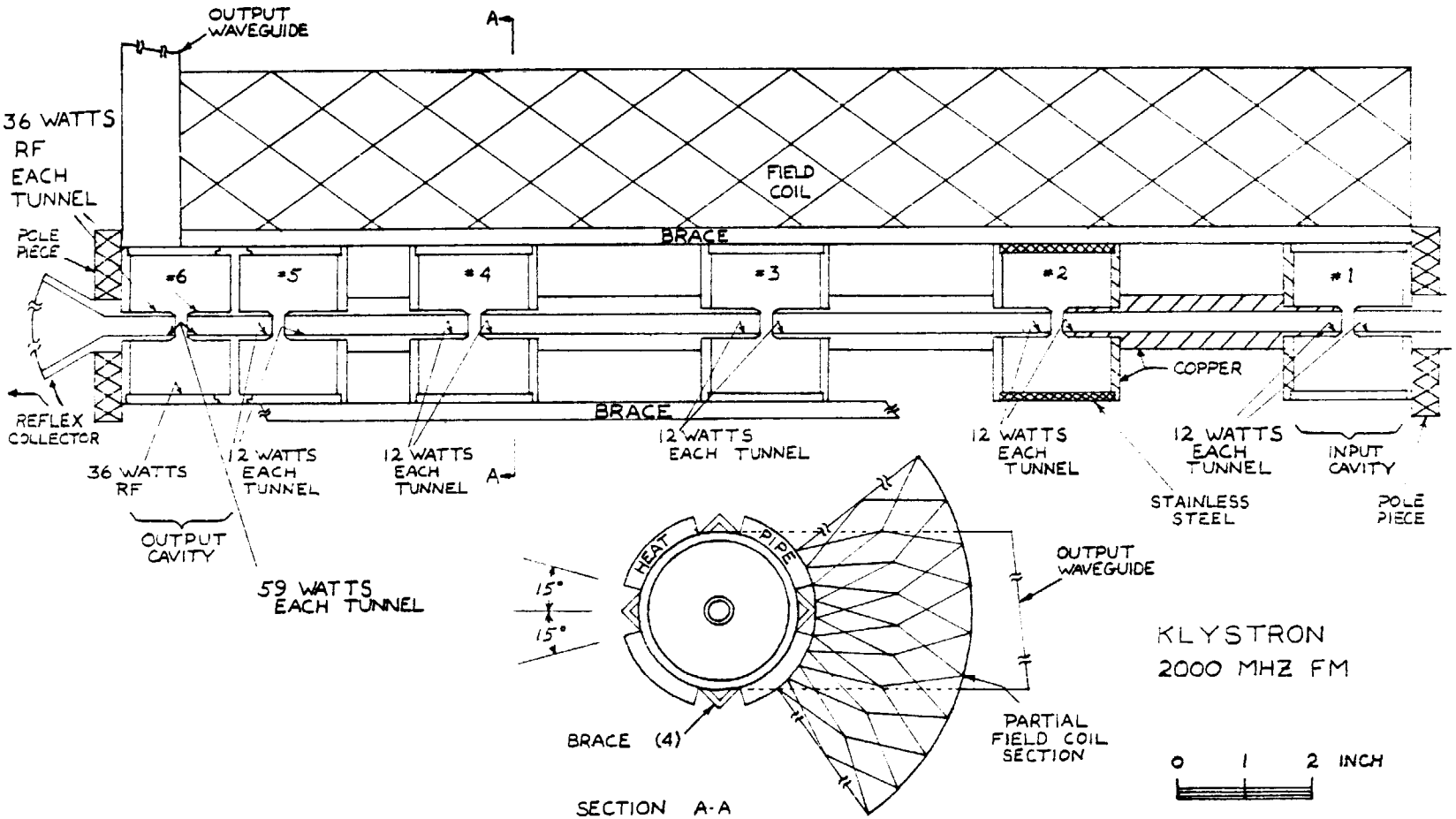

Figure 72 - Layout Sketch of Main Body of 2000-MHz FM Klystron with Single-Gap Output Cavity

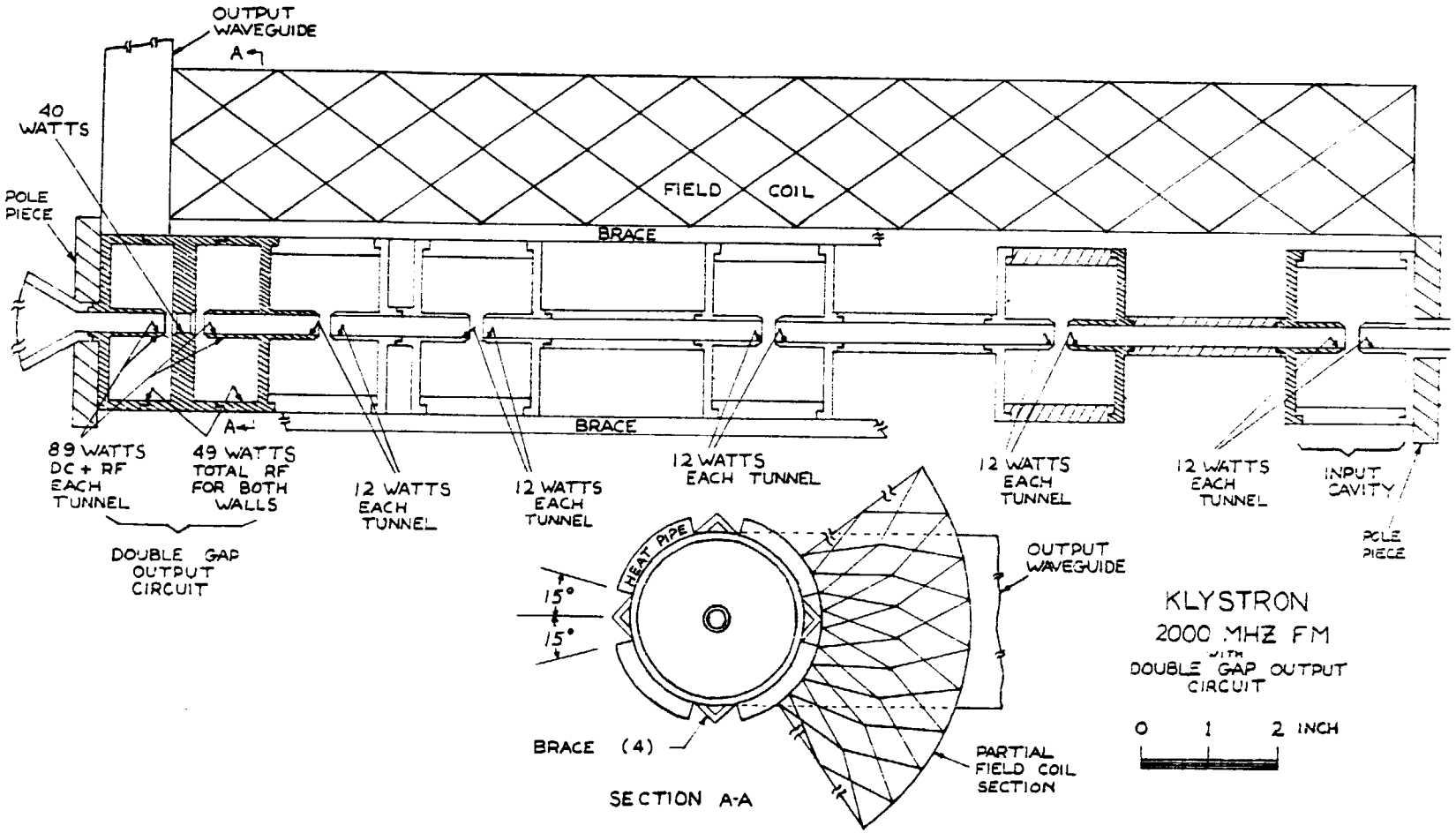

Figure 73 - Layout Sketch of Main Body of 2000-MHz FM Klystron with Double-Gap Extended Interaction Output Cavity

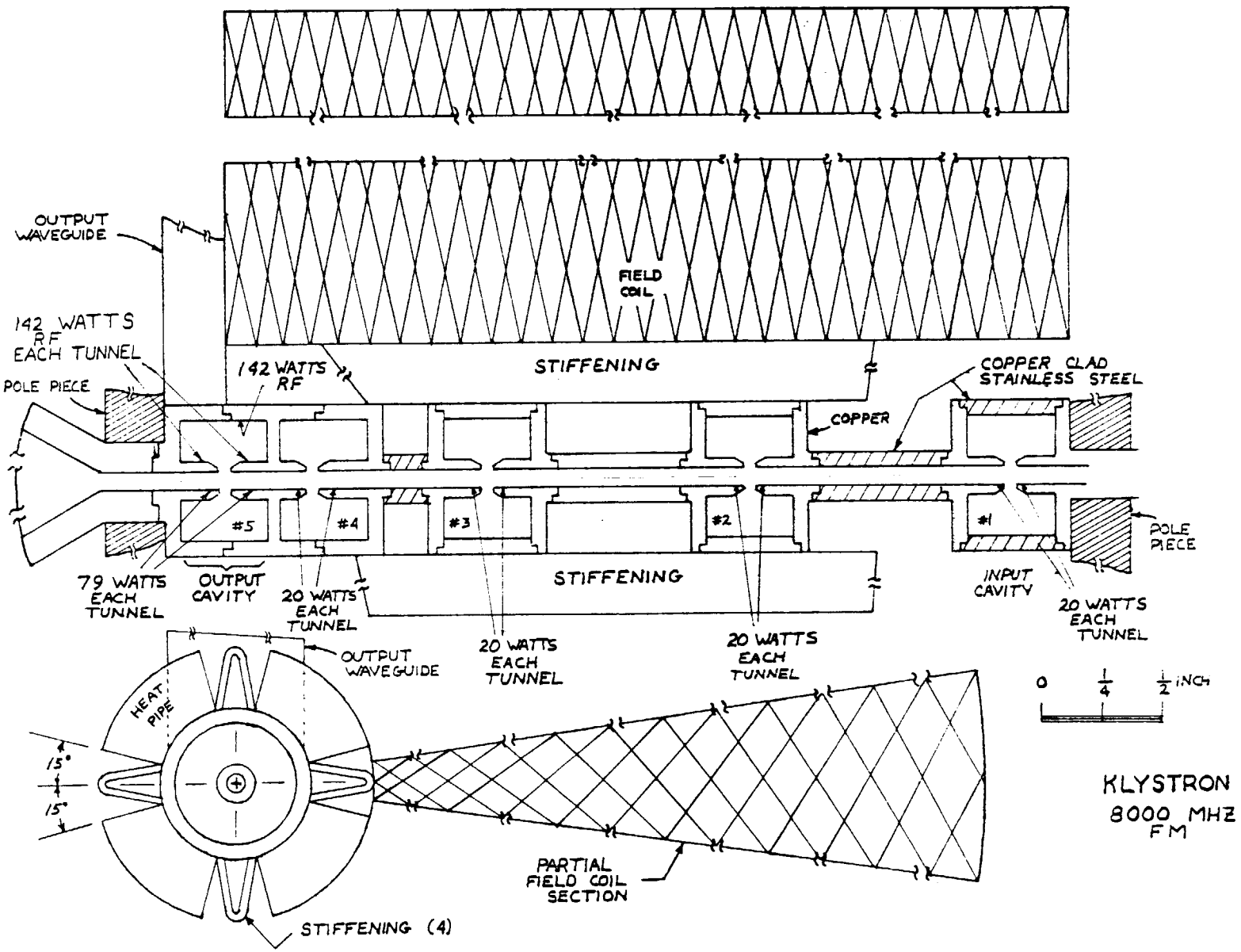

Figure 74 - Layout Sketch of Main Body of 8000-MHz FM Klystron

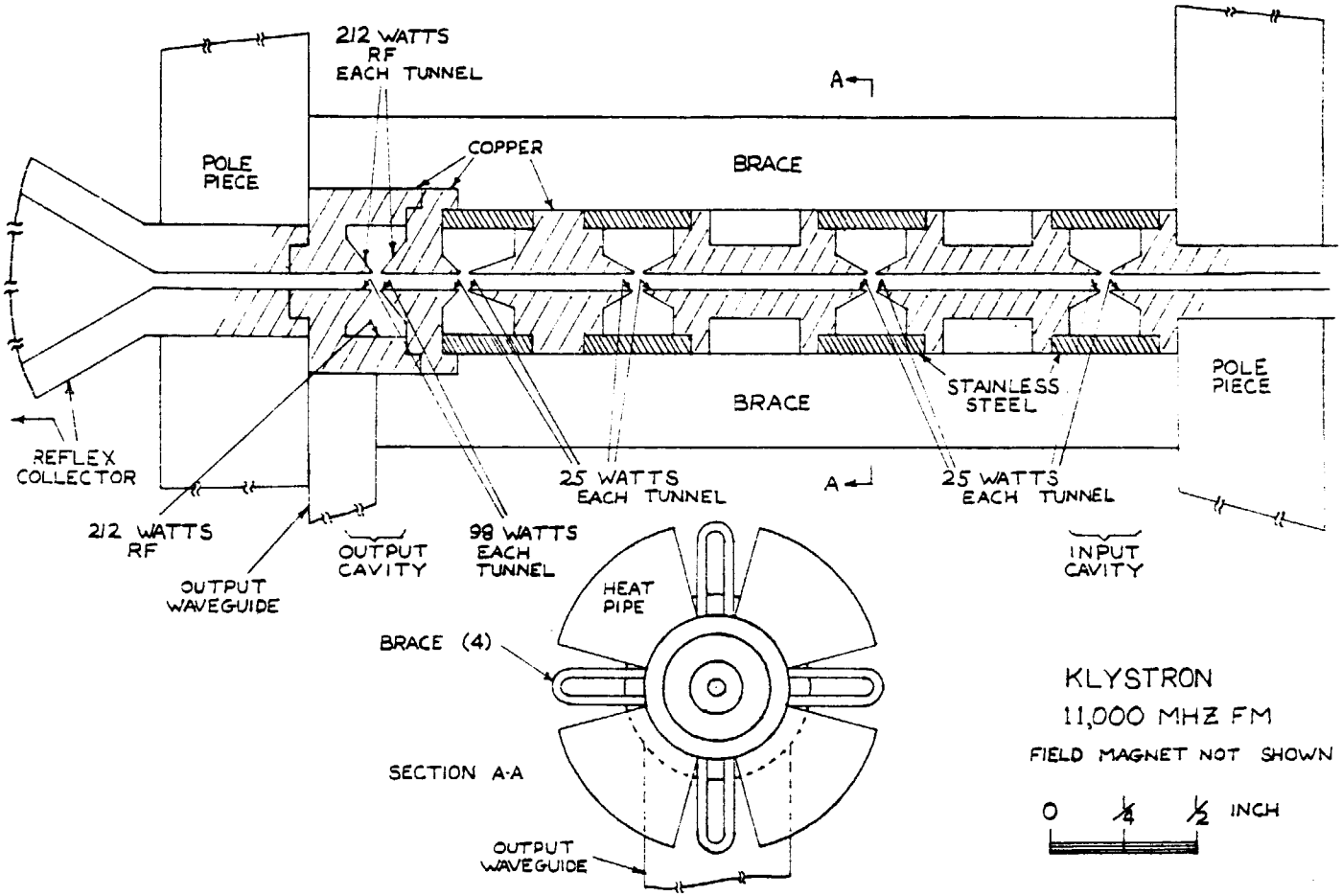

Figure 75 - Layout Sketch of Main Body of 11,000-MHz FM Klystron

(4) Apply and adjust beam and collector voltages. Both body current and ion pump current should be monitored to assure that normal operation is being achieved. (Refer to Section IX for a discussion of power control circuitry.)

(5) Apply and adjust RF drive power. Again, body current and ion pump current, as well as drive and output power, should be monitored to assure that normal operation is being achieved. This procedure is based on the use of a depressed collector, where the power dissipated in the collector is small, even at zero RF drive. In cases where no collector depression is employed, it is desirable to apply RF drive simultaneously with magnet power and then apply beam power. This avoids the high collector dissipation which would ordinarily take place at zero drive.

The shutdown procedure for the klystron is essentially the reverse of the start-up procedure, with the exception that the beam voltage and RF drive can be removed simultaneously.

(1) Remove beam voltage and RF drive voltage.

(2) Remove heater voltage.

(3) Remove ion pump supply voltage.

(4) Remove magnetic field coil supply voltages.

Pre-Launch Testing

It is assumed that complete quality assurance testing, including a 500 to 1000 hour "burn-in" will have been implemented for each klystron prior to delivery. Testing at the launch site then consists primarily of standard checks of the various components, plus a final full-power run of the transmitter after installation in the spacecraft. Because waste heat is radiated at high temperature, the final power test would be made in a space-simulator chamber. The standard check of klystron components are heater resistance, low-voltage emission test, gas condition (from ion pump reading), resistance of field coil and insulation resistance of the various seals.

Operating During Launch

Normal heater power should be applied during launch and booster acceleration. This will assure that the normally brittle tungsten filament will be at a relatively high temperature and in a ductile condition. No other voltages need be applied during the launch and booster acceleration.

Normal Operating Procedures in Orbit

Operation of the klystron while in orbit would be identical to the operation under ground conditions. The start-up procedure would consist of:

(1) Apply magnetic field coil power, if a solenoid is used rather than a permanent magnet.

(2) Apply ion pump supply voltage.

(3) Apply heater voltage.

(4) Apply beam and collector voltages.

(5) Apply RF drive power.

The shutdown procedure for short periods of time would consist of:

(1) Remove beam and collector voltages and RF drive.

(2) Remove magnetic field coil power, if electromagnetic focusing is used. This would leave the heater power and the ion pump supply voltages on. The vacuum would be maintained and the heater would not suffer a cycling period, and the klystron would be ready for almost instantaneous operation. The start-up procedure from this condition would be:

   (a) Apply magnetic field power, if required.

   (b) Apply beam and collector voltages.

   (c) Apply RF drive power.

The shutdown procedure for longer periods of time would be as follows:

(1) Remove beam and collector voltages, and RF drive power.

(2) Remove heater voltage.

(3) Remove ion pump supply voltage.

(4) Remove magnetic field coil power, if used.

KLYSTRON-SPACECRAFT INTERFACE

The klystron and its solenoid (or permanent magnet), its heat pipe and direct radiator cooling systems, and its power supplies may be integrated into a single modular self-contained subsystem. The only necessary connections to the remainder of the spacecraft would be the RF input signal from the video modulator, the low-voltage DC mains connections from the solar array, and the high-power RF output connection to the antenna.

The bulk of the klystron body, including the input and output waveguide connections, operates at the spacecraft frame potential. The problem of extending high-voltage leads from the main body power supply to the electron gun cathode assembly, and from the depressed collector supply to the reflex collector electrodes, may be eliminated by enclosing the cathode end of the klystron with its power supply in a hermetic shield, and the collector and its power supply in a second hermetic shield. However, because of the lower operating temperature required for the power supplies, and the separate heat pipe cooling systems for the collector and the collector power supply, it might be more desirable that they be in two separate enclosures connected by short high-voltage cables. The output end of the klystron should be located near the antenna to minimize transmission line losses between the klystron and the antenna.

The klystron amplifier module may be prefabricated and tested as an independent structure and subsequently bolted to the surface of the spacecraft. In order to keep the heat pipe system to a minimum weight and to permit direct radiation of a portion of the waste heat generated in the klystron, the klystron amplifier module is preferably located on a surface of the spacecraft orientated away from the sun. The primary consideration is to isolate the high temperatures of the klystron and radiators from surrounding parts of the vehicle. Insulation should be provided at all surfaces in contact with the vehicle structure. Surfaces of the klystron-radiator assembly which can radiate to the interior of the vehicle should be insulated. A blanket of 15 layers of aluminized or gold coated Kapton will provide almost total isolation for surfaces below 300°C. The collector, which operates in the 600 to 700°C range, should be insulated using the same type of multilayer insulation, except the Kapton must be replaced by 1 or 2 mil thick stainless steel, titanium or other suitable material.

Figure 76 shows a typical configuration. Although the illustration depicts for a 2000-MHz AM klystron, it is representative of all of the klystrons considered in this study. In the event the beam disperser cannot be positioned to radiate directly to space, a sodium heat pipe can be used to transport the heat to the radiator used for the collector elements. If this is required, it would simplify the design if the beam disperser operates at ground potential.

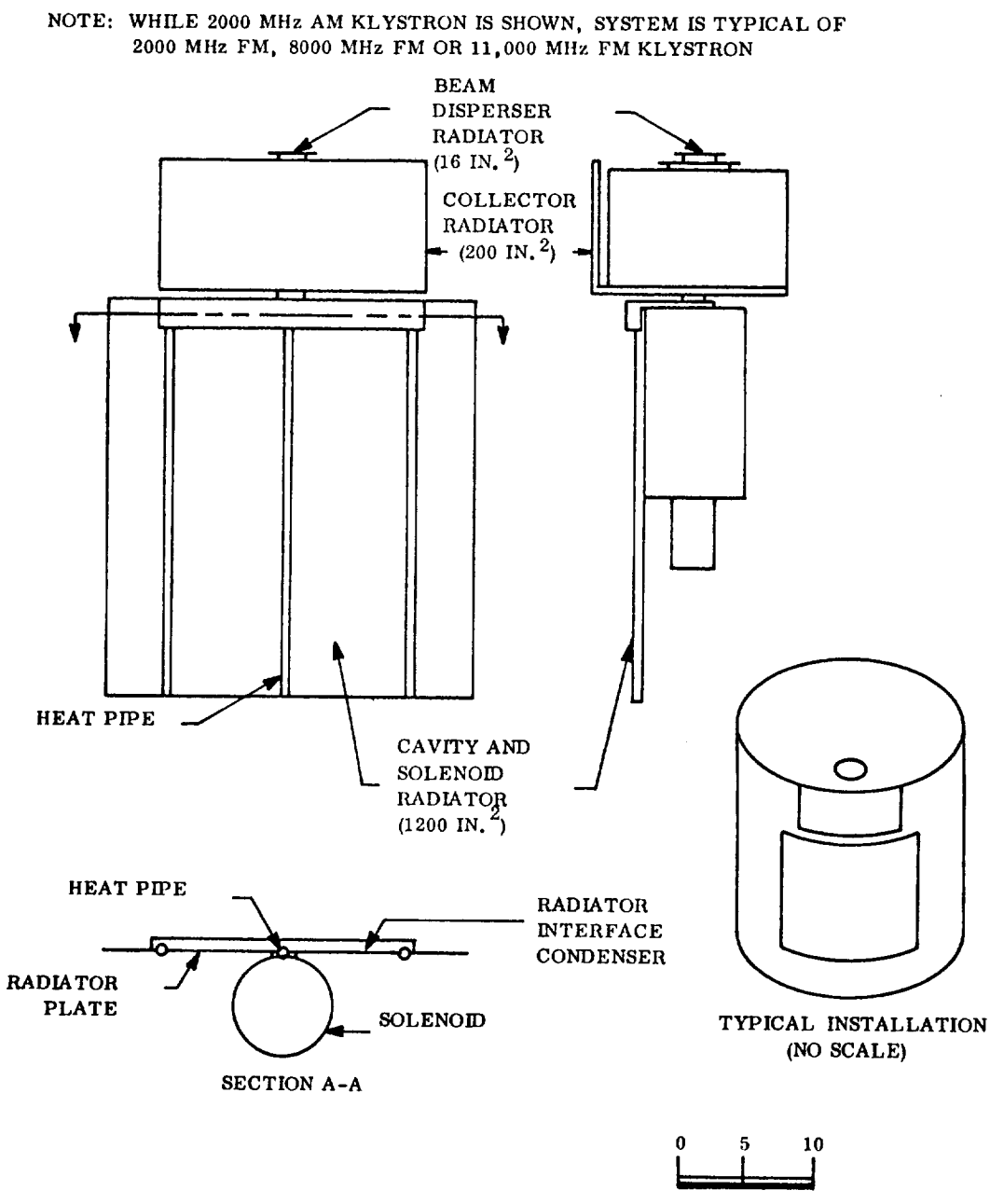

Figure 76 - Sketch of Typical Magnetically-Focused Klystron and Associated Thermal Control System Installation in Spacecraft

Section XI

EFFICIENCY ANALYSIS AND TRADE-OFFS

The overall output efficiency η_o of a high-gain klystron with a reflex depressed collector may be written as:

$$\eta_o = \eta_t \eta_{ckt} \eta_i / \left[1 + \Sigma - \eta_{rc} (1 - \eta_i) \eta_t \right] \qquad (37)$$

where: η_t = the beam transmission fraction

η_{ckt} = the klystron output circuit efficiency

η_i = is the klystron internal conversion efficiency

Σ = the sum of all external input power, exclusive of beam power, normalized to the beam power

η_{rc} = the reflex collector recovery efficiency

Σ in this case includes the electron gun heater power and the solenoid power if a permanent magnet is not employed.

The useful fraction of the beam power that is converted into RF power within the klystron is the product $\eta_t \eta_i$. Since a portion of this is unavoidably dissipated as heat in the output circuit, the remaining fraction of the beam power converted into useful microwave power is $\eta_{ckt} \eta_t \eta_i$. It is therefore of primary importance for maximum efficiency that the circuit efficiency, the beam transmission efficiency, and the internal conversion efficiency be independently made as near 100 percent as possible.

Although microwave cavities have internal losses several magnitudes smaller than lumped parameter resonant circuits at low frequencies, the circuit efficiency with conventional doubly-reentrant single-gap cavities can be as low as 89 percent in the case of the 11,000-MHz FM klystron design. Admittedly, the figure quoted here is a lower limit. With an optimized toroidal design having conical reentrant tunnels, and with especially treated copper surfaces, the internal losses might be decreased by a factor of 2, to raise the circuit efficienty to the vicinity of 95 percent at this beam impedance and power level.

The internal conversion efficiency η_i may be increased further by a continuation of the type of analytic investigation undertaken in this study. In the present study, investigation was made of many klystrons for either AM or FM service, over a wide range of frequencies. Additional detailed study of a specific klystron could result in a further increase in efficiency.

A factor having a directly deleterious effect on efficiency is beam interception on the tunnel walls. Even if the intercepted electrons have already given up their energy in the output gap, they should not be allowed to collect on the distant tunnel of the output cavity because of the danger of secondary electrons returning toward the input of the klystron to spoil its phase or gain linearity. Consequently, an important goal to pursue is more nearly perfect beam transmission at large-signal levels. The best method of achieving high beam transmission appears to be through stiffening the electron beam with carefully designed solenoidal electromagnets rather than with permanent magnets. The improvement in overall efficiency with an improvement in beam transmission will be illustrated in tables and graphs to be presented below.

The next variable in Eq. (37) affecting the overall efficiency is Σ, the normalized sum of power inputs other than the beam power required for the operation of the klystron. The heater power is almost negligibly small in comparison with the beam power, but may be decreased further by improved insulation and heat-shielding of the thermionic cathode. However, this should not be done at the expense of mechanical strength of the cathode support. Although the solenoid power can be eliminated if a permanent magnet of acceptable weight and magnetic properties can be developed, it seems likely that for light weight and precision of electron beam formation and stiffening, a solenoid is more desirable. Other focusing methods such as periodic permanent magnet focusing and electrostatic focusing would be less desirable because of less rigid control of the electron trajectories in a high-power klystron and the additional mechanical complexity and cavity compromises that are entailed.

Both solenoid power input and weight decrease linearity with a reduction in the value of the magnetic field strength used for beam focusing. It is desirable, therefore, that studies be conducted to determine the feasibility of employing a less rigid electron beam than was considered in this study -- i.e., an electron beam collimated by a magnetic field less than three times the Brillouin value for a beam from a shielded cathode. Curves given later in this section show the expected efficiency improvement with the present klystron designs if the same internal conversion efficiency can

be achieved with weaker collimating fields, with normalized values of solenoid power ranging from 0 (permanent magnet focusing) to 3. The normalization of these powers is with respect to the solenoid power required for Brillouin focusing.

The next term in the overall efficiency expression is η_{rc}, the reflex collector energy recovery efficiency. The fractional energy in the portion of the spent beam reaching the collector is given by the product $(1 - \eta_i)\eta_t$; hence, the recovered fraction of beam energy is $(1 - \eta_i)\eta_t\eta_{rc}$. It is considered that a reflex collector having a recovery efficiency of 85 percent can be developed and that perhaps 95 percent is achievable. To illustrate these two cases, as well as the effect of having no depressed collection at all, η_{rc} values of 0, 85 and 95 percent are considered below.

Tables XVIII through XXIII present the computed overall efficiencies at the average picture level for AM klystrons, and at saturation power output for the FM klystrons. In all cases the beam transmission is allowed to take on values of 95, 96, 97, 98, 99, and 100 percent, and the normalized solenoid power ranges from 0 (permanent magnet focusing) in steps of 1 to 3 (solenoid providing three times the field for Brillouin focusing). These data are also presented graphically in Figures 77 through 82.

Several deductions may be made from the curves with respect to the importance of high reflex collector recovery efficiency, high beam transmission, and low magnetic field strength. In the case of the 850-MHz klystron, for example, the average picture level efficiency is the range of 17 to 18 percent for virtually all solenoid or permanent magnets considered at all beam transmission efficiencies, for the case of no potential depression in the collector. With a reflex collector recovery efficiency of 85 percent, however, the efficiency is increased by a factor of 3. Consequently, for AM klystrons, the most significant first step to be made in increasing klystron efficiency is the early development of a reflex depressed collector with a high energy-recovery efficiency.

In the case of the 850-MHz AM klystron with a reasonable beam transmission of 98 percent and reflex collector recovery efficiency of 85 percent, the solenoid for producing the Brillouin field reduces the efficiency by 2.4 percentage points, and for the solenoid designed for three times the Brillouin field 6.5 percentage points. At 8000-MHz, where present technology would allow a beam transmission of about 96 percent, a solenoid for the Brillouin field would cost 1.9 efficiency percentage points, and for the limiting case of three times the Brillouin field 5.6 percentage points. Since the interaction

Table XVIII - Efficiency Trade-Offs for 850-MHz AM Klystron

Reflex Collector Recovery Efficiency: 0 (No potential depression)

Solenoid Power (Normalized)	Beam Transmission - Percent					
	95	96	97	98	99	100
0 (PM)	17.5	17.7	17.9	18.1	18.3	18.4
1	17.3	17.4	17.6	17.8	18.0	18.2
2	17.0	17.2	17.4	17.6	17.7	17.9
3	16.8	16.9	17.1	17.3	17.5	17.7

Reflex Collector Recovery Efficiency: 85%

Solenoid Power (Normalized)	Beam Transmission - Percent					
	95	96	97	98	99	100
0 (PM)	50.0	51.5	53.1	54.8	56.5	58.3
1	48.0	49.4	50.9	52.4	54.1	55.7
2	46.1	47.5	48.8	50.3	51.8	53.3
3	44.4	45.6	46.9	48.3	49.7	51.1

Reflex Collector Recovery Efficiency: 95%

Solenoid Power (Normalized)	Beam Transmission - Percent					
	95	96	97	98	99	100
0 (PM)	64.0	66.5	69.2	72.0	75.0	78.3
1	60.7	63.0	65.4	68.0	70.7	73.6
2	57.7	59.8	62.1	64.4	66.9	69.5
3	55.0	57.0	59.0	61.2	63.5	65.8

Table XIX - Efficiency Trade-Offs for 2000-MHz AM Klystron

Reflex Collector Recovery Efficiency: 0 (No potential depression)

Solenoid Power (Normalized)	Beam Transmission - Percent					
	95	96	97	98	99	100
0 (PM)	18.1	18.3	18.5	18.7	18.9	19.1
1	18.0	18.1	18.3	18.5	18.7	18.9
2	17.8	17.9	18.1	18.3	18.5	18.7
3	17.6	17.8	17.9	18.1	18.3	18.5

Reflex Collector Recovery Efficiency: 85%

Solenoid Power (Normalized)	Beam Transmission - Percent					
	95	96	97	98	99	100
0 (PM)	50.7	52.2	53.8	55.4	57.1	58.9
1	49.2	50.6	52.1	53.7	55.3	57.0
2	47.8	49.2	50.6	52.1	53.6	55.2
3	46.4	47.8	49.1	50.5	52.0	53.5

Reflex Collector Recovery Efficiency: 95%

Solenoid Power (Normalized)	Beam Transmission - Percent					
	95	96	97	98	99	100
0 (PM)	64.2	66.7	69.3	72.1	75.0	78.1
1	61.8	64.2	66.6	69.1	71.9	74.7
2	59.6	61.8	64.1	66.5	69.0	71.7
3	57.6	59.6	61.7	64.0	66.3	68.8

Table XX - Efficiency Trade-Offs for 2000-MHz FM Klystron (Single-Gap Output)

Reflex Collector Recovery Efficiency: 0 (No potential depression)

Solenoid Power (Normalized)	Beam Transmission - Percent					
	95	96	97	98	99	100
0 (PM)	62.4	63.1	63.7	64.4	65.0	65.7
1	61.4	62.0	62.7	63.3	64.0	64.6
2	60.4	61.0	61.6	62.3	62.9	63.5
3	59.4	60.0	60.6	61.3	61.9	62.5

Reflex Collector Recovery Efficiency: 85%

Solenoid Power (Normalized)	Beam Transmission - Percent					
	95	96	97	98	99	100
0 (PM)	83.4	84.6	85.8	87.0	88.2	89.4
1	81.6	82.7	83.9	85.0	86.2	87.4
2	79.8	80.9	82.0	83.1	84.3	85.4
3	78.1	79.2	80.3	81.4	82.5	83.6

Reflex Collector Recovery Efficiency: 95%

Solenoid Power (Normalized)	Beam Transmission - Percent					
	95	96	97	98	99	100
0 (PM)	86.8	88.1	89.4	90.7	92.0	93.3
1	84.8	86.1	87.3	88.6	89.9	91.1
2	82.9	84.1	85.3	86.6	87.8	89.0
3	81.1	82.3	83.4	84.6	85.8	87.0

Table XXI - Efficiency Trade-Offs for 2000-MHz FM Klystron (Double-Gap Output)

Reflex Collector Recovery Efficiency: 0 (No potential depression)

Solenoid Power (Normalized)	Beam Transmission - Percent					
	95	96	97	98	99	100
0 (PM)	60.2	60.8	61.4	62.1	62.7	63.3
1	59.1	59.8	60.4	61.0	61.6	62.3
2	58.2	58.8	59.4	60.0	60.6	61.2
3	57.2	57.8	58.4	59.0	59.6	60.2

Reflex Collector Recovery Efficiency: 85%

Solenoid Power (Normalized)	Beam Transmission - Percent					
	95	96	97	98	99	100
0 (PM)	83.5	84.7	86.0	87.2	88.5	89.7
1	81.6	82.8	84.0	85.2	86.4	87.6
2	79.7	80.9	82.1	83.2	84.4	85.6
3	78.0	79.1	80.2	81.4	82.5	83.7

Reflex Collector Recovery Efficiency: 95%

Solenoid Power (Normalized)	Beam Transmission - Percent					
	95	96	97	98	99	100
0 (PM)	87.5	88.9	90.2	91.6	93.0	94.4
1	85.4	86.7	88.0	89.3	90.7	92.0
2	83.4	84.7	85.9	87.2	88.5	89.8
3	81.5	82.7	83.9	85.1	86.4	87.7

Table XXII - Efficiency Trade-Offs for 8000-MHz FM Klystron

Reflex Collector Recovery Efficiency: 0 (No potential depression)

Solenoid Power (Normalized)	Beam Transmission - Percent					
	95	96	97	98	99	100
0 (PM)	58.7	59.3	59.9	60.5	61.1	61.8
1	57.6	58.2	58.8	59.4	60.0	60.7
2	56.6	57.2	57.8	58.4	59.0	59.6
3	55.6	56.2	56.8	57.4	58.0	58.5

Reflex Collector Recovery Efficiency: 85%

Solenoid Power (Normalized)	Beam Transmission - Percent					
	95	96	97	98	99	100
0 (PM)	79.8	80.9	82.1	83.3	84.4	85.6
1	77.9	79.0	80.1	81.2	82.4	83.5
2	76.0	77.1	78.2	79.3	80.4	81.5
3	74.2	75.3	76.3	77.4	78.5	79.6

Reflex Collector Recovery Efficiency: 95%

Solenoid Power (Normalized)	Beam Transmission - Percent					
	95	96	97	98	99	100
0 (PM)	83.3	84.6	85.8	87.1	88.4	89.7
1	81.2	82.4	83.6	84.9	86.1	87.4
2	79.2	80.4	81.6	82.7	83.9	85.2
3	77.3	78.4	79.6	80.7	81.9	83.1

Table XXIII - Efficiency Trade-Offs for 11,000-MHz FM Klystron

Reflex Collector Recovery Efficiency: 0 (No potential depression)

Solenoid Power (Normalized)	Beam Transmission - Percent					
	95	96	97	98	99	100
0 (PM)	52.8	53.4	53.9	54.5	55.0	55.6
1	51.4	51.9	52.5	53.0	53.6	54.1
2	50.1	50.6	51.1	51.6	52.2	52.7
3	48.8	49.3	49.8	50.3	50.8	51.3

Reflex Collector Recovery Efficiency: 85%

Solenoid Power (Normalized)	Beam Transmission - Percent					
	95	96	97	98	99	100
0 (PM)	75.3	76.5	77.6	78.8	79.9	81.1
1	72.5	73.6	74.6	75.7	76.9	78.0
2	69.8	70.7	71.9	73.0	74.0	75.1
3	67.4	68.4	69.4	70.4	71.4	72.4

Reflex Collector Recovery Efficiency: 95%

Solenoid Power (Normalized)	Beam Transmission - Percent					
	95	96	97	98	99	100
0 (PM)	79.3	80.6	81.8	83.1	84.4	85.7
1	76.1	77.3	78.5	79.8	81.0	82.2
2	73.2	74.4	75.5	76.7	77.8	79.0
3	70.5	71.6	72.7	73.8	74.9	76.0

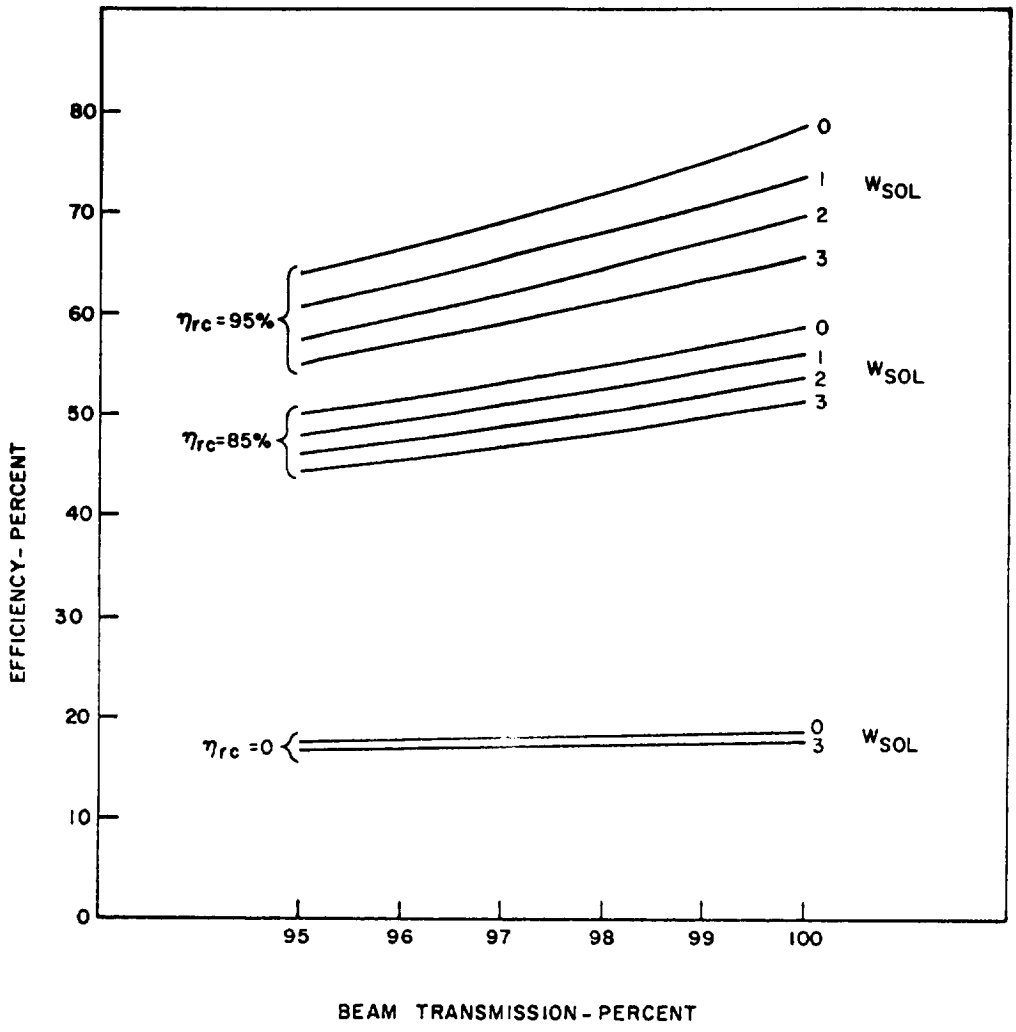

Figure 77 - Efficiency Trade-Offs in 850-MHz AM Klystron (Overall output efficiency versus beam transmission for three values of reflex-collector energy recovery efficiency, η_{rc}, and four values of normalized solenoid power, W_{sol})

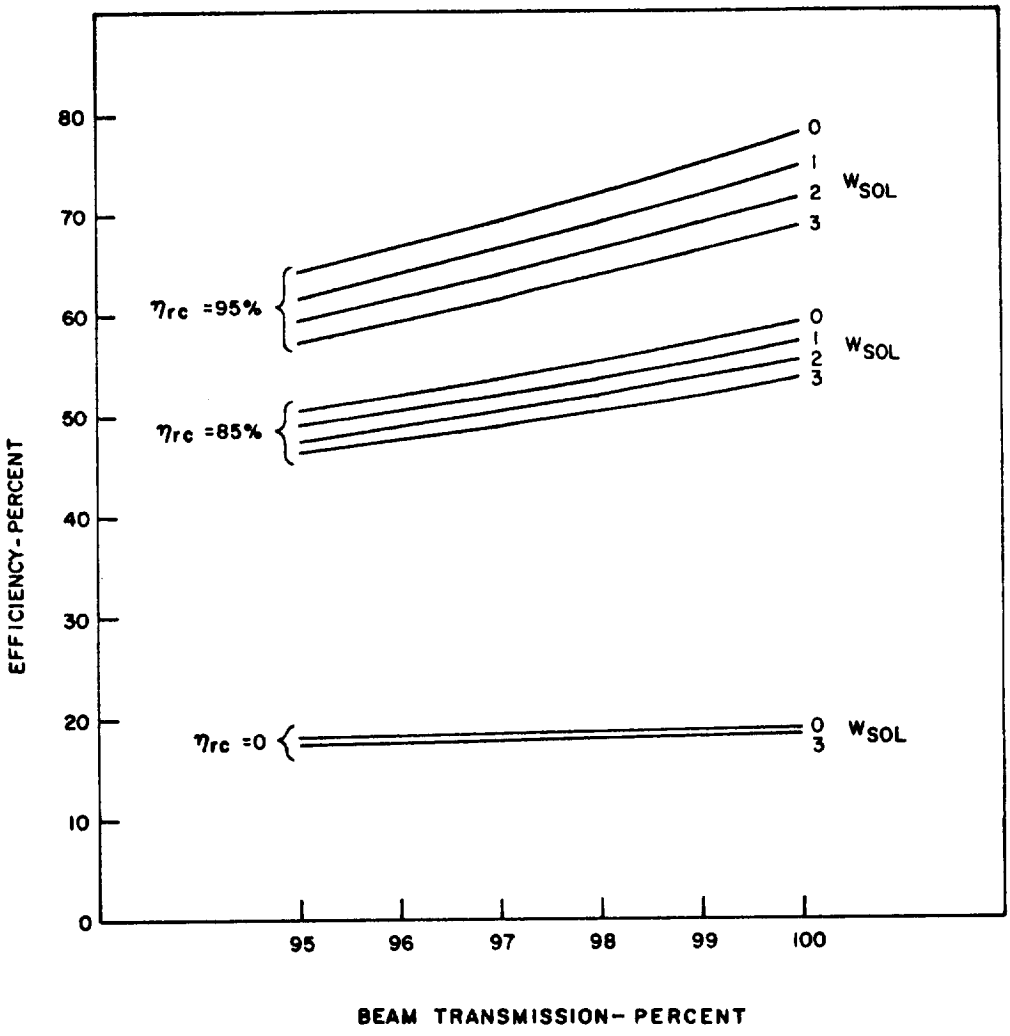

Figure 78 - Efficiency Trade-Offs in 2000-MHz AM Klystron (Overall output efficiency versus beam transmission for three values of reflex-collector energy recovery efficiency, η_{rc}, and four values of normalized solenoid power, W_{sol})

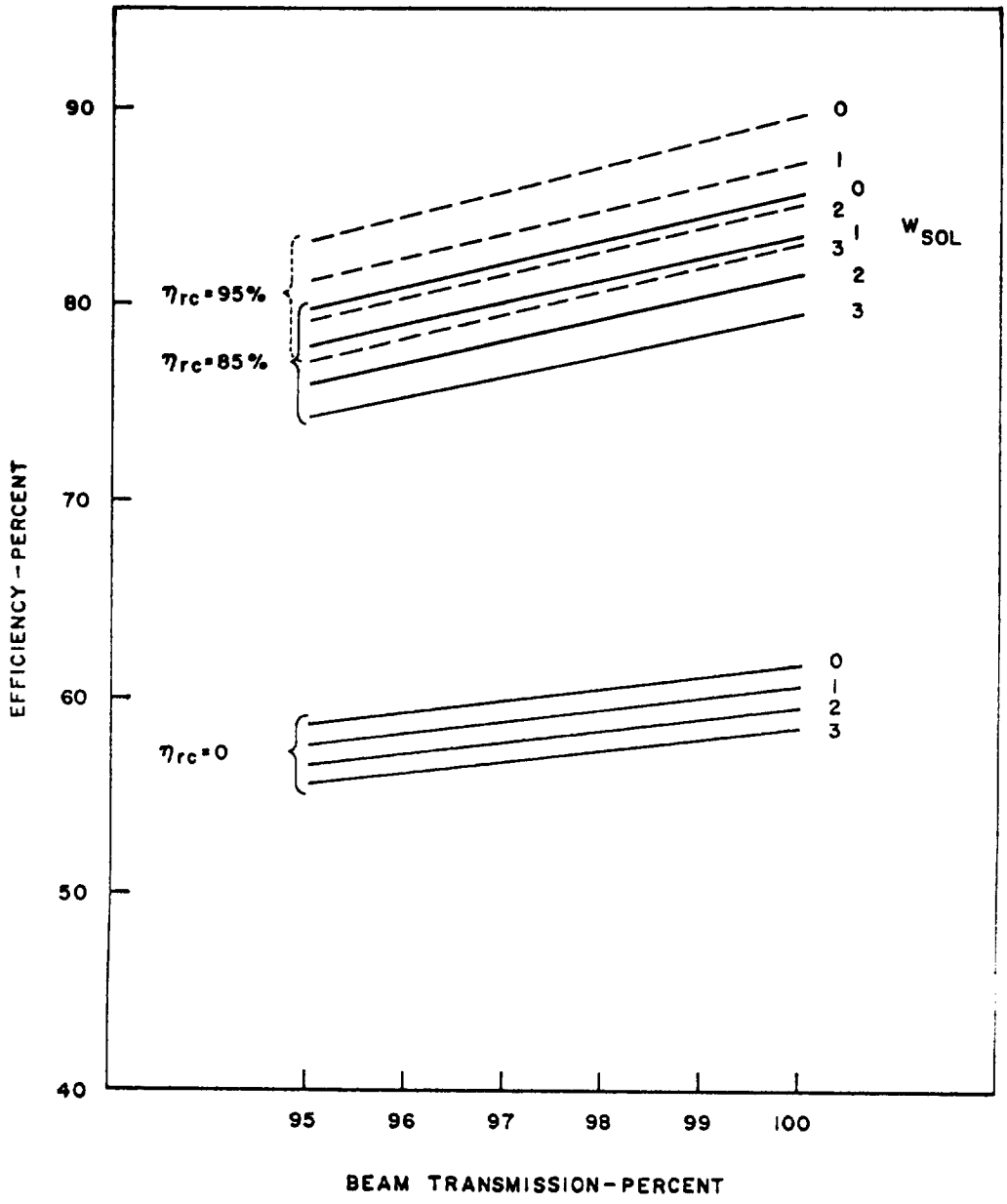

Figure 79 - Efficiency Trade-Offs in 2000-MHz FM Klystron with Single-Gap Output (Overall output efficiency versus beam transmission for three values of reflex-collector energy recovery efficiency, η_{rc}, and four values of normalized solenoid power, W_{sol})

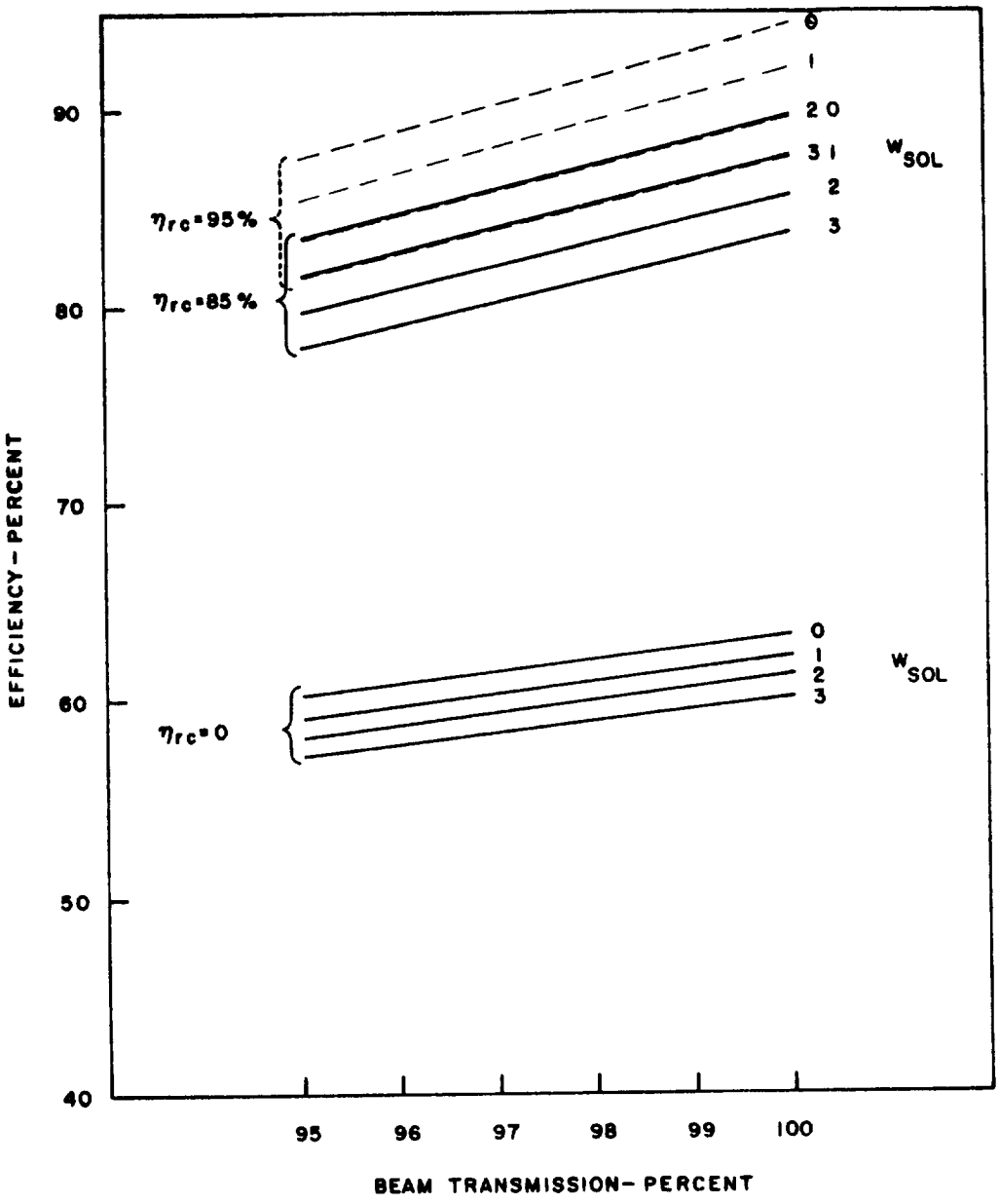

Figure 80 - Efficiency Trade-Offs in 2000-MHz FM Klystron with Double-Gap Output (Overall output efficiency versus beam transmission for three values of reflex-collector energy recovery efficiency, η_{rc}, and four values of normalized solenoid power, W_{sol})

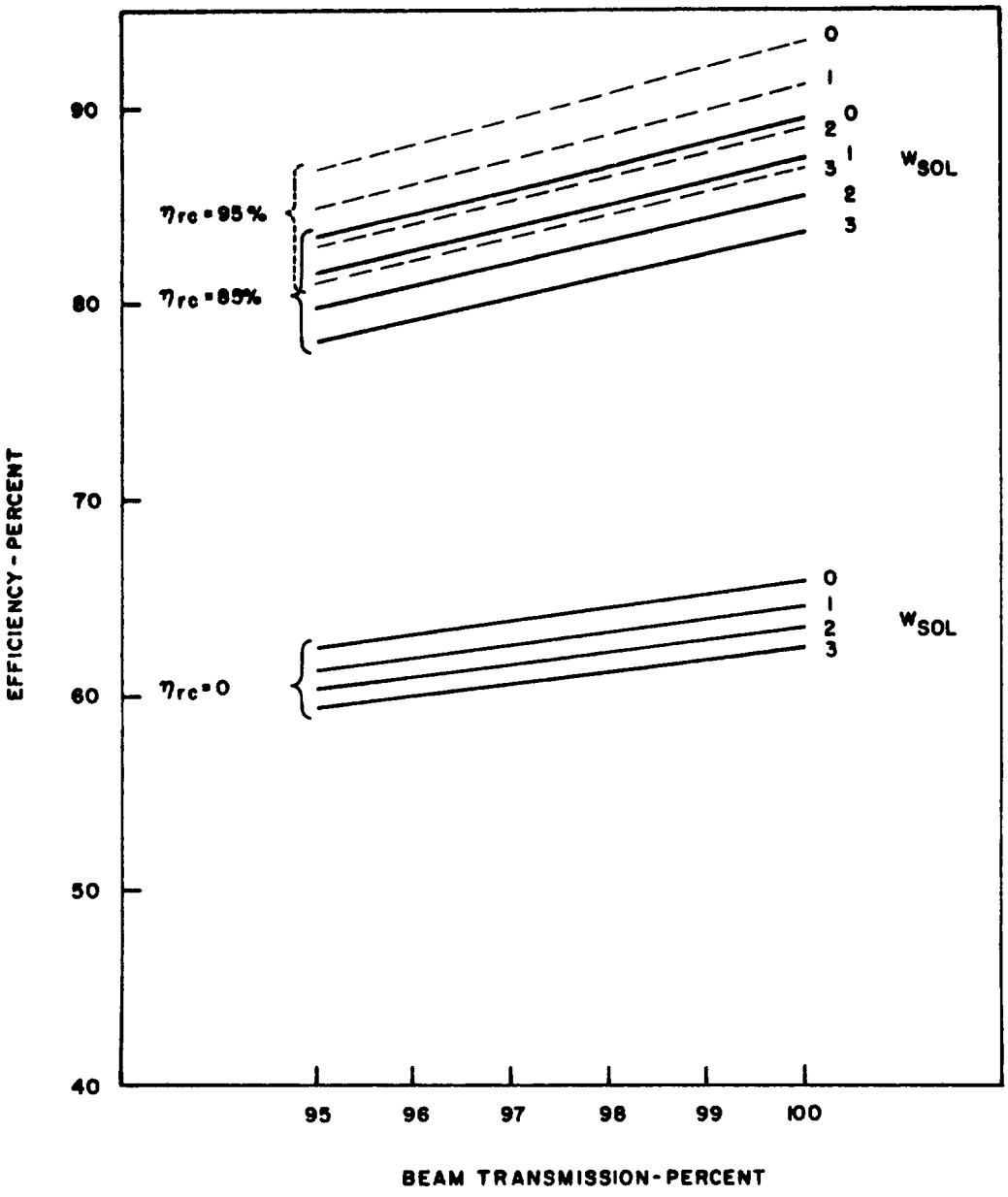

Figure 81 - Efficiency Trade-Offs in 8000-MHz FM Klystron (Overall output efficiency versus beam transmission for three values of reflex-collector energy recovery efficiency, η_{rc}, and four values of normalized solenoid power, W_{sol})

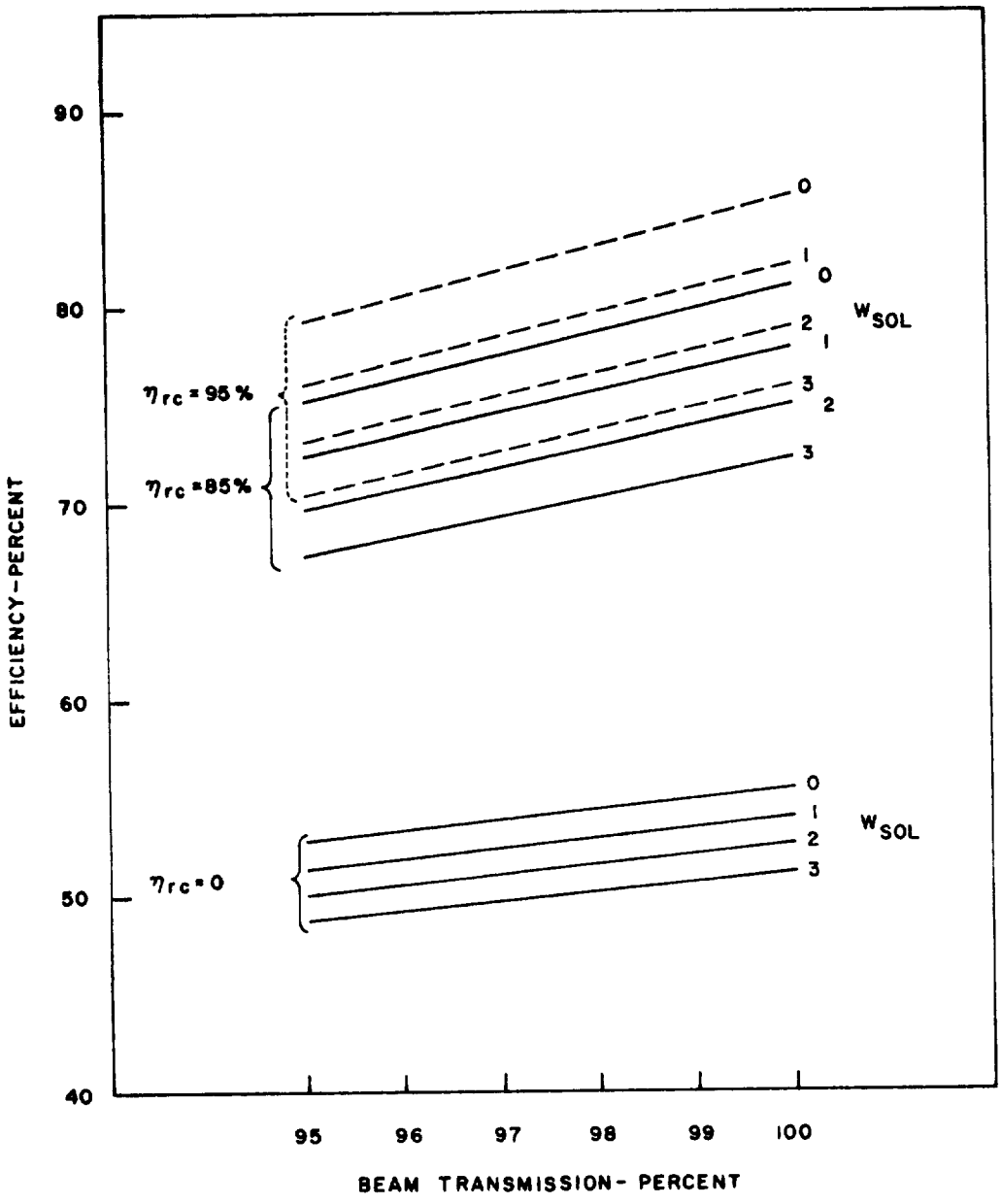

Figure 82 - Efficiency Trade-Offs in 11,000-MHz FM Klystron (Overall efficiency versus beam transmission for three values of reflex-collector energy recovery efficiency, η_{rc}, and four values of normalized solenoid power, W_{sol})

efficiency of klystrons with permanent magnet focusing is currently in the range of 5 percentage points lower than those with electromagnet focusing, it appears that the use of permanent magnet focusing to increase efficiency should not take precedence over such approaches as the depressed collector and better beam transmission.

In Figures 83 through 86 are plotted overall output efficiencies over the specified 30-MHz bandwidths of the 2000-MHz FM klystrons (both single-gap and double-gap output versions), the 8000-MHz klystron, and the 11,000-MHz klystron. The nominal design values of beam transmission of 97 percent at 2000 MHz, 96 percent at 8000 MHz, and 95 percent at 11,000 MHz, were used in the computation of these curves from Eq. (35). Although the depressed collector cannot increase the power output at the band edges, it can make the operation of the klystron more uniform in efficiency across the band.

The effect of beam interception in decreasing the available power output can be compensated to achieve a specified power output by adjusting the beam voltages. In these designs a slight increase in voltage will not appreciably alter the klystron efficiency characteristics but will increase the power output according to the 5/2 power of the voltage. The present designs were made for the nominal 2 to 5 percent interception discussed above. Figure 87 shows the voltage required to yield the specified power outputs for each klystron as a function of beam transmission, ranging from 95 to 100 percent. Table XXIV also gives the required beam voltages to meet the power specifications at the nominal beam transmission considered as the present state-of-art.

- - - - - - -

Table XXIV - Required Beam Potential for Specified Power at Nominal Beam Transmission

Service	t	P_o	V_o
850-MHz AM	98%	9.5 kW	15.9 kV
2000-MHz AM	97	6.25	13.5
2000-MHz FM	97	5.0	11.9
8000-MHz FM	96	5.0	12.3
11,000-MHz FM	95	5.0	12.9

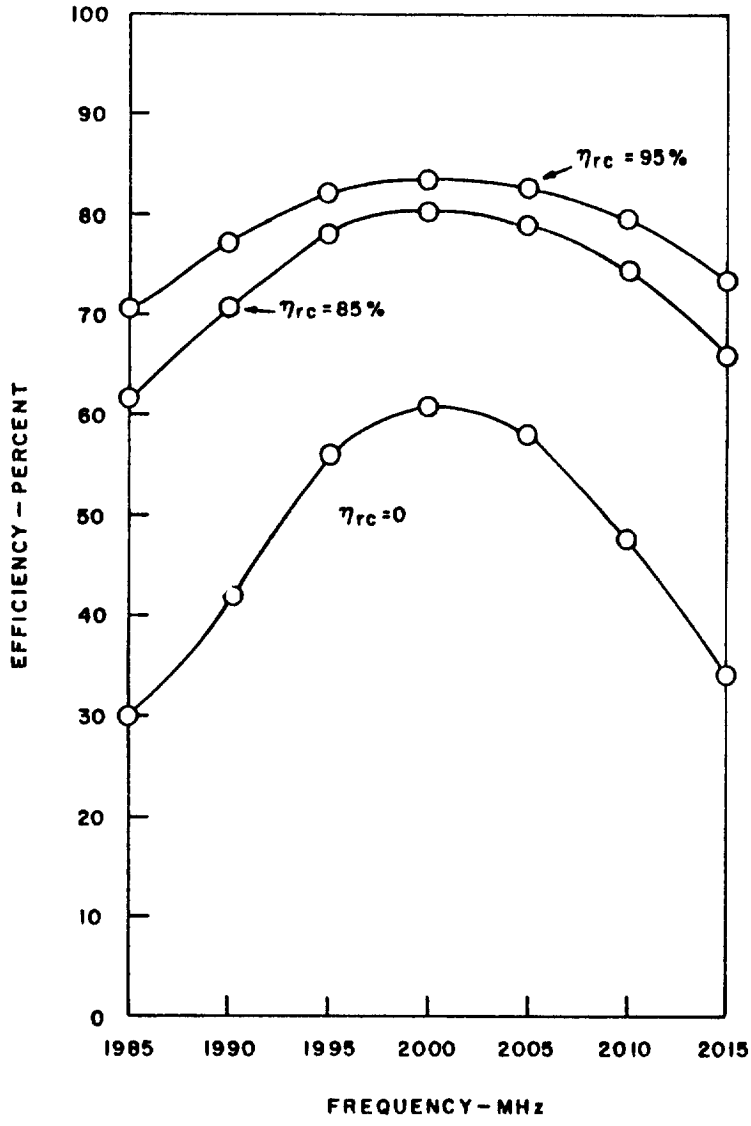

Figure 83 - Efficiency of 2000-MHz FM Klystron Across the Band at Three Values of Reflex-Collector Energy Recovery Efficiency η_{rc} (Single-Gap Output)

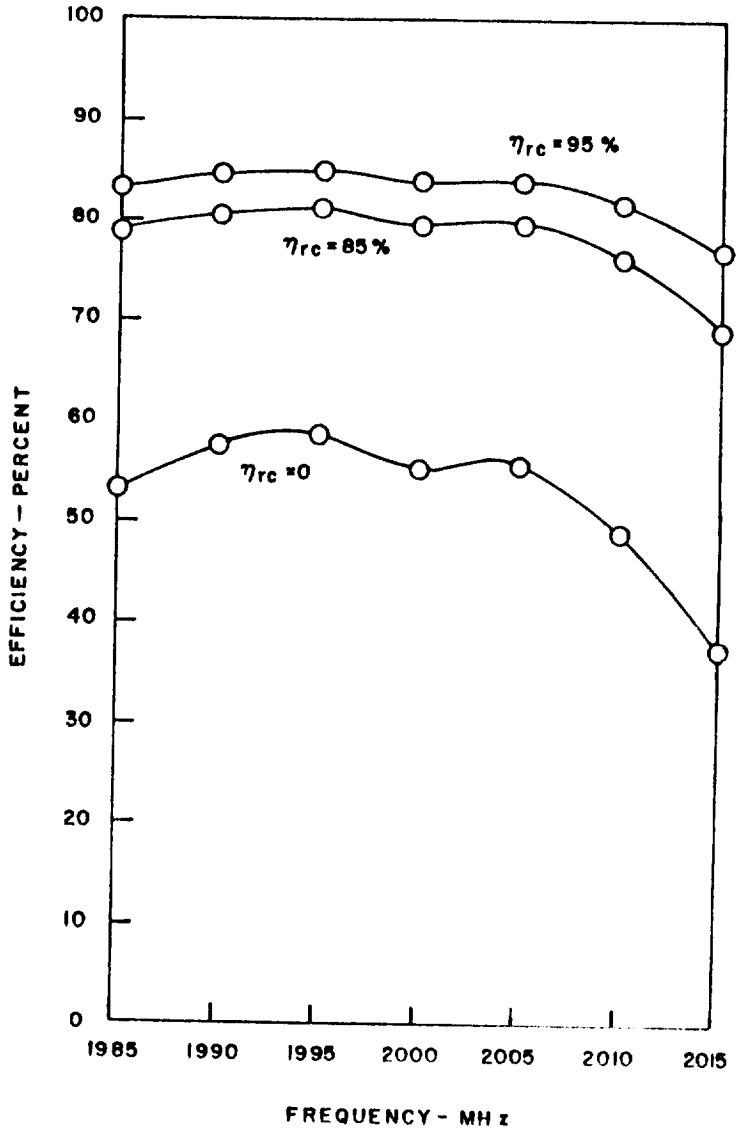

Figure 84 - Efficiency of 2000-MHz FM Klystron Across the Band at Three Values of Reflex-Collector Energy Recovery Efficiency η_{rc} (Double-Gap Output)

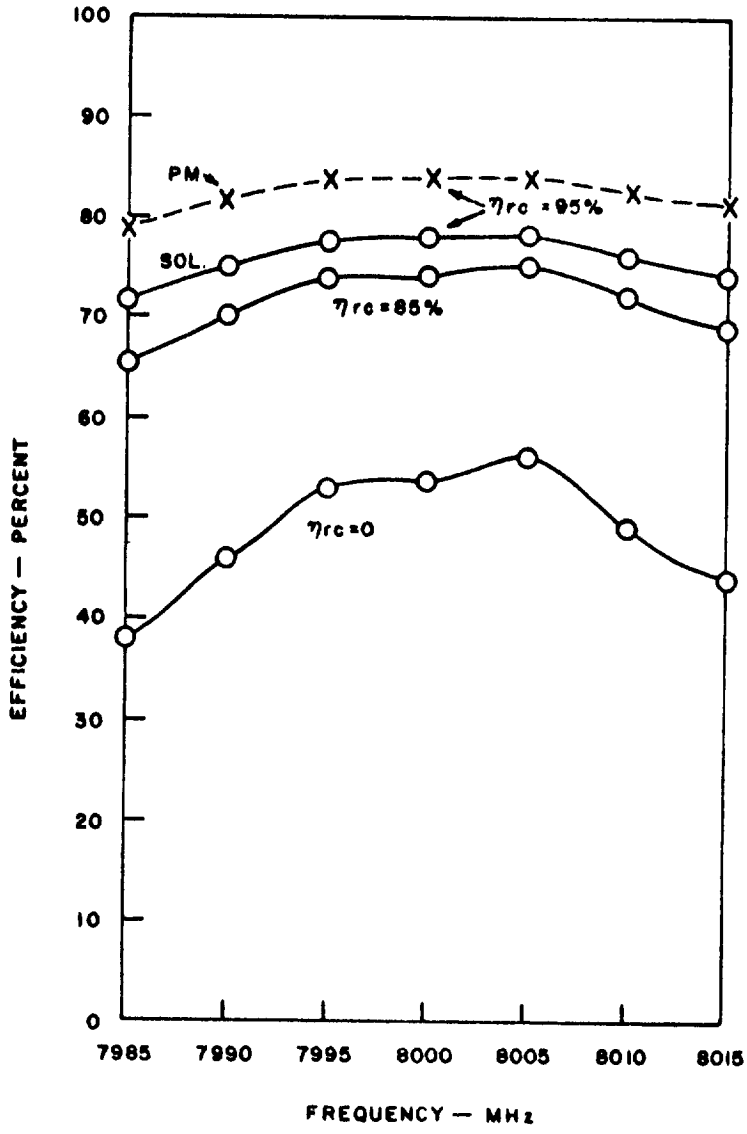

Figure 85 - Efficiency of 8000-MHz FM Klystron Across the Band at Three Values of Reflex-Collector Energy Recovery Efficiency, η_{rc}

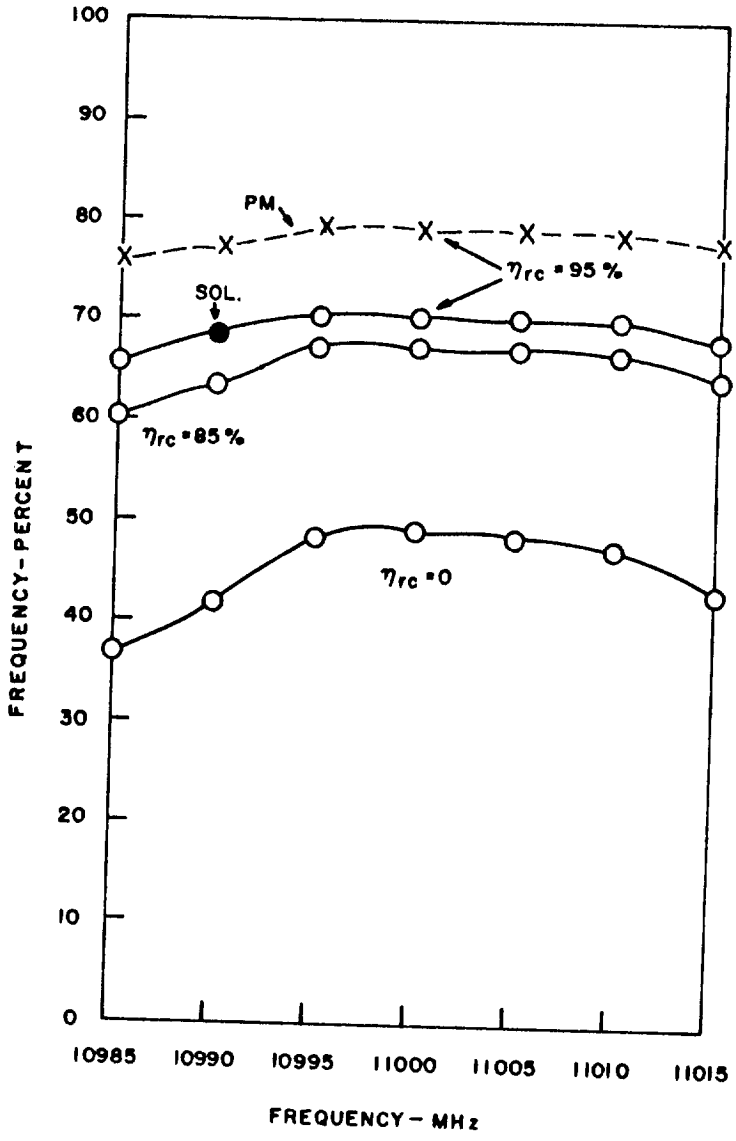

Figure 86 - Efficiency of 11,000-MHz FM Klystron Across the Band at Three Values of Reflex-Collector Energy Recovery Efficiency, η_{rc}

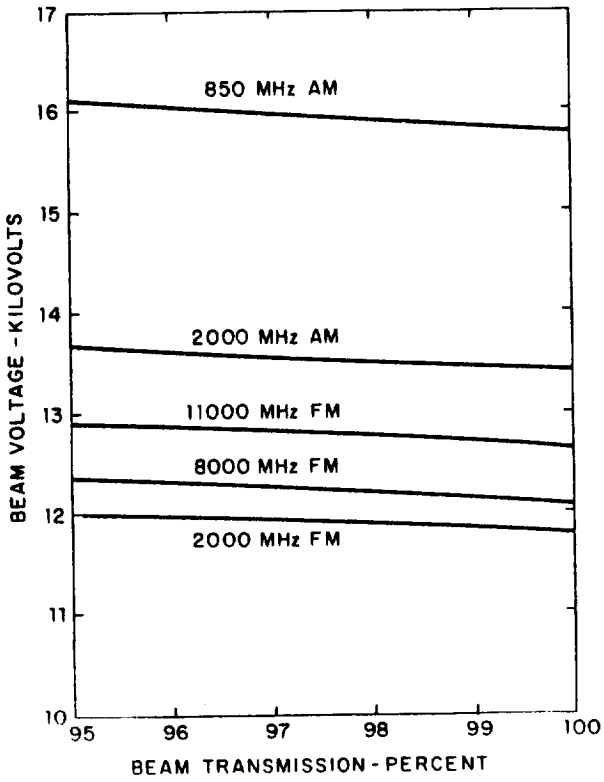

Figure 87 - Beam Voltage Required for Specified Saturation Output Power as Function of Beam Transmission

Section XII
CONCLUSIONS

The development and evaluation of five klystron designs which substantially meet NASA specifications have been successfully carried out, with the following conclusions:

(1) The application of interaction efficiency optimization principles shows that significant increase in klystron power amplifier efficiency is possible. Efficiency at saturation drive can exceed 80 percent.

(2) A new form of depressed collector conceived during the course of this study has inherent secondary electron suppression. This reflex collector may bring the average efficiency of the video amplitude-modulated klystron up from 18 percent to above 50 percent. Frequency modulated klystron efficiency may be brought up to the 75-85 percent range by the same collector technique.

(3) An analytic expression for the R/Q and Q of reentrant cavity resonators has been derived and correlated with previously published results.

(4) Klystron designs for the five different specifications have been prepared. All meet the power output, gain, and bandwidth objectives. All but the 2000-MHz FM design meet the phase specifications. Additional design optimization, curtailed by the end of the study time interval, probably will enable the 2000-MHz design to also meet the phase objective.

(5) Practical thermal control techniques have been designed. Heat transfer to the radiators is either by conduction or by means of two-phase fluid "heat pipes".

(6) The power supply requirements for all of the klystrons appear to be within presently known design capability. No extraordinary control circuits are required.

(7) The electron beams required by the various designs are within the capability of present beam optics techniques, although the larger area convergence required at 8000 and 11,000-MHz may result in 3 to 6 percent beam-energy waste on the drift tube walls. Refinement of beam optics for these high frequency cases is desirable.

(8) The objective 20,000-hour minimum life is well within the capability of the Ba-Sr oxide cathode system for the 850-MHz and 2000-MHz tubes. The 8000-MHz and 11,000-MHz designs require a different cathode type; the tungstate cathode appears to be a good choice, based on continuing life tests which have exceeded 15,000 hours at an emission density in excess of that required by the designs.

(9) All klystron designs, including the largest at 850 MHz appear well adapted for integration with the spacecraft. Waste heat radiator panels can be located at appropriate points on the external surface of the craft. Known mechanical design and fabrication techniques are directly applicable to the klystrons as designed.

(10) For the 850-MHz and 2000-MHz designs, electromagnetic focusing is clearly superior to permanent magnet focusing because it is much lighter and the solenoid power has a second order effect on efficiency. At 8000 and 11,000-MHz, the choice is not as clear and will depend on the degree of beam transmission achievable with each system.

Section XIII
RECOMMENDATIONS FOR VERIFICATION EXPERIMENTS

In the course of this study, several design concepts relative to high-efficiency klystron amplifiers have shown promise of performance significantly better than that achieved by tubes currently being produced. While the trade-off considerations have included those considered to be attainable, as well as those which might be achieved with additional effort, it will be necessary to conduct planned experiments to verify many of the design factors before detailed planning of an orbiting transmitter can be undertaken. In addition, the unusual environment existing both during the launching and orbiting phases of the vehicle will require mechanical design and fabrication techniques that will ensure a long operational life.

A series of confirming experiments have been outlined to enable the verification of the design concepts and to acquire the necessary special technology before a specific klystron transmitter is designed. Identification of these experiments and their interrelationship is shown in Figure 88. Those activities shown below the dashed line and labeled "Technology Acquisition" are considered preliminary to the two stages of specific klystron development and production shown as Experiments 10 and 11.

The estimated time intervals (in months) required for the experiments are indicated within the boxes, and the elapsed time to achieve particular results is shown as a circled figure. Thus, the technology acquisition is estimated to require 27 months, and the specific amplifier development would take an additional 33 months. No attempt has been made to delineate the activities required to pursue the development of other transmitter components such as diplexer, antenna, modulator, or RF driver. However, the experimental investigation of modulation systems coordinated with the demonstration of a depressed collector and its multi-voltage power supply is recommended. Moreover, overall optimization is best achieved by the coordinated efforts of technical people of various specialties.

Specific descriptions of the recommended demonstrations are given below:

(1) Verify Depressed Collector Design Concept

The most significant improvement in overall amplifier efficiency, particularly under modulation conditions, is achieved by use of a multisegment

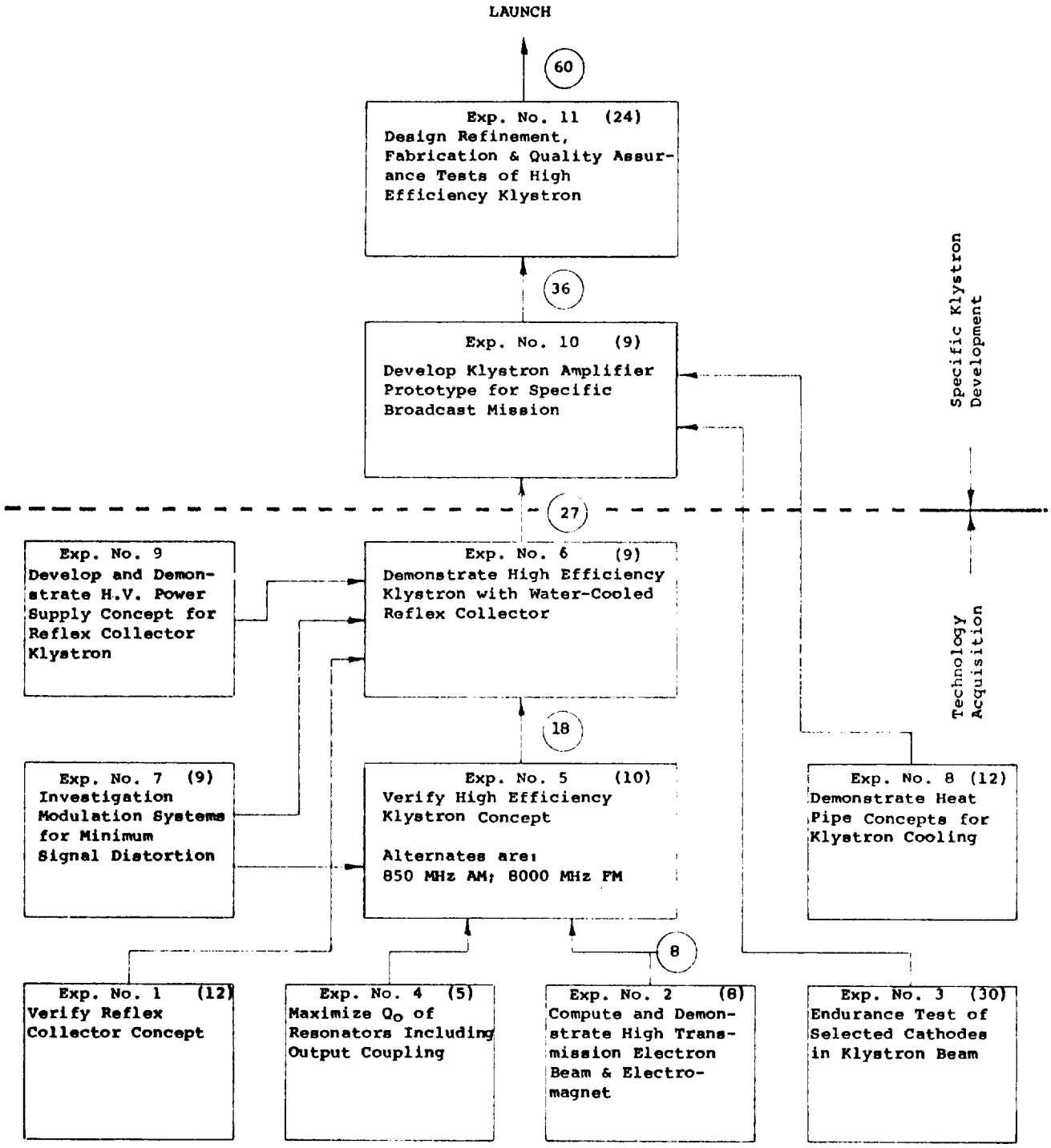

Note: Figures in parentheses ( ) indicate duration of the given project in months. Figures in the circles ○ indicate total elapsed time from the start of technology acquisition in months.

Figure 88 - Recommendations for Verification Experiments

depressed collector. However, this design concept as formulated during this program is unproven. Thus, an experimental verification of this collector is recommended. A demonstration with an unmodulated beam is deemed a necessary prerequisite; the collector should later be fitted to a power klystron and its performance verified under various RF modulation conditions. A twelve-month period is estimated as being required to investigate depressed collector capabilities.

(2) Improve Electron Beam Formation and Collimation

It is evident that beam current intercepted by drift tubes is completely wasted and represents a heat source at a point where heat removal may be difficult. At the higher frequencies where the ratio of cathode area to drift tube cross section is large, beam interception may reach as much as five percent of the input power. It is therefore recommended that beam formation and collimation be investigated in steps which optimize beam system, including the demonstration of a magnet structure adapted for satellite operation. While an arbitrarily high beam transmission could be achieved by the use of excessive magnetic fields, this would not be commensurate with high interaction efficiency. Thus, a nominal maximum field of three times the Brillouin value for a chosen beam diameter is suggested. Also the beam structure (diameter, potential depression, etc.) should be demonstrated by measurement with appropriate probing equipment. This activity is estimated to require eight months.

(3) Endurance Test Selected Cathodes

The realization of a well-focused electron beam will be easier if a smaller area convergence in the gun is used. This requires increased current density from the emitter. However, increased current density may mean reduced life or a change to an emitter system other than the conventional oxide coating on a nickel base. The 8000-MHz and 11,000-MHz designs studied during this contract require cathode current densities in excess of 1 ampere per square centimeter. There are at least two cathode systems which are potentially capable of greater than 20,000 hours life at this loading, but operating experience in high-voltage beam tubes is minimal. We believe that accelerated life tests of cathodes are not sufficiently definitive, and it is recommended that selected cathodes be operated in full scale electron beams for the anticipated lifetime period. By starting early in the program, sufficient data could be accumulated to ensure a long-lived klystron for the space transmitter. Hence, a thirty-month time period is recommended.

An additional question concerns the effects on cathode life of venting the klystron to the environment around the spacecraft at an appropriate time after orbit is reached. While it is true that pressures in orbit have been measured as less than 10^{-12} Torr (even 10^{-14} Torr), the effect of this environment on the cathode is unknown. Also, it is impractical to achieve this low pressure in the laboratory, particularly in the presence of a hot cathode and a moderate power electron beam. It is therefore recommended that several low-power thermionic diodes be orbited in experimental vehicles and that some of these diodes be equipped with venting means while a control group remain sealed. Monitoring of emission activity over an extended time period would provide the desired information.

(4) Reduce Losses in RF Circuitry

Even as beam power intercepted by the drift tube walls is not recoverable by a depressed collector, the RF power lost in the resonators or in the output coupling means is also lost as heat. At the higher frequencies of interest; i.e., above 7000 MHz, losses in the output resonator system will be five to ten percent of the RF power generated. These losses have been computed with presently attainable values of unloaded Q as reference. While these Q values are representative of current design and construction practice, it is worthwile to investigate means for increasing the Q, particularly in resonators which are tightly coupled to a transmission line. A five-month analytic and experimental investigation to reduce RF losses in resonator systems appropriate to klystron amplifiers is recommended.

(5) Verify High-Efficiency Klystron Design Concepts

The klystron designs prepared in the present study are the result of optimization via computer simulation. While this simulation has proven to be accurate for conventional klystron designs, the extension of these concepts to the high-efficiency regime has not been fully verified. One of the klystron designs which have resulted from the present study should be fabricated and tested under various signal conditions. The results of the demonstrations of improved beam formation and reduced RF circuit losses should be applied to the fabrication of this klystron. The frequency chosen for this demonstration would depend on consideration of the most appropriate frequency for a final system. An early choice of frequency or frequency range would maximize the utility of the results in future projects. A ten-month period is estimated to be required to demonstrate the high-efficiency design.

(6) Demonstrate High-Efficiency Klystron with Reflex Depressed Collector

The klystron resulting from Experiment No. 5 will be a good vehicle for demonstration of the multi-segment reflex collector which would have been reduced to practice in Experiment No. 1. It is recommended that this klystron be fitted with a water-cooled, multi-segment collector and that measurement of efficiency enhancement be made under both AM and FM signal conditions. Detailed measurements of signal distortion should also be made under both normal modulation conditions as well as with other modulation systems which may result from Experiment No. 7. Coordination of the activities of microwave tube specialists and modulation circuit specialists will enable effective optimization of the tube-modulator subsystem.

Similarly, power supply concepts resulting from Experiment No. 9 could be tested on this high-efficiency klystron. The special power supply requirements of the multi-electrode depressed collector also offer opportunities for optimization of the power supply-collector subsystem.

These activities are estimated to require a nine-month time interval.

(7) Investigate Modulation Systems for Minimum Signal Distortion

It is recommended that various modulation approaches to be explored both by analysis using computer simulation of the klystron, and by tests conducted on available klystron amplifiers. The primary objective will be to optimize overall transmitter efficiency while achieving the desired quality of radiated signal. This activity should include use of video feedback to compensate for non-linear amplitude response, filters for unwanted sideband energy, means for processing both aural and visual signals through the same klystron, and/or the design of diplexer equipment for combining separate aural and visual signals. Results of this investigation are expected to have a bearing on the klystron design in Experiment No. 6.

(8) Demonstrate Heat Pipe Cooling Concepts for Klystrons

In the present study it was concluded that heat pipes could be effectively employed to transfer heat from various portions of the klystron to appropriate radiating surfaces. While heat pipes of varied geometries have been demonstrated, the specific forms required to transfer the heat from klystron resonator tips or from the multi-segment depressed collector

have not been verified. Of particular interest will be high-temperature heat pipes which will permit heat rejection from small radiating surfaces that are little affected by solar radiation.

It is recommended that heat pipe concepts appropriate for cooling power klystrons be designed and demonstrated in experiments where the heat sources in various portions of the klystron are simulated by radiation or conduction of heat to models of the klystron component under investigation. The demonstration of high-temperature heat pipes in which liquid metals may be in contact with both conductors and insulators will require some investigation of fabrication techniques to contain the working fluid.

A twelve-month time period is suggested as appropriate for this investigation.

(9) Demonstrate Multi-Tap High-Voltage Power Supply

The multi-segment depressed collector concept for achieving high efficiency presents special power supply requirements in that currents at the various taps vary with the modulation level. This is particularly true in the AM case. In order to avoid the weight penalty of overdesign and yet provide adequate voltage regulation for the klystron supplies, various power supply concepts should be evaluated with respect to voltage and current requirements determined in Experiments No. 1 and No. 5. The most appropriate power supply system should then be fabricated as a laboratory version which would be demonstrated in conjunction with the demonstration of the high-efficiency klystron in Experiment No. 6.

A seven-month time period is estimated to be adequate to accomplish this investigation.

(10) Develop Klystron Amplifier Prototype for Specific Broadcast Mission

With the completion of the nine demonstration experiments which have been outlined, a sufficient body of technology will have been acquired to permit the design and development of a klystron amplifier for a specific broadcast mission. When the parameters of the transmitter have been established, it is recommended that a two-stage program of development, refinement, fabrication and quality selection be undertaken.

Assuming the planning of Experiment No. 6 was well coordinated with planned broadcast needs, the design of the prototype klystron will utilize many of the components from the earlier work. These would include resonators, electron gun, and basic collector design. The new work to be done would include mechanical and thermal design to meet the expected environmental factors during both launch and orbit phases. In particular, the heat pipe concepts proven in Experiment No. 8 would be adapted to all parts of the amplifier, including the multi-segment collector.

Test of this klystron would be conducted in a space simulator where all environmental factors except the zero gravitational field would be present. While it is not possible to evaluate the heat pipe cooling in zero gravitational field, it will be possible to test the tube in various orientations in the earth's gravity and thus place various portions of the structure in either a positive or negative field.

During this developmental program, it is expected that prototypes for other transmitter components will become available and can therefore be tested in conjunction with the klystron.

(11) Design Refinement, Fabrication, Endurance Testing, and Quality Assurance Selection of Klystron

In order to obtain space-qualified klystrons based on the prototype klystron development, a program of product refinement, endurance testing, and quality assurance selection will be required.

At the start, those design changes indicated by tests of the prototype amplifier should be incorporated in at least four tubes which will be given rigorous shock and vibration tests. Electrical performance should be evaluated before and after each mechanical test and the severity of the tests should be increased to a point somewhat beyond the values expected in service. This testing would preferably be done with the tube mounted in a mock-up of the space vehicle in order to duplicate the various mechanical constraints as accurately as possible.

Design deficiencies identified in the above tests would be rectified and eight additional amplifiers representative of the best design would be fabricated. After a burn-in test of 500 to 1000 hours to eliminate possible early failures, two tubes would be selected for extended endurance testing in a space simulator chamber. The endurance test would be planned to allow at least 15,000 hours of accumulated test time before a planned launch. In

any case, the endurance testing would be continued until the end of useful life was reached. Data on tube performance would be recorded and analyzed at frequent intervals. The performance evaluation would include diagnostic tests which will permit identification of incipient failures before actual malfunction occurs.

All twelve of these klystrons would be fabricated under stringent quality control. A comprehensive quality assurance plan would be established to control all materials and processes. Complete documentation at all stages will enable direct correlation of performance with fabrication procedures.

The objective of this program will be a yield of at least two space-qualified high efficiency klystrons. The elapsed time required to reach this point is estimated to be 60 months from the start of verification experiments.

Appendix A

DOUBLY-REENTRANT UNGRIDDED CAVITY COMPUTER PROGRAM

1. LISTING

```
80 REM PROPERTIES OF "DOUBLE-SQUARE" DOUBLY-REENTRANT CAVITIES
85 REM WRITTEN BY G.M. BRANCH ON MAY 24, 1966.  REVISED MAY 29,1966.
86 REM REVISED MAY 30, 1966.
90 REM BEGINNING IN STATEMENT 500 INPUT FREQUENCY IN MHZ,
92 REM BEAM POWER IN WATTS, INTERNAL
94 REM CONVERSION EFFICIENCY AS A FRACTION, GAP TRANSIT ANGLE IN
96 REM RADIANS, GAP LENGTH IN INCHES, INITIAL VALUE OF TUNNEL
98 REM O.D. IN INCHES, FINAL VALUE OF TUNNEL O.D. IN INCHES, TUNNEL
100 REM I.D. IN INCHES, DESIRED NORMALIZED GAP IMPEDANCE, AND BEAM IMPED.
101 READ F0,P0,E1,T3,D1,D8,D9,D5,R2,R3
109 LET R0=R2*R3
110 FOR D0=D8 TO D9 STEP .01
120 LET K1=D0*F0/3756.97
125 LET D2=2*D1/D0
130 LET D3=SQR(D2)
140 LET H2=(2*D3-.24*D2)/K1
150 LET H1=H2*D0/2
160 LET D4=H1+D0
180 LET K1=(.461*D3+(.762*K1-.244)*D2)*(120/K1-43.2)
190 LET Q1=4.09E7*D2/(SQR(F0)*K1)
200 PRINT "FREQUENCY ="F0"MHZ","KA ="K1
210 PRINT "TUNNEL DIAM ="D0"INCHES","CAVITY DIAM ="D4"INCHES"
220 PRINT "GAP LENGTH ="D1"INCHES","CAVITY LENGTH ="H1"INCHES"
222 PRINT "GAP TRANSIT ANGLE ="T3"RADIANS"
230 PRINT "R/Q ="K1"OHMS","Q O ="Q1
231 LET Q2=R0/K1
232 LET W1=E1*Q2/Q1*P0/3
233 LET W2=.01*P0
234 LET T1=.065*(W1+W2)*(H1-D1)/(D0^2-D5^2)
235 LET W2=.02*P0
236 LET T2=.065*(W1+W2)*(H1-D1)/(D0^2-D5^2)
237 PRINT "TUNNEL I.D. ="D5"INCHES","Q L ="Q2
238 PRINT "W RF ="W1"WATTS","W DC (1 PERCENT) ="1.01*P0"WATTS"
239 PRINT "TEMP RISE (1) ="T1"DEG C TEMP RISE (2) ="T2"DEG C"
240 PRINT "1 - ETA CKT ="Q2/Q1,"CONV. EFF ="E1
241 PRINT "NORMALIZED CKT IMPED ="R2
242 PRINT "EFFICIENCY ="E1*(1-Q2/Q1)
245 PRINT
250 NEXT D0
280 STOP
500 DATA 2000,7888
501 DATA .711,1,.2
502 DATA .35,.39
503 DATA .3
504 DATA 1.01
505 DATA 18257
999 END
```

2. SAMPLE OUTPUT

```
FREQUENCY = 2000     MHZ          KA = .18632
TUNNEL DIAM = .35      INCHES     CAVITY DIAM = 2.10056 INCHES
GAP LENGTH = .2       INCHES      CAVITY LENGTH = 1.75056 INCHES
GAP TRANSIT ANGLE = 1     RADIANS
R/Q = 226.059 OHMS                Q U = 4623.58
TUNNEL I.D. = .3       INCHES     Q L = 81.5697
W RF = 32.9811 WATTS              W DC (1 PERCENT) = 78.88    WATTS
TEMP RISE (1) = 346.896 DEG C     TEMP RISE (2) = 591.513 DEG C
1 - ETA CKT = 1.76421 E-2         CONV. EFF = .711
NORMALIZED CKT IMPED = 1.01
EFFICIENCY = .698456

FREQUENCY = 2000     MHZ          KA = .191644
TUNNEL DIAM = .36      INCHES     CAVITY DIAM = 2.08963 INCHES
GAP LENGTH = .2       INCHES      CAVITY LENGTH = 1.72963 INCHES
GAP TRANSIT ANGLE = 1     RADIANS
R/Q = 219.826 OHMS                Q U = 4622.62
TUNNEL I.D. = .3       INCHES     Q L = 83.8828
W RF = 33.9235 WATTS              W DC (1 PERCENT) = 78.88    WATTS
TEMP RISE (1) = 283.222 DEG C     TEMP RISE (2) = 481.271 DEG C
1 - ETA CKT = 1.81462 E-2         CONV. EFF = .711
NORMALIZED CKT IMPED = 1.01
EFFICIENCY = .698098

FREQUENCY = 2000     MHZ          KA = .196967
TUNNEL DIAM = .37      INCHES     CAVITY DIAM = 2.07946 INCHES
GAP LENGTH = .2       INCHES      CAVITY LENGTH = 1.70946 INCHES
GAP TRANSIT ANGLE = 1     RADIANS
R/Q = 213.849 OHMS                Q U = 4623.38
TUNNEL I.D. = .3       INCHES     Q L = 86.227
W RF = 34.8658 WATTS              W DC (1 PERCENT) = 78.88    WATTS
TEMP RISE (1) = 237.956 DEG C     TEMP RISE (2) = 402.974 DEG C
1 - ETA CKT = 1.86502 E-2         CONV. EFF = .711
NORMALIZED CKT IMPED = 1.01
EFFICIENCY = .69774

FREQUENCY = 2000     MHZ          KA = .202291
TUNNEL DIAM = .38      INCHES     CAVITY DIAM = 2.07     INCHES
GAP LENGTH = .2       INCHES      CAVITY LENGTH = 1.69     INCHES
GAP TRANSIT ANGLE = 1     RADIANS
R/Q = 208.118 OHMS                Q U = 4625.68
TUNNEL I.D. = .3       INCHES     Q L = 88.6015
W RF = 35.8081 WATTS              W DC (1 PERCENT) = 78.88    WATTS
TEMP RISE (1) = 204.183 DEG C     TEMP RISE (2) = 344.616 DEG C
1 - ETA CKT = 1.91543 E-2         CONV. EFF = .711
NORMALIZED CKT IMPED = 1.01
EFFICIENCY = .697361

FREQUENCY = 2000     MHZ          KA = .207614
TUNNEL DIAM = .39      INCHES     CAVITY DIAM = 2.06122 INCHES
GAP LENGTH = .2       INCHES      CAVITY LENGTH = 1.67122 INCHES
GAP TRANSIT ANGLE = 1     RADIANS
R/Q = 202.621 OHMS                Q U = 4629.35
TUNNEL I.D. = .3       INCHES     Q L = 91.0054
W RF = 36.7504 WATTS              W DC (1 PERCENT) = 78.88    WATTS
TEMP RISE (1) = 178.062 DEG C     TEMP RISE (2) = 299.531 DEG C
1 - ETA CKT = 1.96584 E-2         CONV. EFF = .711
NORMALIZED CKT IMPED = 1.01
EFFICIENCY = .697023
```

Appendix B
SOLENOID DESIGN COMPUTER PROGRAM

1. LISTING

```
050 REM THIS PROGRAM COMPUTES THE TOTAL WEIGHT, COIL WEIGHT,
055 REM COIL POWER AND COIL O.D. FOR A RANGE OF FOIL THICKNESSES
060 REM DATA REQUIRED*  500 MAGNETIC FIELD
065 REM IN GAUSS,COIL LENGTH IN INCHES,COIL I.D. IN INCHES
070 REM INSULATOR THICKNESS IN INCHES, COND. DENSITY
075 REM IN LBS/CU.IN., RESISTIVITY IN OHM-IN., COIL CURRENT,
080 REM NUMBER OF FOIL WIDTHS PER TOTAL SOLENOID WIDTH.
100 READ B,L1,A,D2,S,Q
102 READ I,N1
105 PRINT"FIELD=";B, "LENGTH=";L1, "COIL I.D.=";A
107 PRINT "INSUL. THKNSS=";D2,"DENSITY=";S
115 PRINT "RESISTIVITY=";Q, "COIL CURRENT=";I
120 LET H=L1/N1
218 PRINT "FOIL WIDTH=";H
219 PRINT
220 PRINT"FOIL THK'S","TOTAL WEIGHT","COIL WEIGHT","O.D.","PWR KW"
222 PRINT
230 FOR D1=.005 TO .006 STEP .0001
235 LET K=D1/(D1+D2)
238 LET B3=B/I
240 LET L2=6.35*B3*L1*A + 12.6*B3↑2*H/K*D1
250 LET C=H*D1*L2*S
260 LET R=Q*L2/(H*D1)
265 LET O=A+4.04*B3*H*D1/K
270 LET P=R*I↑2/1000
280 LET V=C+100*P
290 PRINT D1,          R,          C,          O,          P
300 NEXT D1
500 DATA 845
502 DATA 14.26,2.815,.0005
503 DATA .097
504 DATA 1.823E-6
510 DATA 10,6
999 END
```

2. SAMPLE OUTPUT

```
FIELD= 845      LENGTH= 14.26                    COIL I.D.= 2.815
INSUL. THKNSS= .0005            DENSITY= .097
RESISTIVITY= 1.82300 E-6        COIL CURRENT= 10
FOIL WIDTH= 2.37667

FOIL THK'S      TOTAL WEIGHT    COIL WEIGHT     O.D.            PWR KW

 .005           61.0804         26.2049         7.27741         .348755
 .0051          60.9769         26.7545         7.35654         .342244
 .0052          60.9034         27.3052         7.43967         .335963
 .0053          60.8526         27.8566         7.52061         .329958
 .0054          60.825          28.4095         7.60194         .324156
 .0055          60.8196         28.9631         7.68306         .318565
 .0056          60.8351         29.5177         7.76421         .313174
 .0057          60.8706         30.0734         7.84535         .307972
 .0058          60.925          30.63           7.92648         .302949
 .0059          60.9974         31.1877         8.00762         .298097
 .006           61.087          31.7463         8.08875         .293406
```

Appendix C
UNDULATION OF LARGE-SIGNAL PHASE SHIFT AND EFFICIENCY

An unexpected and undesirable feature of the phase shift curves of Figures 37(c) and 38(c) is the development of an undulation at large-signal levels which causes the phase shift to exceed the phase specification by a factor of two to three. In this appendix we will show that this undulation apparently is an artifact of the large-signal disk model due to the fact that a finite number of disks is used in the digital computation.

In Figures 89(a) and 89(b), the phase midway in the output gap of the fundamental component of current i_1/I_o at saturation drive is plotted (dashed lines) as a function of frequency for the 8000-MHz and 11,000-MHz tubes, respectively. In addition, the phase locations of several anti-bunch electrons are plotted, as indicated by the solid lines labeled with electron number. It is significant to note that the phase of the current cuts across several of the electron trajectory curves in both diagrams. It would not be surprising to find that some calculated quantities show a periodic disturbance with frequency as the phase of the current alternately coincides with and lies midway between the phases of the individual electrons. Indeed, a small undulation in gain and efficiency and a large undulation in the second derivative of phase shift appear to be synchronous with this "granularity", as discussed below.

In Figure 37(a), the efficiency curve shows an upward bulge of a few percent at 8005 MHz. From Figure 89(a), it is evident that the phase of the RF current falls midway between adjacent electron trajectory phases at this frequency. This evidently is a favorable condition in the output gap calculation, and efficiency is enhanced by two or three points due to this anti-coincidence of phases. In similar manner, the coincidence of phases at midband probably depresses the efficiency by a point or two. This combination of effects apparently is responsible for the small undulation of efficiency and gain evident in Figures 37(a) and 37(b) just above midband. The inverse effect can be seen at 11,000 MHz in Figures 38(a) and 38(b). Here the gain and efficiency are flattened just above midband due to the coincidence of the current phase and the phase of electron No. 10, as evident in Figure 89(b). In both cases the undulation of efficiency is of the order the reciprocal of the number of disks used in the calculation, i.e., ± 2.5 percent for 20 disks. Thus undulation, while troublesome, is not large enough to cause the efficiency to fail to meet the desired specification.

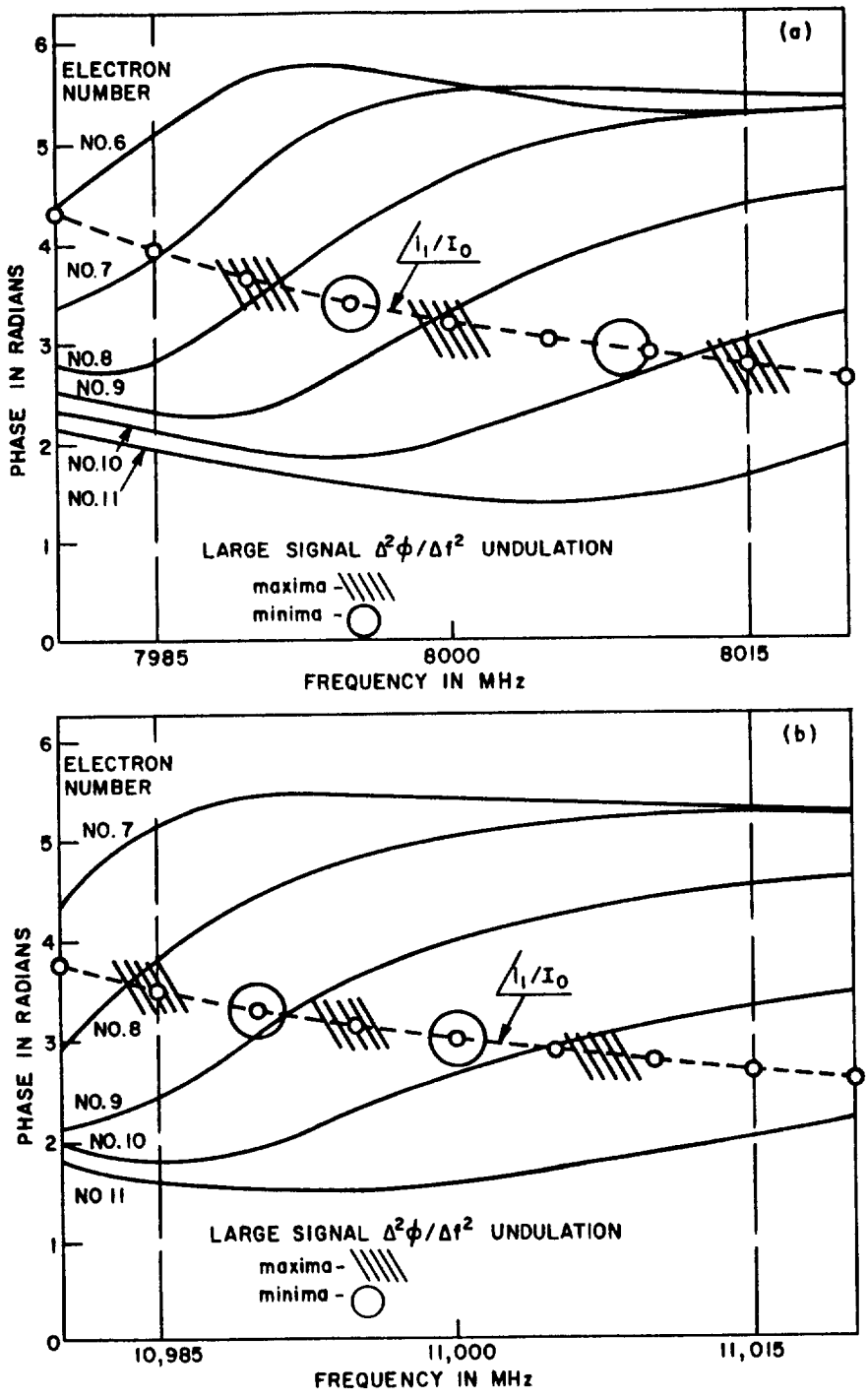

Figure 89 - Phase of Fundamental Component of RF Current at Large Signal and Phase Location of Antibunch Electrons as a Function of Frequency at (a) 86 GHz and (b) 11 GHz

The second derivative of phase shift under large-signal conditions is much more sensitive than efficiency to the number of electron disks used in the digital calculation. The large undulations of the second derivative of phase shown in the lower plots of Figures 37(c) and 38(c) apparently stem from the same source as the small variations in the gain and efficiency curves. This conclusion can be justified by noting along the current phase curves in Figures 89(a) and 89(b) the frequencies at which the maxima and minima of the second derivative curve of phase shift occur, as taken from Figures 37(c) and 38(c). The frequencies at which the maxima of these curves occur are indicated by the shaded areas in Figures 89(a) and 89(b), and the frequencies of the second derivative minima are indicated by the circles. It is evident that the maxima and minima occur more or less synchronously with the coincidence and anti-coincidence of the dashed current phase curve with the various curves of electron phases. The correlation is not perfect, perhaps due to the additional phase shift introduced in the output gap calculation due to the large-signal coupling coefficient. However, the correlation is close enough to strongly suggest that the granularity due to a finite number of disks is responsible for what apparently is a spurious undulation in phase shift at large-signal levels.

REFERENCES

1. Clough, L. D., Dix, J. F., Monk, A. J. and Rowcroft, P., "A High Efficiency 15 Mw, 400 Mc/s Pulsed Klystron", Jour. of Electronics and Control, pp. 105-118

2. Walder, J., "The Biased Gap Klystron", M. Sc. Thesis, Cornell University, February 1965

3. Chodorow, M. and Wessel-Berg, T., "A High Efficiency Klystron with Distributed Interaction", Trans. IRE, Vol. ED-8, pp. 44-55; January 1961

4. Priest, D. H. and Leidigh, W. J., "Experiments with High Power CW Klystrons with Extended Interaction Catchers", IEEE Trans. on Elec. Dev., Vol. ED-10, pp. 201-211; May 1963

5. Priest, D. H. and Leidigh, W. J., "A Two-Cavity Extended Interaction Klystron Yielding 65 Percent Efficiency", IEEE Trans. on Elec. Dev., Vol. ED-11, pp. 369-373; August 1964

6. Met, V., "Depressed Collector Studies for High Power Klystrons", Final Tech. Report, Contract AF 30(602)-1500, Task 45083, March 1961

7. Webber, S. E., "Large Signal Analysis of the Multi-Cavity Klystron", IRE Trans. on Elec. Dev., Vol. ED-5, pp. 306-316; October 1958

8. Rowe, J. E., Nonlinear Electron-Wave Interaction Phenomena, Academic Press, N. Y., Cap. V; 1965

9. Sun, C. and Dalman, G. C., "Large Signal Behavior of Distributed Klystrons", IEEE Trans. on Elec. Dev., Vol. ED-15, pp. 60-69; February 1968

10. Hahn, W. C. "Small Signal Theory of Velocity-Modulated Electron Beams", G.E. Rev., Vol. 42, pp. 258-270: 1939

11. Hahn, W. C., "Wave Energy and Transconductance of Velocity-Modulated Electron Beams", G.E. Rev., Vol. 42, pp. 597-602; Nov. 1939

12. Ramo, S., "The Electronic-Wave Theory of Velocity Modulated Tubes", Proc. IRE, Vol. 27, pp. 757-763; Dec. 1939

13. Branch, G. M. and Mihran, T. G., "Plasma Frequency Reduction Factors in Electron Beams", Trans. IRE, Vol. ED-2, pp. 3-11; April 1955

14. Webber, S. E., "Ballistic Analysis of a Two-Cavity Finite Beam Klystron", Trans. IRE, Vol. ED-5, pp. 98-108; April 1958

15. Webber, S. E., "Some Calculation on the Large Signal Energy Exchange Mechanisms in Linear Beam Tubes", Trans. IRE, Vol. ED-7, pp. 154-162; July 1960

16. Mihran, T. G., "The Effect of Space Charge on Bunching in a Two Cavity Klystron", Trans. IRE, Vol. ED-6, pp. 54-64; Jan. 1959

17. Mihran, T. G., "Plasma Frequency and Velocity Spread in Bunched Electron Beams at Finite Diameter", Jour. Appl. Phys., Vol. 38, pp. 159-166; Jan. 1967

18. Mihran, T. G., "The Effect of Drift Length, Beam Radius and Perveance on Klystron Power Conversion Efficiency", Trans. IRE, Vol. ED-14, pp. 201-206; April 1967

19. Branch, G. M., Mihran, T. G., Neugebauer, W. and Pohl, W. J., "Space-Charge Wavelengths in Electron Beams", Trans. IEEE, Vol. ED-14, pp. 350-357; July 1967

20. Beck, A. H. W., Thermionic Valves, Cambridge, Univ. Press, p. 370; 1953

21. Branch, G. M., "Electron Beam Coupling in Interaction Gaps of Cylindrical Symmetry", Trans. IRE, Vol. ED-8, pp. 193-206; May 1961

22. Tien, P. K., Walker, L. R. and Wolontis, V. M., "A Large Signal Theory of Traveling-Wave Amplifiers", Proc. IRE 43, pp. 260-277; March 1955

23. Hamilton, D. R., Knipp, J. K. and Kuper, J. B. H., "Klystrons and Microwave Triodes", pp. 73-80, McGraw-Hill Book Co., New York, 1948

24. Ginzton, E. L. and Nalos, E. J., "Shunt Impedance of Klystron Cavities", Trans. IRE, Vol. MTT-3, pp. 4-7; Oct. 1955

25. Ramo, S., Whinnery, J. R. and VanDuzer, T. R.: "Modern Communications Electronics", 3rd. Ed., p. 289, John Wiley & Sons, New York; 1965

26. Langmuir, I. and Blodgett, K., Phys. Rev. 22, Series 2, 1923, p. 347

27. Prince, D. C., Jr., "Computer Evaluation of Ion Engines", TIS Report R63FPD128, General Electric Company, Cincinnati, Ohio; March 1963

28. COSMIC Computer Center, Univ. of Georgia; Directory of Computer Programs Available from COSMIC, Vol. 1, "Computer Evaluation of Ion Engines", MFS-0143; July 1967

29. Branch, G. M., Jr. and Neugebauer, Wendell, "Applications of Computers to Tube Design", Invited Paper, Proc. Eighth IEEE Conference on Tube Techniques; Sept. 1966

30. Cockroft, J. D., "Production of Strong Magnetic Fields", Phil. Trans. Roy. Soc. 227, p. 325; 1928

31. Bozorth, R. M., Ferromagnetism. Princeton: D. Van Nostrand Co., Inc., 1951, pp. 344-364

32. Chambers, R. L. and Somers, E. V., "Radiation Fin Efficiency for One Dimensional Heat Flow in a Circular Fin", ASME Paper No. 59-HT-8; 1959

33. Lieblein, S., "Analysis of Temperature Distribution and Radiant Heat Transfer Along a Rectangular Fin of Constant Thickness", NASA TN D-196; 1959

DISTRIBUTION LIST
FINAL REPORT
Contract NAS3-11514

	No. of Copies
National Aeronautics and Space Administration Headquarters Washington, D.C. 20546	
Attention: SA/L. Jaffe	1
SAC/A.M.G. Andrus	10
National Aeronautics and Space Administration Lewis Research Center 21000 Brookpark Road Cleveland, Ohio 44135	
Attention: C. C. Conger, MS 54-1	1
R. E. Alexovich, MS 54-3	1
Dr. H. G. Kosmahl, MS 54-3	1
Technology Utilization Officer, MS 3-19	1
Spacecraft Technology Procurement Sec., MS 54-2	1
Library, MS 60-3	2
Report Control Office, MS 5-5	1
N. T. Musial, MS 501-3	1
G. J. Chomos, MS 54-3	50
Communication Systems Inc. 5817 Columbia Pike Falls Church, Virginia 22046	
Attention: J. Bisaga	1
Rand Corporation 1700 Main Street Santa Monica, California 90404	
Attention: Dr. J. Holt	1
National Aeronautics and Space Administration Electronics Research Center 575 Technology Square Cambridge, Massachusetts 02139	
Attention: E/Dr. L. Vanatta	1
EM/C. Veronda	1
Library	1

	No. of Copies
National Aeronautics and Space Administration George C. Marshall Space Flight Center Huntsville, Alabama 35812	
Attention: RASTR-A/E. C. Hamilton	1
Library	1
National Aeronautics and Space Administration Goddard Space Flight Center Greenbelt, Maryland 20771	
Attention: 733/R. Pickard	1
Library	1
National Aeronautics and Space Administration Ames Research Center Moffett Field, California 94035	
Attention: OART-MAO/E. Van Vleck, MS 202-6	1
Library	1
National Aeronautics and Space Administration Langley Station Hampton, Virginia 23365	
Attention: B. Kendall, MS 173	1
Library, MS 185	1
National Aeronautics and Space Administration Manned Spacecraft Center Houston, Texas 77001	
Attention: Library	1
Jet Propulsion Laboratory 4800 Oak Grove Drive Pasadena, California 91103	
Attention: L. Derr	1
Library	1
National Aeronautics and Space Administration Scientific and Technical Information Facility P.O. Box 5700 Bethesda, Maryland	
Attention: NASA Representative	3
Radio Corporation of America Astro-Electronics Division Princeton, New Jersey 08540	
Attention: R. B. Marstin	1

	No. of Copies
TRW Systems One Space Park Redondo Beach, California 90278 Attention: W. A. Finley/Space Vehicle Division	1
General Dynamics Convair Division P.O. Box 1128 San Diego, California 92112 Attention: F. J. Dore/Advanced Programs	1
Hughes Aircraft Company Space Systems Division 1194 West Jefferson Boulevard Culver City, California 90230 Attention: H. A. Rosen/Satellite Systems Laboratory	1
General Electric Company Missile and Space Division Valley Forge Space Technology Center P.O. Box 8555 Philadelphia, Pennsylvania 19101 Attention: H. Collins P. Nadler	1 1
Federal Communications Commission 521 Twelfth Street Washington, D.C. 20554 Attention: H. Fine	1
U. S. Information Agency 25 M Street S.W. Washington, D.C. 20547 Attention: IBS/EF/G. Jacobs	1
General Electric Company Tube Department Microwave Tube Business Section Schenectady, New York Attention: R. A. Dehn	1
Litton Industries Electron Tube Division 960 Industrial Road San Carlos, California 94070 Attention: Dr. G. Pokorny J. Orr	1 1

	No. of Copies
S-F-D Laboratories Inc. 800 Rahway Avenue Union, New York 07083 Attention: Dr. G. Farney	1
Hughes Aircraft Company Electron Dynamics Division P.O. Box 2999 Torrence, California 90509 Attention: Dr. J. Mendel	1
Watkins Johnson Company 333 Hillview Avenue Palo Alto, California 94304 Attention: Dr. D. Watkins	1
Varian Associates 611 Hansen Way Palo Alto, California 94303 Attention: F. Melzer	1
Radio Corporation of America Industrial Tube Division Lancaster, Pennsylvania Attention: W. P. Bennett	1